Universidade de Lisboa

Faculdade de Medicina de Lisboa

NUTRIENT UPTAKE AND METABOLISM IN *PLASMODIUM*-INFECTED HEPATIC CELLS

Patrícia dos Santos Meireles

Orientador: Doutor Miguel Prudêncio

Tese especialmente elaborada para obtenção do grau de Doutor em Ciências Biomédicas, Especialidade de Microbiologia e Parasitologia.

2016

Universidade de Lisboa
Faculdade de Medicina de Lisboa

NUTRIENT UPTAKE AND METABOLISM IN *PLASMODIUM*-INFECTED HEPATIC CELLS

Patrícia dos Santos Meireles

Orientador: Prof. Doutor Miguel Prudêncio

Tese especialmente elaborada para obtenção do grau de Doutor em Ciências Biomédicas, Especialidade de Microbiologia e Parasitologia.

Júri:

Presidente: Doutor José Augusto Gamito Melo Cristino, Professor Catedrático e Presidente do Conselho Cientifico da Faculdade de Medicina da Universidade de Lisboa.

Vogais:
- Doutora Anne-Kristin Mueller, Research Group Leader da Heidelberg University Hospital, Alemanha;
- Doutor Henry Staines, Researcher da St. George's University of London, Reino Unido;
- Doutor Luís Jaime Gomes Ferreira da Silva Mota, Professor Auxiliar da Faculdade de Ciências e Tecnologia da Universidade Nova de Lisboa;
- Doutor João António Augusto Ferreira, Professor Associado da Faculdade de Medicina da Universidade de Lisboa;
- Doutor Rui Miguel Prudêncio Cunha Pignatelli, Investigador do Instituto de Medicina Molecular da Faculdade de Medicina da Universidade de Lisboa; (Orientador)
- Doutora Luísa Miranda Figueiredo, Investigadora do Instituto de Medicina Molecular da Faculdade de Medicina da Universidade de Lisboa;
- Doutora Liliana Mâncio Silva, Investigadora do Instituto de Medicina Molecular da Faculdade de Medicina da Universidade de Lisboa.

Fundação para a Ciência e Tecnologia

2016

A impressão desta tese foi aprovada pelo Conselho Cientifico da Faculdade de Medicina de Lisboa na reunião de 16 de Fevereiro de 2016.

Summary

Malaria is an acute febrile illness and one of the most prevalent infectious diseases in the world. It is caused by protozoan parasites of the genus *Plasmodium* that are transmitted to their mammalian hosts through the bite of an infected female *Anopheles* mosquito [1, 2]. In 2015, there were an estimated 214 million cases of malaria, which resulted in 438 000 deaths, most of them occurring in sub-Saharan Africa [1]. Overall, 3.2 billion people are estimated to be at risk of being infected by *Plasmodium* and developing the disease [1].

Upon the bite of an infected mosquito, *Plasmodium* parasites, termed sporozoites at this stage of the lifecycle, are deposited under the skin of their mammalian host, and are carried by the circulatory system to the liver, where they traverse several hepatocytes before productively invading a final cell [3]. Inside hepatocytes, each sporozoite develops into an exoerythrocytic form (EEF), containing thousands of newly formed merozoites that are eventually released into the bloodstream where they invade red blood cells, initiating the symptomatic, erythrocytic stage of the disease [4].

During the asymptomatic liver stage of *Plasmodium* infection, the parasite undergoes a remarkably rapid growth, with 10^4- to 10^5-fold replication of its genome [5, 6]. To support their rapid multiplication and supply their metabolic pathways, parasites scavenge nutrients from the host hepatocyte [7-10]. It was previously shown that glucose plays a crucial role during the liver stage of *P. berghei*, establishing the importance of the import of this nutrient through the parasite's membrane hexose transporter (HT) for its replication inside liver cells [8]. On the other hand, microarray analyses of *P. berghei*-infected hepatoma cells and *P. yoelii*-infected mouse hepatocytes revealed that *Plasmodium* modulates the host cell's transcriptome towards biosynthetic pathways and identified 63 transport proteins or regulatory subunits whose expression is altered in infected cells [11].

We employed RNA interference (RNAi) to down-modulate the expression of a selected group of genes, in order to identify host cell membrane transporters that play a role during *Plasmodium* infection of hepatic cells. This approach led to the identification of glucose transporter 1 (GLUT1) and cationic amino acid transporter

2 (CAT2) as major players in this process and warranted further investigation of the host-parasite interaction in which they are involved.

GLUT1 is one of the 14 members of the family of integral membrane glucose transporter (GLUT) molecules. It is expressed in liver cells and is overexpressed in various tumors [12, 13]. Glucose is transported by GLUT1 from the plasma into the cytosol of *Plasmodium*-infected erythrocytes, and is then taken up by the parasite via a parasite-encoded facilitative hexose transporter (HT) [14-16]. This transporter is also expressed during the liver and transmission phases of *Plasmodium* parasites, suggesting that glucose might be essential also for these stages [8, 17]. In this study, we employed rodent *P. berghei* parasites, a well-established model of malaria infection, to investigate the uptake and utilization of glucose by *Plasmodium* liver stages. We established the importance of glucose availability for the intra-hepatic development of the malaria parasite. We observed that glucose uptake increases specifically in infected cells from 30 hours post-infection onwards and identified GLUT1 as the major host transporter involved in glucose uptake by those cells. The importance of this molecule during hepatic infection was further validated by employing a specific GLUT1 inhibitor, both *in vitro* and *in vivo*. Finally, we demonstrated that *P. berghei* infection leads to a small depletion of intracellular ATP and enhances the translocation of GLUT1 to the cell membrane of infected hepatoma cells in a phosphoinositide 3-kinase (PI3K)-independent manner, contributing to the significantly higher uptake of glucose by infected cells, when compared with their non-infected counterparts. This increase in glucose uptake was not observed when hepatic cells were subjected to a variety of other stimuli, including temperature and oxidative stress, and viral infection, suggesting that it constitutes a specific response to *Plasmodium* infection. Overall, these data suggest that the extensive replication of intra-hepatic *Plasmodium* parasites leads to a decrease of intracellular glucose availability, consequently decreasing the host cells' ATP levels. GLUT1 translocation to the plasma membrane of *Plasmodium*-infected cells compensates for this decrease by enhancing glucose uptake and preventing further ATP depletion that could lead to cell death.

CAT2, encoded by SLC7A2, is part of the CAT family of Na^+-independent y^+ transporters, which constitute the main mechanism of cellular uptake of cationic amino acids, such as arginine, lysine and ornithine [18-20]. Arginine is involved in

many metabolic pathways, including the synthesis of nitric oxide (NO), polyamines, agmatine, creatine, proline, glutamate, and urea [21]. Arginine and the arginase pathway have been implicated in several infections, including *Trypanosoma spp.*, *Leishmania spp.*, *Toxoplasma gondii*, *Shistosoma mansoni*, *Candida albicans*, and *Helicobacter pylori* (reviewed in [22]). *Plasmodium* parasites were also shown to express arginase, the first enzyme of the metabolism of arginine into polyamines, and to be dependent on polyamines for survival in the blood stage of infection [23-28]. Our results showed that the normal developmental process of liver stage *P. berghei* parasites is also dependent on arginine availability and that this arginine is acquired by the infected host cell mostly via the CAT2A and CAT2B transporters, the two splice variants encoded by the *SLC7A2* gene [29]. We also showed that the arginine taken up by the infected cell is mainly employed as a precursor of polyamine synthesis, to promote parasite growth. Because the inhibition of polyamine production by the host cell alone has no impact on *P. berghei* development in Huh7 cells, we hypothesize that the parasite relies mostly on its own polyamine synthesis pathway to fulfill its developmental needs. The bimodal hepatic infectivity behavior displayed by the arginase-KO *P. berghei* parasite partially supports this hypothesis but also suggests that the parasite may have compensatory mechanisms to guarantee its survival when this pathway is compromised.

Finally, we investigated whether *Plasmodium* infection could be impaired by appropriate amino acid supplementation. Lysine, ornithine and valine have been described as arginase inhibitors and could therefore be employed to inhibit polyamine synthesis [30, 31]. Under these conditions, increasing the amount of arginine available might in turn enhance the production of NO, which was previously shown to kill malaria parasites *in vitro* [32-39]. For these reasons, we investigated the effect of these 4 amino acids, individually and in combination, on liver stage *Plasmodium* infection. Our data showed that *P. berghei* hepatic infection can be markedly inhibited *in vitro* and *ex vivo* through supplementation with lysine and valine, either alone or in combination. Importantly, we further showed that the simultaneous administration of lysine, valine and arginine in the drinking water of mouse models of *P. berghei* infection resulted in a striking decrease of *in vivo* liver parasite load. We showed that this decrease results from an impairment of parasite growth, as well as a significant reduction in the number

of *P. berghei*-infected hepatocytes, suggesting that this combination of amino acids effectively inhibits parasite growth and contributes to its elimination. Our data strongly suggest that the lysine and valine employed in the supplementation lead to arginase inhibition and consequent impairment of the synthesis of polyamines, which are important for parasite development. Concurrently, the extra arginine provided in the supplementation stimulates NO production by inducible NO synthase (iNOS), leading to parasite death.

Overall, this dissertation highlights the relevance of glucose and arginine uptake and metabolism for parasite survival and intra-hepatic development in *Plasmodium*-infected cells. This work elucidates hitherto unknown host-parasite interactions and identifies a novel, drugless and non-toxic approach to modulate liver-stage of *Plasmodium* infection.

Resumo

A malária é uma doença febril aguda e uma das doenças infecciosas mais prevalentes no mundo. É causada por parasitas protozoários do género *Plasmodium*, os quais são transmitidos aos seus hospedeiros mamíferos através da picada de um mosquito *Anopheles* fêmea infetado [1, 2]. Estima-se que em 2015 ocorreram 214 milhões de casos de malária, dos quais resultaram 438 000 mortes, a maioria das quais na África sub-Sahariana [1]. Globalmente estima-se que 3.2 biliões de pessoas corram o risco de serem infetadas pelo *Plasmodium* e desenvolverem a doença [1].

Aquando de uma picada por um mosquito infectado, os parasitas *Plasmodium*, denominados esporozoítos nesta fase do seu ciclo de vida, são depositados na pele do seu hospedeiro mamífero, e são transportados pela circulação sanguínea até ao fígado, onde atravessam diversos hepatócitos até invadirem produtivamente uma célula final [3]. Dentro dos hepatócitos, cada esporozoíto transforma-se numa forma exo-eritrocitária (EEF) contendo milhares de merozoítos recém-formados, que acabam por ser libertados para a corrente sanguínea, onde invadem os eritrócitos, dando início à fase eritrocitária, sintomática, da doença [4].

Durante a fase hepática, assintomática, da infecção por *Plasmodium*, o parasita cresce de forma extremamente rápida, replicando o seu genoma 10^4 a 10^5 vezes [5, 6]. Para sustentar a sua rápida multiplicação e alimentar as suas vias metabólicas, os parasitas obtêm nutrientes a partir do seu hepatócito hospedeiro [7-10]. Foi anteriormente mostrado que a glucose desempenha um papel crucial durante a fase hepática de *P. berghei*, tendo sido demonstrada a importância do transporte deste nutriente pelo transportador de hexoses (HT) membranar do parasita para a replicação deste dentro das células hepáticas [8]. Por outro lado, estudos de transcriptómica de células de hepatoma infetadas por *P. berghei* e de fígados de ratinho infetados por *P. yoelii* mostraram que o parasita modula o transcriptoma da célula hospedeira no sentido de favorecer vias biossintéticas, e permitiu identificar 63 proteínas transportadoras cuja expressão está alterada em células infetadas [11].

Neste trabalho, utilizámos técnicas de RNA de interferência (RNAi) para diminuir a expressão de um grupo de genes selecionados, de modo a identificar

transportadores membranares das células hospedeiras envolvidos na infecção hepática por *Plasmodium*. Esta abordagem conduziu à identificação do importante papel do transportador de glucose 1 (GLUT1) e do transportador de aminoácidos catiónicos 2 (CAT2) neste processo, abrindo caminho para uma investigação mais aprofundada das interações hospedeiro-parasita em que estão envolvidos.

O GLUT1 é um de 14 membros da família de moléculas membranares transportadoras de glucose (GLUT), sendo expresso em células hepáticas e sobre-expresso em diversos tumores [12, 13]. A glucose é transportada pelo GLUT1 do plasma para o citosol dos eritrócitos infetados por *Plasmodium*, sendo depois transportado para o parasita através de um transportador de hexoses parasitário (HT) [14-16]. Este transportador também é expresso durante as fases hepáticas e de transmissão de parasitas *Plasmodium*, sugerindo que a glucose poderá também ser essencial nestas fases [8, 17]. No presente estudo, utilizámos parasitas *P. berghei* de roedores, um modelo bem estabelecido de infeção de malária, para investigar a aquisição e utilização da glucose por parasitas *Plasmodium* hepáticos. Demonstrámos a importância da disponibilidade de glucose para o desenvolvimento intra-hepático do parasita da malária. Observámos que durante o desenvolvimento hepático de *P. berghei*, a aquisição de glucose aumenta especificamente em células infetadas a partir de 30 horas de infeção, e identificámos o GLUT1 como sendo o principal transportador responsável pela entrada de glucose nessas células. A importância desta molécula durante a infeção hepática foi adicionalmente validada através da utilização de um inibidor específico de GLUT1, quer *in vitro*, quer *in vivo*. Finalmente, demonstrámos que a infeção por *P. berghei* leva a uma pequena depleção do ATP intracelular e conduz à translocação de GLUT1 para a membrana celular de células de hepatoma infetadas, num processo independente da cinase PI3K. Isto contribui para que o aumento da aquisição de glucose seja significativamente maior nas células infetadas do que nas não-infetadas. Este aumento de aquisição de glucose não foi observado quando as células hepáticas foram sujeitas a diversos outros estímulos, incluindo *stress* de temperatura, *stress* oxidativo, e infeção viral, sugerindo que se trata de uma resposta específica à infeção por *Plasmodium*. Globalmente, estes dados sugerem que a enorme taxa de replicação dos parasitas *Plasmodium* intra-hepáticos conduz a uma diminuição da disponibilidade de glucose intracelular, o que leva ao decréscimo dos níveis de

ATP da célula hospedeira. A translocação do GLUT1 para a membrana celular compensa esta diminuição, aumentando a aquisição de glucose e impedindo uma maior depleção de ATP, que poderia conduzir à morte celular.

O CAT2, codificado pelo gene *SLC7A2*, faz parte da família CAT de transportadores y^+ independentes de Na^+, que constituem o principal mecanismo de aquisição celular de aminoácidos catiónicos, tais como a arginina, a lisina e a ornitina [18-20]. A arginina está envolvida em diversas vias metabólicas, incluindo a síntese de óxido nítrico (NO), poliaminas, agmatina, creatina, prolina, glutamato e ureia [21]. A arginina e a via da arginase foram já implicadas em diversas infeções, incluindo *Trypanosoma spp.*, *Leishmania spp.*, *Toxoplasma gondii*, *Shistosoma mansoni*, *Candida albicans*, e *Helicobacter pylori* (revisto em [22]). No que diz respeito a parasitas *Plasmodium*, foi demonstrado que eles expressam arginase, a primeira enzima do metabolismo de arginina a poliaminas, e que dependem de poliaminas para a sua sobrevivência durante a fase sanguínea da infeção [23-28]. Os nossos resultados mostram que o processo de desenvolvimento normal de parasitas *P. berghei* hepáticos também depende da disponibilidade de arginina, a qual é adquirida pela célula hospedeira principalmente através de transportadores CAT2A e CAT2B, as duas variantes codificadas pelo gene *SLC7A2* [29]. Também demonstrámos que a arginina adquirida pela célula infectada é utilizada principalmente como precursor da síntese de poliaminas, para permitir o crescimento do parasita. O facto de a inibição da produção de poliaminas apenas pela célula hospedeira não ter qualquer impacto no desenvolvimento de *P. berghei* em células Huh7, sugere a hipótese de que o parasita depende principalmente da sua própria via de síntese de poliaminas para preencher as suas necessidades de desenvolvimento. O comportamento bimodal de infectividade hepática apresentado pelo parasita *P. berghei* arginase-KO sustenta em parte esta hipótese mas também sugere que o parasita poderá dispor de mecanismos compensatórios para assegurar a sua sobrevivência quando essa via está comprometida.

Finalmente, investigámos se a infeção por *Plasmodium* poderia ser inibida através de uma suplementação adequada com aminoácidos. A lisina, a ornitina e a valina foram identificadas como inibidores da arginase, podendo pois ser utilizadas para inibir a síntese de poliaminas [30, 31]. Nessas condições, um aumento na quantidade de arginina disponível poderia por sua vez aumentar a produção de

NO, o qual se demonstrou previamente ser capaz de matar parasitas da malária *in vitro* [32-39]. Por estas razões, investigámos o efeito destes 4 aminoácidos, individualmente e em combinação, na infeção hepática por *Plasmodium*. Os nossos resultados mostraram que a infeção hepática por *P. berghei* pode ser fortemente inibida *in vitro* e *ex vivo* pela suplementação com lisina e valina, quer individualmente, quer em combinação. Crucialmente, mostrámos ainda que a administração simultânea de lisina, valina e arginina na água de modelos roedores de infeção por *P. berghei* conduziu a um enorme decréscimo da carga parasitária hepática *in vivo*. Mostrámos que este decréscimo resulta de uma inibição do crescimento do parasita, a par de uma significativa diminuição do número de hepatócitos infetados por *P. berghei*, sugerindo que esta combinação de aminoácidos inibe eficazmente o desenvolvimento do parasita e contribui para a sua eliminação. Os nossos dados sugerem fortemente que a lisina e a valina empregues na suplementação conduzem à inibição da arginase e à consequente inibição da síntese de poliaminas necessárias ao desenvolvimento do parasita. Concomitantemente, a arginina fornecida na suplementação estimula a produção de NO pela enzima iNOS, conduzindo à morte do parasita.

Globalmente, esta dissertação demostra a relevância da aquisição e metabolismo da glucose e arginina para a sobrevivência e o desenvolvimento intra-hepático do parasita em células infetadas por *Plasmodium*. Este trabalho elucida novas interacções hospedeiro-parasita e identifica uma nova abordagem para modular a infeção hepática por *Plasmodium* sem recorrer ao uso de fármacos e sem toxicidade associada.

Acknowledgements

I am truly thankful to my supervisor, Miguel Prudêncio, for accepting me as his first PhD student and for being the best supervisor I could have asked for. Thank you for trusting me and letting me do things my way, have my own ideas and solve my own problems, but also for knowing how to say “No” whenever I had crazy ideas. Thank you for always pushing me to work harder and become better, being it in the bench or for a presentation. Thank you for always worrying about me and for supporting me every time I felt disheartened. You are an amazing person and I am very happy that I had the chance to meet you. I am very proud to be your student.

I want to thank Cláudia Cunha for helping me give my first steps in the malaria field and for teaching me everything I needed to start working by myself. You were a wonderful colleague and I really miss having you in the lab.

I also want to thank António Mendes for all his ideas and for his contagious enthusiasm. You are a brilliant scientist and a spectacular person. Absolutely marvelous! I am very happy that I had the chance to meet and work with you.

I am very thankful to the current members of the lab, Marta Machado, Filipa Teixeira, Carolina Andrade, Margarida Vaz, Raquel Azevedo and João Sinfrónio, but also to the previous members, Jorge Santos, Marija Markovic, Joana Pissarra and Miguel Duarte, for being absolutely amazing! Thank you for your friendship, your incredible energy and for all the unforgettable moments we lived together. I feel very lucky to have met each and every one of you!

I want to thank everyone in Mota Lab, both current and past members, for their companionship and for all their scientific input. My special thanks to Joana Dias, Aparajita Lahree, Fernanda Baptista, Sofia Marques, Daniel Carapau, Margarida Ruivo, Liliana Mâncio, Peter Liehl, Patrícia Inácio, Lénia Rodrigues, Vanessa Luís and Ângelo Chora.

I also want to thank everyone in Figueiredo Lab for being wonderful lab colleagues. Since we started sharing the lab with you, our days have been energetic and fun. You are all truly wonderful people!

A huge thank you to all my PhD colleagues, especially Rosangela Frita, Diogo Fonseca-Pereira, Rita Aroeira, André Santos, Inês Perpétuo, Vânia Batalha, Catarina Pato, Rita Domingues, Cristina Silva and Mariana Oliveira for their friendship.

Also at iMM, many thanks go to everyone from the Bioimaging, Cytometry and Rodent Facilities, namely, António Temudo, Ana Nascimento, José Rino, Ana Vieira, Ana Isabel Pinto, Iolanda Moreira, Carlos Silva, Olena Pinho, and also to Dinora Levy for all the help and joyful conversations.

A very special thanks to my three musketeers, Sara Pais, Ana Parreira and Inês Albuquerque, with whom I shared so many good experiences and memories. Thank you for your friendship and for always being there whenever I needed the most.

A huge thanks to Neuza Duarte, Ricardo Serra, Cristiana Robalo e João Inácio for being such extraordinary friends. Thank you for always being there for me. Your energy is absolutely contagious! I really cherish all the time we spend together.

I also want to thank my precious High School friends, Tânia Cristina, Tânia João, Ana Jacinta and Paula, who I have known for almost half of my life now. Thank you for always being there for me! I always feel home when I am with you, girls!

I cannot thank my parents enough for all they have done for me and for all their love. I am who I am because of both of you. An enormous thank you to my sister, Sandra, for listening to me whenever I needed to get something off my chest and with whom I share so many similarities. Finally, I want to thank my little brother Filipe and the closest members of my family for all their love and support.

Last but not least, I want to thank my dear João, who has been by my side for a long time now and has been tirelessly supporting me in these last months of my PhD. Thank you for continuously making me happy and for all the good memories were already share. You always turn a bad day into a good day. I feel very lucky to have such a wonderful person by my side.

These last five years, I grew a lot both as a researcher and as a person, and it is mostly because of all the amazing people I had the chance to meet both at iMM and outside it. Thank you everyone!

Table of Contents

Figure and Table Index

I) General Introduction

II) GLUT1-mediated glucose uptake during Plasmodium hepatic infection

III) The role of L-arginine uptake and polyamine production during liver stage infection by the malaria parasite

IV) Inhibition of *Plasmodium* liver infection by amino acid supplementation and modulation of arginine metabolism

Abbreviations

2-NBDG	2-[N-(7-nitrobenz-2-oxa-1,3-diazol-4-yl)amino]-2-deoxy-D-glucose
A. atroparvus	*Anopheles atroparvus*
A. maculipennis	*Anopheles maculipennis*
A. maculipennis atroparvus	*Anopheles maculipennis atroparvus*
A. stephensi	*Anopheles stephensi*
AAAP	amino acid/auxin permease
Acetyl-CoA	acetyl coenzyme A
ACTs	artemisinin-based combination therapies
AD	*anno domini*
AdoMet	S-adenosylmethionine
AdoMetDC	S-adenosylmethionine decarboxylase
AMP	adenosine monophosphate
AMPK	AMP-activated protein kinase
AMPK-dKO	AMPK double knockout
AQ+SP	amodiaquine plus sulfadoxine-pyrimethamine
Arg	L-arginine
ART	artemisinin
ATP	adenosine triphosphate
BC	before Christ
BCAA	branched-chain amino acid
Bcl-2	B-cell lymphoma 2
BSA	bovine serum albumin
CAT	cationic amino acid transporter
CD81	cluster of differentiation 81
cDNA	complementary DNA
CelTOS	cell traversal protein for ookinetes and sporozoites
CFP	cyan fluorescent protein
$CoCl_2$	cobalt (II) chloride
CQ	chloroquine
CSP	circumsporozoite protein
CT	cycle threshold
DDT	dichlorodiphenyltrichloroethane
DFMO	α-difluoromethylornithine

DHA	dihydroartemisinin
DNA	deoxyribonucleic acid
DV	digestive vacuole
EDTA	ethylenediaminetetraacetic acid
EEF	exoerythrocytic form
EMA	European Medicines Agency
ER	endoplasmic reticulum
ETRAMP	early transcribed membrane protein
EXP1	exported protein 1
F6P	fructose-6-phosphate
FACS	fluorescence-activated cell sorting
FAS-II	type II fatty acid synthesis pathway
FBS	fetal bovine serum
FDA	Food and Drug Administration
FELASA	Federation of European Laboratory Animal Science Associations
FGF15/19	gastrointestinal-secreted fibroblast growth factor 15/19
FP2ase	fructose-1,6-bisphosphatase
FRET	fluorescence resonance energy transfer
G3P	glyceraldehyde-3-phosphate
G6P	glucose 6-phosphate
G6Pase	glucose-6-phosphatase
G6PD	glucose-6-phosphate dehydrogenase
GA-I	glutaric aciduria type I
GAMT	guanidinoacetate methyltransferase
GCK	glucokinase
GFP	green fluorescent protein
GLUT	glucose transporter
GPI	glycophosphatidylinositol
HCU	homocystinuria
HCV	hepatitis C virus
HEK	human embryonic kidney
HEPES	4-(2-hydroxyethyl)-1-piperazineethanesulfonic acid
HGF	hepatocyte growth factor
HHH	hyperammonaemia-hyperornithinaemia-homocitrullinuria

HIF-1α	hypoxia inducer factor-1α
Hnf4α	hepatocyte nuclear factor 4 alpha
hpi	hours post-infection
HPRT	hypoxanthine-guanine phosphoribosyltransferase
HRP-2	histidine-rich protein-2
hsHSPGs	highly sulfated-heparan sulfate proteoglycans
HSP70	Heat Shock Protein 70
HT	hexose transporter
iNOS	inducible nitric oxide synthase
i.p.	intraperitoneal injection
i.v.	intravenous injection
IPTi	intermittent preventive treatment for infants
IPTp	intermittent preventive treatment in pregnancy
IRS	indoor residual spraying
ITNs	insecticide-treated mosquito nets
IVC	inferior vena cava
KO	knockout
LDM	liver digestion medium
L-FABP	liver fatty acid binding protein
LLNs	long-lasting nets
L-NAME	N_{ω}-Nitro-L-arginine methyl ester
LPI	lysinuric protein intolerance
L-PK	liver pyruvate kinase
LPM	liver perfusion medium
LPS	lipopolysaccharide
L-SDMA	N^{G},N^{G}-dimethyl-L-arginine
LSECs	liver sinusoidal endothelial cells
Lys	L-lysine
MEFs	mouse embryonic fibroblasts
MHV68	murine gammaherpesvirus 68
MMA	methylmalonic acidemia
MOI	multiplicity of infection
MPAC	Malaria Policy Advisory Committee
mRNA	messenger ribonucleic acid
MSUD	maple syrup urine disease
NADPH	nicotinamide adenine dinucleotide phosphate
NFLD	non-alcoholic fatty liver disease

NO	nitric oxide
Nor-NOHA	N^{ω}-hydroxy-nor-arginine
NOS	nitric oxide synthase
OAT	ornithine aminotransferase
ODC	ornithine decarboxylase
Orn	L-ornithine
P. cynomolgi	*Plasmodium cynomolgi*
P. falciparum	*Plasmodium falciparum*
P. gallinaceum	*Plasmodium gallinaceum*
P. knowlesi	*Plasmodium knowlesi*
P. malariae	*Plasmodium malariae*
P. ovale	*Plasmodium ovale*
P. relictum	*Plasmodium relictum*
P. vivax	*Plasmodium vivax*
PA	propionic acidemia
PALM	*Plasmodium*-specific Apicoplast protein important for Liver Merozoite formation
PbHT	*P. berghei* hexose transporter
PBS	phosphate-buffered saline
PCR	polymerase chain reaction
PDKs	pyruvate dehydrogenase kinases
PEPCK	phosphoenolpyruvate carboxylase
PFA	paraformaldehyde
PfCRT	*P. falciparum* chloroquine resistance transporter
PfEMP1	*P. falciparum* erythrocyte membrane protein 1
PfHT	*P. falciparum* hexose transporter
PFK	6-phosphofructo-1 kinase
PFK-2/FBP-2	6-phosphofructo-2-kinase/fructose-2,6-bisphosphatase
PFU	plaque-forming units
$PI(3,5)P_2$	phosphatidylinositol 3,5-bisphosphate
PI3K	phosphoinositide 3-kinase
PKC	protein kinase C
PL	phospholipase
pLDH	*Plasmodium* lactate dehydrogenase
PLP1	perforin-like protein 1
PPP	Pentose Phosphate Pathway

PQ	primaquine
PV	parasitophorous vacuole
PVM	parasitophorous vacuole membrane
qPCR	quantitative PCR
RBCs	red blood cells
RDT	rapid diagnostic test
RFP	red fluorescent protein
RNA	ribonucleic acid
RNAi	RNA interference
ROM1	rhomboid 1
SAGE	Strategic Advisory Group of Experts on Immunization
SD	standard deviation
SEM	standard error of the mean
SERA	serine repeat antigen
shRNA	short hairpin RNA
SLC	solute carrier
SMC	seasonal malaria chemoprevention
SP	sulfadoxine-pyrimethamine
SPECT	sporozoite microneme protein essential for cell traversal
SpdS	spermidine synthase
SpmS	spermine synthase
SR-BI	scavenger receptor BI
TCA	tricarboxylic acid
TPA	12-O-tetradecanoyl-phorbol-13-acetate
TRAP	thrombospondin-related anonymous protein
TSR	thrombospondin repeat
TVN	tubovesicular network
UDP	uridine diphosphate
UIS3	upregulated in infectious sporozoites 3
UIS4	upregulated in infectious sporozoites 4
Val	L-valine
WHO	World Health Organization
Wnt	Wingless-related integration site
WT	wild type
YFP	yellow fluorescent protein

General Introduction

Malaria – general considerations

Malaria is an acute febrile illness and one of the most prevalent infectious diseases in the world [1, 2]. It is caused by a protozoan parasite of the genus *Plasmodium* that is transmitted through the bite of an infected female *Anopheles* mosquito [1, 2]. There are five species of *Plasmodium* that can cause malaria in humans [1, 40, 41]. Four of these (*Plasmodium falciparum*, *P. vivax*, *P. malariae* and *P. ovale*) are human malaria species, which are spread from one person to another by the bite of an infected mosquito [1, 2, 40]. Additionally, in recent years, human cases of malaria have also been recorded due to *P. knowlesi*, a species that causes malaria among monkeys, and occurs in certain forested areas of South-East Asia [1, 42, 43].

P. falciparum and *P. vivax* malaria pose the greatest public health challenge [1, 2, 40, 41]. *P. falciparum* is most prevalent in Africa but also occurs in South and East Asia, South America, the Caribbean and the Middle East, and is responsible for most deaths from malaria [1, 40, 42, 44]. *P. vivax* has a wider geographic distribution because it can develop in the *Anopheles* mosquito vector at lower temperatures and survive at higher altitudes and in cooler climates [1, 40, 42, 44, 45]. Additionally, it can generate cryptic forms, known as hypnozoites, which can remain dormant for long periods of time as potential reservoirs of infection, leading to disease relapses after the initial symptomatic infection has been treated [1, 40, 44]. Although *P. vivax* can occur throughout Africa, the risk of infection with this species in this continent is lower, because of the absence of the Duffy gene in many African populations, which codes for a protein necessary for red blood cell invasion by *P. vivax* [1, 46]. Recently, however, several reports have surfaced, describing *P. vivax* mono and mixed malaria parasite infections in Duffy-negative individuals from several countries, such as Brazil, Angola, Equatorial Guinea, Mauritania, Cameroon and Ethiopia [46-50]. *P. ovale* and *P. malariae* are two rare, nonlethal parasites, most commonly found in Africa and Papua New Guinea [42, 45].

In a non-immune individual, malaria symptoms include fever, headache, chills, sweating, fatigue and vomiting, and appear seven days or more after the infective mosquito bite [2, 51, 52]. If not treated within 24 hours, *P. falciparum* malaria can progress to severe illness, defined as a malaria episode with signs and symptoms

of organ dysfunction or high levels of parasitaemia, which often leads to death [2, 40, 52]. Children with severe malaria frequently develop severe anaemia, respiratory distress, metabolic acidosis and/or cerebral malaria [2, 51]. In pregnant women, malaria increases the risk of maternal death, miscarriage, stillbirth, and low birth weight, as well as the associated risk of neonatal death [2]. In endemic countries, partial immunity develops over years of exposure [2, 52]. Although this does not provide complete protection, it does reduce the risk of developing severe disease [2, 52].

The History of Malaria

From Superstition to Disease

Possible references to malaria may be traced back to antiquity considering its clinical signatures, specifically, recurrent periodic fevers and splenomegaly [53, 54]. The most ancient records were found in a Chinese document from about 2700 BC, clay tablets from Mesopotamia from 2000 BC, Egyptian papyri from 1570 BC and Hindu texts as far back as 6 BC [53-55]. Numerous other ancient Chinese documents provided valuable information about how the infection was transmitted [53]. Indeed, two documents dating back as far as the period 476 to 221 BC mentioned that malaria was caused by mosquito bites, especially during the late summer and early autumn [53]. Nonetheless, in ancient times malarial manifestations were usually attributed to supernatural influences, namely to the anger of a deity or to the devils that governed the destiny of men and nature; their curses could be inactivated through specific rites, sacrifices, exorcisms or magic potions [53, 54].

The early Greeks, including Homer in about 850 BC, Empedocles of Agrigentum in about 550 BC, and Hippocrates in about 400 BC, were well aware of the characteristic poor health, fevers and enlarged spleens seen in people living in marshy places [55, 56]. In fact, Hippocrates was the first physician who described the malarial paroxysm (chills, fever, sweats and exacerbation) and the different clinical types of malaria depending on the periodicity of the fevers (tertian and quartan fever, depending on whether the person has fever every 3 or 4 days, respectively) [53, 54, 56].

Throughout history, several designations were used to describe malaria: ägue, paludisme, Wechselfieber, Dardag Kolle, triasuchka, likhoradka, the fever, febris ardens, accessia, paludal fever, fièvе äigue, marsh fever, seasonal fevers, fever of summer/fall (estivoautumnal fever), autumnal fever, intermittent fever, periodical fever, the quakes, the Bailiff of the Marshes, Lord John's fever and Old Johnny Axey [53, 56]. The word *malaria* used nowadays derives from the Italian words *mal'aria* meaning bad air, evil air or corrupted air, since for hundreds of years the supposition of the miasmatic nature of the illness was widely spread [53-56]. The first attested mention of the term *mal aere* dates from 1440 [53]. Malaria, the finally settled word for the disease, was used for the first time in the first half of the nineteenth century [53]. The overlapping clinical features between malaria and typhoid fever created difficulties in the diagnosis of malaria by clinicians, hence the usage of the term typhomalaria was widespread for several decades [56]. This term was mostly abandoned when William Osler described the specific differences in the clinical features of each disease, and established the susceptibility of the malaria parasite to quinine as a simple clinical test for malaria [56, 57].

Discovery of *Plasmodium* parasites – the Erythrocytic Stage

With the discovery of bacteria by Antonie van Leeuwenhoek in 1676, the incrimination of microorganisms as causes of infectious diseases and the development of the germ theory of infection by Louis Pasteur and Robert Koch in 1878-1879, the search for the causative agent of malaria deepened [55]. At first, it was thought that malaria was caused by a bacterium present in marshy waters, *Bacillus malariae*, but this theory was proven wrong by Alphonse Laveran, a French military surgeon, in 1880 [53-55]. Starting from the known fact that the spleens of malaria patients contained a dark pigment, Laveran began to look for pigment in the fresh unstained blood of 200 patients and observed it first in leucocytes and then in red blood cells, exclusively in patients with malaria [55, 57]. He observed several different forms of erythrocytic organisms including crescents, spherical motionless bodies with pigment, spherical moving bodies with pigment and bodies that extruded flagella-like structures, all of which he thought were on the outside of the red blood cells (Fig. 1.1) [55, 57]. He also suggested a course of events that began with clear spots that grew, acquired pigment and filled the cell,

which then burst, coinciding with the fevers associated with malaria [55]. Laveran quickly realized that he had found a parasitic protozoan which he called *Oscillaria malariae* [55]. He presented his findings to the French Academy of Medical Sciences and, after overcoming the skepticism of all microbiologists, zoologists and malariologists of his time, he was awarded the Nobel Prize for Medicine in 1907 [55, 58].

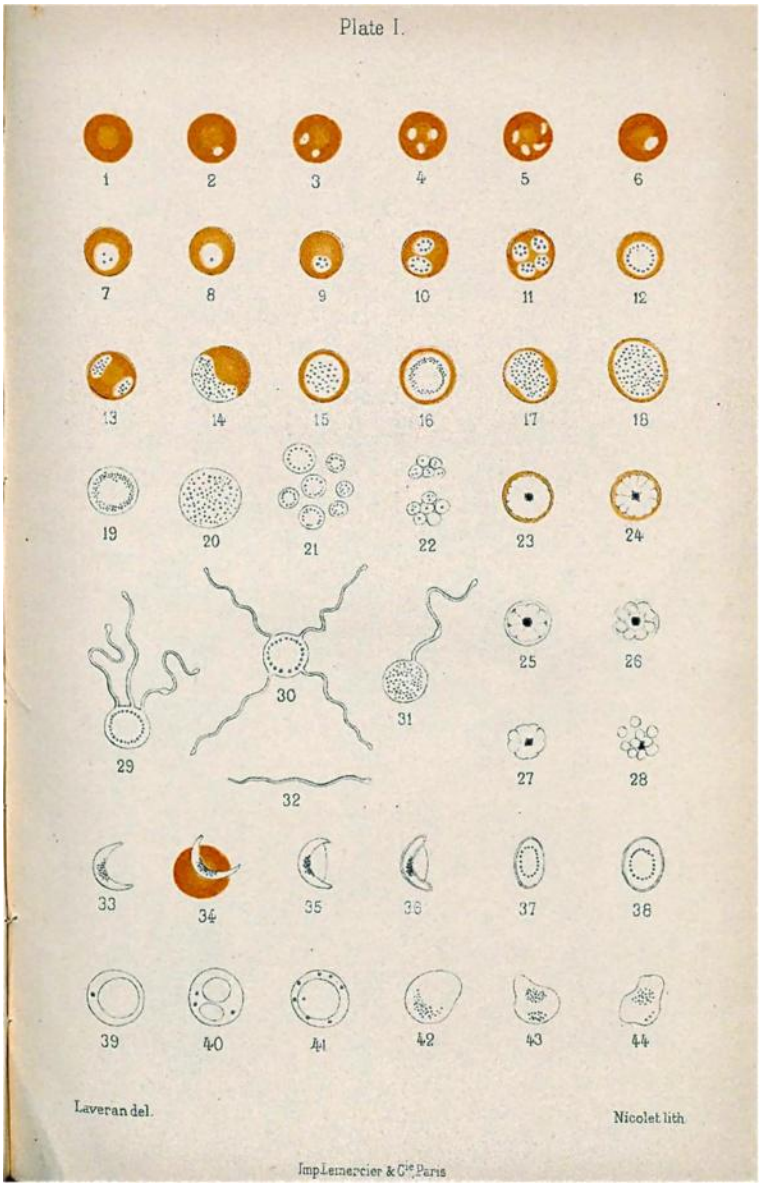

Figure 1.1 - Laveran's drawings of malaria parasites. From [57].

At around the same time, the Russian physiologist Vassily Danilewsky observed a number of parasites, including trypanosomes and others, that he identified as "pseudovacuoles", later confirmed as unstained malaria parasites, while examining

the blood of birds and reptiles in the Ukraine [55]. In fact, by 1885 Danilewsky had recognised the three most common genera of intraerythrocytic blood parasites of birds (*Plasmodium*, *Haemoproteus* and *Leucocytozoon*) [55]. However, as he had published much of his work in Russian, only in 1889 did this information become widely available in French [55]. The accidental discovery of a methylene blue-eosin stain by Dimitri Leonidovitch Romanowsky in 1891 greatly facilitated the search for other malaria parasites in reptiles, birds and mammals [55, 59]. This stain became popular at the beginning of the twentieth century and nowadays remains the basis of blood stains, such as Leishman's, Giemsa's and Wright's [55].

By 1890, with the contributions of Marchiafava, Bignami and Golgi, it was well established that malaria was caused by a protozoan parasite that invaded and multiplied in red blood cells, that there were three species with specific periodicities responsible for benign tertian (*Haemamoeba vivax*), malignant tertian (*Laverania malariae*) and quartan malaria (*Haemamoeba malariae*), currently known as *P. vivax*, *P. falciparum* and *P. malariae*, respectively, and that the paroxysms of fever coincided with the rupture and release of merozoites into the bloodstream [54, 55, 57]. *P. ovale*, a fourth species that resembled *P. vivax,* was only described in 1922 by John Stephens while working in West Africa [55].

The Mosquito Stage

Throughout centuries, circumstantial evidence accumulated suggesting that mosquitoes could be the explanation for how the parasite spread from one human to another [55]. By 1883, the American physician Albert King had assembled 19 facts in support of this theory [57].

The first person to provide definitive proof that mosquitoes carried malaria was Ronald Ross while working in India in 1897 [54, 55, 57, 60]. Under the tutelage of his mentor, Patrick Manson, he discovered that culicine mosquitoes transmitted the avian malaria parasite *Plasmodium relictum* [55, 60]. He found that after feeding on infected birds, the mosquitoes developed pigmented bodies in their guts, which he called "spores", leading him to conclude that the mosquitoes would take up male and female gametocytes from the infected bird, very similarly to what had been described by William MacCallum for the haematozoan *Haemoproteus*

columbae [55, 60]. These gametocytes would undergo fertilization in the mosquito gut, developing into spores, within which rod-like structures were produced that invaded the mosquito's salivary glands and were injected into a new host when the infected mosquito fed [55, 60]. Later, when working in Sierra Leone in 1899, he observed that mosquitoes fed on a malaria patient also contained spores in their guts, proving that the human malaria parasites were transmitted by anopheline mosquitoes [53, 55, 61]. Ross was awarded the Nobel Prize for Physiology and Medicine in 1902 [53, 58].

Bignami and Grassi had reached the same conclusions one year earlier in sites near Rome and in Sicily, where malaria was present; they fed local *Anopheles claviger* mosquitoes on infected patients and subsequently transmitted the infection to uninfected individuals through the bite of the same mosquitoes [54, 55, 57, 62]. These observations were confirmed by Manson in London by using *P. vivax*-infected *A. maculipennis* mosquitoes to infect two healthy volunteers, one of them his own son [55, 57]. Over the next two years Bignami, Grassi and Bastianelli proved that only female *Anopheles* mosquitoes could transmit malaria and described the whole blood-mosquito life cycles of *P. vivax*, *P. falciparum* and *P. malariae* [53-55, 62]. The discovery of the role of mosquitoes in the transmission of malaria was essential because it raised the possibility of controlling the disease by reducing contact with infected mosquitoes, a malaria control strategy that is still used presently [55].

Plasmodium's Elusive Exoerythrocytic Stage

At this point in time, although the blood and mosquito stages were mostly understood, nobody knew where the parasites developed in the first days after infection, during which they could not be seen in the blood [55]. Grassi and his colleagues, in the late 1890's, were the first ones to postulate that another developmental stage should exist in cells other than red blood cells, possibly white blood cells [55]. Their theory was quickly abandoned due to what is nowadays known as "Schaudinn's fallacy" [55]. In 1903, the German scientist Fritz Schaudinn described the direct penetration of red blood cells by *P. vivax* sporozoites, without further development [55, 57]. Even though, in 1898, MacCallum had observed developmental stages of *P. relictum* in the liver and spleen of infected birds and no

one else was able to reproduce Schaudinn's results, his ideas dominated the scientific opinion for over 40 years [55, 57].

It was only in 1937 that Sydney James and Parr Tate conclusively demonstrated that in sporozoite-induced *P. gallinaceum* infections in chickens, a phase of multiplication in cells of the reticuloendothelial system preceded the appearance of parasites in the blood [55, 63]. One decade later, Henry Shortt and Cyril Garnham, working in London, finally confirmed that in primates this exoerythrocytic phase occurs in the liver [55, 57, 64]. Their clue came from the monkey parasites *Hepatocystis kochi*; while being related to malaria parasites, they do not have an erythrocytic stage in their life cycles, only an exoerythrocytic stage in the parenchyma cells of the liver [55, 65]. Shortt and Garnham found exoerythrocytic stages in the livers of rhesus monkeys seven days after the bites of five hundred *A. maculipennis atroparvus* mosquitoes infected with *P. cynomolgi* [55, 66]. In subsequent years, they found exoerythrocytic forms of *P. vivax*, *P. falciparum* and *P. ovale* in human volunteers [55, 67-69]. The exoerythrocytic stages of *P. malariae* were only demonstrated experimentally in infected chimpanzees in 1960 by Robert Bray [55, 70]. It took nearly 70 years for the elucidation of the life cycle of the human malaria parasites to be almost complete [55]. The last piece of the puzzle, the dormant exoerythrocytic stages of *P. vivax*, called hypnozoites, was described by Wojciech Krotoski in 1982 [55, 71].

Malaria in Portugal

In Portugal, in the beginning of the 1900's, malaria was mostly endemic in the alluvial valleys of the main rivers with extensive rice cultivation, where the mosquito *A. atroparvus* had its breeding places [72]. Control programs in the Tagus river basin were initiated in 1931 and, seven years later, the Institute for Malaria Research and Training (Instituto de Malariologia) was established by the Rockefeller Foundation, under the direction of Francisco Cambournac [72]. Only in the 1950's were plans for eradication of the disease with dichlorodiphenyltrichloroethane (DDT) spraying put into motion [72, 73]. By 1958 transmission of the infection was interrupted in nearly all areas of Portugal and the country was placed in the maintenance phase of malaria eradication [72, 73]. The

certification of malaria eradication was confirmed by the World Health Organization (WHO) in 1973 [72, 73].

Nowadays, the only cases of malaria in Portugal are imported [74]. Approximately 40 to 50 cases are notified every year, mostly due to the increasing international travel and expatriation to sub-Saharan countries where malaria is endemic [74]. In fact, from 2009 to 2012, there was a 60% increase in malaria hospitalizations, contradicting the declining trend observed since 2003 in Europe [74]. This raises the possibility of reappearance of autochthonous malaria, which has already occurred in other European countries once officially considered malaria-free like France, Spain, Italy, and Greece [74]. Malaria might be spread by *A. atroparvus*, which is widely distributed in Portugal and might be susceptible to African *P*. *vivax* strains, despite being non-susceptible to the African *P*. *falciparum* strains [74].

Antimalarials with History

Over the centuries, several antimalarial compounds with different origins and efficacies have been used to treat malaria.

One of the most famous antimalarials is quinine. Quinine is the main alkaloid extracted from the powdered bark from the cinchona tree from South America [42, 54, 59]. The name of the tree resulted from the successful treatment of the countess of Chinchon, wife of the Spanish Vice-king of Peru, who was suffering from fever [54]. In 1633, an Augustinian monk called Calancha, from Lima, Peru, was the first to report that the powder of the cinchona plant “given as a drink cures fever and tertian” [54]. Cinchona was imported into Europe by the Jesuit Fathers to cure fever and, for almost two centuries, the bark of the cinchona tree was used in medicine as a powder [54]. Quinine was finally isolated in 1820 by Pelletier and Caventou [54]. Although its mode of action remains incompletely understood, it is thought to inhibit the formation of hemozoin in the digestive vacuole (DV) of blood stage *Plasmodium* parasites, a process indispensable for the disposal of the heme generated by the digestion of host’s hemoglobin [42, 75, 76]. The quinoline moiety of quinine, essential for the antimalarial properties of the compound, is present in the numerous analogues synthesized subsequently, including chloroquine (CQ) and primaquine (PQ) [42].

Chloroquine (CQ) is a quinoline analogue that was found during a collaborative program of research into antimalarial drugs during the Second World War [42, 54]. At the end of the war, however, it was discovered that the same compound had been synthesized and studied under the name of Resochin by the German researcher Johann “Hans” Andersag and his coworkers at the Bayer laboratories since 1934, but it had been rejected because it was considered too toxic for human use [54, 59, 77]. CQ can freely diffuse across membranes in its neutral form, allowing it to concentrate inside the acidic DV of *Plasmodium* parasites inside red blood cells (RBCs) and prevent hemozoin formation [78-81]. It was used as first-line antimalarial therapy for many years due to its effectiveness and relatively low cost, but after 20 years of use resistant *Plasmodium* strains eventually appeared in Southeast Asia, South America and the Western Pacific region, and spread progressively throughout malaria-endemic areas [42, 59, 78, 82]. The primary determinant for CQ resistance was shown to be the *P. falciparum* CQ resistance transporter (PfCRT), which is involved in excreting CQ from the DV [78, 83].

Primaquine (PQ) is an 8-aminoquinoline [42, 84]. Its first mass use occurred in the 1950s during the Korean War to eliminate long latency *P. vivax* infections [84, 85]. Since then, it has been administered to millions of people, mostly in China, Azerbaijan, Tajikistan, Northern Afghanistan and North Korea [84]. Despite its weak asexual stage activity, PQ is able to kill mature gametocytes of *P. falciparum* (with a single dose) and developing parasites of all species in the liver, and is currently the only clinically available drug that is active against hypnozoites from *P. vivax* and *P. ovale* [1, 42, 84, 86-89]. Unfortunately, PQ has a short plasma half-life (approximately 6 hours) as a result of oxidative deamination to carboxyprimaquine, and causes mild to severe and possibly fatal acute hemolytic anemia, particularly in patients bearing an inborn deficiency of glucose-6-phosphate dehydrogenase (G6PD), which has an 8% average prevalence in malaria-endemic regions [42, 44, 84, 86, 90]. Recently, a mutation in the human cytochrome P-450 2D6 enzyme with a serious impact on PQ metabolism and decreasing its efficacy against relapse was uncovered [44, 91].

Artemisinin (ART) is the endoperoxide of a sesquiterpene lactone derived from the infesting plant *Qing hao*, also known as sweet or annual wormwood [54, 92]. The medical properties of this plant were well known by the Chinese more than 2000

years ago [54]. In 340 AD, Ge Hong prescribed tea of *Qing hao* as a remedy for feverish attacks and in 1596, Li Shizhen recommended it for the relief of the symptoms of malaria [54]. The antimalarial component, artemisinin, was extracted and crystallized in 1972 by Chinese researchers from 'project 523' [54, 92]. One of these researchers, Tu Youyou, was recently awarded the 2015 Nobel Prize in Physiology or Medicine [58]. It is a potent treatment for malaria due to its low toxicity, rapid killing of malaria parasites in several stages of their life cycle and its nanomolar potency *in vivo* against *P. falciparum*, including multi-resistant strains. However, it has low solubility in water and oil and a very short half-life of only 2 hours *in vivo* [42, 92-97]. Nowadays, ART has been replaced by three more powerful semi-synthetic derivatives: dihydroartemisinin (DHA), artemether and artesunate [42, 54]. In addition, to overcome their short half-lives, ART-based combination therapies (ACTs), in which a potent, short-acting ART derivative is simultaneously administered with one or more longer-acting drug with independent mode of action, are the current first-line antimalarials recommended by the WHO [42, 78, 98, 99].

The Public Health Challenge Currently Posed by Malaria

Nowadays, malaria exerts a heavy burden on several low- and lower-middle-income countries, especially in Africa [1, 100]. Within malaria-endemic countries, the poorest communities are the most severely affected, having the highest risks associated with malaria and the least access to effective services for prevention, diagnosis and treatment [1, 101].

The 2015 World Malaria Report, which summarizes information received from 96 malaria-endemic countries, estimated that 3.2 billion people are at risk of being infected by *Plasmodium* and developing malaria [1]. In 2015, there were an estimated 214 million cases of malaria, which resulted in 438 000 deaths, 90% of which in sub-Saharan Africa (Table 1.1) [1]. The number of malaria deaths in children aged under 5 years is estimated to have decreased to 306 000, which accounts for only 10% of total child deaths in sub-Saharan Africa [1]. As a result, malaria is no longer the leading cause of death among children in this region [1]. Substantial progress has been accomplished in the past few years, with a 60%

reduction in global malaria deaths between 2000 and 2015 due to an increase in international and domestic funding for malaria control and elimination [1].

Table 1.1 - Estimated malaria cases and deaths, by WHO region, 2000–2015. From [1].

	Estimated number of malaria cases (000's)				Change	Estimated number of malaria deaths				Change
WHO region	**2000**	**2005**	**2010**	**2015**	**2000–2015**	**2000**	**2005**	**2010**	**2015**	**2000–2015**
African	214 000	217 000	209 000	188 000	-12%	764 000	670 000	499 000	395 000	-48%
Americas	2 500	1 800	1 100	660	-74%	1 600	1 200	1 100	500	-69%
Eastern Mediterranean	9 100	8 600	4 000	3 900	-57%	15 000	15 000	7 000	6 800	-51%
European*	36	5.6	0.2	0	-100%	0	0	0	0	
South-East Asia	33 000	34 000	28 000	20 000	-39%	51 000	48 000	44 000	32 000	-37%
Western Pacific	3 700	2 300	1 700	1 500	-59%	8 100	4 200	3 500	3 200	-60%
World	**262 000**	**264 000**	**243 000**	**214 000**	**-18%**	**839 000**	**738 000**	**554 000**	**438 000**	**-48%**
Lower bound	205 000	203 000	190 000	149 000		653 000	522 000	362 000	236 000	
Upper bound	316 000	313 000	285 000	303 000		1 099 000	961 000	741 000	635 000	

* There were no recorded deaths among indigenous cases in WHO European Region for the years shown.
Source: *WHO estimates*

Besides the significant impact on the demographic structure of endemic countries caused by the preferential mortality of infants and children, malaria has a profound impact on households, health systems and national economies [100-102].

At the household level, malaria imposes both direct and indirect costs [100, 103]. Direct costs include time lost from work, as well as medical treatment and prevention costs, while indirect costs include loss of work efficiency and work reallocation within the household [100-103]. In the case of the children, indirect costs include nutritional deficiencies, cognitive and educational disabilities and physical retardation [100-102]. Notably, malaria is responsible for 15% of health-related absenteeism from school, contributing to poor educational performance and high failure and school drop-out rates [101, 102, 104].

Public health systems of endemic countries spend a high proportion of their resources on malaria treatment [102]. Additionally, malaria has an adverse impact on foreign investment, tourism and trade in endemic countries, impairing their economic linkage with the rest of the world [101, 102].

Ultimately, malaria costs Africa more than US$12 billion annually and is estimated to have slowed down economic growth in African countries by as much as 1.3%

per year [54, 100, 101, 105]. Malaria is, therefore, a cause of poverty; conversely, poverty promotes malaria transmission [101, 102].

Strategies for Malaria Control and Elimination

Prevention

Malaria interventions comprise vector control, which reduces transmission by the mosquito vector from humans to mosquitoes and then back to humans and can be achieved using insecticide-treated mosquito nets (ITNs), long-lasting nets (LLNs) or indoor residual spraying (IRS); chemoprevention, which prevents blood stage infections in humans; and case management, which includes diagnosis and treatment of infections [1, 2].

ITNs and IRS are currently the preferred methods of malaria vector control and, in many cases, are used together in the same households, conferring increased protective benefits [106]. In 2015, 67% of the population at risk in sub-Saharan Africa had access to an ITN and, in 2014, 116 million people were protected from malaria through the use of IRS [1]. IRS makes use of 12 WHO-approved insecticides from 4 different classes, namely organochlorines (namely, DDT), organophosphates, carbamates and pyrethroids [106, 107]. On the other hand, ITNs show a high degree of personal protection but rely mainly on pyrethroids, to which malaria vectors in most countries around the world have acquired resistance [1, 108-118].

Chemoprevention is particularly important for pregnant women and young children [1, 86]. Intermittent preventive treatment in pregnancy (IPTp), through the administration of sulfadoxine-pyrimethamine (SP) during the second and third trimester of pregnancy, has been shown to reduce severe maternal anaemia, low birth weight and perinatal mortality [1, 54, 86, 119]. In 2014, only 17% of the pregnant women received the recommended three or more SP doses [1]. For children, the WHO recommends the implementation of seasonal malaria chemoprevention (SMC) with amodiaquine plus SP (AQ+SP) and intermittent preventive treatment for infants (IPTi) with SP [1, 86]. SMC can be used in children aged 3–59 months living in areas of highly seasonal malaria transmission and it works by maintaining therapeutic antimalarial drug concentrations in the blood

during periods of greatest malaria risk [1, 86]. IPTi is delivered at routine infant immunization, providing protection in the first year of life against clinical malaria and anaemia [1, 86]. In 2014, only 8 countries had adopted SMC and only one country, Chad, had adopted IPTi [1].

Chemoprophylaxis is also recommended for travelers from non-endemic countries to countries with ongoing local malaria transmission, preferably in addition to other personal protective measures, such as the use of insect repellents, ITNs, long sleeves and long pants [52, 120]. Currently, the most common prophylactic drugs for travelers are CQ, Proguanil, Atovaquone/Proguanil (known as Malarone), Doxycycline, Mefloquine and PQ [120, 121]. The preventive drug recommended varies with the country of origin and the availability of antimalarial drugs in that country, the species of *Plasmodium* and the presence or not of drug resistance in the country of destination, as well as, the time the traveler will spend there [52, 120].

There is still no licensed vaccine available against malaria, mainly due to the complex life cycle of *Plasmodium*, which makes the selection of targeted antigens more challenging, and by our lack of understanding of the immune response against malaria [1, 51, 122]. Even so, four candidate vaccines are currently undergoing field trials: three of these are in Phase 2B clinical trials and one, the RTS,S/AS01 vaccine, has completed Phase 3 trials [1, 123, 124]. This vaccine is based on the repetitive sequence of 4 amino acids of the *P. falciparum* surface circumsporozoite protein (CSP) and its administration led to a 46% reduction in malaria incidence in children and a 27% reduction in infants [1, 54, 122-124]. The RTS,S/AS01 candidate vaccine, known as Mosquirix^{TM}, was reviewed for its quality, safety and efficacy by the European Medicines Agency (EMA) earlier this year and was considered to have a favourable risk-benefit balance for active immunization of children aged 6 weeks up to 17 months [122, 125]. WHO's Strategic Advisory Group of Experts on Immunization (SAGE) and the Malaria Policy Advisory Committee (MPAC) recommend that pilot implementations should be the next step with this vaccine and regard it as a complementary tool that could potentially be added to, but not replace, the core package of proven malaria preventive measures [126]. Nonetheless, efforts towards the generation of a vaccine with higher efficacy levels are still ongoing [122].

Diagnostic and Treatment

Early diagnosis and treatment of malaria reduces disease and prevents deaths [2]. The WHO recommends that all patients with suspected malaria (i.e., people who had fever for a week or more in an area of malaria transmission) should be examined for evidence of infection with *Plasmodium* parasites by either microscopy or a rapid diagnostic test (RDT) [1, 2, 86]. The accuracy of the diagnostic test by microscopy depends on the expertise of the personnel [52, 127]. RDTs rely on the detection of two major antigens: the histidine-rich protein-2 (HRP-2) / aldolase system and the *Plasmodium* lactate dehydrogenase (pLDH) system [52, 127]. Although these RDTs have limited sensitivity to non-*falciparum* and non-*vivax Plasmodium* species, respectively, they are quick and easy to perform, contrary to microscopy, which requires significant expertise [52, 127]. In general, RDTs detecting HRP2 are most commonly used, because they are less expensive, more stable across a wider temperature range and have a lower detection threshold than pLDH-based tests [127, 128]. Other alternatives for malaria diagnosis are DNA/RNA-based detection techniques, such as the polymerase chain reaction (PCR), which is considered to have the most sensitive parasite detection level [127, 129]. However, it requires trained staff and specialized equipment, which are seldom available in resource-poor settings [127, 130, 131].

By the end of 2013, ACTs were adopted as national policy for first-line treatment of *P. falciparum* uncomplicated malaria, as recommended by the WHO [1, 52, 86]. The five ACTs currently in use are artemether plus lumefantrine, artesunate plus AQ, artesunate plus mefloquine, artesunate plus SP, and dihydroartemisinin plus piperaquine [2, 42, 52]. The choice of the ACT is usually based on the therapeutic efficacy of the combination in the country or area of intended use [2, 52]. Importantly, although the transmission of the parasite is reduced by decreasing the amount of gametocytes in the blood of subjects treated with an ACT, they can still transmit malaria [52, 86]. The only licensed drug that can completely prevent transmission of *P. falciparum* is PQ [1, 42, 84, 86-89]. As for the treatment of severe malaria, quinine, which has a fatality rate around 10% and is difficult to administer, remains the official first-line treatment in most countries, even though artesunate was shown to function better [52, 54, 132].

All African countries have reported *P. falciparum* resistance to CQ treatment and resistance to SP is increasing [52, 133, 134]. In fact, in many areas along the Cambodia-Thailand border, *P. falciparum* has become resistant to most available antimalarial medicines, the most worrisome being the reports of changes in sensitivity to ART since 2007 [1, 133, 135, 136]. It is arguable whether this lower sensitivity to ART can be considered resistance because, even though there is a slower parasite clearance due to the reduced susceptibility of ring-stage parasites, the parasites are still eliminated [133, 135-141]. But the fact is that, on the Thailand-Myanmar border, the geometric mean half-life for parasite clearance increased from 2.6 hours in 2001 to 3.7 hours in 2010, as compared with a half-life of 5.5 hours in western Cambodia between 2007 and 2010 (Fig. 1.2) [133, 142, 143]. Recently, this slow clearance has been linked with point mutations in the "propeller" region of a *P. falciparum* kelch protein gene on chromosome 13 (*kelch13*) [143, 144]. Nevertheless, ACTs have generally remained clinically and parasitologically efficacious, provided the partner drug remains efficacious and the treatment is prolonged from 3 to 6 days [1, 133].

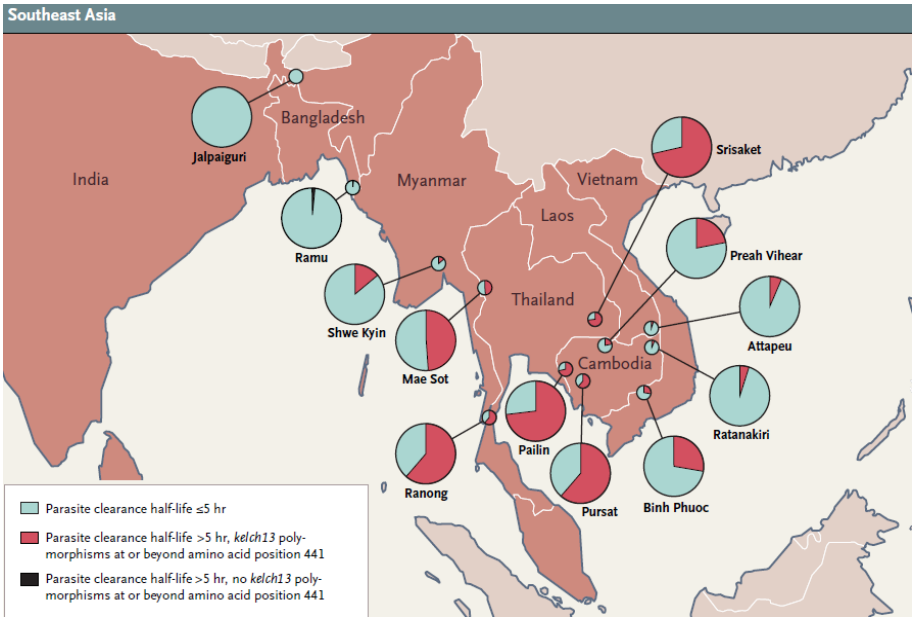

Figure 1.2 – Distribution of *Plasmodium* clearance time with ART treatment in Southeast Asia and its association with *kelch13* mutations. Adapted from [133].

CQ is still used in 10 Central American and Caribbean countries for the treatment of *P. vivax* malaria, where it remains efficacious [1, 78]. Alternatively, both CQ and ACTs can be combined with a 14-day course of PQ for the radical cure of *P. vivax*

malaria, the latter being the only licensed drug effective against hypnozoites of *P. vivax* [2, 44, 84, 86]. Confirmed *P. vivax* resistance to CQ has been emerging at least since 1990 and, currently, has been detected in 10 countries; ACTs are now recommended for the treatment of CQ-resistant *P. vivax* [1, 44].

Plasmodium Life Cycle

As previously mentioned, *Plasmodium* parasites cycle between a mosquito vector and a vertebrate host, and are obligate intracellular pathogens within the latter (Fig. 1.3) [5, 6, 51].

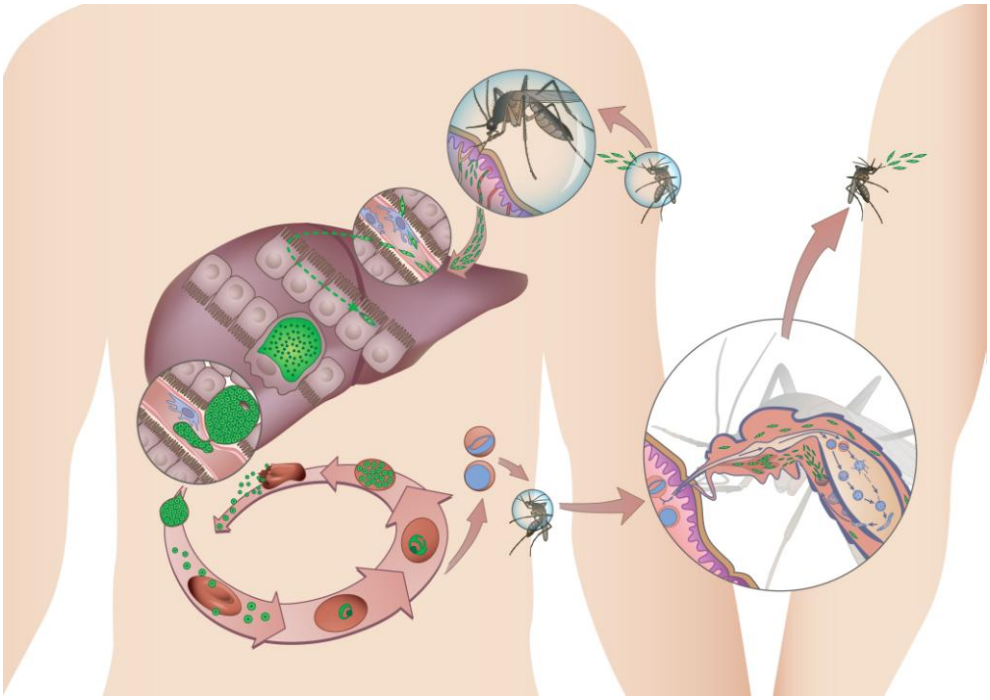

Figure 1.3 – Life cycle of the *Plasmodium* parasite.

Upon a bite of an infected female *Anopheles* mosquito, *Plasmodium* parasites, termed sporozoites at this stage, are deposited under the skin of the mammalian host [5, 40, 41, 145, 146]. Sporozoites then use a form of locomotion known as gliding motility to reach the host's vasculature, and a form of host interaction (cell traversal) to enter circulation [5, 40, 41, 145, 146]. Within a few minutes to a few hours after inoculation, these highly motile forms are passively carried to the liver by the circulatory system, where they traverse several hepatocytes before invading a final cell [5, 40, 41, 145, 147]. Recently, it was shown that sporozoites traverse cells inside transient vacuoles that precede PV formation [148].

Sporozoites initially invade cells inside transient vacuoles by an active moving junction-independent process and then, using pH sensing and perforin-like protein 1 (PLP1), they exit these vacuoles and, only then, enter the PV [148]. Once established inside hepatocytes, each sporozoite develops into an exoerythrocytic form (EEF), through a process called schizogony [5, 40, 41, 145]. This pre-erythrocytic phase of infection is completely asymptomatic and lasts 5-17 days in humans, depending on the *Plasmodium* species [6, 40, 41]. Once parasite replication and cellularization are completed, the newly formed haploid parasites (termed merozoites) are packaged into vesicles called merosomes, which are then released into the bloodstream and eventually burst in the vasculature of the lung, releasing merozoites that will initiate the erythrocytic stage of infection [5, 40, 41, 51, 149, 150]. The liver stage of *Plasmodium* infection will be further detailed in a section below.

P. vivax and *P. ovale* are capable of forming dormant pre-erythrocytic forms, called hypnozoites, which hugely magnify their epidemiological and clinical complexity [6, 44, 51, 151]. These dormant parasites can cause multiple clinical attacks (called relapses) for up to about 2 years [40, 44, 51]. The risk, timing, and frequency of the relapses appear to coincide with both a relatively high likelihood of encountering a different strain of the parasite in the blood and of the presence of anopheline mosquitoes in the environment, in which sexual recombination with that other strain may occur [44].

During the symptomatic erythrocytic stage of infection, the parasites use the erythrocytes as sites of asexual replication, with cycles of replication of 24, 48 or 72 hours, depending on parasite species [40, 51]. The parasite progresses from a ring-stage, which is the earliest form of the parasite that is established following invasion of the red blood cell by a merozoite, to a more metabolically active trophozoite and, finally, to a schizont, characterized by asexual replication and cell division [51, 152]. At the end of each cycle, the newly formed merozoites burst from the erythrocytes and infect more cells, leading to the classic symptoms of the disease [6, 40, 51, 149]. *Plasmodium* blood stages extensively remodel their erythrocyte host cell, establishing several endomembrane structures, such as the Maurer's clefts, Schueffner's dots, J-dots and the tubovesicular network (TVN) [6, 153-156]. These structures allow the export of virulence factors, such as the *P. falciparum* erythrocyte membrane protein 1 (PfEMP1) family, that mediate

adhesion of the infected cell to the vascular endothelium and avoid parasite clearance by the spleen [157].

Throughout the blood stage of infection, some parasites differentiate into the sexual forms, called gametocytes, which are eventually taken up by an uninfected female *Anopheles* mosquito [51, 152]. This process of gametocytogenesis occurs in only a small proportion of blood stage parasites, but is an essential step in the *Plasmodium* life cycle, as it ensures continued transmission [152, 158]. Following ingestion by the mosquito, gametocytes experience a drop in temperature, a change in pH and exposure to xanthurenic acid, which together trigger their maturation into gametes in the mosquito midgut [152, 159]. These gametes then fuse, forming diploid zygotes that develop into ookinetes before burrowing into the midgut epithelium and develop into oocysts [51, 152, 160]. The oocysts burst after one or two weeks of incubation in the midgut and release sporozoites into the hemolymph [51, 152, 160]. Finally, these sporozoites invade the salivary glands and are then transmitted to the next mammalian host that is bitten [51, 160].

The Pre-Erythrocytic Stage of *Plasmodium* Infection

The pre-erythrocytic stage of *Plasmodium* infection includes all the steps since *Plasmodium* sporozoite deposition under the skin of the mammalian host until the release of the first generation merozoites into the bloodstream, where they will invade red blood cells and initiate the erythrocytic stage of infection. The pivotal stage of pre-erythrocytic infection occurs in the liver. Sporozoites selectively infect hepatocytes because these cells are able to support their massive replication, ensuring life cycle progression with the release of red blood cell-infectious merozoites [6]. This hepatic stage of *Plasmodium* infection takes 5-17 days in humans and constitutes an appealing target for the development of an anti-malarial vaccine or prophylactic drug because it would act before the onset of pathology [5, 40, 149, 161].

The present section of this thesis is divided in two parts. The first part addresses the most commonly used tools to investigate *Plasmodium* hepatic infection. In the second part, each step of the pre-erythrocytic stage of infection is described in detail. Liver structure and metabolism are outlined in the following section of the thesis.

Experimental Address of *Plasmodium* Hepatic Infection

The study of human malaria relies mainly on epidemiological analyses, population genetics, clinical studies of patients, and *post-mortem* biopsies [40]. This entails several limitations, such as the difficult access to *post-mortem* tissues and the lack of proper control subjects for most studies [40]. Additionally, the data obtained from *post-mortem* studies represents solely the end stage of a long process; consequently, it is not informative of the sequence of events that led to pathology, particularly the liver stage of infection [40, 41]. Therefore, several models have been developed to enable effective experimental approaches to study hepatic *Plasmodium* infection [41].

Rodent parasite models

P. berghei was the first rodent malaria parasite identified and was isolated from wild rodents in Central Africa by Ignace Vincke and Marcel Lips in 1948 [41, 55]. It was subsequently adapted to mice, rats, hamsters and gerbils and it can be easily maintained in laboratory-bred mosquitoes such as *A. stephensi* [55]. Since then three other species, *P. yoelii*, *P. vinckei* and *P. chabaudi*, have been identified, isolated and adapted to laboratory rodents [41, 55]. Several strains of each parasite are currently available, with distinct courses and outcomes of infection, depending on the host-mouse strain combination [40].

In vitro hepatic infection systems

Liver stage malaria research has made use of several cell lines, which are easy to maintain and propagate in the laboratory, have a well-defined genome and transcriptome, and are very permissive to genetic manipulation [41]. The cell lines most commonly used with rodent *Plasmodia* are HepG2, Huh7 and Hepa1-6; HepG2 and HC04 cells are used for *P. vivax* infections, being HC04 the only cell line known to support in *vitro* growth of *P. falciparum* [162-166]. However, one negative aspect of cell lines is the fact that they are modified, immortalized cells that may have lost some of the features of the cells they were derived from [41]. An alternative approach relies on the *ex vivo* use of primary hepatocyte cultures, which retain more characteristics of liver hepatocytes [41, 167]. Primary

hepatocytes can either be acquired commercially or purified in the laboratory [41, 168].

In vivo infection models

The use of mosquito-borne human-infective *Plasmodium* species in the laboratory poses obvious safety concerns and several technical challenges [41]. Hence, most liver stage malaria research has employed parasite species that infect other mammals, namely rodents and non-human primates [41].

Mouse models of malaria infection have been used for several decades, as they can be infected by a variety of *Plasmodia* that mimic human parasites [41, 169]. They are particularly useful for understanding of the basic biology of the parasite, the response of the organism to infection as a whole, and to perform drug delivery or toxicity studies [40, 41]. Distinct courses and outcomes of infection can be obtained, depending on the host-mouse model and the parasite used [40, 41].

Although the heterogeneity in outcome observed with different parasite and mouse combinations generates concerns about the translational utility of animal models in understanding human malaria, it can also be considered a reflection of the diversity of the human pathology [40, 169, 170]. The availability of inbred/congenic/transgenic animals and the ability to manipulate and control different aspects of the host, including the immune system, make the mouse model a precious tool [40, 151]. Additionally, the use of rodent models enables maintaining the entire life cycle of the parasite in controlled and optimized laboratory conditions [40, 41].

Nevertheless, the results obtained with mouse models should be interpreted with caution because mice are physiologically and genetically different from humans and the *Plasmodium* species infecting each host are highly divergent [40, 161, 169, 170]. In fact, rodent malaria parasites have only around 70% and 60% identity in nucleotide and protein sequence, respectively, with *P. falciparum* [151]. Consequently, not all aspects of *P. falciparum* biology can be modeled using rodent malaria models [171]. *P. falciparum* exhibits a diversity of unique traits and harbors several genes that lack orthologous genes in the rodent *Plasmodium* parasites [171]. Additionally, many rodent parasite genes diverge functionally from their human parasite orthologs or have different times of expression [171].

Besides humans, only large apes, including gorillas and chimpanzees, and possibly other smaller, non-human primate species, are natural hosts for *P. falciparum* and *P. vivax* [41, 151, 171]. However, their use is hampered by ethical and economic constraints [41, 151, 171]. Recently, mouse models with human tissues (liver and blood) have been developed to enhance our biological knowledge of human parasites, allowing their study in a physiologically relevant model [151, 161, 171]. These humanized mouse models share a set of mutations and genetically deficient backgrounds for immunocompromised status that facilitate engraftment with human cells and have already been shown to support the development of blood and liver stages of *P. falciparum*, when transplanted with human RBCs or hepatocytes, respectively [161, 171]. A mouse with a dual humanization of the erythrocytic and hepatic compartments would support the entire mammalian life cycle stages of human malaria parasites, enabling to study all the transition points in the cycle, to assess the safety of live-attenuated vaccine strains and to test pre-clinically the efficacy of therapeutics blocking different parts of the parasite life cycle *in vivo* [151, 171]. To date, only one study has recapitulated *P. falciparum* entire life cycle *in vivo* [151, 172]. In order to study immune responses and vaccine immunogenicity and efficacy, these humanized mouse models still need further improvement [171].

The First Step of *Plasmodium* Infection – The Skin

Sporozoites residing in the mosquito salivary glands exit with the saliva into the skin of the vertebrate host as the mosquito probes for blood [147]. Salivation stops when the mosquito begins to take in blood [173-175]. Consequently, sporozoites are primarily deposited into the dermis of the skin and not directly into the bloodstream [173-175]. A single infected mosquito can inject between 0 and 1300 sporozoites, with the average inoculum being approximately 125 sporozoites [176]. However, these numbers correspond to laboratory-raised mosquitoes where infection is optimized and salivary gland sporozoite numbers tend to be high [147]. In the field, mosquitoes harbor lower numbers of parasites, and therefore, it is likely that the inoculum is smaller than 100 sporozoites [177, 178].

To exit the skin, sporozoites move randomly using gliding motility until they contact with endothelial cells of the blood system [147, 175, 179, 180]. They glide around

and along these vessels, enter them by a cell traversal process, and are swiftly carried away by the blood circulation [147, 179]. Although some sporozoites leave the injection site very rapidly, many take up to 2 to 3 hours to exit the dermis and enter the bloodstream [181]. Fifteen to 20% of the inoculated sporozoites do not enter the bloodstream and, instead, reach the lymphatic circulation and go to the draining lymph node, where they are eliminated by the immune system [179, 181, 182]. Finally, 0.5-5%, of the inoculated sporozoites were shown to remain in the dermis and begin to develop into exoerythrocytic stages at the inoculation site [183, 184]. This has only been observed using laboratory rodent malaria parasites [147]. Hence, it is possible that the development of exoerythrocytic parasite forms in the skin results either from a non-optimal host-parasite combination or is an evolutionary remnant from the common ancestry with the avian malaria parasites [147]. Notably, parasites developing in the skin are not able to initiate a blood stage infection; even though the merozoites seem fully mature, they are probably unable to penetrate the closed endothelium of the blood vessels [147, 183, 184]. Sporozoites that remain at the inoculum site are possibly destroyed by the innate immune cells, contributing to the initiation of the immune response [40, 147]. In the end, only 10 - 25% of the inoculated sporozoites reach and develop within the liver [185, 186].

The Arrival to the Liver – *Plasmodium*'s Cell Traversal Ability

Liver sinusoids have a fenestrated endothelium and are lined with liver-resident macrophages called Kupffer cells [5]. Once the sporozoites injected by an infected mosquito reach the blood capillaries in the liver, parasites traverse liver sinusoidal endothelial cells (LSECs) or Kupffer cells to exit the bloodstream and gain access to the hepatocytes [5, 6, 187-189]. Kupffer cells have been shown to undergo apoptosis after exposure to sporozoites [5, 190]. Thus, the traversal of these cells might constitute a strategy to resist phagocytosis [5, 190].

After traversing the sinusoidal barrier, sporozoites traverse several hepatocytes before invading one that will serve as host cell (Fig. 1.4) [145]. The role of this migration process is still unclear but it was postulated to render the sporozoites competent for invasion and/or the host cell permissive to infection [5, 191]. Sporozoites that have traversed cells were shown to be more infectious than non-

traversing parasites, probably due to induction of exocytosis of apical organelles necessary for invasion [191]. On the other hand, during traversal, sporozoites are exposed to increased levels of potassium inside the traversed cells which reduces their cell passage activity and enhances their infectivity [192]. Finally, wounded/traversed hepatocytes secrete hepatocyte growth factor (HGF), which conditions neighbouring cells to be more susceptible to infection [193]. Nevertheless, mutant parasites lacking one of the proteins that are known to be involved in cell traversal, namely sporozoite microneme protein essential for cell traversal (SPECT), PLP1, cell traversal protein for ookinetes and sporozoites (CelTOS) and phospholipase (PL), are able to infect cells *in vitro* with efficiencies similar to those of wild type parasites, suggesting that traversal is not a pre-requisite for cell invasion by sporozoites [194-199]. Another hypothesis as to how the sporozoite switches to an infectious mode is related to their interaction with highly sulfated-heparan sulfate proteoglycans (hsHSPGs) present on hepatocytes [6, 200]. Exposure to hsHSPGs induces the proteolytic cleavage of the N-terminus of the surface CSP by a parasite cysteine protease, exposing the type I thrombospondin repeat (TSR), a cell adhesive domain that is otherwise masked, and thus allows the sporozoite to shift to an invasive state [147, 201].

The Process of Hepatocyte Invasion

Similarly to gliding motility, the invasion process relies on the actin-myosin motor beneath the parasite's plasma membrane and requires the formation of a moving junction to form an interface between the parasite and the hepatocyte [5, 147]. The proteins necessary for host cell invasion are stored and released from specialized apical organelles called micronemes [5]. One such protein is thrombospondin-related anonymous protein (TRAP), which connects host cell and parasite by using its cytoplasmic tail to bind parasite actin via aldolase and its extracellular adhesive domains to bind hepatocytes, as has been shown using both gene deletion and mutagenesis of functional domains [5, 147, 202, 203]. TRAP is secreted from micronemes at the sporozoite's anterior end and is translocated to the posterior end, thus providing the propulsion used by the sporozoite during invasion [5, 147, 203]. Parasite proteins stored in the rhoptries, another type of secretory organelle,

might also be involved in the hepatocyte invasion process because of their demonstrated roles in invasion of red blood cells by merozoites [5, 204].

Several host factors are also important for invasion of hepatocytes. The actin nucleating complex Arp2/3 is required for the parasite-induced formation of a ring-shaped F-actin structure in the host cell at the moving junction [205]. A successful invasion requires *de novo* polymerization of host actin at the entry site, which is likely involved in anchoring the tight junction so that the parasite can pull upon it to penetrate the host cell [5]. The tetraspanin cluster of differentiation 81 (CD81), present in cholesterol-rich lipid rafts on the surface of hepatocytes, has been shown to be involved in sporozoite invasion by some species of *Plasmodium* [5, 6]. HepG2 cells expressing CD81 are more permissive to invasion by *P. yoelii*; on the other hand, CD81 is not required for invasion by *P. berghei* and its presence is necessary but not sufficient for invasion by *P. falciparum* [206-209]. Scavenger receptor BI (SR-BI) is a high-density lipoprotein receptor that, along with CD81, is present in cholesterol-rich microdomains on the hepatocyte surface and is necessary for efficient sporozoite invasion [210, 211]. SR-BI normally functions to facilitate the uptake of high-density lipoprotein cholesteryl-esters, and thus may indirectly promote sporozoite invasion by providing the cholesterol necessary for appropriate CD81 cell-surface localization [5, 6]. Another hepatocyte receptor, c-Met, has been implicated in hepatocyte infection by *P. berghei* but not by *P. falciparum* or *P. yoelii* [193, 212].

Host-Parasite Interface - The Parasitophorous Vacuole

During the invasion of hepatocytes, the parasite forms a parasitophorous vacuole (PV), within which it resides throughout its liver stage development (Fig. 1.4) [5, 6]. The sporozoites that enter hepatocytes without a PV are rapidly cleared by host cells through a Bcl-2-dependent apoptosis mechanism, whereas the sporozoites that form a PV render host cells less susceptible to apoptosis [213-215]. The PV membrane (PVM) is porous, allowing the entrance of small host factors into the vacuole [5, 6, 216]. It is derived from the host plasma membrane, which is significantly remodeled with proteins of parasite origin [5, 6, 216].

The parasite proteins P36 and P52 (P36p) are involved in the formation of the PV, as a *P. yoelii p52*/*p36* double gene knockout and *P. berghei* and *P. falciparum p52*

single gene deletion are unable to form a PVM and arrest early in liver stage development [213, 217, 218]. Very recently, it was shown that the hepatocyte EphA2 receptor is likely to play a role in establishing a PV, probably via an interaction with P36 [219]. A secreted protease from *P. yoelii*, rhomboid 1 (ROM1), was found to be involved in liver stage PV formation, with 50% of *rom1* knockout parasites developing abnormal vacuoles and aborting growth within the first 12 hours of infection [220]. Several liver stage PVM-resident proteins have been identified, including upregulated in infectious sporozoites (UIS) 3, UIS4, exported protein 1 (EXP1), and two members of the early transcribed membrane protein (ETRAMP) family [221-223]. These PVM-resident proteins might have a role on parasite growth and survival, as evidenced by the deletion mutants of UIS3 or UIS4 that are not able to develop beyond early liver stages *in vivo* [5]. Both UIS3 and UIS4 have their carboxyl-termini in direct contact with host hepatocyte, therefore they are likely involved in host-parasite interactions [5]. In fact, UIS3 was shown to bind host liver fatty acid binding protein (L-FABP), indicating an involvement in the uptake of fatty acids by the parasite [9]. It is likely that other PVM proteins are also involved in nutrient uptake or other forms of host cell manipulation [5].

Plasmodium Hepatic Schizogony

After the successful invasion of a hepatocyte, each sporozoite dedifferentiates from an invasive form to an active replicative form, the liver stage trophozoite (Fig. 1.4) [5, 6]. This process takes approximately one-third of the time the parasite spends inside the hepatocyte and begins with the breakdown of the sporozoite's inner membrane complex, a cytoskeletal structure located beneath the plasma membrane, which leads to the formation of a central spherical bulb around the nucleus with the simultaneous retraction of the sporozoite's two distal ends [216, 224]. Simultaneously, the parasite expels the remnants of its invasion machinery by an active exocytic process, retaining only those organelles that are necessary for parasite replication [5]. Dedifferentiation to a trophozoite was shown to be triggered by extracellular bicarbonate concentrations and a raise in temperature that mimic host conditions, leading to increased intracellular calcium levels, especially in the centre of the spherical bulb [225, 226]. Additionally, the

translational repression of specific mRNAs packaged into storage granules also plays a major role in sporozoite transformation [5].

Once dedifferentiated, the trophozoite enters schizogony, a process during which it undergoes rapid growth with 10^4- to 10^5-fold replication of its genome, ultimately forming a multinucleate syncytium (Fig. 1.4) [5, 6]. During nuclear division, the apicoplast and mitochondrion become two extensively branched and intertwining structures that undergo morphological and positional changes before segregating into individual merozoites [227]. This cellular and genomic expansion happens at a remarkable speed, taking only 2 days for the rodent-infective *P. yoelii* and *P. berghei* parasites [5].

To support their rapid multiplication, parasites derive nutrients from the host hepatocyte both by passive diffusion through pores in the PVM and by active processes such as those that take up glucose, fatty acids and cholesterol [7-10]. Indeed, microarrays of *P. berghei*-infected hepatoma cells and *P. yoelii*-infected mouse hepatocytes revealed that the parasite modulates the host cell's transcriptome towards biosynthetic pathways including carbohydrate and fatty acid metabolism [11]. Recently, it was demonstrated that the developing EEF scavenges phosphatidylcholine from their hepatocyte host [228]. Liver stage parasites also scavenge $PI(3,5)P_2$ by sequestration of late endosomes and lysosomes around their PVM and subsequent fusion with the TVN during development [229-231]. Iron availability also plays a role on *Plasmodium* liver development. It was shown that blood stage parasite density above a certain threshold can inhibit the next wave of sporozoite invasion and development through modulation of hepcidin, the host iron regulatory hormone, to redistribute iron away from the liver [232]. Certainly, several other nutrients are also acquired from the host to sustain parasite growth and development.

Merozoite Formation and Release

Formation of the individual hepatic merozoites occurs through several invaginations of the parasite plasma membrane that eventually package the individual daughter merozoites with a single nucleus and the necessary organelles [5]. This massive expansion of the parasite plasma membrane relies on the endogenous generation of fatty acids via the type II fatty acid synthesis (FAS-II)

pathway in the apicoplast [5]. The components of this pathway were shown to be upregulated in liver stages; if deleted, rodent malaria parasites arrest their liver stage development before merozoite formation, indicating that fatty acid synthesis is essential for late liver stage development [233-235].

Plasmodium-specific apicoplast protein important for liver merozoite formation (PALM) was also implicated in efficient merozoite formation and segregation because its absence results in a significant defect in late liver stage development [236]. In fact, the apicoplast seems to play an important role in the development of the parasite given that using antibiotics to inhibit the bacterial-like protein translation processes of this organelle hinders its development and, consequently, disrupts the maturation of the parasite [236].

During merozoite formation, the cysteine protease-dependent degradation of the PVM leads to the release of merozoites into the host cell cytoplasm [237]. These cysteine proteases are probably serine repeat antigen (SERA) proteases, which are present in all *Plasmodium* species and are essential for merozoite egress from erythrocytes and sporozoite egress from oocysts in the mosquito midgut [238]. In fact, *P. berghei* proteases SERA-1 and SERA-3 were found in the hepatocyte cytoplasm during merozoite development, probably due to PVM breakdown [239, 240]. Nevertheless, it is still unknown if these proteases are involved in the breakdown of the PVM or whether they play a role during merozoite release from the hepatocyte [5].

Following the breakdown of the PVM, from a few to several thousand merozoites are packaged into vesicles termed merosomes that are extruded from the infected hepatocyte into the liver sinusoids (Fig. 1.4) [237, 241]. The parasite induces a non-apoptotic/non-necrotic cell death program in the hepatocyte causing it to detach from surrounding tissue and delays the fragmentation of the host genomic DNA [5, 237]. Additionally, it inhibits phosphotidylserine display on the outer leaflet of the plasma membrane of these dying hepatocytes, as well as, on the surface of merosomes, whose membrane is comprised of the host hepatocyte plasma membrane [242]. This allows the merozoites to evade detection by immune cells present in the liver [5]. Merosomes then travel passively in the bloodstream and burst in the narrow vasculature of the lung, releasing merozoites that initiate blood stage infection [150].

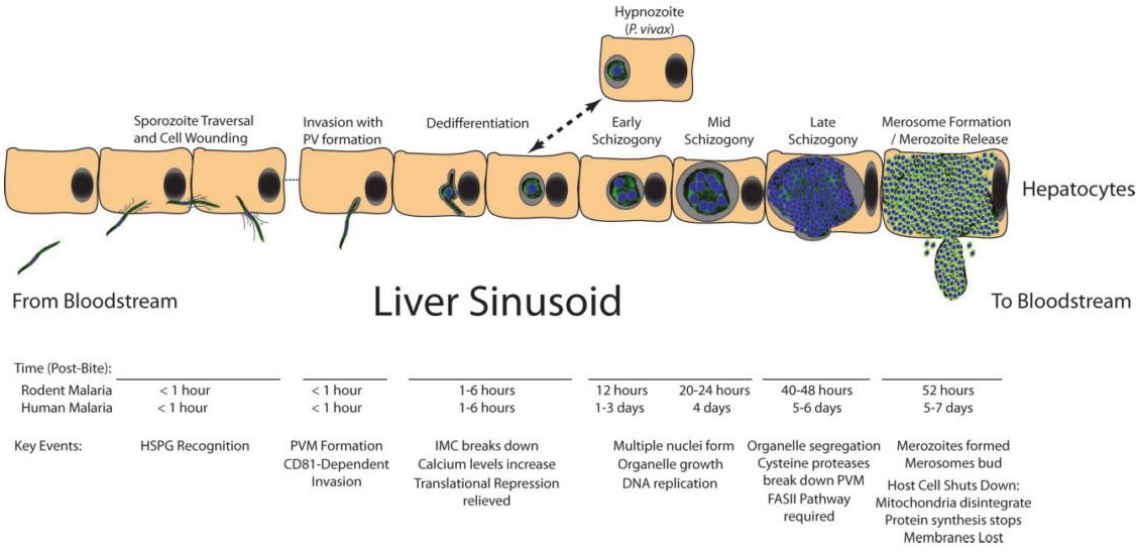

Figure 1.4 – The liver stage of *Plasmodium* parasites. After traversing the endothelium, each sporozoite traverses several hepatocytes until it productively invades one, with formation of a PV. Then, it actively expels and disassembles organelles involved in the invasion process and dedifferentiates into a trophozoite. Liver stage parasites scavenge nutrients from the hepatocyte and extensively replicate their genome and organelles, which are segregated during schizogony into each of the newly formed merozoites. Late in schizogony, the PVM breaks down and merozoites are enclosed in merosomes, which are released into the liver sinusoid, enter circulation and eventually burst in the lung microvasculature to release the merozoites. Infections by *P. vivax* and *P. ovale* also produce hypnozoites that can reactivate months or years later. From [5].

Liver Structure and Metabolism

Liver Anatomy

The liver is the largest gland in the body, accounting for 2 to 5% of body weight [243-245]. It sits in the right upper abdominal cavity beneath the diaphragm and is protected by the rib cage and by a thin connective tissue capsule known as Glisson's capsule [244, 245].

This organ has a dual blood supply consisting of the hepatic artery, which delivers around 25% of the blood supply, and the portal vein that accounts for the remaining 75% [245]. All nutrients absorbed by the intestinal system reach the liver through the portal vein and are processed through the hepatic metabolism of glucose, lipids and proteins [245, 246].

The liver possesses a repeated, multicellular architecture, composed of five types of specialized cells, classifiable into parenchymal (hepatocytes) and nonparenchymal cells (sinusoidal endothelial cells, Kupffer cells, biliary ductal cells and stellate cells) [243-245]. The vast majority of liver functions, including synthesis and storage functions and filtration of the portal venous blood, are mediated by the hepatocytes, which constitute about two-thirds of the liver cell mass [243-245]. These cells are structurally and functionally polarized, with three distinct membrane domains, sinusoidal (basal), lateral and canalicular (apical) [245, 247]. Kupffer cells are the specialized liver macrophages, responsible for immunological and phagocytic functions [248]. Bile duct epithelial cells are involved in the transport of bile and maintenance of its pH [249]. Finally, hepatic stellate cells store retinoids (retinol and retinyl esters) in perinuclear fat droplets and have been implicated in the pathological remodeling process associated with hepatic fibrosis [250, 251].

The liver parenchyma is arranged in hexagonal lobules in a honey-comb-like pattern; at the periphery of each lobule, branches of the hepatic artery, portal vein and bile duct form three to six portal triads (Fig. 1.5A) [244, 245, 252, 253]. Both portal vein venules and portal arterioles of each portal triad branch into the lobules to form the sinusoids, blood vessels with fenestrated, discontinuous endothelium that serve to provide nutrients and oxygen to the surrounding hepatocytes [244, 245, 253]. The sinusoids are positioned radially in the liver lobule and ultimately

converge and form the central vein at the center of the lobule [244, 245]. The direction of blood flow of each liver lobule is from the periphery to the center, generating a gradient in oxygen, nutrients, hormones and growth factors (Fig. 1.5B) [243, 245].

Hepatocytes are the building blocks of the liver lobules [245, 253]. They are arranged in liver cell plates and positioned radially with individual sinusoidal capillaries (Fig. 1.5B) [243-245, 254]. This unique architectural arrangement allows for bi-directional permeability and exchange of materials from both the hepatocyte and blood [245, 253]. The space of Disse is a subendothelial area that separates the endothelial cells from the hepatocytes [244, 245]. Many hepatic nonparenchymal cells are located in the sinusoids and space of Disse, allowing for efficient immune surveillance as well as other metabolic functions [245].

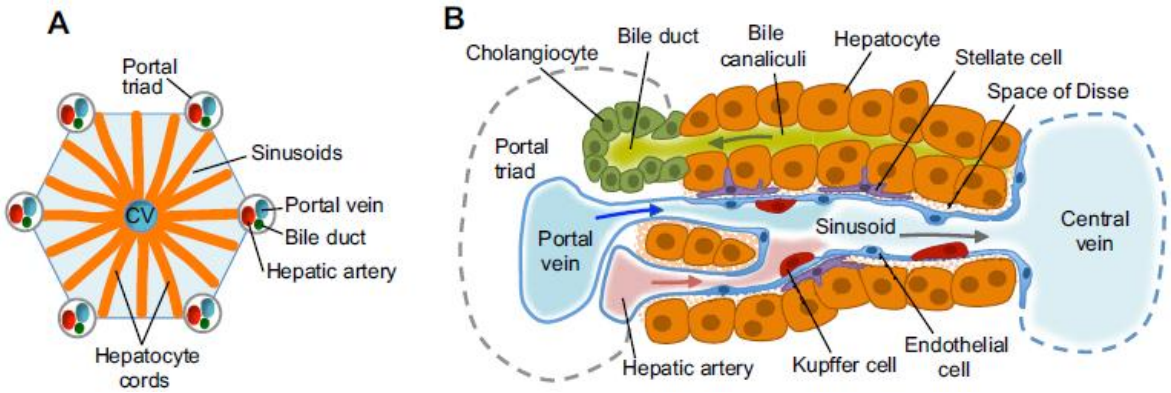

Figure 1.5 - Liver structure and cell types. **A)** The liver is organized in many lobules, its functional units. The portal triad consists of a portal vein, hepatic artery and biliary duct. Hepatocyte cords are separated by sinusoids that carry blood from the portal triads to the central vein. **B)** Within each lobule are a number of sinusoids, which are discontinuous vessels built from specialized fenestrated endothelial cells of the liver. Stellate cells are located in the space of Disse between the hepatocyte cords and sinusoids. Kupffer cells also reside in sinusoids. Hepatocytes secrete bile salts into the bile canaliculi that lead to the bile duct. Cholangiocytes are the epithelial cells lining the bile ducts. From [255].

Liver Zonation

The liver cell plate consists of 15–25 hepatocytes that extend from the portal triad to the hepatic venule [245, 253]. Although histologically indistinguishable, each hepatocyte specializes in certain metabolic functions based on its position along

the porto-central axis of the liver lobule, which determines their fate as either periportal or perivenous hepatocytes [245, 253, 256]. Zone 1 is composed by six to eight periportal hepatocytes that surround the portal triad and are in close contact with the afferent blood [245]. Close to the efferent centrilobular vein, two to three perivenous hepatocytes are considered zone 3 [245]. The midlobular population of six to ten hepatocytes make up zone 2 [245]. The concept of zonation, in which opposing or complementary metabolic pathways are carried out within distinct non-overlapping regions of the liver lobule, was proposed by Jungermann thirty years ago [245, 253, 257]. This metabolic zonation is thought to contribute to the maintenance of optimal metabolic homeostasis and to optimize liver function [253].

The zonated functions include glucose metabolism, ammonia detoxification, metabolism of drugs and xenobiotics, lipid metabolism, synthesis of bile acids and the metabolism of several amino acids [245, 253]. In the case of glucose metabolism, gluconeogenesis is mostly periportal whereas glycolysis is mostly perivenous [245, 256]. Ammonia detoxification relies firstly on periportal hepatocytes and, later, on perivenous hepatocytes [245, 258, 259]. The metabolism of drugs and xenobiotics occurs mostly in the perivenous area [245, 257]. Importantly, not all hepatic processes are zonal [245]. For example, the synthesis of transthyretin and transferrin transporters and albumin appears to occur in all hepatocytes [245].

Functional zonation is mainly controlled by differential expression of genes encoding the enzymes responsible for the functions concerned [245, 260]. This control may involve transcriptional or posttranscriptional regulation along the portocentral axis [245]. The Wnt/β-catenin pathway is one critical player in liver zonation [253, 261-263]. The transcription factor Hnf4α is also a modulator of the zonal expression of genes, acting through cross-talk with the Wnt pathway [245, 264].

Liver Function

The liver functions as a metabolic hub, performing a complex array of more than 500 functions, including synthesis of serum proteins, metabolism of amino acids, lipids and carbohydrates and detoxification of xenobiotic compounds [243, 245]. For the sake of simplicity, only glucose and protein metabolisms will be introduced.

Hepatic Glucose Metabolism

The liver plays a unique role in controlling carbohydrate metabolism by maintaining glucose concentrations in a normal range through a tight regulation of glucose breakdown, synthesis and storage as glycogen in hepatocytes [245]. Additionally, it acts as a sensory organ; the intrahepatic sensory-effector nerves detect glucose concentration gradients between the hepatic artery and the portal vein and, subsequently, generate a cholinergic signal for an insulin-dependent net hepatic glucose uptake [265, 266].

Blood glucose enters hepatocytes mainly via plasma membrane glucose transporter 2 (GLUT2), a high capacity transporter that also mediates glucose release [245, 246, 267]. Upon uptake, glucose is phosphorylated by glucokinase (GCK), the rate-limiting enzyme for further glucose utilization, to generate glucose 6-phosphate (G6P) (Fig. 1.6) [245, 246, 268]. G6P is then channeled to several pathways such as glycogen synthesis, glycolysis and pentose phosphate pathway (PPP) in the fed state, or is transported into the endoplasmic reticulum (ER) and dephosphorylated by glucose-6-phosphatase (G6Pase) to release glucose in the fasted state [246].

Glycogen Metabolism

With 10% of its weight, the liver has the highest specific glycogen content of any tissue [245]. Glycogen is synthesized from G6P by glycogen synthase in the fed state and is metabolized by glycogen phosphorylase in the fasted state, both enzymes regulated by phosphorylation [245, 246, 269].

In the fed state, pancreatic β-cells secret insulin, that stimulates the synthesis of glycogen and suppresses glycogenolysis, the process of glycogen breakdown [246, 270]. Glycogen synthesis is also stimulated by the GI-secreted fibroblast growth factor 15/19 (FGF15/19) [246, 271]. In the fasted state, glucagon and catecholamines, such as epinephrine and norepinephrine, are secreted by pancreatic α-cells and the adrenal medulla, respectively, and stimulate glycogen breakdown [246, 272].

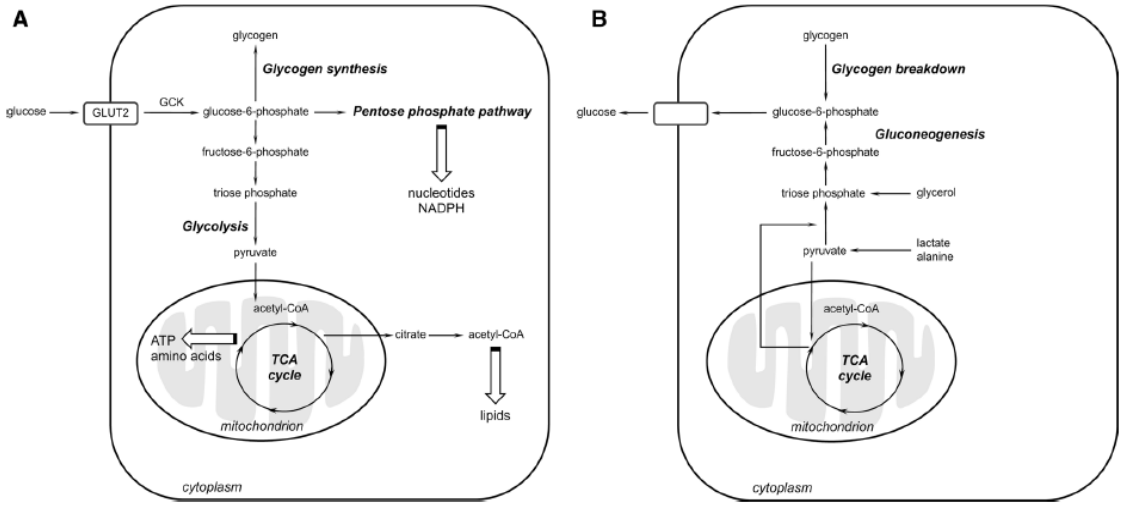

Figure 1.6 - Pathways of hepatic glucose metabolism. **A)** Simplified scheme depicting the major biochemical pathways activated during postprandial glucose consumption and storage. **B)** Simplified scheme depicting the major biochemical pathways activated during post-absorptive glucose production. Acetyl-CoA, acetyl-coenzyme A; GCK, glucokinase; GLUT2, glucose transporter 2; TCA, tricarboxylic acid. From [273].

Glycolysis

In the fed state, when glucose is abundant, glycolysis is the preferred pathway for energy supply by hepatocytes [246]. The generated glycolytic intermediates are completely oxidized in the tricarboxylic acid (TCA) cycle to generate adenosine triphosphate (ATP) and are used to synthesize lipids, amino acids and other important molecules (Fig. 1.6A) [245, 246]. The glycolytic flux is mainly controlled by four kinases, GCK, 6-phosphofructo-1 kinase (PFK), liver pyruvate kinase (L-PK) and pyruvate dehydrogenase kinases (PDKs), whose levels and activity increase after food ingestion [274].

Hepatic glycolysis is also controlled by insulin and glucagon. In the fed state, insulin stimulates glycolysis while in the fasted state, glucagon inhibits it; both act via a single enzyme called bifunctional 6-phosphofructo-2-kinase/fructose-2,6-bisphosphatase (PFK-2/FBP-2) [275, 276].

Pentose Phosphate Pathway (PPP)

The PPP, also known as the hexose monophosphate shunt or the phosphogluconate pathway, branches from glycolysis at the first committed step

and consumes G6P as a primary substrate [277]. Besides generating phosphopentoses and ribonucleotides, the PPP plays a pivotal role in the cellular redox state because it is a major source of nicotinamide adenine dinucleotide phosphate (NADPH) [277].

The PPP comprises two branches: the oxidative branch and the nonoxidative branch [277-279]. The oxidative branch generates NADPH and ribonucleotides via three irreversible reactions [277-279]. The non-oxidative branch comprises a series of reversible reactions that recruit additional glycolytic intermediates, such as fructose-6-phosphate (F6P) and glyceraldehyde-3-phosphate (G3P), which can be converted into pentose phosphates and vice versa [277-279].

Gluconeogenesis

The liver produces glucose through glycogenolysis in short-term fasting (2-6 hours after a meal) [245, 246]. In more prolonged fasting, after depletion of hepatic glycogen, hepatocytes start synthesizing glucose through gluconeogenesis using lactate, pyruvate, glycerol and amino acids, such as alanine (Fig. 1.6B) [245, 246, 272].

The rate of gluconeogenesis is determined by the availability of its substrates, which are either generated within the liver or delivered through the circulation from extra-hepatic tissues, such as skeletal muscle and adipose tissue, and by the activity of the unidirectional enzymes, phosphoenolpyruvate carboxylase (PEPCK), fructose-1,6-bisphosphatase (FP2ase) and G6Pase [245, 246, 272].

Gluconeogenesis is a highly regulated process. Insulin is a very well-known suppressor of gluconeogenesis [245, 246, 280]. On the other hand, glucagon, whose secretion is higher in the fasted state and during exercise, is a stimulator [245, 281]. Several GI hormones, including glucagon-like peptide 1, FGF15/19 and serotonin, also regulate this process [246, 282, 283].

Hepatic Protein Metabolism

Under steady-state conditions the body cannot store protein [245]. All amino groups of the protein component of the food have to be deaminated [245]. The resulting ammonia has to be detoxified and excreted (mainly as urea), whereas the carbohydrate component is metabolized or stored as glycogen or fat [245].

The liver is the main responsible for the detoxification of the ammonia generated by metabolization of amino acids in the intestines, converting 75% of it into urea [245, 284]. Several amino acids, such as alanine and glutamine, are also directly used in hepatic urea synthesis [245, 253]. Although relatively independent from feeding, the capacity to synthesize urea corresponds directly to the protein content of the food [284-286].

Urea excretion via the urine accounts for 70-80% of the urea synthesized [287-289]. The remaining is lost through the gut or reabsorbed in the form of ammonia to reenter the urea cycle, or rescued for amino acid synthesis via microbial urease [287, 289-291].

The liver is also able to produce amino acids, such as glutamine or, alternatively, to convert some amino acids into others [284, 292, 293]. Distinct hepatocytes express the enzymes involved in hepatic ammonia and glutamine metabolism [245]. Urea cycle enzymes are found in periportal hepatocytes, whereas glutamine synthesis is mostly confined to pericentral hepatocytes [294, 295]. Enzymes involved in the metabolism of histidine, histamine, glycine and serine are mostly periportal [253, 260].

Plasmodium Metabolism

Most of what is known about *Plasmodium* metabolism regards the blood stage of infection. Information concerning mosquito and liver stages has arisen more recently. In the following two sections, the parasite´s carbon and polyamine metabolisms will be addressed.

Carbon Metabolism

Glucose is the major carbon source for *Plasmodium* blood stage parasites [296, 297]. In fact, the glucose consumption rate of an erythrocyte is estimated to increase up to 100-fold when containing the metabolically active trophozoite and schizont stages of *Plasmodium* [297, 298].

Most of the glucose consumed by the malaria parasite is incompletely oxidized to lactic acid, which is excreted; other metabolites include pyruvate, alanine and glycerol, the latter being an unusual product of anaerobic catabolism of glucose only found in yeast and other protozoan parasites, such as *Leishmania* and *Trypanosomes* [296, 299-301]. Only a small fraction is completely oxidized to carbon dioxide, suggesting that blood stage *Plasmodium* relies primarily on glucose fermentation for energy supply [297, 302, 303]. Similarly to all proliferating cells, *Plasmodium* parasites also utilize glucose to synthesize nucleic acids and NADPH via the PPP [304-307]. Among the other sugars, only fructose can support *Plasmodium* growth, but at a reduced rate [15, 308].

As previously mentioned, blood stage malaria parasites generate energy mainly through anaerobic glycolysis. However, a canonical oxidative TCA cycle is also active and uses both glucose and glutamine as carbon sources [309, 310]. Glutamine-derived carbon enters the cycle via α-ketoglutarate, whereas glucose provides oxaloacetate and acetyl-CoA [309-311]. Glucose-derived acetyl-CoA is also used in the synthesis of UDP-N-acetyl-glucosamine, which is involved in the production of glycophosphatidylinositol (GPI) anchors of glycoconjugated proteins [312]. Knockout parasites for the TCA cycle enzymes grow normally in asexual blood stages but their life cycle progression is halted at later stages, such as gametocyte and mosquito stages [313].

Plasmodium parasites lack the ability to generate carbohydrate stores such as glycogen and, for that reason, they are dependent on a constant and abundant

supply of glucose [297, 302, 303, 314]. This is achieved by the presence of sugar transporters on the erythrocyte and on the parasite plasma membranes [17, 315]. Glucose is first transported from the blood plasma into the erythrocyte cytosol by GLUT1, the most abundant facilitative glucose transporter in the erythrocyte membrane [315, 316]. Glucose molecules then pass from the erythrocyte cytoplasm to the vacuolar space through high-capacity, low selectivity channels present in the PVM [317]. Finally, glucose uptake into the parasite is mediated by a facilitative hexose transporter (HT) [315, 318]. Inhibition of HT by 3-O-[undecyl-10-en]-1-yl-D-glucose, also known as compound 3361, highly impacts *P. falciparum in vitro* survival and suppresses *P. berghei* parasitaemia *in vivo* [16]. Deletion of this gene is lethal for the parasite, further proving its essentiality for asexual blood stages [7, 17].

Glucose also plays a pivotal role in other stages of the parasite's life cycle. The hemolymph of *A. stephensi* is rich in glucose and in the storage carbohydrate trehalose; likewise, the liver of the mammalian host is rich in glucose and glycogen [245, 319]. Additionally, HT is expressed throughout development in the mosquito vector, as well as during the liver stage [8, 17, 233, 320, 321]. Inhibition of glucose uptake with compound 3361 affects both these stages of the parasite life cycle [7, 8]. Finally, glucose concentration in the culture medium was established as a key factor for *P. berghei* development into infective merozoites inside hepatoma cells [322].

Polyamines Metabolism

Polyamines (putrescine, spermidine and spermine) are low molecular weight organic cations that are synthesized in all cells but occur in particularly high concentrations in rapidly proliferating cells, such as cancer cells and protozoan parasites [323-325]. These molecules and their derivatives have the ability to interact electrostatically with most polyanionic macromolecules in the cells and thereby mediate several important cellular processes, including cellular differentiation and proliferation, embryonic development and stress responses [326-329].

Polyamine biosynthesis pathways start with the conversion of L-arginine into L-ornithine by arginase, which is then metabolized into putrescine (1,4-diaminobutane) by ornithine decarboxylase (ODC) [329, 330]. In parallel, S-

adenosylmethionine decarboxylase (AdoMetDC) catalyses the formation of decarboxylated S-adenosylmethionine (AdoMet) [331, 332]. AdoMet then donates the aminopropyl group for the conversion of putrescine into spermidine and, subsequently, of spermidine into spermine, by spermidine synthase (SpdS) and spermine synthase (SpmS), respectively [331-333].

Polyamines make up 14% of the total metabolome of isolated intraerythrocytic *Plasmodium* parasites and their availability is essential for the survival and rapid proliferation of the parasite [328, 329, 334]. This pool of polyamines is mainly composed of putrescine and spermidine [26, 329]. Spermine is only present in very low levels because the parasite lacks a SpmS; however, its SpdS is somewhat promiscuous and can also metabolize spermidine into spermine [328, 329, 335]. The most distinctive feature of polyamine biosynthesis in the malaria parasite is that a single open reading frame encodes the two rate-limiting enzymes in the pathway, ODC and AdoMetDC, originating a unique protein, AdoMetDC/ODC [328, 329, 336]. Even though each decarboxylase active site functions independently of the other, ODC activity seems to be allosterically stimulated by the presence of the AdoMetDC domain and, conversely, AdoMetDC activity is inhibited by the presence of the ODC domain, resulting in the production of equimolar levels of putrescine and AdoMet [337-339].

Polyamine metabolism can be targeted either by preventing intracellular polyamine biosynthesis with enzyme inhibitors or by competitively displacing the functional polyamine pool within cells with non-functional polyamine analogues [324, 329]. Inhibition of AdoMetDC/ODC with ODC inhibitors, the most well-known being α-difluoromethylornithine (DFMO), has a cytostatic effect on *P. falciparum* proliferation *in vitro* that is reversible by exogenous polyamines; additionally, it is not curative in an *in vivo* infection with *P. berghei* [26, 328, 340, 341]. Similar results were obtained when inhibiting the AdoMetDC activity of the bifunctional protein with the compound MDL 73811 [328, 342]. Co-inhibition of both decarboxylase activities displays a non-synergistic but additive effect on infection [340, 342]. Although not so extensively studied, inhibition of SpdS also impacts *P. falciparum* growth *in vitro* [28, 335]. Polyamine analogues inhibit *P. falciparum* and *P. berghei* growth *in vitro* and *in vivo*, respectively [343-345]. Notably, administration of one of the bis(benzyl)polyamine analogs, MDL 27695, in combination with DFMO, effectively cured 47 out of 54 mice infected

with *P. berghei*; these mice were found to be immune upon re-challenge with the same *P. berghei* strain 4 months after the initial infection [343].

The cytostatic effects of the inhibitors of both activities of the AdoMetDC/ODC enzyme and of SpdS are probably due to the ability of the parasite to take up exogenously provided polyamines to replenish intracellular pools [328, 329]. Both putrescine and spermidine can be taken up into the parasite via a saturable temperature-dependent process, with competition between different polyamines, the precursor ornithine and other basic amino acids [346]. This transport is dependent on extracellular pH and on the parasite's membrane potential but independent of extracellular Na^+ concentration [346]. Putrescine and spermidine uptake is increased when polyamine biosynthesis is inhibited [346].

The polyamine biosynthesis pathway is likely to play an important role on other stages of *Plasmodium* life cycle. DFMO was shown to impair exoerythrocytic development of *P. berghei* both in mice and in cultured human hepatoma cells [347]. Similarly, DFMO also impacts the sporogonous cycle of *P. berghei* in *Anopheles* mosquitos [348].

Parasites scavenge nutrients from the host hepatocyte to feed into their metabolic pathways and support their rapid multiplication. It is, therefore, expected that this utilization of nutrients by the parasite, making them unavailable for the host cell, will affect the cell's metabolism.

Thesis Aims

During the liver stage of *Plasmodium* infection, the parasite undergoes a remarkably rapid growth, with 10^4- to 10^5-fold replication of its genome, ultimately forming thousands of new parasites [5, 6]. In order to support their rapid multiplication and feed their metabolic pathways, parasites scavenge nutrients from the host hepatocyte [7-10, 228-232, 322].

The host lab previously showed that glucose plays a crucial role during the liver stage of *P. berghei*, establishing the importance of the import of this nutrient through the parasite's membrane hexose transporter (HT) for its replication inside liver cells [8]. On the other hand, a previous microarray study from the host lab showed that *Plasmodium* development inside hepatic cells induces the coordinated and sequential expression of host genes [11]. Prominent among these are genes encoding membrane transporters, including several genes involved in amino acid transport, whose expression is consistently altered in infected cells.

These observations led to the formulation of two hypotheses, which the present thesis aimed to address: the uptake of glucose by the host cell constitutes a crucial requirement for the parasite's ability to develop normally; and, the intra-hepatic *Plasmodium* parasites modulate host membrane transporters, most likely to ensure their own survival and development.

At the onset of this work, we established a number of specific aims. Firstly, to employ an RNA interference (RNAi)-based approach to identify, from among a panel of selected genes encoding the membrane transporters that might play a role during *Plasmodium* infection of liver cells. Secondly, to characterize the molecular function of these transporters and the role of their downstream metabolic pathways during the parasite's intracellular development. And, finally, to identify molecular targets and infection modulation strategies that can impact *Plasmodium* development or survival during the hepatic stage of the parasite's life cycle.

The pursuit of these objectives relied upon the use of an extensive array of methodological approaches and experimental tools, including established *in vitro*, *ex vivo* and *in vivo* infection models, selected transgenic rodent models, RNAi, immunofluorescence microscopy, flow cytometry and quantitative real-time PCR techniques, and the use of specific competitors and inhibitors of the transport

proteins identified and of the enzymes of the downstream pathways, as well as nutrient depletion and supplementation studies. With these approaches, we expected to unravel novel host transport proteins and metabolic pathways that play a crucial role on *Plasmodium* exoerythrocytic development, and which may constitute suitable targets for malaria prophylaxis and thereby contribute to the development of new intervention strategies against this disease.

GLUT1-mediated glucose uptake during *Plasmodium* hepatic infection

Patrícia Meireles[1], Joana Sales-Dias[1], Carolina M. Andrade[1], João Mello-Vieira[1], Liliana Mancio-Silva[1], J. Pedro Simas[1], Henry M. Staines[2], Miguel Prudêncio[1]

[1] Instituto de Medicina Molecular, Faculdade de Medicina, Universidade de Lisboa, Avenida Professor Egas Moniz, 1649-028, Lisboa, Portugal

[2] Institute for Infection & Immunity, St. George's, University of London, Cranmer Terrace, London, UK

Author Contributions

PM, MP and LMS designed the experiments. PM performed all the experiments. JSD helped with the FACS experiments with the different concentrations of glucose and with the 2-NBDG uptake at different time points of infection. CMA helped with the WZB117 *in vivo* experiments. JMV performed microscopy analysis of WZB117-treated liver slices and helped with other microscopy analyses. PS provided the murine gammaherpesvirus. LMS and HMS gave intellectual input to the work. PM wrote the chapter. MP supervised the work and revised the text.

Introduction

Glucose is the primary source of energy and a key substrate for most cells. Glucose and other carbohydrates are transported into cells by members of a family of integral membrane glucose transporter (GLUT) molecules. To date 14 members of this family, also called the solute carrier 2A (SLC2A) family, have been identified, which are divided into several families (classes I to III) based on their transport characteristics and sequence similarities [349, 350].

GLUT1 is a class I facilitative glucose transporter expressed in liver cells and overexpressed in various tumors [12, 13]. GLUT1 expression is highest in the human erythrocyte membrane, and has been shown to play a critical role in cerebral glucose uptake [351]. GLUT1 is also a receptor for the human T cell leukemia virus (HTLV) and GLUT1-mediated glucose transport in T-cells has been shown to regulate HIV infection [352, 353].

As mentioned in the *Plasmodium* Metabolism section on the general introduction of this thesis, blood stages of malarial parasites are dependent on glycolysis as their main ATP source, a process that has recently been modeled for the human malaria parasite *P. falciparum* [315, 354-356]. Glucose has been shown to be transported from human blood plasma into the erythrocyte cytosol by GLUT1, and then taken up by the parasite via a parasite-encoded facilitative hexose transporter (PfHT) [14-16]. This finding supports novel chemotherapeutic interventions that target PfHT [316, 357]. Furthermore, studies in the rodent malaria model, *P. berghei*, found that the orthologous hexose transporter (PbHT) is expressed not only throughout the parasite's development within the mosquito vector, but also during liver and transmission stages [8, 17].

During their extensive intra-hepatic replication, developing *Plasmodium* parasites likely require the availability of large amounts of nutrients and energy. The availability of appropriate amounts of glucose in infected hepatic cells is thus expected to play an essential role in the development of liver stage *Plasmodium* parasites. In fact, inhibition of PbHT by compound 3361, a specific inhibitor of plasmodial HTs, impairs hepatic *P. berghei* development, supporting the essentiality of glucose uptake for *Plasmodium* liver stages [8]. Accordingly, a recent study established D-glucose concentration in the culture medium as a key factor for *in vitro* hepatic parasite development [322].

In this study, we employed rodent *P. berghei* parasites, a well-established model of malaria infection, to elucidate the uptake and utilization of glucose by *Plasmodium* liver stages [41]. We confirmed the importance of glucose availability for the intra-hepatic development of the malaria parasite. We also investigated the glucose requirements during the course of *P. berghei* development in hepatic cells as well as the host molecular receptors involved in glucose uptake by those cells. The importance of GLUT1 in glucose uptake by infected hepatic cells was validated with a specific inhibitor, both *in vitro* and *in vivo*. Finally, we demonstrate that *P. berghei* infection leads to a small intracellular ATP depletion and enhances the translocation of GLUT1 to the cell membrane of infected hepatoma cells, which contribute to their significantly higher uptake of glucose comparing to non-infected cells. This higher glucose uptake was not observed with any of the other stimuli tested, suggesting specificity to *Plasmodium* infection.

Materials and Methods

Chemicals

RPMI 1640, PBS pH 7.4, trypsin, fetal bovine serum (FBS), non-essential amino acids, penicillin/streptomycin, glutamine, HEPES pH 7, OptiMEM and Lipofectamine RNAiMAX were purchased from Gibco/Invitrogen. All other chemicals were obtained from Sigma, unless otherwise specified.

Cells

Huh7 cells, a human hepatoma cell line, and mouse embryonic fibroblasts (MEFs) were cultured in RPMI 1640 or DMEM medium, respectively, supplemented with 10% FBS, 1% non-essential amino acids, 1% penicillin/streptomycin, 1% Glutamine and 1% HEPES, pH 7 and maintained at 37°C with 5% CO_2.

Mice

C57BL/6 mice were purchased from Charles River and housed in a 12 hour night-light cycle. All animal experiments were performed in strict compliance to the guidelines of our institution´s animal ethics committee and the Federation of European Laboratory Animal Science Associations (FELASA).

Parasites

Green fluorescent protein (GFP)-, red fluorescent protein (RFP)-, or luciferase-expressing *P. berghei* ANKA sporozoites were dissected in non-supplemented RPMI medium from the salivary glands of infected female *A. stephensi* mosquitoes, bred at Instituto de Medicina Molecular (Lisbon, Portugal), prior to being employed for *in vitro* and *in vivo* infections [358, 359].

Overall *in vitro* infection by luminescence

Overall hepatic infection was determined by measuring the luminescence intensity in Huh7 cells infected with a firefly luciferase-expressing *P. berghei* line, as previously described [358]. Briefly, Huh7 cells ($1.0x10^4$ per well) were seeded in 96-well plates the day before infection. Sporozoite addition was followed by centrifugation at 1800xg for 5 minutes and the medium was replaced

approximately 2 hours after infection by the appropriate medium. Parasite infection load was measured 48 hours after infection by a bioluminescence assay (Biotium) using a multiplate reader Infinite M200 (Tecan). The effect of the different treatments on the viability of Huh7 cells was assessed by the CellTiter-Blue assay (Promega) according to the manufacturer's protocol.

Quantification of *P. berghei* invasion and development by flow cytometry

Invasion of hepatoma cells and intracellular parasite development were assessed by determining the percentage of GFP^+ cells 2 hours after infection with a GFP-expressing *P. berghei* line and by measuring the intensity of the GFP signal of the infected cells 48 hours after infection, respectively, as previously described [163]. Huh7 cells ($5.0x10^4$ per well) were seeded in 24-well plates the day before infection. The medium was replaced by the appropriate medium 1 hour prior or 2 hours after infection, for invasion and development quantification, respectively. Cells were then collected for flow cytometry analysis at 2 hours or 48 hours after infection and analyzed on a Becton Dickinson FACSCalibur. Data acquisition and analysis were carried out using the CELLQuest (version 3.1.1 f1, Becton Dickinson) and FlowJo (version 6.4.7, FlowJo) software packages, respectively.

Immunofluorescence imaging of *P. berghei* in Huh7 cells

For immunofluorescence microscopy analyses, cells were seeded on glass coverslips in 24-well plates and infected with sporozoites as described above. Forty-eight hours after infection, cells were rinsed with 1x PBS and fixed with 4% paraformaldehyde (PFA; Santa Cruz Biotechnology) for 20 minutes at room temperature and stored at 4°C in PBS 1x until being stained. Cells were incubated with the permeabilization/blocking solution (0.1% triton X-100, 1% bovine serum albumin (BSA) in 1x PBS) for 30 minutes at room temperature. Parasites were stained with a parasite specific anti-Heat Shock Protein 70 (Hsp70) antibody (2E6; dilution 1:100) and an anti-UIS4 antibody (dilution 1:1000) for 1 hour at room temperature, followed by three washes with permeabilization/blocking solution. Cells were further incubated in a 1:400 dilution of anti-mouse Alexa-Fluor 488 (Jackson ImmunoResearch Laboratories) or anti-goat Alexa-Fluor 568 (Life

Technologies) secondary antibodies in the presence of a 1:1000 dilution of Hoechst 33342 (Invitrogen) for nuclei staining. An additional three washes were carried out with permeabilization/blocking solution. Coverslips were mounted on microscope slides with Fluoromount (SouthernBiotech). Confocal images were acquired using a Zeiss LSM 710 confocal microscope. Widefield images for size determination were acquired in a Zeiss Axiovert 200M microscope. Images were processed with ImageJ software (version 1.47).

Quantification of glucose uptake by flow cytometry

Glucose uptake into Huh7 cells was quantified by flow cytometry using a fluorescent D-glucose derivative, 2-[N-(7-nitrobenz-2-oxa-1,3-diazol-4-yl)amino]-2-deoxy-D-glucose (2-NBDG; Molecular Probes, Life Technologies) as a tracer [360, 361]. Shortly, Huh7 cells ($1.0x10^4$ per well) were seeded in 96-well plates the day before infection with RFP-expressing *P. berghei* sporozoites. At several time points after infection, the medium was replaced by RPMI without glucose supplemented with 1 mM of glucose and 0.1 mM of 2-NBDG, and cells were incubated for 5 min at 37°C to allow uptake. Cells were then collected for flow cytometry analysis and analyzed on a BD LSR Fortessa flow cytometer with the DIVA software (version 6.2). Analysis was carried out using the FlowJo software (version 6.4.7, FlowJo).

Temperature shocks and ethanol-induced oxidative stress

Huh7 cells ($1.0x10^4$ per well) were seeded in 96-well plates and incubated at 37°C for 48 hours. To induce a mild cold stress response, one of the plates was incubated at 27°C for 1 hour [362]. To induce a heat stress response, another plate was incubated at 43°C for 1 hour [363]. Control plate was maintained at 37°C. Ethanol-induced oxidative stress was attained by incubating Huh7 cells in complete RPMI with 50 mM of ethanol for 24 hours [364, 365]. Following temperature shocks and ethanol-induced oxidative stress, the uptake of 2-NBDG by the cells was determined as previously described.

Stress induced by viral infection

Huh7 cells ($5.0x10^4$ per well) were seeded in 24-well plates and, on the following day, were infected with 0.01, 1 and 5 plaque-forming units (PFU)/cell of wild type

murine gammaherpesvirus 68 (MHV68) or YFP-expressing MHV68 (MHV68-YFP) [366]. Twenty-four hours later, the uptake of 2-NBDG by the MHV68-infected cells was determined as previously described. The percentage of MHV68-infected cells in each condition was estimated by determining the percentage of YFP^+ cells after infection with the same amount of PFU/cell of MHV68-YFP.

Assessment of the impact of glucose transporters on *Plasmodium* infection by RNA interference (RNAi)

Down-modulation of the genes encoding selected glucose transporters employed short hairpin RNAs (shRNAs). All shRNAs were purchased from the MISSION TRC library (Sigma) in the form of bacterial glycerol stocks which were grown to obtain the purified plasmids. Each gene was targeted by using three distinct shRNAs, used individually (Table 2.1). For the lentiviral production, HEK 293FT cells ($2.0x10^4$ per well) were seeded in 96-well plates. On the following day, cells were transfected with the packaging vectors and each individual shRNA plasmid in a final concentration of 100 ng/well using the FuGENE 6 reagent (Promega), according to the manufacturer's instructions. The lentiviral particles were collected in the supernatant of these cells approximately 60 hours after transfection and stored at - 80°C. For the transduction of Huh7 cells and subsequent generation of cell lines with stable knockdown of the genes of interest, cells ($1.0x10^5$ per well) were seeded in 12-well plates. On the following day, the medium was replaced by 400 µL of supplemented RPMI with 8 µg/mL of polybrene, on top of which were added 100 µL of lentiviral particles-containing supernatant (approximate MOI of 1:1) and the plates were centrifuged for 30 minutes at 1200xg and 37°C. Twenty-four hours after transduction, the medium was replaced by supplemented RPMI with 5 µg/mL of puromycin (Calbiochem) for the selection of the transduced cells which were allowed to grow for at least a week before being used for infections with luciferase- or GFP-expressing *P. berghei* sporozoites to determine overall infection and parasite development by luminescence, flow cytometry and microscopy, as described above. Cells transduced with lentiviral particles carrying a negative control shRNA (SHC002) not targeting any annotated gene in the human genome were used as negative control. A stable cell line with the knockdown of SR-BI was used as positive control in the luminescence assays [210]. The knockdown efficiency of each shRNA sequence (Table 2.1) was

assessed by quantitative PCR (qPCR) with specific primers for each gene (Table 2.2).

siRNA transfection

$4.0x10^4$ Huh7 cells were reverse-transfected with 30nM of target specific (human AMPK α1: ref. L-005027-00-0005; human AMPK α2: ref. L-005361-00-0005) or control siRNA sequence pools (ON-TARGETplus SMARTpool, Dharmacon), using Lipofectamine RNAiMAX (Gibco/Invitrogen) according to the manufacturer´s instructions. Twenty-four hours after transfection, the cells were infected with $3.0x10^4$ GFP-expressing *P. berghei* sporozoites. Cells were collected for flow cytometry analysis at 48 hpi and analyzed on a BD LSR Fortessa flow cytometer with the DIVA software (version 6.2). Analysis was carried out using the FlowJo software (version 6.4.7, FlowJo). The efficiency of knockdown was assessed with specific primers by qPCR (Table 2.2).

FACS-sorting of *P. berghei*-infected and non-infected Huh7 cells

Huh7 cells ($1.0x10^5$ per well) were seeded in 24-well plates and infected 24 hours later with $1.0x10^5$ GFP-expressing *P. berghei* sporozoites. Cells were collected at 2 hpi and FACS-sorted on a BD FACSAria III Cell Sorter (BD Biosciences). Non-infected and GFP-expressing *P. berghei*-infected cells were gated on the basis of their different fluorescence intensity, as previously established, and collected simultaneously [11, 163]. Immediately after FACS-sorting, both infected and non-infected cells were washed and seeded in 24-well plates at a density of $1.5x10^5$ per well. Infected cells were diluted 1:1 with non-infected cells to allow replicates. Cells were then incubated until being collected at 30 or 48 hpi. In the case of the 6 hpi time point, *P. berghei*-infected cells were FACS-sorted at this time, diluted 1:1 with non-infected cells, pelleted, snap-frozen and stored until RNA extraction using the High Pure RNA Isolation kit (Roche) according to the manufacturer´s instructions.

Table 2.1 - List of shRNA sequences used, with the corresponding knockdowns.

Protein	Gene	Gene ID	Sequence	Clone ID	Oligonucleotide Sequence	Knockdown
GLUT1	*SLC2A1*	NM_006516	#01	TRCN0000043583	CCGGGCCACACTATTACCATGAGAACTCGAGTTCTCATGGTAATAGTGTGGCTTTTTG	90%
			#02	TRCN0000043584	CCGGGCGGAATTCAATGCTGATGATCTCGAGATCATCAGCATTGAATTCCGCTTTTTG	80%
			#03	TRCN0000043585	CCGGCTTCTATTACTCCACGAGCATCTCGAGATGCTCGTGGAGTAATAGAAGTTTTTG	40%
GLUT2	*SLC2A2*	NM_000340	#01	TRCN0000043598	CCGGGCCCACAATCTCATACTCAATCTCGAGATTGAGTATGAGATTGTGGGCTTTTTG	0%
			#02	TRCN0000043600	CCGGGCAAACATTCTGTCATTAGTTCTCGAGAACTAATGACAGAATGTTTGCTTTTTG	45%
			#03	TRCN0000043601	CCGGCGACGTTCTCTCTTTCTAATTCTCGAGAATTAGAAAGAGAGAACGTCGTTTTTG	70%
GLUT3	*SLC2A3*	NM_006931	#01	TRCN0000043614	CCGGCCTGAGAAGATCATAAAGGAACTCGAGTTCCTTTATGATCTTCTCAGGTTTTTG	80%
			#02	TRCN0000043615	CCGGAGTAGCTAAGTCGGTTGAAATCTCGAGATTTCAACCGACTTAGCTACTTTTTTG	95%
			#03	TRCN0000043617	CCGGCCCAGATCTTTGGTCTGGAATCTCGAGATTCCAGACCAAAGATCTGGGTTTTTG	60%
GLUT4	*SLC2A4*	NM_001042	#01	TRCN0000043629	CCGGCCTTCTTAAGAGTACCTGAAACTCGAGTTTCAGGTACTCTTAAGAAGGTTTTTG	90%
			#02	TRCN0000043630	CCGGCTTGAGTATTTAGGGCCAGATCTCGAGATCTGGCCCTAAATACTCAAGTTTTTG	60%
			#03	TRCN0000043632	CCGGGTGATTGAACAGAGCTACAATCTCGAGATTGTAGCTCTGTTCAATCACTTTTTG	80%
GLUT9	*SLC2A9*	NM_001001290	#01	TRCN0000043683	CCGGACGTTGGACAATTATGTCAAACTCGAGTTTGACATAATTGTCCAACGTTTTTTG	70%
			#02	TRCN0000043684	CCGGCGCTTCATCATGGGCATAGATCTCGAGATCTATGCCCATGATGAAGCGTTTTTG	25%
			#03	TRCN0000043685	CCGGCCATACCTGTTTGGAGTGATTCTCGAGAATCACTCCAAACAGGTATGGTTTTTG	70%
SR-BI	*SCARB1*	NM_005505		TRCN0000056966	CCGGGCAAGGTTGACTTCTGGCATTCTCGAGAATGCCAGAAGTCAACCTTGCTTTTTG	85%

In vivo WZB117 treatment and *P. berghei* sporozoites infection and quantification of parasite liver load by qPCR

Six weeks old male C57BL/6 mice were injected intraperitoneally (i.p.) with 10 mg/kg of WZB117 in PBS/DMSO 1:1 (v/v), or with vehicle alone, immediately before intravenous (i.v.) injection of $3.0x10^4$ GFP-expressing *P. berghei* sporozoites [367]. The administration of the drug or vehicle was repeated at 15 and 30 hours post-infection (hpi) and the livers were collected at 44 hpi and homogenized in 3 mL of denaturing solution (4 M guanidine thiocyanate; 25 mM sodium citrate pH 7, 0.5% *N*-lauroylsarcosine and 0.7% β mercaptoethanol in DEPC-treated water). Total RNA was extracted from the livers with the NZY Total RNA Isolation Kit (NZYTech), according to the manufacturer's protocol, and parasite load was quantified by qPCR using primers specific to *P. berghei* 18S RNA (Table 2.2). Mouse Hprt expression was used for normalization.

Immunohistochemical staining of liver sections

For microscopy, PFA-fixed liver lobes were cut in 50 µm sections and were incubated in permeabilization/blocking solution (1% w/v BSA, 0.5% v/v Triton-X100 in PBS) at room temperature for 1 h, followed by a 2 h incubation at room temperature with an anti-UIS4 antibody (dilution 1:500). Slices were further incubated in a 1:300 dilution of anti-GFP-Alexa488 antibody (Invitrogen) and anti-goat Alexa-Fluor 568 (Invitrogen) in the presence of a 1:1000 dilution of Hoechst 33342 (Invitrogen) and a 1:100 dilution of Phalloidin-660 (Invitrogen) for actin staining for 1 h. After washing, slices were mounted on microscope slides with Fluoromount (SouthernBiotech). Images were acquired and processed as previously described.

RNA extraction and quantification

RNA was extracted from cultured Huh7 cells using the High Pure RNA Isolation kit (Roche) according to the manufacturer´s instructions. The amount of RNA in each sample was assessed with a NanoDrop® ND-1000 spectrophotometer.

cDNA synthesis and qPCR

Complementary DNA (cDNA) was synthesized from 1 µg of RNA using the Roche cDNA synthesis kit, according to the manufacturer´s instructions. The cDNA was synthesized employing the following thermocycling parameters: 25°C for 10 minutes, 55°C for 30 minutes, and 85°C for 5 minutes. qPCR reaction was performed in a total volume of 20 µL in a ABI Prism 7500 Fast system (Applied Biosystems) using the iTaq^{TM} Universal SYBR® Green kit (BioRad) as follows: 50°C for 2 minutes, 95°C for 10 minutes, 40 cycles at 95°C for 15 seconds and 60°C for 1 minute, melting stage was done at 95°C for 15 seconds, 60°C for 1 minute, and 95°C for 30 seconds. Primers for the housekeeping gene hypoxanthine-guanine phosphoribosyltransferase (*HPRT*) were used for normalization in all experiments (Table 2.2). For qPCR, the delta-delta CT relative quantification method was used.

Table 2.2 - List of primer sequences used.

Gene	forward primer (5' - 3')	reverse primer (5' - 3')
SLC2A1	CGTCGCCACCCGCGTAC	AACTCCTCGATCACCTTCTGGGG
SLC2A2	AGATAAGGTCACTGGGACCCTGGT	GCTTTTCGGTCATCCAGTGGAACA
SLC2A3	GGACGTGGAGAAAACTTGCTGCTG	GCCGATTGTAGCAACTGTGATGGCA
SLC2A4	AGACGAGATGCCGTCGGGCT	TGTTCAATCACCTTCTGAGGGGCA
SLC2A9	CAAGAGCTGTGAAAGCCTTCC	ATGGTGACAATCACGGTGACC
SCARB1	AGAATAAGCCCATGACCCTGAA	TGAGCTCAGCAAATAATCCGAA
AMPK α1	AGGAGAGCTATTTGATTATATCTGTAAGAATG	ACACCAGAAAGGATCTGTTGGAA
AMPK α2	CGGCTCTTTCAGCAGATTCTGT	ATCGGCTATCTTGGCATTCATG
Pb18S	AAGCATTAAATAAAGCGAATACATCCTTAC	GGAGATTGGTTTTGACGTTTATGTG
HPRT	TTTGCTGACCTGCTGGATTAC	CAAGACATTCTTTCCAGTTAAAGTTG

Determination of ATP levels inside single cells by live microscopy

Huh7 cells (2.0x10^5 cells) were seeded on glass bottom microwell dishes (MatTek). The following day, 1 µg of ATeam plasmid carrying the ATP indicator (pRSET-AT1.03) was transfected into the cells with FuGENE 6 (Roche) according to the manufacturer's instructions [368]. Twenty-four hours after transfection, cells were infected with RFP-expressing *P. berghei* sporozoites and, at selected time points of infection, were visualized at 37°C on a Zeiss LSM 710 confocal microscope as described previously [369]. Huh7 cells incubated for 6 hours in

RPMI without glucose with 10 mM of galactose and 10 µM of Oligomycin were used as positive controls for ATP depletion. Image analysis was performed using the ImageJ software (version 1.47). The Venus/CFP emission ratio was calculated for each cell dividing its mean intensity in the Venus channel by the mean intensity in the CFP channel.

Quantification of GLUT1 at the plasma membrane of infected cells by flow cytometry

Huh7 cells ($1.0x10^4$ per well) were seeded in 96-well plates and were infected with RFP-expressing *P. berghei* sporozoites on the following day. Thirty and 48 hours after infection, cells were detached using PBS containing 1 mM EDTA, centrifuged at 4°C, and the cell pellet was resuspended in cold RPMI containing 10% FBS. Cells were further incubated with supernatant obtained from 293T cells transfected with a vector encoding the H_{RBD}-EGFP fusion protein (dilution 1:50 in PBS with 2% FBS) [352, 370]. Following incubation at 37°C for 30 minutes, cells were harvested by centrifugation, washed one time with PBS with 2% FBS, resuspended in the same buffer and analyzed with a BD LSR Fortessa cytometer with the DIVA software (version 6.2). Huh7 cells incubated overnight in complete RPMI with 250 µM of cobalt (II) chloride ($CoCl_2$) were used as positive controls [371]. Analysis was carried out using the FlowJo software (version 6.4.7, FlowJo).

Statistical Analyses

Statistical analyses were performed using the GraphPad Prism 5 software. One-way ANOVA, Two-way ANOVA, Chi-Square, Mann-Whitney U test or Student's t-test were used for significance of differences observed, as indicated in each figure. ns – not significant, * $p < 0.05$, ** $p < 0.01$ and *** $p < 0.001$.

Results

Effect of glucose on *P. berghei* hepatic infection

In order to evaluate glucose requirements throughout the liver stage of infection, Huh7 cells, a human hepatoma cell line, were infected with luciferase-expressing *P. berghei* sporozoites in the presence of varying concentrations of glucose. Glucose concentrations ranged from 1.25 to 20 mM, which includes and expands the physiological range of glucose concentrations, 2.5-10 mM [372]. Luminescence intensity, a correlate of parasite load, and cell viability were measured near the end of hepatic parasite development, at 48h after infection [358]. Our results show that an increase in glucose availability correlates with an increase of overall *Plasmodium* infection (Fig. 2.1A). In contrast, any glucose concentration below the standard medium ≈10 mM concentration significantly impairs infection (Fig. 2.1A), demonstrating that glucose is required for a successful hepatic *Plasmodium* infection. Cell viability was not affected by the presence of an excess of glucose in the medium, but decreased for 2.5 and 1.25 mM of glucose (Fig. 2.1A).

In order to dissect how glucose influences hepatic infection, we employed an established flow cytometry-based approach that makes use of GFP-expressing *P. berghei* parasites to determine the number of infected cells and to measure parasite development [163]. The analysis of cells 2 hours after sporozoite addition, when the invasion process is virtually completed, shows that glucose concentration does not affect the ability of parasites to invade cells (Fig. 2.1B) [163]. Conversely, when cells were analyzed 48 hours after infection, a glucose-dependent increase in parasite development was observed (Fig. 2.1C). These results also showed that the number of infected cells is higher at 20 mM glucose concentration than at glucose concentrations below the physiological range, suggesting that glucose availability influences the survival of infected cells. These results were further confirmed by immunofluorescence microscopy analysis, which demonstrated that parasite size is proportional to the amount of glucose in the medium and that the survival of intra-hepatic parasites 48 hours after infection depends on the availability of glucose (Fig. 2.1D, E). In fact, at low glucose concentrations, not only are most parasites very small (<50 μm^2) but also the

number of infected cells is very low. Increasing concentrations of glucose lead to higher numbers of parasites and favor parasite growth, with approximately 40% of the parasites being larger than 200 µm^2 at 10 and 20 mM glucose (Fig. 2.1E). Overall, these results demonstrate that glucose availability plays an important role in the intra-hepatic development and survival of *Plasmodium* parasites.

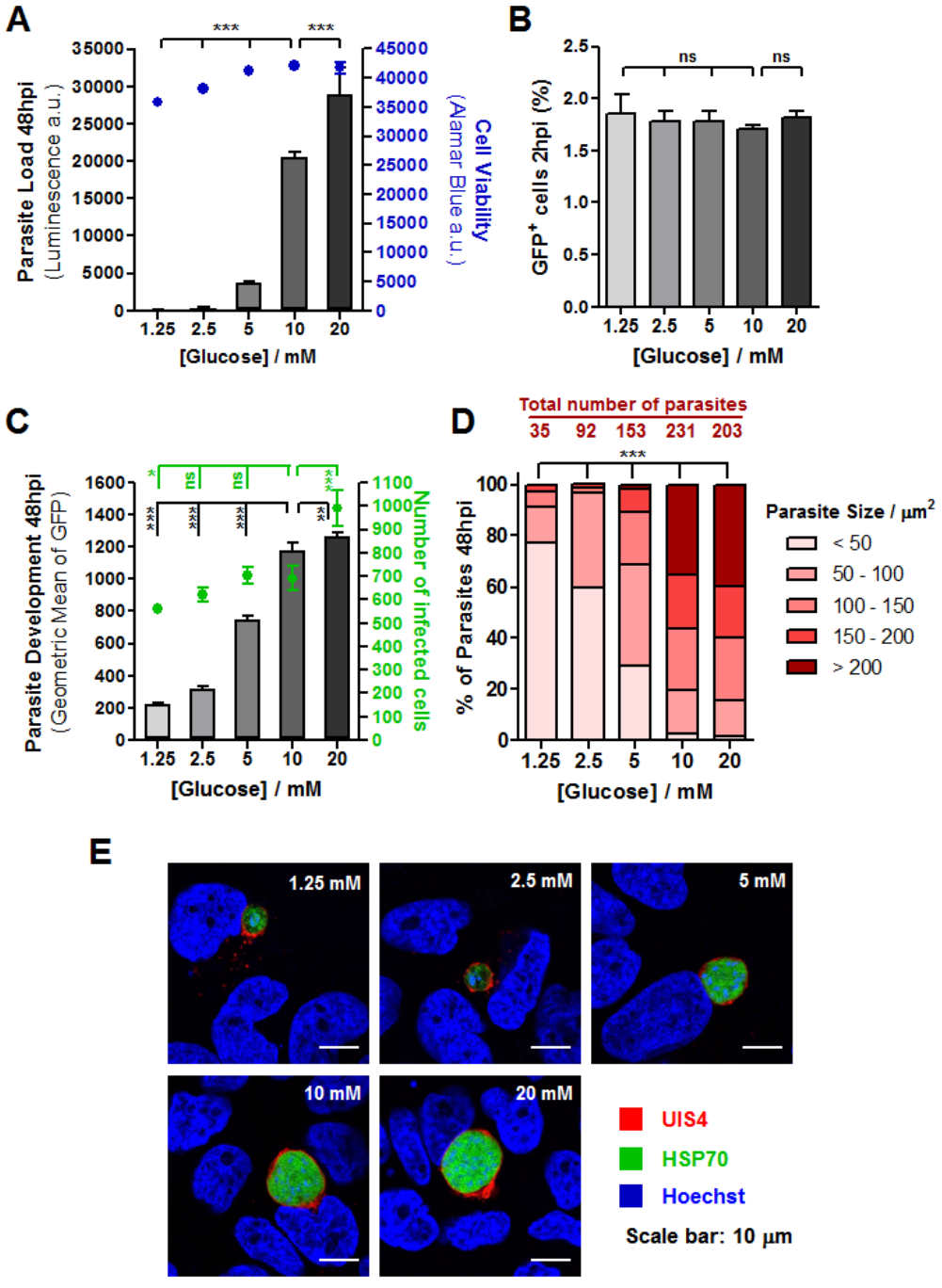

Figure 2.1 - Glucose availability highly impacts *P. berghei* hepatic infection. (A) Huh7 cells were infected with luciferase-expressing *P. berghei* sporozoites and the culture medium was replaced 2 hpi by medium with different concentrations of glucose. Parasite load (luminescence) and cell viability were assessed after 48 hours. Representative

experiment out of 2 independent experiments. Error bars represent SD. One-way ANOVA with post-test Dunnett. **(B)** The culture medium of Huh7 cells was replaced by medium with different concentrations of glucose 1 hour prior to infection with GFP-expressing sporozoites. Cell invasion was quantified by determining the percentage of GFP^+ cells 2 hpi by flow cytometry. Representative experiment out of 2 independent experiments. Error bars represent SD. One-way ANOVA with post-test Dunnett. **(C)** Huh7 cells were infected with GFP-expressing *P. berghei* sporozoites and the culture medium was replaced 2 hpi by media with different concentrations of glucose. Parasite development and the total number of infected cells were assessed by flow cytometry by determining the fluorescence intensity and the number of GFP^+ cells at 48 hpi, respectively. Representative experiment out of 5 independent experiments. Error bars represent SD. One-way ANOVA with post-test Dunnett. **(D)** For each glucose concentration, the EEFs in the acquired fluorescent microscopy images were counted and their area was determined. EEFs were divided into 5 different size classes. Pool of 2 independent experiments. Chi-square test. **(E)** Representative confocal images of Huh7 cells infected with sporozoites and incubated in medium with different concentrations of glucose for 48 hours. The cells were immunostained with anti-UIS4 (red), anti-HSP70 (green) and Hoechst (blue). Scale bar, 10 µm. ns - not significant, * $p < 0.05$, ** $p < 0.01$ and *** $p < 0.001$.

Glucose uptake is specifically increased in hepatic cells containing replicating *P. berghei* parasites

Having demonstrated a fundamental role for glucose during intra-hepatic *P. berghei* development, we then sought to determine whether glucose uptake is specifically enhanced in infected cells and whether this is linked to parasite replication within these cells. To this end, we employed flow cytometry to monitor the uptake of a fluorescent glucose derivative, 2-NBDG, by *P. berghei*-infected cells [360, 361]. Huh7 cells were incubated with 2-NBDG and analyzed at different time points following addition of RFP-expressing *P. berghei* sporozoites. The uptake of 2-NBDG was measured as an increase in green fluorescence intensity, whereas parasite development was monitored as a function of red fluorescence intensity. The latter enables distinguishing the population of cells containing replicating parasites from a smaller population of cells containing parasites whose development is impaired (Fig. 2.2A) [163]. Our results clearly show that glucose uptake is highly increased in cells containing developing parasites, from 30 hpi onwards (Fig. 2.2B). A smaller increase in glucose uptake is also observed at

around the same time in non-infected cells and in cells containing non-developing parasites, present in the same well (Fig. 2.2B).

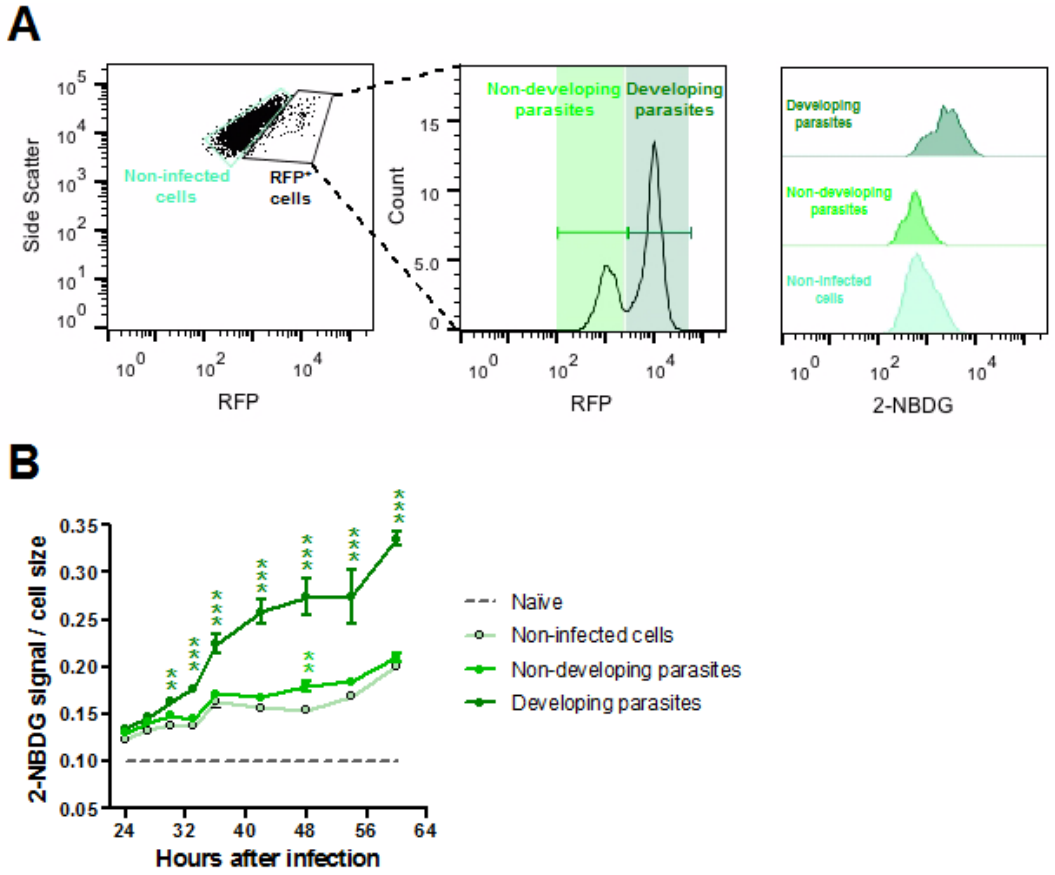

Figure 2.2 - Glucose uptake is increased in hepatoma cells containing developing P. *berghei* parasites. (A) Huh7 cells were infected with RFP-expressing *P. berghei* sporozoites and incubated with medium with 2-NBDG, a fluorescent glucose derivative, at different time points of infection. Dot plot represents non-infected and infected (RFP^+) cells of one replicate from the 48 hours time point. Left histogram shows the different fluorescence intensity displayed by non-developing (RFP^{low}) and developing (RFP^{high}) parasites. Right histogram exemplifies the 2-NBDG uptake by the different cell populations (non-infected, non-developing and developing parasites), assessed as an increased fluorescence intensity in the green channel. **(B)** 2-NBDG uptake by the several cell populations, normalized to cell size, at different time points of infection, assessed by flow cytometry. Error bars represent SD. Two-way ANOVA with post-test Bonferroni. ** $p < 0.01$ and *** $p < 0.001$.

Since it is known that hepatic glucose uptake and metabolism are influenced by factors such as feeding/fasting, exposure to low/high temperature, exercise, oxidative stress, several liver pathologies, such as steatosis and non-alcoholic fatty liver disease (NFLD), and liver infections, for example, by hepatitis

C virus (HCV), we sought to assess the specificity of the *P. berghei*-induced increase in glucose uptake by infected Huh7 cells [373-379]. To this end, we measured 2-NBDG by Huh7 cells subjected to conditions known to induce low-temperature stress in various types of mammalian cells, high-temperature stress in a chicken hepatocellular carcinoma cell line or oxidative stress in rat hepatocytes [362-365] (Fig. 2.3).

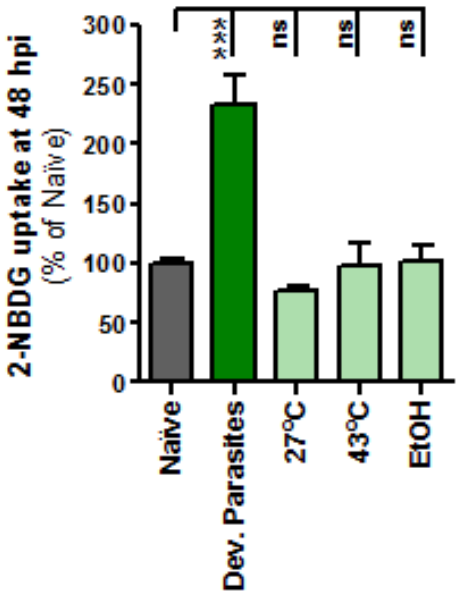

Figure 2.3 – The increased glucose uptake by *P. berghei*-infected cells is not recapitulated by exposure to temperature or oxidative stresses. 2-NBDG uptake by naïve Huh7 cells, cells containing developing *P. berghei* parasites and cells subjected to low-temperature, high-temperature and ethanol-induced oxidative stresses, assessed by flow cytometry. Pool of 2 independent experiments. Error bars represent SD. One-way ANOVA with post-test Dunnet. ns - not significant and *** $p < 0.001$.

Finally, we infected Huh7 cells with the wild type MHV68 at different MOI and did not observe any increase on 2-NBDG uptake 24 hours after infection (Fig. 2.4A). The percentage of virus-infected cells was estimated by infecting Huh7 cells with MHV68-YFP with the same MOI as the wild type and determining the percentage of YFP^+ cells 24 hours later by flow cytometry (Fig. 2.4B) [366]. Our data show that 2-NBDG is neither affected by any of the stress-inducing treatments employed, nor by any of the conditions of viral infection assessed, suggesting that the increase in glucose uptake by *P. berghei*-infected cells is not the result of an unspecific response to stress or to infection. Overall, these results show that *P. berghei* development inside infected Huh7 leads to a specific enhancement of glucose uptake by these cells.

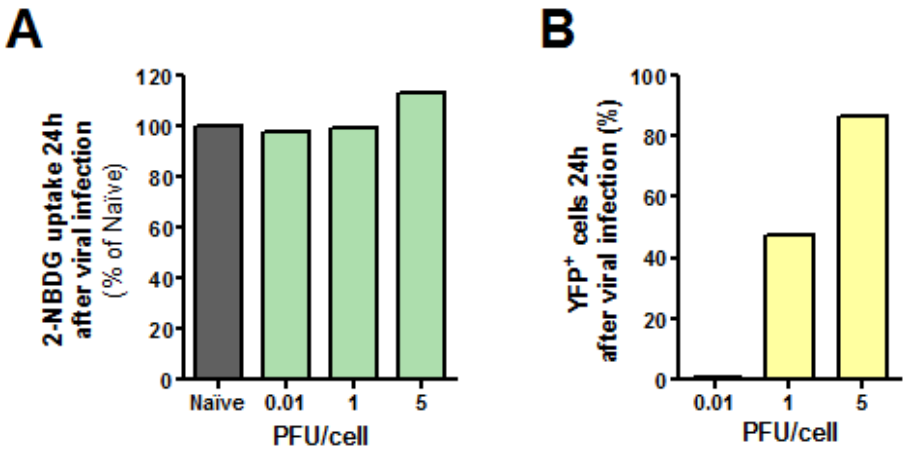

Figure 2.4 – Infection with MHV68 does not increase glucose uptake by virus-infected cells. (A) 2-NBDG uptake by naïve Huh7 cells and cells infected with MHV68 at different MOI, assessed by flow cytometry. **(B)** Percentage of YFP^+ cells 24 hours after infection with different loads of MHV68-YFP, assessed by flow cytometry.

RNAi study implicates GLUT1 in glucose uptake by *P. berghei*-infected hepatic cells

The results so far suggest that infection of hepatic cells by *Plasmodium* modulates the uptake of glucose by these cells, possibly through the enhancement of the activity of membrane glucose transporters in the cell. To ascertain this, we decided to carry out a small-scale RNAi study to evaluate the effect of the down-regulation of the expression of 5 membrane glucose transporters on *P. berghei* infection (see Table 2.1 from the Materials and Methods section). The screen included all class I GLUT transporters (GLUT1-4) as well as GLUT9, a major regulator of influx in HepG2 hepatoma cells [380].

Huh7 cells stably expressing shRNA sequences targeting the selected genes were constructed to be used throughout the RNAi study. The study proceeded in 3 consecutive steps, employing different established methods to measure hepatic infection by *Plasmodium*. In the first step, 3 shRNA sequences were used to silence each of the selected genes and the resulting stable cell lines were infected with luciferase-expressing *P. berghei* sporozoites. Forty-eight hours later, the parasite load in these cells was determined by measuring the bioluminescence of cell lysates. Each sequence was used in at least 4 independent experiments and a shRNA targeting SR-BI was employed as a positive control for infection decrease [210]. GLUT1 emerged as the transporter whose knockdown leads to the

strongest decrease in infection, with GLUT4 and GLUT9 knockdown yielding a more moderate effect (Fig. 2.5A). We then carried out a second step of the RNAi study, where the expression of only GLUT1, GLUT4 and GLUT9 was silenced prior to infection with GFP-expressing *P. berghei* parasites. The extent of parasite development was assessed 48 hours later by flow cytometry determination of GFP intensity [163]. The results showed that the knockdown of GLUT1 leads to the strongest impairment of parasite development among the transporters assessed (Fig. 2.5B). Therefore, GLUT1 was selected for a final confirmation step using the three shRNA sequences targeting the GLUT1-encoding gene and assessment of parasite development by immunofluorescence microscopy (Fig. 2.5C). Interestingly, these imaging data demonstrated that parasite size correlates with the expression levels of GLUT1, suggesting that GLUT1-mediated glucose uptake is required for the parasite's replication.

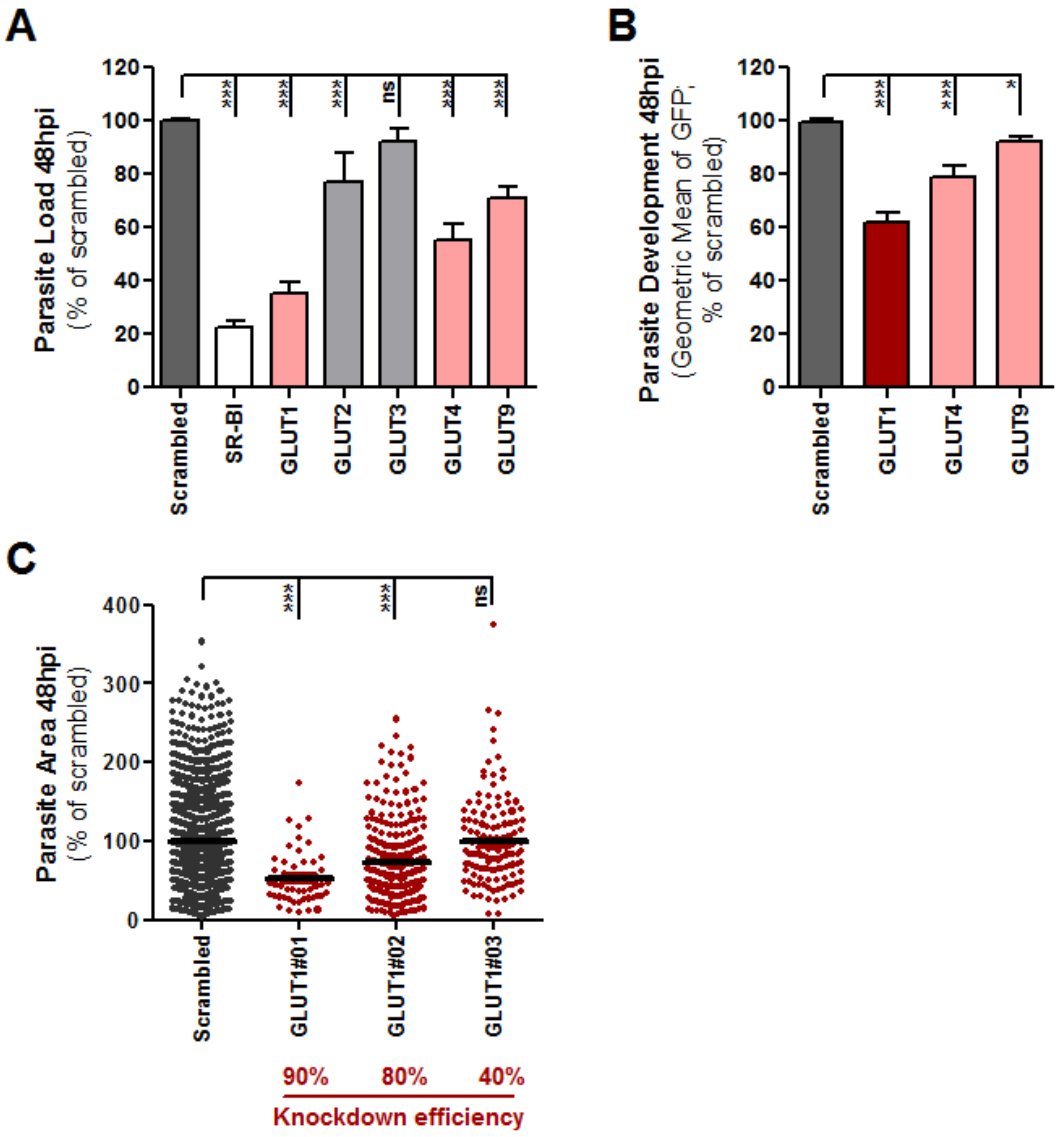

Figure 2.5 - GLUT1 knockdown significantly impairs *P. berghei* intra-hepatic development. (A) Huh7 cells with stable knockdown of one of the 5 GLUTs tested were infected with luciferase-expressing *P. berghei* sporozoites and parasite load (luminescence) was assessed after 48 hours. A scrambled shRNA sequence was used as a negative control and a cell line with stable knockdown of SR-BI as positive control. Pool of 4 independent experiments. Error bars represent SEM. **(B)** Huh7 cells with the knockdown of GLUT1, GLUT4 or GLUT9 were infected with GFP-expressing *P. berghei* sporozoites and parasite development was assessed by flow cytometry at 48 hpi. Pool of 3 independent experiments. Error bars represent SEM. **(C)** Quantification of the area of the EEFs in each of the 3 different cell lines with GLUT1 knockdown at 48 hpi by immunofluorescence microscopy. The knockdown efficiency of each shRNA sequence is indicated. Pool of 3 independent experiments. All panels: one-way ANOVA with post-test Dunnett. ns - not significant, * $p < 0.05$ and *** $p < 0.001$.

To further establish a link between the uptake of glucose by GLUT1 and *Plasmodium* infection, we assessed the difference of 2-NBDG uptake by infected and non-infected Huh7 cells expressing the same three GLUT1-targeting shRNA sequences as above. As previously shown, infected control cells were found to uptake significantly more fluorescent glucose than their non-infected counterparts at 48 hpi. However, this difference in 2-NBDG uptake by infected and non-infected cells was reduced by up to 40% in the GLUT1-knockdown stable cell lines, a decrease that is proportional to the extent of the down-modulation of GLUT1 (Fig. 2.6A). Only when GLUT1 expression is 90% reduced, we can see a decrease in glucose uptake by non-infected cells, thus it seems that GLUT1 knockdown primarily affects glucose uptake by infected cells (Fig. 2.6B). As control, we assessed the 2-NBDG uptake following knockdown of GLUT2, the main glucose transporter in the liver, showing that the down-modulation of the expression of this transporter does not affect 2-NBDG uptake by infected cells (Fig. 2.6A).

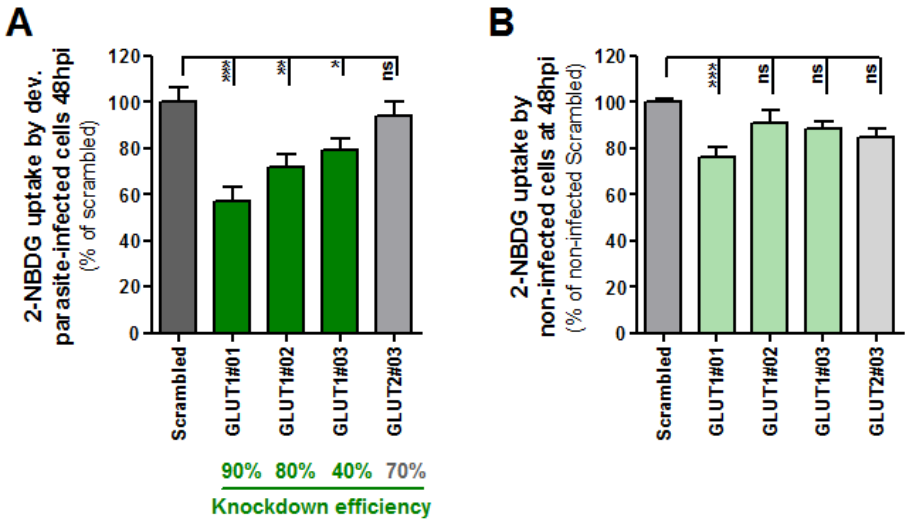

Figure 2.6 - GLUT1 knockdown significantly impairs glucose uptake into *P. berghei*-infected cells. (A) Difference of 2-NBDG uptake in the several cell lines with GLUT1 knockdown by developing parasites-containing cells and non-infected cells at 48 hpi, assessed by flow cytometry. A cell line with the knockdown of GLUT2 was used as a control. Pool of 4 independent experiments. Error bars represent SEM. **(B)** 2-NBDG uptake only by non-infected cells in the several cell lines with GLUT1 knockdown at 48hpi, assessed by flow cytometry. Pool of 4 independent experiments. Error bars represent SEM. Both panels: one-way ANOVA with post-test Dunnett. ns - not significant, * $p < 0.05$, ** $p < 0.01$ and *** $p < 0.001$.

To provide a chemical validation of the results obtained by the previously employed genetic approach, we assessed infection, parasite development, and 2-NBDG uptake by infected cells, in the presence of WZB117, a specific inhibitor of GLUT1-mediated glucose transport [367]. Our results show a clear dose-dependent effect of WZB117 on *P. berghei* infection of Huh7 cells (Fig. 2.7A), which correlates to a decreased parasite development, as assessed by flow cytometry (Fig. 2.7B). Similarly, 2-NBDG uptake by infected cells is affected in a dose-dependent manner (Fig. 2.7C). Taken together, these data indicate that the membrane transporter GLUT1 has a pivotal contribution to glucose uptake by the infected host cell, as required by the replicating parasite during its hepatic developmental process.

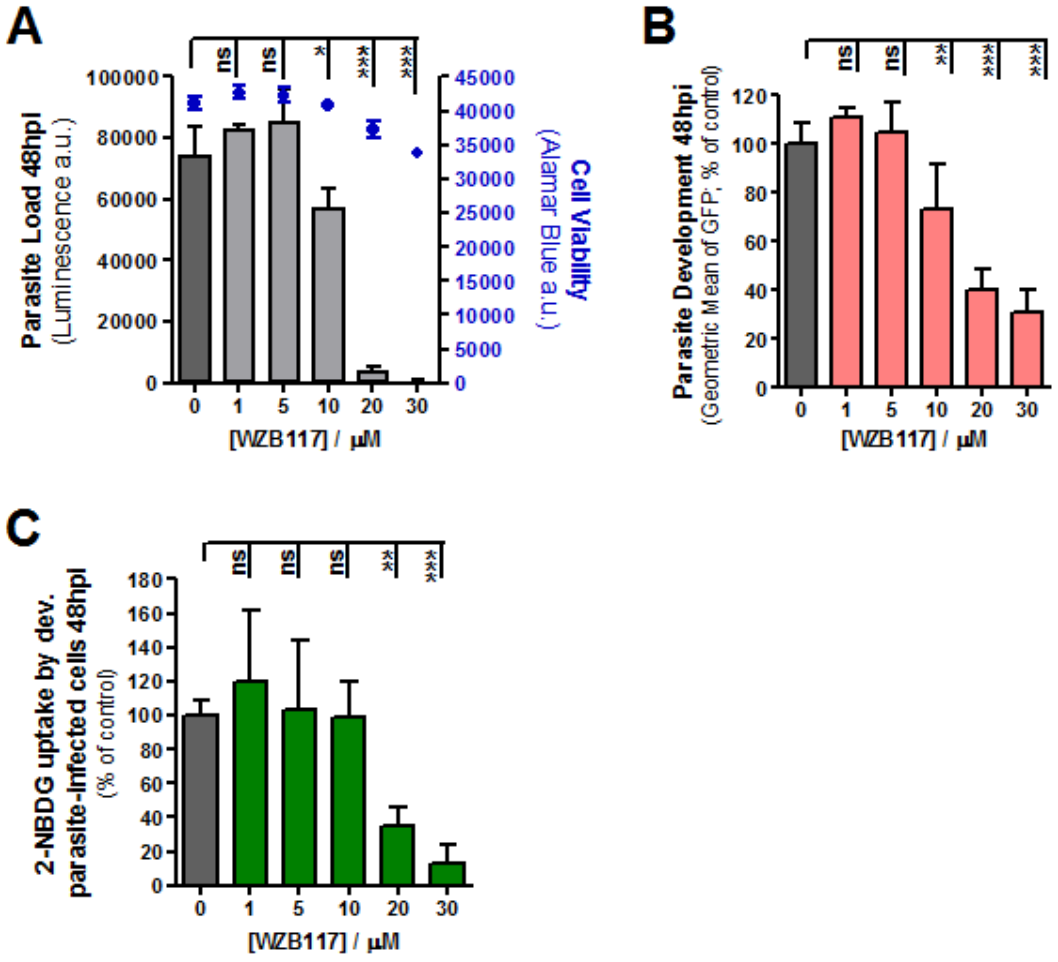

Figure 2.7 – Chemical inhibition of GLUT1-mediated glucose transport with WZB117 impairs *P. berghei* intra-hepatic development and glucose uptake by infected cells. **(A)** Huh7 cells were infected with luciferase-expressing *P. berghei* sporozoites and 2 hours later the culture medium was replaced by medium with increasing concentrations of WZB117. Parasite load (luminescence) was assessed at 48 hpi. Representative

experiment out of 2 independent experiments. Error bars represent SD. **(B)** Huh7 cells were infected with RFP-expressing *P. berghei* sporozoites and 2 hours later the culture medium was replaced by medium with increasing concentrations of WZB117. Parasite development was assessed by flow cytometry at 48 hpi. Pool of 2 independent experiments. Error bars represent SD. **(C)** 2-NBDG uptake by RFP-expressing *P. berghei*-infected cells at 48 hpi after treatment with increasing concentrations of WZB117, assessed by flow cytometry. Pool of 2 independent experiments. All panels: one-way ANOVA with post-test Dunnett. ns - not significant, * $p < 0.05$, ** $p < 0.01$ and *** $p < 0.001$.

Finally, we evaluated the role of GLUT1 on *Plasmodium* hepatic infection *in vivo*. C57BL/6 mice received three i.p. injections of 10 mg/kg of WZB117 in PBS/DMSO 1:1 (v/v), or vehicle alone, the first administration being immediately before the i.v. injection of $3.0x10^4$ GFP-expressing *P. berghei* sporozoites, and the other two at 15 and 30 hpi [367]. Livers were collected at 44 hpi and parasite load was determined by qPCR. Our results show a statistically significant 50% reduction on *P. berghei* liver load upon treatment with WZB117 (Fig. 2.8A). This decrease is mainly explained by a reduction in the number of parasites per area of liver (Fig. 2.8C), although a small effect on parasite size was also observed (Fig. 2.8B and D). Even though GLUT1 is not the main glucose transporter in the liver, its inhibition with WZB117 has a high impact on the survival of *P. berghei* parasites *in vivo*. Because GLUT1 is only at the membrane of the few pericentral hepatocytes of each chord, we hypothesize that the parasites inside these specific hepatocytes might be preferentially targeted by the treatment with this inhibitor.

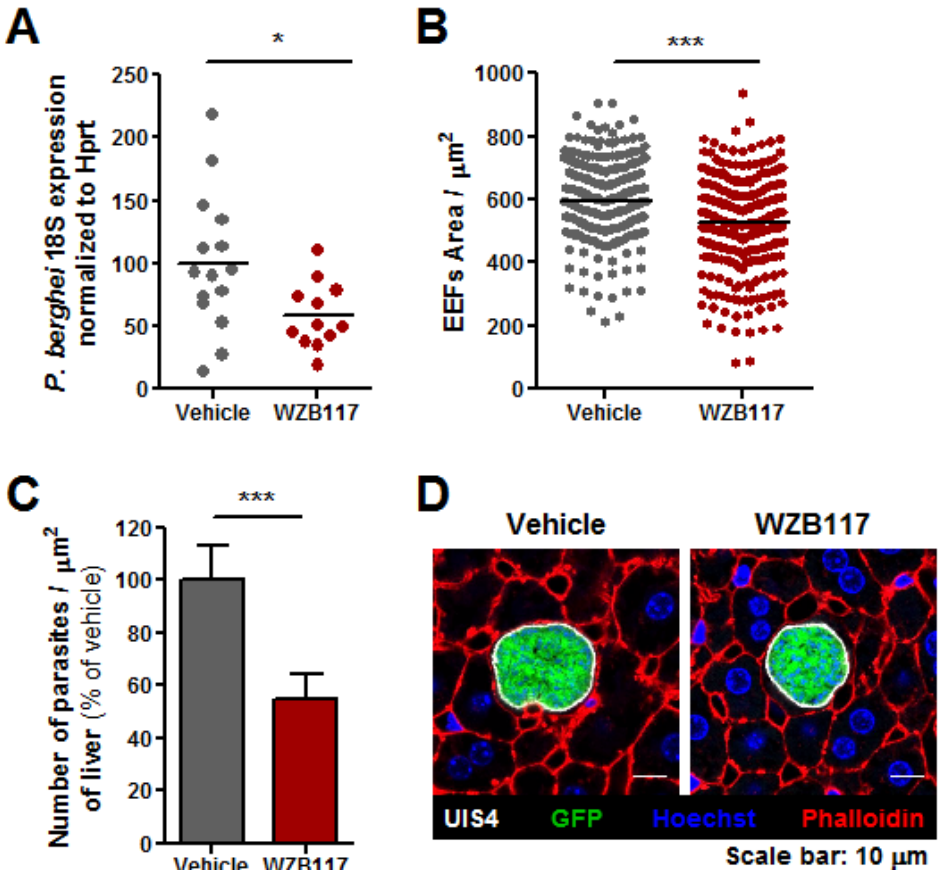

Figure 2.8 – *In vivo* inhibition of GLUT1-mediated glucose transport with WZB117 decreases the number of *P. berghei* parasites in the liver of C57BL/6 mice. (A) Mice received three doses of 10 mg/kg of WZB117 i.p., the first immediately before infection with *P. berghei* sporozoites and the other two at 15 and 30 hpi. Parasite load was assessed at 44 hpi by qPCR. Pool of 3 independent experiments. Vehicle: n = 15 mice; WZB117-treated: n = 12 mice. Two-tailed Mann-Whitney test. **(B)** A liver lobe of one mouse from each group was cut in 50µm sections and the parasites were stained with anti-UIS4 (red) and Hoechst (blue) for area determination by fluorescence microscopy. Representative experiment out of 2 independent experiments. Two-tailed Mann-Whitney test. **(C)** Number of parasites observed per area of liver in the control (vehicle) or the WZB117-treated mouse. Two-tailed Mann-Whitney test. **(D)** Representative confocal images of *P. berghei* parasites in both groups of mice. Scale bar, 10 µm. * $p < 0.05$ and *** $p < 0.001$.

GLUT1 expression is not enhanced in *Plasmodium*-infected cells

Having established a role for GLUT1 on the specific uptake of glucose by infected cells, we hypothesized that *Plasmodium* infection might lead to an increase in the expression of that transporter. To address this, we compared GLUT1 expression

levels in non-infected and infected Huh7 cells at 6, 30 and 48 hpi with GFP-expressing *P. berghei* parasites. Following the separation of infected and non-infected cells by fluorescence-activated cell sorting (FACS), cells were analyzed by qPCR, employing GLUT1-specific primers (see Table 2.2) [11]. The data showed no significant differences in GLUT1 expression between infected and non-infected cells, at the selected time points (Fig. 2.9). As such, we concluded that the increase in GLUT1-mediated glucose uptake by *Plasmodium*-infected cells does not result from an infection-induced enhancement of the expression of this transporter.

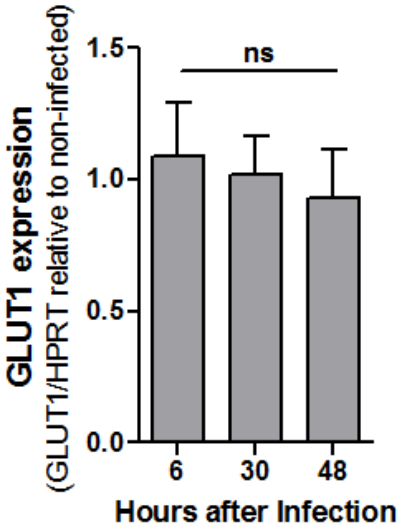

Figure 2.9 - GLUT1 expression is not altered in *P. berghei*-infected cells. Quantification of GLUT1 transcriptional expression on sorted infected and non-infected Huh7 cells by qPCR. Each time point is a pool of 2 independent sortings. Error bars represent SD. Two-tailed Mann-Whitney test. ns – not significant.

P. berghei development leads to cytoplasmic ATP depletion

It has been shown that cytoplasmic ATP interacts with GLUT1 to induce conformational changes that inhibit GLUT1-mediated glucose transport [381, 382]. This modulation by ATP is inhibited by AMP and ADP [383]. We thus wondered whether the observed increase in glucose uptake by *Plasmodium*-infected cells would correlate to a decrease in ATP levels in these cells. To investigate this, we employed a fluorescence resonance energy transfer (FRET)-based indicator for ATP (ATeam), composed of the ε subunit of the bacterial F_oF_1-ATP synthase sandwiched by the cyan- and Venus fluorescent proteins (CFP and Venus, respectively), which enables monitoring intracellular ATP levels as a function of the Venus/CFP ratio [368]. Using RFP-expressing *P. berghei* parasites and live fluorescence microscopy, we specifically monitored ATP levels in non-infected and infected cells at 30 and 48h after infection. Interestingly, we observed that ATP

levels of infected cells were significantly lower than those of naïve cells (Fig. 2.10). In agreement with the results in Figure 2.2B, we also detected a smaller but significant ATP reduction in the non-infected cells present in the same well, when compared to naïve cells (Fig. 2.10). These results indicate that intra-hepatic parasite development leads to a small but significant decrease in the ATP/AMP ratio inside the host cell, which could result in the well-described ATP/ADP/AMP-driven conformational changes in GLUT1 and ultimately lead to an increased glucose uptake [381-383].

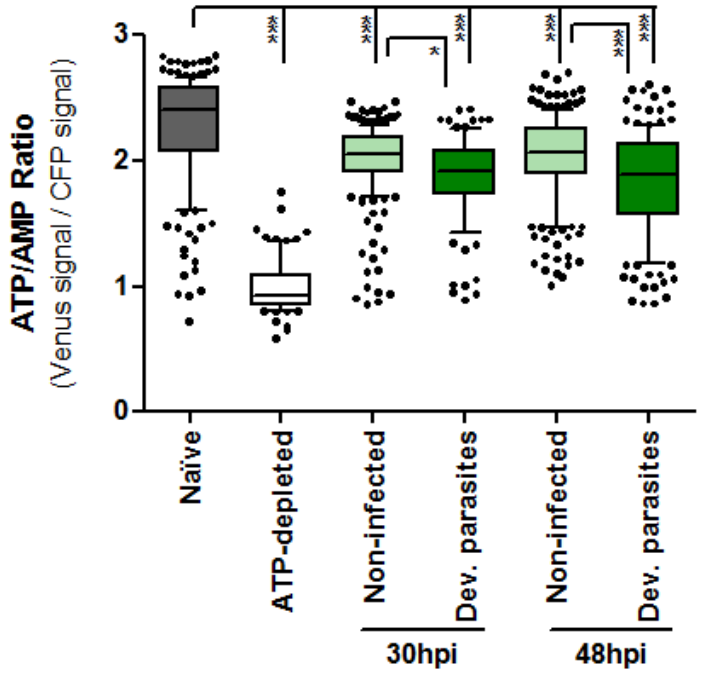

Figure 2.10 - *P. berghei* development inside Huh7 cells results in a decreased ATP/AMP ratio. Huh7 cells were transfected with an ATP probe, AT1.03, and infected with RFP-expressing *P. berghei* sporozoites. Thirty and 48 hpi, the Venus/CFP emission ratio in the cytoplasm of each individual cell (non-infected and cells containing developing parasites) was calculated from the fluorescent images acquired in both channels. Huh7 cells incubated in RPMI without glucose with 10 mM of galactose and 10 µM of oligomycin were used as positive controls for ATP depletion. Pool of 2 and 3 independent experiments for the 30 hours and 48 hours time points, respectively. One-way ANOVA with post-test Tukey. * $p < 0.05$ and *** $p < 0.001$.

A pathogen-induced decrease in cytoplasmic ATP is typically associated with activation of AMP-activated protein kinase (AMPK) [384]. Also, an enhancement of glucose transport by GLUT1 transporters preexisting in the plasma membrane has

been associated with stimulation of AMPK activity [385, 386]. Thus, we next compared 2-NBDG uptake by infected and non-infected wild type (WT) and AMPK-deficient (knockout for both α1 and α2 AMPK subunits, AMPK-dKO) mouse embryonic fibroblasts (MEFs). Crucially, 2-NBDG uptake was not impaired by AMPK-deletion (Fig. 2.11A), suggesting that this kinase does not play a role in the increase of glucose uptake in *Plasmodium*-infected hepatic cells. This was further confirmed by measuring *P. berghei* infection of Huh7 cells and 2-NBDG uptake by infected and non-infected cells, following the knockdown of the expression of both the α1 and the α2 subunits of AMPK by RNAi. Our results show that the effective knockdown of gene expression (Fig. 2.11B) did not impair parasite development (Fig. 2.11C), nor did impact the uptake of 2-NBDG by infected cells (Fig. 2.11D). Collectively, these results rule out a role for AMPK in the increased uptake of glucose by cells containing developing *Plasmodium* parasites.

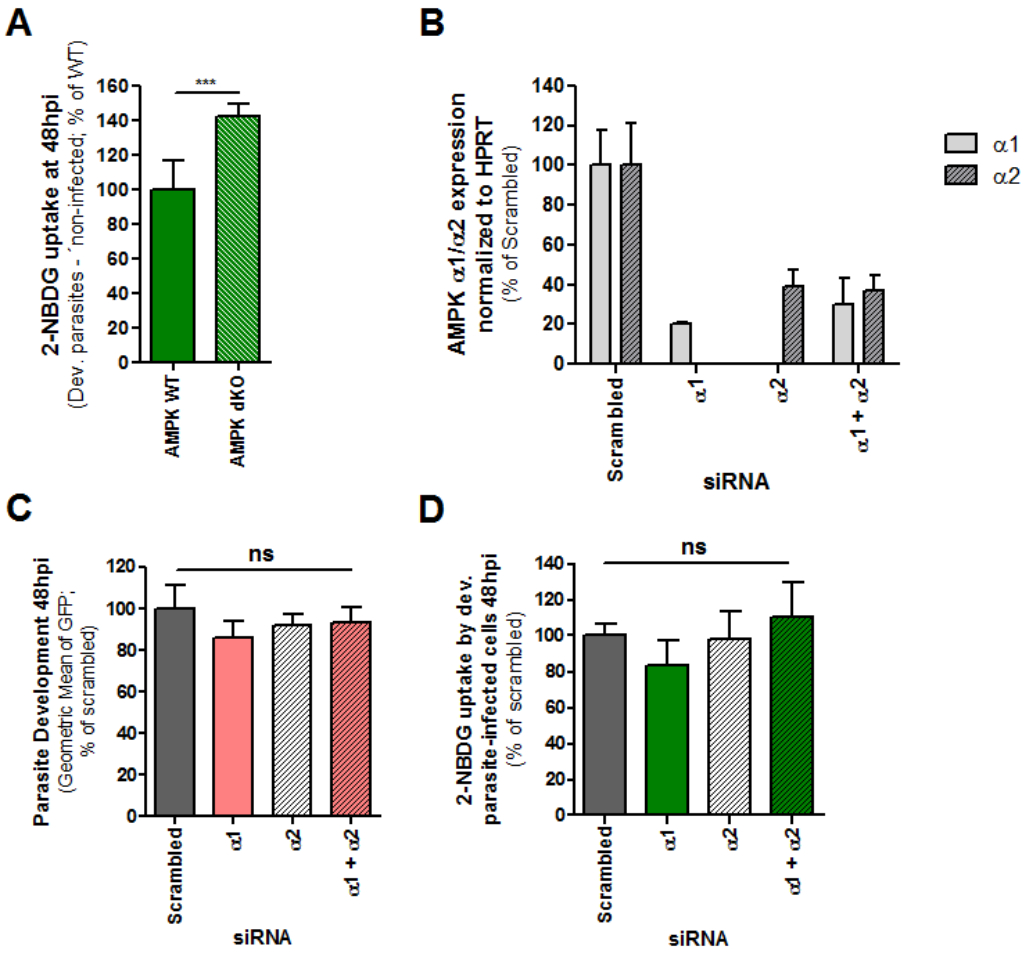

Figure 2.11 – Increased GLUT1-dependent glucose uptake into *P. berghei*-infected cells is independent of AMPK. (A) WT and AMPK-dKO MEFs were infected with RFP-expressing sporozoites and incubated with medium with 2-NBDG, 48 hours after infection.

The difference of 2-NBDG uptake by cells containing developing parasites and non-infected cells was assessed for both cell lines by flow cytometry. Pool of 2 independent experiments. Error bars represent SD. Two-tailed unpaired t-test. **(B)** Knockdown efficiency upon transfection in Huh7 cells of the siRNAs used against the α1 and α2 subunits of AMPK. **(C)** Huh7 cells with the knockdown of α1 or/and α2 subunits of AMPK were infected with GFP-expressing *P. berghei* sporozoites and parasite development was assessed by flow cytometry at 48 hpi. Pool of 2 independent experiments. Error bars represent SD. One-way ANOVA with post-test Dunnett. **(D)** 2-NBDG uptake at 48 hpi by developing parasites-containing cells with the knockdown of α1 or/and α2 subunits of AMPK, assessed by flow cytometry. Representative experiment out of 2 independent experiments. Error bars represent SD. One-way ANOVA with post-test Dunnett. ns - not significant, *** $p < 0.001$.

P. berghei infection leads to GLUT1 translocation to the plasma membrane

It has been shown that GLUT1 translocation to the plasma membrane may be triggered by different factors, such as ischemia and insulin, in a phosphoinositide 3-kinase (PI3K)-dependent fashion [387, 388]. Although no effect on parasite load (Fig. 2.12A and B), nor on the specific uptake of glucose by infected cells (Fig. 2.12C and D), was observed in the presence of increasing concentrations of insulin or of the PI3K irreversible inhibitor, Wortmannin, we hypothesized that there could exist a PI3K-independent mechanism responsible for the translocation of GLUT1 to the membrane of *P. berghei*-infected cells that could contribute to the observed increase in GLUT1-mediated glucose uptake upon infection.

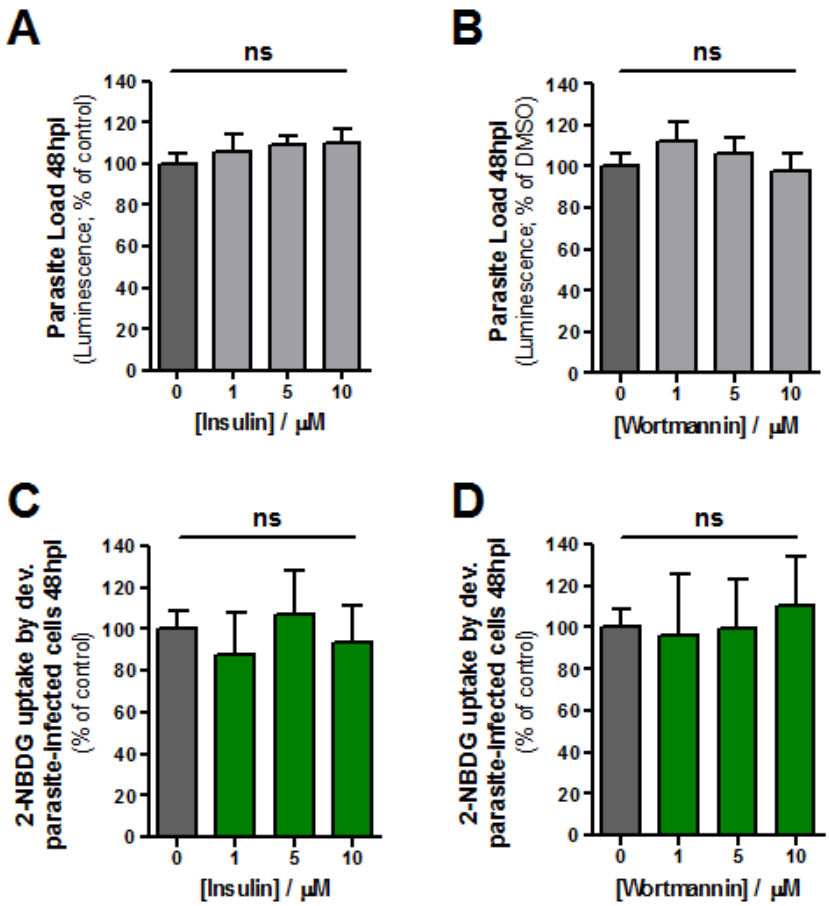

Figure 2.12 - PI3K stimulation or inhibition does not impact *P. berghei* infection of Huh7 cells neither does it alter glucose uptake by infected cells. Huh7 cells were infected with luciferase-expressing *P. berghei* sporozoites and 2 hours later were treated with different concentrations of **(A)** insulin or **(B)** Wortmannin. Parasite load (luminescence) was assessed after 48 hours. Representative experiment out of 2 and pool of 3 independent experiments, respectively. Error bars represent SD. To evaluate possible effects on glucose uptake, Huh7 cells were infected with RFP-expressing *P. berghei* sporozoites and the treatment with different concentrations of insulin **(C)** and Wortmannin **(D)** was initiated 2 hpi. 2-NBDG uptake by developing parasites-containing cells was assessed at 48 hpi by flow cytometry. Pool of 2 independent experiments for both insulin and Wortmannin. Error bars represent SD. All panels: one-way ANOVA with post-test Dunnett. ns - not significant.

To compare the amount of GLUT1 present on the membrane of infected and non-infected cells, Huh7 cells were infected with RFP-expressing *P. berghei* parasites and incubated with the fusion peptide H_{RBD}-EGFP (consisting of the Receptor Binding Domain of the human T cell leukemia virus fused to enhanced green fluorescent protein), which specifically binds to GLUT1 at the cell membrane [352,

370]. $CoCl_2$ was used as positive control as it has been shown to enhance GLUT1 translocation to the plasma membrane [371]. Flow cytometry analysis showed a small, non-significant increase in the amount of membrane-located GLUT1 in both non-infected and infected cells at 30 hpi, relative to naïve cells (Fig. 2.13). However, at 48 hpi, the amount of GLUT1 on the membrane is specifically and significantly enhanced in infected cells (Fig. 2.13). This suggests that an enhancement of GLUT1 availability at the plasma membrane facilitates the uptake of glucose required for the later stages of parasite development, the time at which there is a dramatic increase in glucose uptake (Fig. 2.2B). Overall, these data support the notion that *P. berghei* development inside hepatic cells results in the PI3K-independent translocation of GLUT1 to the host cell's membrane, leading to increased glucose uptake.

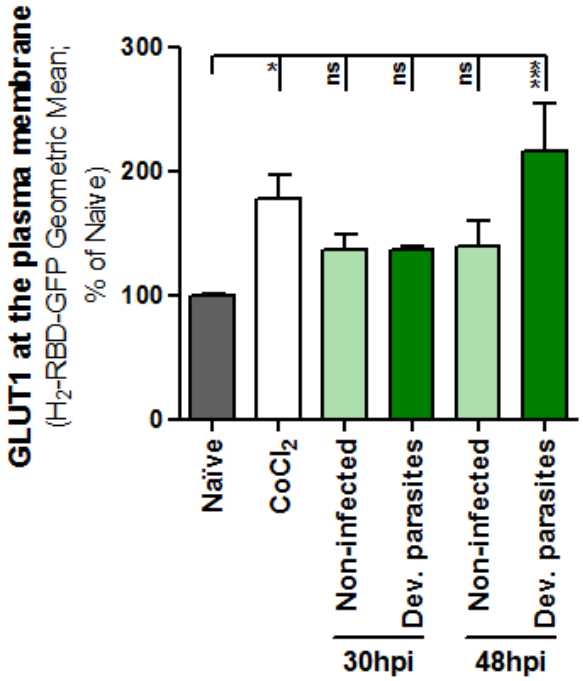

Figure 2.13 - *P. berghei* development inside Huh7 cells results in an increased GLUT1 content at the plasma membrane. Huh7 cells were infected with RFP-expressing sporozoites and, at 30 and 48 hpi, were incubated with the H^{RBD}-EGFP peptide that binds specifically to GLUT1 at the surface of the cells and were analysed by flow cytometry. Huh7 cells incubated overnight in complete RPMI with 250 µM of $CoCl_2$ were used as positive controls. Pool of 2 and 4 independent experiments for the 30 hours and 48 hours time points, respectively. Error bars represent SEM. One-way ANOVA with post-test Tukey. ns - not significant, * $p < 0.05$ and *** $p < 0.001$.

Discussion

Glucose is ubiquitously used as the common currency of metabolism, and the ability to transport this hexose across the plasma membrane is a feature of nearly all cells [389]. Although GLUT2 is the major glucose transporter of hepatocytes, where it is involved in glucose uptake and release in the fed and fasted states, respectively, GLUT1 is also present in the liver, where it is transcribed and expressed by both periportal and perivenular hepatocytes [349, 350, 390]. Interestingly, membrane localization of GLUT1 under basal conditions is restricted to hepatocytes proximal to the hepatic venule [12, 391]. Since the liver cell plate is perfused unidirectionally from portal to hepatic venule, the concentration of several substrates, such as oxygen and glucose, decreases as blood moves closer to the hepatic venule [391]. This is consistent with the observation that GLUT1 expression is enhanced by a decrease in circulating glucose levels as well as by hypoxia [392, 393]. Importantly, it has recently been shown that hypoxia enhances liver stage infection by malaria parasites, an effect that is also observed following treatment with an activator of hypoxia inducer factor (HIF)-1α or with the hypoxia mimetic $CoCl_2$ [394]. Interestingly, increased HIF-1α levels have been shown to upregulate expression of GLUT1 and $CoCl_2$ has been shown to enhance GLUT1 translocation to the plasma membrane (Fig. 2.13) [371, 395]. In this context, our results suggest that the high capacity GLUT1 transporter provides a crucial link to explain the observed preferential infectivity of hypoxic liver cells by *Plasmodium* parasites. Indeed, our *in vivo* data support this hypothesis, as the chemical inhibition of GLUT1-mediated glucose uptake had a considerable impact on the survival of *P. berghei* parasites (Fig. 2.8). Although it has been suggested that the effect of hypoxia on liver stage parasite development might be mediated by the AMPK pathway, our data do not indicate any effect of AMPK on parasite development nor on glucose uptake by infected cells (Fig. 2.11) [396]. This is also in agreement with the results of our previously published kinome RNAi screen, which did not identify AMPK as one of the kinases implicated on infection of hepatoma cells by *P. berghei* [397].

Our data suggest a model in which the extensive replication of intra-hepatic parasites leads to a depletion in intracellular glucose concentration and, consequently, affects the host cells' ATP levels due to the lack of its main

substrate. This effect is compensated for by an increase in glucose uptake that results from the likely activation of GLUT1 transporters at the plasma membrane via AMP-dependent conformational changes and from GLUT1 translocation to the plasma membrane that, consequently, do not allow further decrease in ATP levels that could lead to cell death (Fig. 2.14). Still, the levels of ATP are not completely restored in infected cells, possibly contributing to the activation of the GLUT1 transporters at the plasma membrane via AMP-dependent conformational changes in the transporter (Fig. 2.10) [381-383].

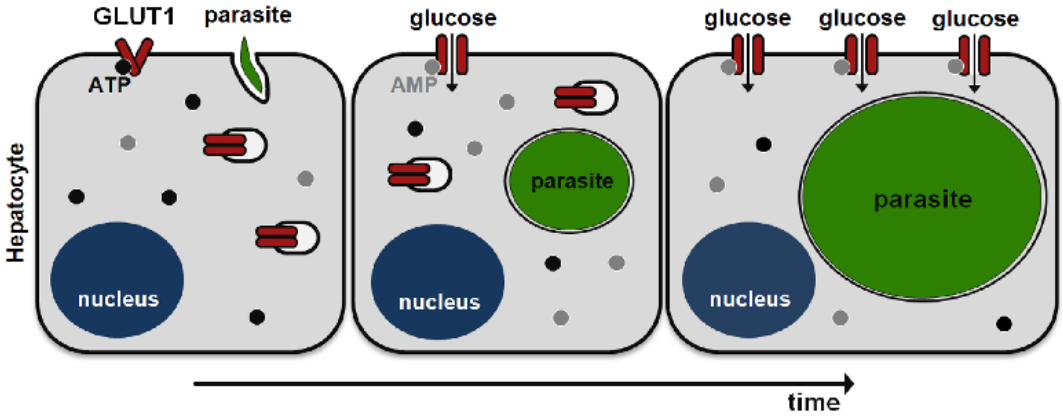

Figure 2.14 - Representative model of GLUT1-mediated glucose uptake during hepatic infection by *Plasmodium*.

The increased glucose uptake by infected cells likely leads to the depletion of this nutrient from the culture medium, which results in a similar, albeit weaker, response by neighboring non-infected cells. In fact, these cells also display a small decrease in ATP levels, as well as some, although not statistically significant, GLUT1 translocation to the membrane (Fig. 2.11 and Fig. 2.13) and a slight increase in glucose uptake from 30 hours of infection onwards (Fig. 2.2B). Importantly, as infection progresses, the amount of GLUT1 on the membrane increases specifically in infected cells (Fig. 2.13), presumably to maintain their energetic balance despite the expectedly high glucose consumption by developing parasites [8]. This is in agreement with the observation that ATP levels in infected cells do not appear to change over the time of infection (Fig. 2.10). Finally, we also showed that *P. berghei* infection of hepatoma cells is neither affected by addition of insulin, nor by inhibition of PI3K (Fig. 2.12). This is consistent with the fact that, although both ischemia and insulin have been shown to promote GLUT1 (and

GLUT4) translocation to the membrane in rat hearts, PI3K is only involved in the insulin-induced signaling, but not in the ischemia-mediated signaling, leading to GLUT1 translocation [388]. Very recently, phosphorylation of GLUT1 by protein kinase C (PKC) has been shown to lead to the rapid increase in glucose uptake and enhanced cell surface localization of GLUT1 induced by 12-O-tetradecanoyl-phorbol-13-acetate (TPA) [398]. Whether a similar mechanism may be at play during *P. berghei* infection of hepatic cells is currently under investigation.

The liver displays the capacity to remove 30-40% of the glucose presented to it following glucose ingestion and therefore must be considered a significant site of postprandial glucose removal [399]. Interestingly, a recent case-control study in Ghana found that patients with type 2 diabetes mellitus had a 46% increased risk for infection with *P. falciparum* [400]. The authors of this study offer a number of possible explanations for this observation, including impaired immune responses, an increased number of infectious mosquito bites, and enhanced parasite growth in the blood of type 2 diabetes mellitus patients [400]. Thus, our results suggest the possibility that the elevated amounts of circulating glucose displayed by diabetic patients may also promote parasite development in the liver, thereby contributing to the increased risk of appearance of clinically relevant malaria. Further investigation of the link between diabetes and malaria is clearly warranted by the fact that sub-Saharan Africa currently faces the world's highest increase in type 2 diabetes mellitus [401].

This work addresses the role of glucose during hepatic infection by *Plasmodium* from a molecular point of view. It identifies GLUT1 as a major player in glucose uptake by infected cells and shows that its function as a glucose transporter is modulated in cells containing replicating parasites. These findings contribute to an understanding of how hepatic host cells meet the energy demands imposed by the parasite's huge replication rate. Such an understanding may help identify strategies to control energy production by infected cells and thereby limit parasite development and survival.

Acknowledgements

We are very grateful to Marc Sitbon and Julie Laval (Institut de Génétique Moléculaire de Montpellier CNRS-UMSF, France) for kindly providing the H_{RBD}-EGFP peptide, to Hiromi Imamura (Graduate School of Biostudies, Kyoto University, Japan) for kindly providing the pRSET-AT1.03 plasmid, to Benoit Viollet (Institut Cochin, France) for providing the AMPK-KO MEFs, to Maria M. Mota (Instituto de Medicina Molecular, Portugal) for critically reviewing the manuscript, to Marta Miranda for help with the viral infections, to Ana Parreira and Filipa Teixeira for producing the various lines of *P. berghei*-infected mosquitoes and to the Bioimaging, Flow Cytometry and Rodent facilities of iMM Lisboa for technical support.

The role of L-arginine uptake and polyamine production during liver stage infection by the malaria parasite

Patrícia Meireles[1], Rita I. Aroeira[2], Henry M. Staines[3], António M. Mendes[1], Miguel Prudêncio[1]

[1] Instituto de Medicina Molecular, Faculdade de Medicina, Universidade de Lisboa, Avenida Professor Egas Moniz, 1649-028, Lisboa, Portugal

[2] Institute of Pharmacology and Neurosciences, Faculty of Medicine and Neurosciences Unit, Instituto de Medicina Molecular, Faculdade de Medicina, Universidade de Lisboa, Avenida Professor Egas Moniz, 1649-028, Lisboa, Portugal

[3] Institute for Infection & Immunity, St. George's, University of London, Cranmer Terrace, London, UK

Author Contributions

PM and MP designed the experiments. PM performed all the experiments. RIA helped with the radioactive uptake experiments. AMM and HMS gave intellectual input to the work. PM wrote the chapter. MP supervised the work and revised the text.

Introduction

Cationic amino acids, including L-arginine (Arg), are transported through biological membranes by various distinct transport systems [19, 402]. Among these is the y^+ system, the main mechanism of cellular uptake of cationic amino acids. The y^+ system is found almost ubiquitously and specifically transports Arg, L-lysine (Lys), and L-ornithine (Orn) through the cationic amino acid transporter (CAT) family of proteins, a subfamily of the solute carrier family 7 (SLC7) [18, 19]. The four members of the CAT family are the nearly-ubiquitous CAT1, encoded by *SLC7A1*, the two products of *SLC7A2*, the gene that encodes through alternative splicing the liver-abundant low affinity CAT2A and the high affinity CAT2B transporters, the brain-specific CAT3, encoded by *SLC7A3*, and CAT4, encoded by *SLC7A4*, whose function is still unknown [19, 403-406].

Once inside the cell, Arg can be degraded via multiple pathways that are initiated by arginase, nitric oxide synthase (NOS), Arg:glycine amidinotransferase, and Arg decarboxylase. These pathways produce polyamines, nitric oxide (NO), proline, glutamate, creatine, and agmatine, each of which has great biological importance [407]. Arginase, the arginine hydrolytic enzyme, catalyzes the hydrolysis of Arg and its activity is important for maintaining Orn levels for polyamine synthesis. There are two isoforms of the enzyme, a cytosolic arginase 1, mostly expressed in the liver, and a more widely distributed mitochondrial arginase 2 [408].

Plasmodium parasites also express arginase and the structure of the *P. falciparum* enzyme has already been reported [23-25]. The dependency of blood stage *P. falciparum* on polyamines for survival has been well established [26-28]. Possibly the most distinctive feature of polyamine biosynthesis in *Plasmodium* parasites is that the two rate-limiting decarboxylase activities are found in a unique protein known as AdoMetDC/ODC, whose bifunctionality is important for the regulation of polyamine pools in the parasite [336-338].

Arg and the arginase pathway have been implicated in several infections, including *Trypanosoma spp.*, *Leishmania spp.*, *Toxoplasma gondii*, *Shistosoma mansoni*, *Candida albicans*, and *Helicobacter pylori* (reviewed in [22]). Most studies concerning the use of Arg by *Plasmodium* parasites have concentrated on the blood stages of infection. *Plasmodium* spp. parasites are incapable of *de novo* amino acid biosynthesis and must therefore acquire the amino acids they require

for protein synthesis and growth [24, 305, 409]. A metabolomics study of *P. falciparum* blood stages has shown that Arg is significantly depleted while Orn and citrulline accumulate in the culture medium during the parasite's trophozoite and schizont stages [24]. This depletion has been associated with the reduced plasma Arg levels observed in severe malaria patients [410].

To overcome the scarcity of information regarding the uptake and role of Arg in *Plasmodium* liver stages we employed a well-established rodent *P. berghei* model of *in vitro*, *ex vivo* and *in vivo* infection [41]. Our results reveal an important role for the CAT2 transporter in the uptake of Arg by infected cells and show that Arg plays an essential role in the development of hepatic parasites by fueling the polyamine synthesis pathway of the parasite and of the infected cell.

Materials and Methods

Chemicals

RPMI 1640, William's E, PBS pH 7.4, trypsin, FBS, non-essential amino acids, penicillin/streptomycin, glutamine, HEPES pH 7, liver perfusion medium (LPM), liver digestion medium (LDM), OptiMEM and Lipofectamine RNAiMAX were purchased from Gibco/Invitrogen. All other chemicals were obtained from Sigma, unless otherwise specified.

Cells

Huh7 cells, a human hepatoma cell line were cultured in RPMI 1640 medium supplemented with 10% FBS, 1% non-essential amino acids, 1% penicillin/streptomycin, 1% Glutamine and 1% HEPES, pH 7 and maintained at 37°C with 5% CO_2. Mouse primary hepatocytes were cultured in William's E medium supplemented with 4% FBS and 1% penicillin/streptomycin and maintained at 37°C with 5% CO_2.

Mice

C57BL/6 mice were purchased from Charles River. A breeding trio of *Slc7a2*$^{+/-}$ mice was kindly provided by Lesley G. Ellies (University of California, San Diego School of Medicine) and the animals were housed and bred in the facilities of the Instituto de Medicina Molecular to obtain *Slc7a2*$^{-/-}$ and corresponding littermate *Slc7a2*$^{+/+}$ mice [411]. All animal experiments were performed in strict compliance to the guidelines of our institution´s animal ethics committee and the Federation of European Laboratory Animal Science Associations (FELASA).

Parasites

WT, arginase-KO, GFP- or luciferase-expressing *P. berghei* ANKA sporozoites were dissected in non-supplemented RPMI medium from the salivary glands of infected female *A. stephensi* mosquitoes, bred at Instituto de Medicina Molecular (Lisbon, Portugal), prior to being employed for *in vitro, ex vivo* and *in vivo* infections [25, 358, 359].

RNAi screen of hepatic transporters on *Plasmodium* infection

Down-modulation of the genes encoding the transporters whose expression was shown to be altered upon *P. berghei* infection was obtained by employing shRNAs. All shRNAs were purchased from the MISSION TRC library (Sigma) in the form of bacterial glycerol stocks which were grown to obtain the purified plasmids. Each gene was targeted by using one to three distinct shRNAs, used individually (Table 3.1). For the lentiviral production, HEK 293FT cells ($2.0x10^4$ per well) were seeded in 96-well plates. On the following day, cells were transfected with the packaging vectors and each individual shRNA plasmid in a final concentration of 100 ng/well using the FuGENE 6 reagent (Promega), according to the manufacturer's instructions. The lentiviral particles were collected in the supernatant of these cells approximately 60 hours after transfection and stored at -80°C. For the transduction of Huh7 cells and subsequent generation of cell lines with stable knockdown of the genes of interest, Huh7 cells ($1.0x10^5$ per well) were seeded in 12-well plates. On the following day, the medium was replaced by 400 µL of supplemented RPMI with 8 µg/mL of polybrene, on top of which were added 100 µL of lentiviral particles-containing supernatant (approximate MOI of 1:1) and the plates were centrifuged for 30 minutes at 1200xg and 37°C. Twenty-four hours after transduction, the medium was replaced by supplemented RPMI with 5 µg/mL of puromycin (Calbiochem) for the selection of the transduced cells which were allowed to grow for at least a week before being used for infections. Cells transduced with lentiviral particles carrying a negative control shRNA (SHC002) not targeting any annotated gene in the human genome were used as negative control. A stable cell line with the knockdown of SR-BI was used as positive control in the luminescence assays [210]. The efficiency of knockdown of each shRNA sequence was assessed by qPCR using specific primers (Table 3.2).

Table 3.1 - List of shRNA sequences used, with the corresponding knockdowns.

Gene	Gene ID	Sequence	Clone ID	Oligonucleotide Sequence	Knockdown
SCARB1	NM_005505		TRCN0000056966	CCGGGCAAGGTTGACTTCTGGCATTCTCGAGAATGCCAGAAGTCAACCTTGCTTTTTG	85%
SLC1A4	NM_003038		TRCN0000038639	CCGGCCATGTTATTCATGGAGGAATCTCGAGATTCCTCCATGAATAACATGGTTTTTG	50%
SLC3A2	NM_002394		TRCN0000043384	CCGGCGAGAAGAATGGTCTGGTGAACTCGAGTTCACCAGACCATTCTTCTCGTTTTTG	40%
SLC6A9	NM_006934	#01	TRCN0000043503	CCGGCCCGCCATCATCTTCTTTATTCTCGAGAATAAAGAAGATGATGGCGGGTTTTTG	25%
		#02	TRCN0000043505	CCGGGACGGCATCATGTACTACCTACTCGAGTAGGTAGTACATGATGCCGTCTTTTTG	65%
		#03	TRCN0000043507	CCGGCATGTTCAAAGGAGTGGGCTACTCGAGTAGCCCACTCCTTTGAACATGTTTTTG	0%
SLC7A2	NM_003046	#01	TRCN0000042973	CCGGGGCCCAAATGTTCTCCTGAGAACTCGAGTTCTCAGGAGAACATTTGGGCTTTTTG	70%*
		#02	TRCN0000042974	CCGGGCTGGGTTTGTGAAAGGAAATCTCGAGATTTCCTTTCACAAACCCAGCTTTTTG	90%*
		#03	TRCN0000042976	CCGGCGTATGTGATAGGTACATCAACTCGAGTTGATGTACCTATCACATACGTTTTTG	N.I.
SLC7A5	NM_003486		TRCN0000043010	CCGGGCCGTGGACTTCGGGAACTATCTCGAGATAGTTCCCGAAGTCCACGGCTTTTTG	70%
SLC7A11	NM_014331		TRCN0000043125	CCGGCCTGCGTATTATCTCTTTATTCTCGAGAATAAAGAGATAATACGCAGGTTTTTG	55%
SLC25A12	NM_003705		TRCN0000044588	CCGGGCCATTAAACTGACTGTTAATCTCGAGATTAACAGTCAGTTTAATGGCTTTTTG	N.I.
SLC38A2	NM_018573	#01	TRCN0000020239	CCGGCCTCCAATCCTCTGGCTATTTCTCGAGAAATAGCCAGAGGATTGGAGGTTTTT	60%
		#02	TRCN0000020240	CCGGCCTGAACAATGAATTCCCATTCTCGAGAATGGGAATTCATTGTTCAGGTTTTT	20%
		#03	TRCN0000020242	CCGGTCTGGCTATTTAAGGTTCAAACTCGAGTTTGAACCTTAAATAGCCAGATTTTT	50%
SLC38A4	NM_018018	#01	TRCN0000044709	CCGGCGGAACCACTTCCTTTGGAATCTCGAGATTCCAAAGGAAGTGGTTCCGTTTTTG	50%
		#02	TRCN0000044710	CCGGCCCAATTCGTACATCAGTGATCTCGAGATCACTGATGTACGAATTGGGTTTTTG	75%
		#03	TRCN0000044711	CCGGGCAGCAATGAGCAGTCAATTTCTCGAGAAATTGACTGCTCATTGCTGCTTTTTG	70%
SLC38A7	NM_018231	#01	TRCN0000060153	CCGGCTGTGCCTCATTCAAGCCAAACTCGAGTTTGGCTTGAATGAGGCACAGTTTTTG	90%
		#02	TRCN0000060154	CCGGCCCTTGGTACACAGACCGCAACTCGAGTTGCGGTCTGTGTACCAAGGGTTTTTG	80%
		#03	TRCN0000060157	CCGGCGGCAAGGTGATCTCAGTCATCTCGAGATGACTGAGATCACCTTGCCGTTTTTG	80%
SCN1A	NM_006920	#01	TRCN0000044308	CCGGCGCATCAATCTGGTGTTCATTCTCGAGAATGAACACCAGATTGATGCGTTTTTG	N.D.
		#02	TRCN0000044310	CCGGGCCAATGTCCAGAGGGATATACTCGAGTATATCCCTCTGGACATTGGCTTTTTG	N.D.
		#03	TRCN0000044311	CCGGCGGAAGACTTTAGTAGTGAATCTCGAGATTCACTACTAAAGTCTTCCGTTTTTG	N.D.
CLCA1	NM_001285	#01	TRCN0000044884	CCGGCGAGTACAATAATGATGAGAACTCGAGTTCTCATCATTATTGTACTCGTTTTTG	N.D.
		#02	TRCN0000044885	CCGGGCCCTGAGTAATTCACTCATTCTCGAGAATGAGTGAATTACTCAGGGCTTTTTG	N.D.
		#03	TRCN0000044887	CCGGGCACAACATGTTGATTCTATACTCGAGTATAGAATCAACATGTTGTGCTTTTTG	N.D.
CLCA2	NM_006536	#01	TRCN0000044288	CCGGCCCTTACACTTTGGCTATGAACTCGAGTTCATAGCCAAAGTGTAAGGGTTTTTG	N.D.
		#02	TRCN0000044289	CCGGGCCGAGTGTTTGTCCATGAATCTCGAGATTCATGGACAAACACTCGGCTTTTTG	N.D.
		#03	TRCN0000044291	CCGGGCTGACTTTCACCACAGCTTTCTCGAGAAAGCTGTGGTGAAAGTCAGCTTTTTG	N.D.
SLC12A2	NM_001046		TRCN0000042944	CCGGGCTCTCTACATGGCATGGTTACTCGAGTAACCATGCCATGTAGAGAGCTTTTTG	50%
SLC20A1	NM_005415		TRCN0000043057	CCGGCCATCAGTACAACACATTGTACTCGAGTACAATGTGTTGTACTGATGGTTTTTG	55%
ATP2A2	NM_001681		TRCN0000038531	CCGGCCCTTGGTTGTACTTCTGTTACTCGAGTAACAGAAGTACAACCAAGGGTTTTTG	90%
ATP2B1	NM_001001323	#01	TRCN0000043069	CCGGCCAGAGAAAGAGGGTGGATTACTCGAGTAATCCACCCTCTTTCTCTGGTTTTTG	0%
		#02	TRCN0000043070	CCGGGCCTCTCATCTCACGTACAATCTCGAGATTGTACGTGAGATGAGAGGCTTTTTG	70%
		#03	TRCN0000043071	CCGGGCAGATTTAGAAAGAAGAGAACTCGAGTTCTCTTCTTTCTAAATCTGCTTTTTG	45%
CACNA2D1	NM_000722	#01	TRCN0000043768	CCGGCCCATCATGTAACGCGGATTTCTCGAGAAATCCGCGTTACATGATGGGTTTTTG	0%
		#02	TRCN0000043770	CCGGGCCAGGGATATTGAGAAACTTCTCGAGAAGTTTCTCAATATCCCTGGCTTTTTG	15%
		#03	TRCN0000043771	CCGGGCACGATTTGTTGTGACTGATCTCGAGATCAGTCACAACAAATCGTGCTTTTTG	0%

N.I. not included in the RNAi screen due to cytotoxicity; N.D. knockdown was not possible to determine; * average knockdown of both splice variants.

Overall *in vitro* infection by luminescence

Overall hepatic infection was determined by measuring the luminescence intensity in Huh7 cells infected with a firefly luciferase-expressing *P. berghei* line, as previously described [358]. Briefly, Huh7 cells ($1.0x10^4$ per well) were seeded in 96-well plates the day before infection. Sporozoite addition was followed by centrifugation at 1800xg for 5 minutes and the medium was replaced approximately 2 hours after infection by the appropriate medium. Parasite infection load was measured 48 hours after infection by a bioluminescence assay (Biotium) using a multiplate reader Infinite M200 (Tecan). The effect of the different treatments on the viability of Huh7 cells was assessed by the CellTiter-Blue assay (Promega) according to the manufacturer's protocol.

Quantification of *P. berghei* invasion and development by flow cytometry

Invasion of hepatoma cells and intracellular parasite development were assessed by determining the percentage of GFP^+ cells 2 hours after infection with a GFP-expressing *P. berghei* line and by measuring the intensity of the GFP signal of the infected cells 48 hours after infection, respectively, as previously described [163]. Huh7 cells ($5.0x10^4$ per well) were seeded in 24-well plates the day before infection. The medium was replaced by the appropriate medium 1 hour prior or 2 hours after infection, for invasion and development quantification, respectively. Cells were then collected for flow cytometry analysis at 2 hours or 48 hours after infection and analyzed on a Becton Dickinson FACSCalibur. Data acquisition and analysis were carried out using the CELLQuest (version 3.1.1 f1, Becton Dickinson) and FlowJo (version 6.4.7, FlowJo) software packages, respectively.

Immunofluorescence imaging of *P. berghei*-infected cells

For immunofluorescence microscopy analyses, cells were seeded on glass coverslips in 24-well plates and infected with sporozoites as described above. Forty-eight hours after infection, cells were rinsed with 1x PBS and fixed with 4% paraformaldehyde (PFA; Santa Cruz Biotechnology) for 20 minutes at room temperature and stored at 4°C in PBS 1x until being stained. Cells were incubated with the permeabilization/blocking solution (0.1% triton X-100, 1% bovine serum

albumin (BSA) in 1x PBS) for 30 minutes at room temperature. Parasites were stained with a parasite specific anti-Hsp70 (2E6) antibody (dilution 1:100) and an anti-UIS4 antibody (dilution 1:1000) for 1 hour at room temperature, followed by three washes with permeabilization/blocking solution. Cells were further incubated in a 1:400 dilution of anti-mouse Alexa-Fluor 488 (Jackson ImmunoResearch Laboratories) or anti-goat Alexa-Fluor 568 (Life Technologies) secondary antibodies in the presence of a 1:1000 dilution of Hoechst 33342 (Invitrogen) for nuclei staining. An additional three washes were carried out with permeabilization/blocking solution. Coverslips were mounted on microscope slides with Fluoromount (SouthernBiotech). Confocal images were acquired using a Zeiss LSM 710 confocal microscope. Widefield images for size determination were acquired in a Zeiss Axiovert 200M microscope. Images were processed with ImageJ software (version 1.47).

P. berghei sporozoites *in vivo* infection and quantification of parasite liver load by qPCR

Mice were infected i.v., through retro-orbital injection, with $1.0x10^4$ *P. berghei* sporozoites. The livers were collected at 44 hpi and homogenized in 3 mL of denaturing solution (4 M guanidine thiocyanate; 25 mM sodium citrate pH 7, 0.5% *N*-lauroylsarcosine and 0.7% β mercaptoethanol in DEPC-treated water). Total RNA was extracted from the livers with the NZY Total RNA Isolation Kit (NZYTech), according to the manufacturer's protocol, and parasite load was quantified by qPCR using primers specific to *P. berghei* 18S RNA (Table 3.2). Mouse Hprt expression was used for normalization.

In vivo inhibition of NO production

Six weeks old male C57BL/6 mice were injected daily with 50 mg/kg of N_ω-Nitro-L-arginine methyl ester (L-NAME) i.p. in saline, or with saline (0.9% NaCl) alone, starting 3 days before and until the day of *P. berghei* sporozoite i.v. injection. The livers were collected at 44 hpi and processed as previously described, for quantification of parasite liver load.

L-Arg *in vivo* supplementation

The drinking water of 4 weeks old male C57BL/6 mice was replaced by sterilized water with 2.5% (w/v) L-arginine hydrochloride (Fisher Scientific) and the mice were allowed to drink *ad libitu*m for 4 weeks. Control mice drank sterilized water alone. Mice were then infected i.v. with $1.0x10^4$ *P. berghei* sporozoites and the livers were collected at 45 hpi and processed as previously described, for quantification of parasite liver load.

Blood Parasite Load

The presence of luciferase-expressing erythrocytic-stage parasites was monitored daily by Giemsa-stained blood smears and luminescence. For luminescence measurements, 5 µL of blood was collected from the tail vein into 50 µL of lysis buffer [412]. Luminescence was determined by adding 50 µL of D-luciferin dissolved in firefly luciferase assay buffer (according to the manufacturer's instructions) to 30 µL of lysate and immediately measured using a multiplate reader (Tecan, Switzerland). Values of luciferase activity are expressed as relative luminescence units.

Isolation and infection of mouse primary hepatocytes

Mouse primary hepatocytes were isolated using a modified two-step perfusion protocol followed by a Percoll purification step [168, 413, 414]. Briefly, mice were euthanized by CO_2 inhalation and immediately processed for cannulation of the portal vein using a 26-gage needle. Upon successful cannulation, the inferior vena cava (IVC) was cut to allow fluid to drain. Liver perfusion medium (LPM) was perfused at 8–9 mL/min for 10 minutes followed by liver digestion medium (LDM) at the same rate. Intermittent clamping of the IVC (3 seconds clamp every 30 seconds) was performed during LDM perfusion to improve tissue digestion. After digestion, the liver was excised and the cells were liberated by tearing and shaking of the liver with forceps. The cell suspension was then sequentially filtered through a 100 µm and a 70 µm cell strainer and spun at 50xg for 3 min. The cell pellet was resuspended in Williams's Medium E with 10% of FBS and carefully overlaid on a 60% Percoll solution (1:1). The cell suspension was fractionated by centrifugation at 750xg for 20 minutes, without break, at 20 °C. Viable hepatocytes deposited in

the pellet were washed with Williams's Medium E with 10% FBS, spun at 50xg for 3 minutes and resuspended in complete Williams's Medium E (supplemented with 4% FBS and 1% penicillin/streptomycin). Hepatocytes were then plated at a density of $2.0x10^4$ in 96-well plates or $1.0x10^5$ in 24-well plates and infected 16 hours later with $1.0x10^4$ or $5.0x10^4$ *P. berghei* sporozoites, respectively. Viability and yield were assessed by trypan blue staining.

FACS-sorting of *P. berghei*-infected and non-infected Huh7 cells

Huh7 cells ($1.0x10^5$ per well) were seeded in 24-well plates and infected 24 hours later with $1.0x10^5$ GFP-expressing *P. berghei* sporozoites. Cells were collected at 2 hpi and FACS-sorted on a BD FACSAria III Cell Sorter (BD Biosciences). Non-infected and GFP-expressing *P. berghei*-infected cells were gated on the basis of their different fluorescence intensity, as previously established, and collected simultaneously [11, 163]. Immediately after FACS-sorting, both infected and non-infected cells were washed and seeded in 24-well plates at a density of $1.5x10^5$ per well. Infected cells were diluted 1:1 with non-infected cells to allow replicates. Cells were then incubated until being collected at 18, 30 or 48 hpi. In the case of the 6 hpi time point, *P. berghei*-infected cells were FACS-sorted at this time, diluted 1:1 with non-infected cells, pelleted, snap-frozen and stored until RNA extraction using the High Pure RNA Isolation kit (Roche) according to the manufacturer´s instructions.

[^{3}H] Arginine Uptake

Arg uptake analysis was performed in naïve and sorted infected and non-infected Huh7 cells at 24 hpi, with CAT2 knockdown (SLC7A2#02 cell line) and corresponding control (scrambled cell line). The [^{3}H] Arg (specific activity 47.7 Ci/mmol; PerkinElmer) transport was initiated by the addition of 100 nM [^{3}H] Arg and 200 µM cold Arg in KHR transport buffer (containing in mM: 137 NaCl, 5.4 KCl, 1.8 $CaCl_2.2H_2O$, 1.2 $MgSO_4$ and 10 HEPES, pH 7.40) for 1 minute. Uptake was stopped by washing the cells twice with ice cold stop buffer (containing in mM: 137 NaCl and 10 HEPES, pH 7.40). Cells were subsequently solubilized with lysis buffer (100 mM NaOH and 0.1 % SDS) at 37°C for 1 hour and scraped from the plates. Protein concentration was quantified using Bio-Rad DC protein assay. The amount of [^{3}H] Arg taken up by the cells was quantified by liquid scintillation

counting (MicroBeta Trilux, PerkinElmer) [415]. The specific CAT2-mediated transport was calculated as the difference between the [^{3}H] Arg uptake in the scrambled cell line (total transport) and in the SLC7A2#02 cell line.

siRNA transfection

4.0x10^4 Huh7 cells were reverse-transfected with 30nM of target specific (human ODC: ref. L-006668-00-0005; human arginase 1: ref. L-009922-00-0005) or control siRNA sequence pools (ON-TARGETplus SMARTpool, Dharmacon), using Lipofectamine RNAiMAX (Gibco/Invitrogen) according to the manufacturer´s instructions. Twenty-four hours after transfection, the cells were infected with 3.0x10^4 GFP-expressing *P. berghei* sporozoites. Cells were collected for flow cytometry analysis at 48 hpi and analyzed on a BD LSR Fortessa flow cytometer with the DIVA software (version 6.2). Analysis was carried out using the FlowJo software (version 6.4.7, FlowJo). The efficiency of knockdown was assessed by qPCR using specific primers (Table 3.2).

RNA extraction and quantification

RNA was extracted from cultured Huh7 cells using the High Pure RNA Isolation kit (Roche) according to the manufacturer´s instructions. The amount of RNA in each sample was assessed with a NanoDrop® ND-1000 spectrophotometer.

cDNA synthesis and qPCR

Complementary DNA (cDNA) was synthesized from 1 µg of RNA using the Roche cDNA synthesis kit, according to the manufacturer´s instructions. The cDNA was synthesized employing the following thermocycling parameters: 25°C for 10 minutes, 55°C for 30 minutes, and 85°C for 5 minutes. qPCR reaction was performed in a total volume of 20 µL in a ABI Prism 7500 Fast system (Applied Biosystems) using the iTaq^{TM} Universal SYBR® Green kit (BioRad) as follows: 50°C for 2 minutes, 95°C for 10 minutes, 40 cycles at 95°C for 15 seconds and 60°C for 1 minute, melting stage was done at 95°C for 15 seconds, 60°C for 1 minute, and 95°C for 30 seconds. Primers for the housekeeping gene hypoxanthine-guanine phosphoribosyltransferase (*HPRT*) were used for

normalization in all experiments (Table 3.2). For qPCR, the delta-delta CT relative quantification method was used.

Table 3.2 - List of primer sequences used.

Gene	forward primer (5' - 3')	reverse primer (5' - 3')
Pb18S	AAGCATTAAATAAAGCGAATACATCCTTAC	GGAGATTGGTTTTGACGTTTATGTG
HPRT	TTTGCTGACCTGCTGGATTAC	CAAGACATTCTTTCCAGTTAAAGTTG
SCARB1	AGAATAAGCCCATGACCCTGAA	TGAGCTCAGCAAATAATCCGAA
SLC1A4	TGTTTGCTCTGGTGTTAGGAGT	CGCCTCGTTGAGGGAATTGAA
SLC3A2	AGTGCCAACATGACTGTGAAG	CCTTACTCCGCTGGTCACTCAG
SLC6A9	CAGATCGAGTTTGTACTGACGAG	GCGATAGCAGAGGTATGGGAAG
SLC7A2 var1	TCACCAGTTGCTGCCACGTTGA	AGCCAGGCTGGTACCTGAGGATGAG
SLC7A2 var2	CGGGTGCAGTGGCAGCTTTGATGG	
SLC7A5	CCAAGCTCGTGGCCTGCCT	GATTGGACACATCACCCTTCCCGA
SLC7A11	TGCTGGCTGGTTTTACCTCAAC	CCAATGGTGACAATGGCCAT
SLC25A12	TGGCGGTCAAGGTGCAGACAACTA	TCCTGCCAAGAGCTGCACGATCTT
SLC38A2	TTGGTTTTATTGGTGCATCTGCAGC	GCCATGCTTCCGGTCATCACCA
SLC38A4	ATTACACCCACCGCAATCCTG	CGTCCGGGAGTTGAATACAAAG
SLC38A7	TTCCCAGGGCTGTGCCTCATTC	TGTTCCCTGGGAGGCAGTGGT
SLC12A2	TCCCACTGGAGAGCAAGAAGCCA	TGGCTGACTGAGGATCTGCAAGA
SLC20A1	TCTTGGTTCGTGTCCCCACTGCTT	TTGTCAAAGCCCAGCAACGGTGC
ATP2A2	AGAACGTGCAAATGCCTGCAACTCA	ATGACACCTTCAGGAGCACCCTTCA
ATP2B1	TGGAAGGCTCTGGAAGAATGGTAGT	CCTGGGCTTTTGCTTTGTTGCGA
CACNA2D1	CGTTCCCTTCGGCCGTCACTATC	GCAATTTCTACCAGCTGGCGTGC
ODC	ATGGCTTCCAGAGGCCGAC	TTGCTGCATGAGTTGCCACGCA
Arginase 1	GAAGTGTCAGAGCATGAGCG	AGCAGACCAGCCTTTCTCAA
mouse *Slc7a2*	TGCTGCTCGTCCAACCTTC	TGGAATCTTCAAGGCTGTCC

Statistical Analyses

Statistical analyses were performed using the GraphPad Prism 5 software. One-way ANOVA, Two-way ANOVA, Survival Test Gehan-Breslow-Wilcoxon, Mann-Whitney U test or Unpaired t-test were used for significance of the differences observed, as indicated in each figure. ns – not significant, * $p < 0.05$, ** $p < 0.01$ and *** $p < 0.001$.

Results

SLC7A2 plays an important role during *P. berghei* intra-hepatic development

Previous microarray results obtained by the laboratory have shown that the expression of several transport proteins is altered during infection of hepatoma cells by *P. berghei* parasites [11]. To investigate the functional role of these proteins during the liver stage of *Plasmodium* life cycle, we employed an RNAi-based strategy to monitor the effect of their down-modulation on *P. berghei* infection. The screen proceeded in 3 consecutive steps, employing different established methods to measure hepatic infection by *Plasmodium*. In the first step, 1 to 3 shRNA sequences were used to silence each of the 18 selected genes and the resulting stable cell lines were infected with luciferase-expressing *P. berghei* sporozoites. Forty-eight hours later, the parasite load in these cells was determined by measuring the bioluminescence of cell lysates. Each sequence was used in at least 4 independent experiments and a shRNA targeting SR-BI was employed as a positive control for infection decrease [210]. Our results showed that the knock-down of 10 of those genes consistently led to a decrease in overall parasite load, as measured by the luminescence of infected cell lysates (Fig. 3.1A). Based on the correlation between the effect on infection and the level of knockdown of gene expression by the different sequences, 7 genes were selected for the second step of the RNAi screen. Then, the stable cells lines with the knockdown of these genes were infected with GFP-expressing *P. berghei* parasites and the extent of the impairment of the parasite's intra-hepatic development was assessed 48 hours later by flow cytometry determination of GFP intensity [163]. Our data showed that down-modulation of both splice variants of the *SLC7A2* gene leads to the strongest impairment of parasite development among the genes assessed, indicating that the transporter encoded by this gene might play an important role in the ability of the parasite to replicate inside hepatic cells (Fig. 3.1B). Therefore, the *SLC7A2* gene was selected for a final confirmation step using two shRNA sequences and through assessment of parasite development by immunofluorescence microscopy (Fig. 3.1C). These imaging data demonstrated that parasite size correlates with the average expression levels of

both variants of *SLC7A2*, suggesting that CAT2A and CAT2B, the two transporters encoded by this gene, are involved in the parasite's hepatic development.

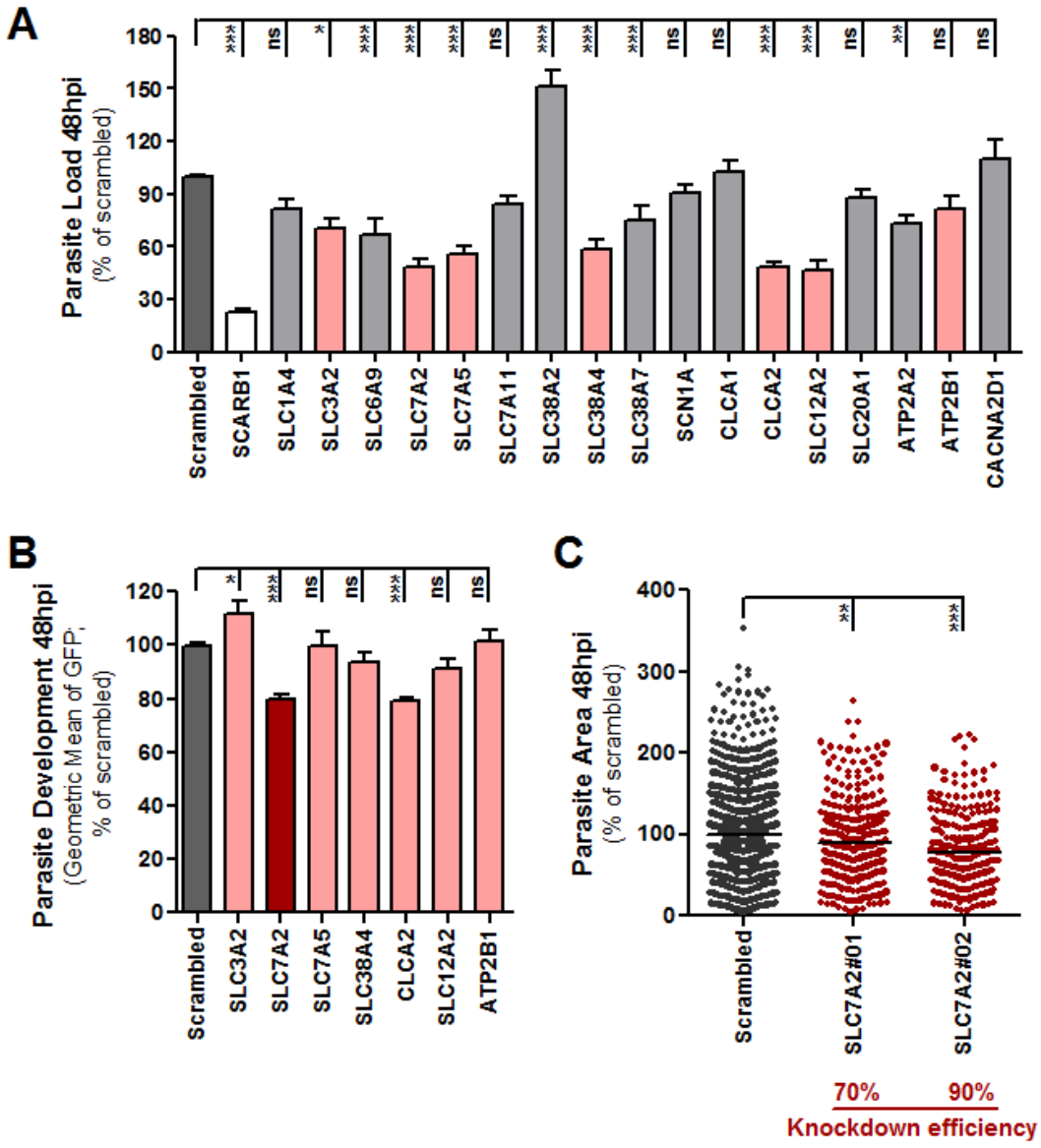

Figure 3.1 – *SLC7A2* knockdown significantly impairs *P. berghei* intra-hepatic development. (A) Huh7 cells with stable knockdown of the selected genes were infected with luciferase-expressing *P. berghei* sporozoites and parasite load (luminescence) was assessed 48 hours later. A scrambled shRNA sequence was used as a negative control and a cell line with stable knockdown of SR-BI was used as positive control. Error bars represent SEM. **(B)** Huh7 cells with the knockdown of the 7 genes selected on the previous step were infected with GFP-expressing *P. berghei* sporozoites and parasite development was assessed by flow cytometry at 48 hpi. Error bars represent SEM. **(C)** Quantification of the area of the EEFs in the 2 different cell lines with *SLC7A2* knockdown at 48 hpi by immunofluorescence microscopy. The knockdown efficiency of each shRNA

sequence is indicated. All panels: Pool of 3 independent experiments. One-way ANOVA with post-test Dunnett. ns - not significant, * $p < 0.05$, ** $p < 0.01$ and *** $p < 0.001$.

Further evidence of a role for *SLC7A2* in *Plasmodium* hepatic development was obtained in *in vivo* and *ex vivo* experiments employing *Slc7a2*$^{-/-}$ mice. In the *in vivo* experiments, male and female *Slc7a2*$^{-/-}$ (KO), *Slc7a2*$^{+/-}$ (heterozygous) and *Slc7a2*$^{+/+}$ (WT) littermate mice were infected by i.v. injection of 1.0x10^4 *P. berghei* sporozoites. Our results show that, in males, parasite burden assessed by qPCR 44 hours after infection was approximately 65% lower in the livers from KO mice compared with their WT counterparts, with the heterozygous mice exhibiting a smaller and non-significant reduction that correlates with *Slc7a2* expression in these mice (Fig. 3.2A, C). In female mice, even though there is an approximately 50% reduction in parasite load in the livers of the KO mice, the difference is not statistically significant (Fig. 3.2B). Additionally, heterozygous female mice do not exhibit an intermediate reduction in infection as observed for the males, although the expression of the gene is reduced by around 40% (Fig. 3.2D).

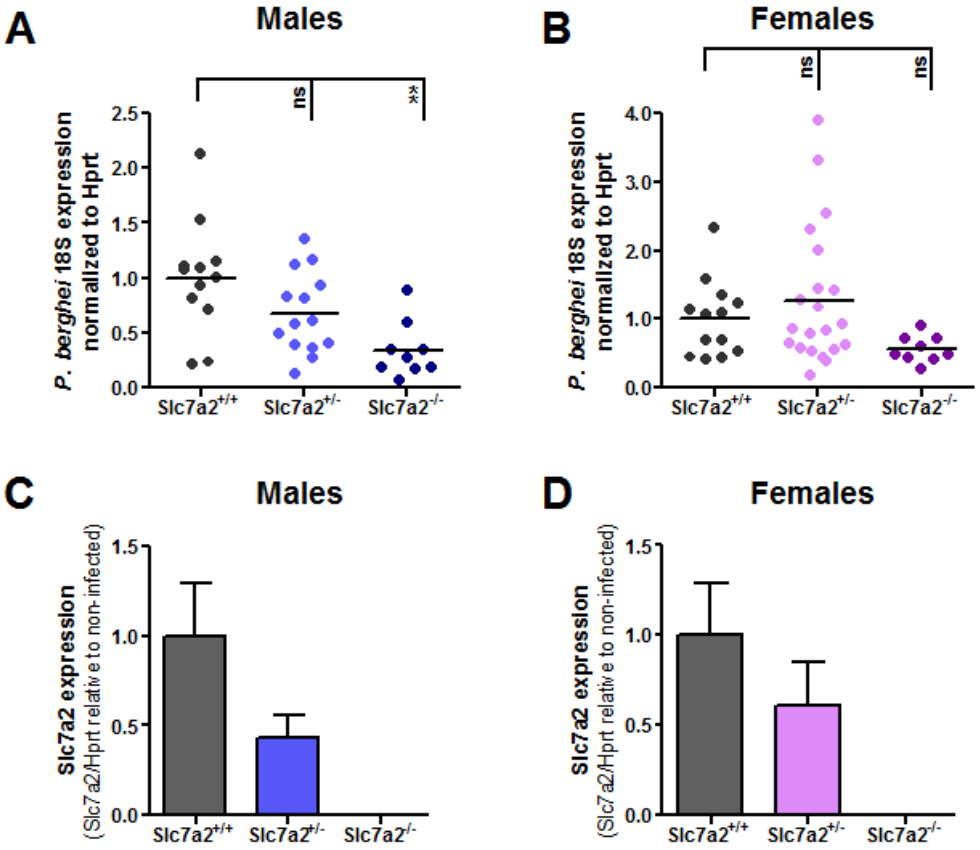

Figure 3.2 - *P. berghei* liver load is reduced in *Slc7a2*$^{-/-}$ mice. *Slc7a2*$^{+/+}$, *Slc7a2*$^{+/-}$ and *Slc7a2*$^{-/-}$ littermate mice were infected with 1.0x10^4 *P. berghei* sporozoites and the

parasite liver load at 44 hpi was determined by qPCR. **(A)** Liver load in males. WT: n= 12; heterozygous: n = 14; KO: n = 9. **(B)** Liver load in females. WT: n= 13; heterozygous: n = 21; KO: n = 9. **(C)** Expression of both variants of *Slc7a2* in the livers of male mice. Error bars represent SD. **(D)** Expression of both variants of *Slc7a2* in the livers of female mice. Error bars represent SD. Pool of 2 independent experiments. Panels **(A)** and **(B)**: One-way ANOVA with Dunnett. ns - not significant and ** $p < 0.01$.

To exclude possible effects of the absence of expression of *Slc7a2* in non-parenchymal liver cells on the observed phenotype, primary hepatocytes were collected from the livers of KO, heterozygous and WT mice and infected with GFP-expressing *P. berghei* parasites. Our *ex vivo* results show that, 48 hours after sporozoite addition, the overall parasite load in KO hepatocytes is approximately 60% lower than in WT liver cells (Fig. 3.3A), in perfect agreement with our *in vivo* observations. Similarly, parasite load in primary hepatocytes from heterozygous mice is reduced when compared with the WT but the reduction is milder. Immunofluorescence microscopy analyses of infected primary hepatocytes further confirmed that in the absence of both transporters encoded by *Slc7a2* the parasite's ability to develop intracellularly is significantly impaired (Fig. 3.3B).

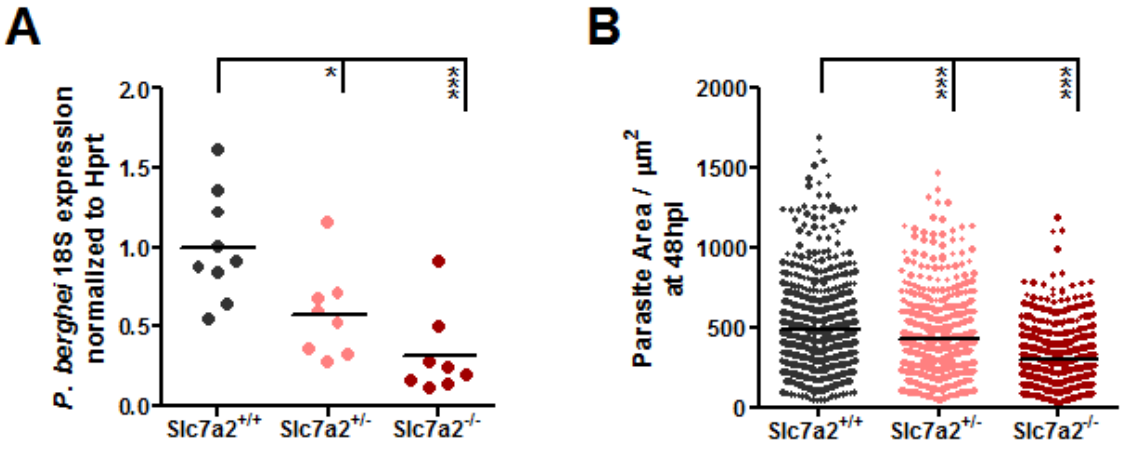

Figure 3.3 – Absence of *Slc7a2* in hepatocytes impairs *P. berghei* development. (A) Primary hepatocytes from *Slc7a2*$^{+/+}$, *Slc7a2*$^{+/-}$ and *Slc7a2*$^{-/-}$ littermate mice were infected *ex vivo* with *P. berghei* sporozoites and parasite load at 48 hpi was determined by qPCR. **(B)** Immunofluorescence microscopy quantification of EEF areas in primary hepatocytes from *Slc7a2*$^{+/+}$, *Slc7a2*$^{+/-}$ and *Slc7a2*$^{-/-}$ littermate mice at 48 hpi. Pool of 3 independent experiments. Both panels: One-way ANOVA with post-test Dunnett. * $p < 0.05$ and *** $p < 0.001$.

Absence of *Slc7a2* does not impact blood stage *P. berghei* infection

Finally, to determine if the absence of *Slc7a2* expression would affect *P. berghei* blood parasite load and mouse survival, both male and female WT and KO mice were injected i.v. with $1.0x10^4$ luciferase-expressing *P. berghei* sporozoites. Blood parasite load was monitored daily, starting on day 2, by a bioluminescence assay [412]. No difference in blood parasite load was observed between the 2 groups of mice (Fig. 3.4A). The survival of the mice was also not affected by the absence of *Slc7a2* (Fig. 3.4B). These data suggest that, contrarily to what we observed in hepatocytes, the two transporters encoded by *Slc7a2* are not important for *Plasmodium* survival inside RBCs and that its absence does not improve the outcome of infection. This is not surprising because, contrarily to hepatocytes, in which CAT2A is the main Arg transporter, RBCs uptake Arg via the ubiquitous CAT1.

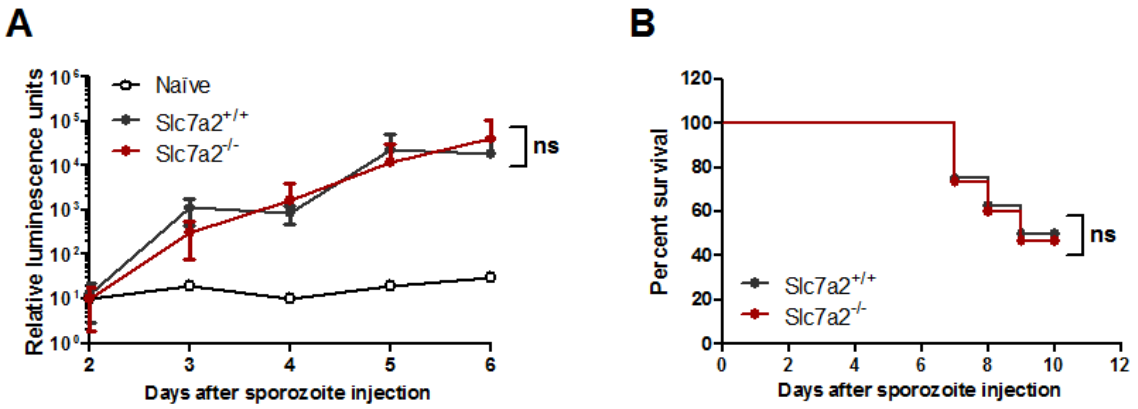

Figure 3.4 – Effect of the absence of *Slc7a2* on blood parasite load and mouse survival. (A) Blood parasite load in WT and KO mice following i.v. injection of $1.0x10^4$ luciferase-expressing *P. berghei* sporozoites, assessed by a bioluminescence assay. Representative experiment out of 2 independent experiments. WT: n = 4; KO: n = 7 mice. Two-way ANOVA with post-test Bonferroni. **(B)** Survival of WT and KO mice infection. Pool of 2 independent experiments. WT: n = 8; KO: n = 15 mice. Gehan-Breslow-Wilcoxon Survival test. ns – not significant.

Arg availability is essential for *Plasmodium* hepatic infection

Since Arg has been shown to play an important role in various infections [416-419], we sought to investigate the effect of the depletion of this amino acid on the outcome of *Plasmodium* infection. We started by showing that a decrease in Arg

availability in the cell culture medium of Huh7 cells infected by luciferase-expressing *P. berghei* sporozoites leads to a decrease in overall parasite load, as measured by the luminescence assay of infected cell lysates, for Arg concentrations below 2.5 µM (Fig. 3.5A). Likewise, addition of increasing concentrations of N^G-N^G-dimethyl-L-arginine (L-SDMA), a competitor for Arg transport, to the culture medium leads to a decrease in parasite load (Fig. 3.5B). Overall, these data indicate that Arg uptake is essential to sustain *Plasmodium* hepatic infection.

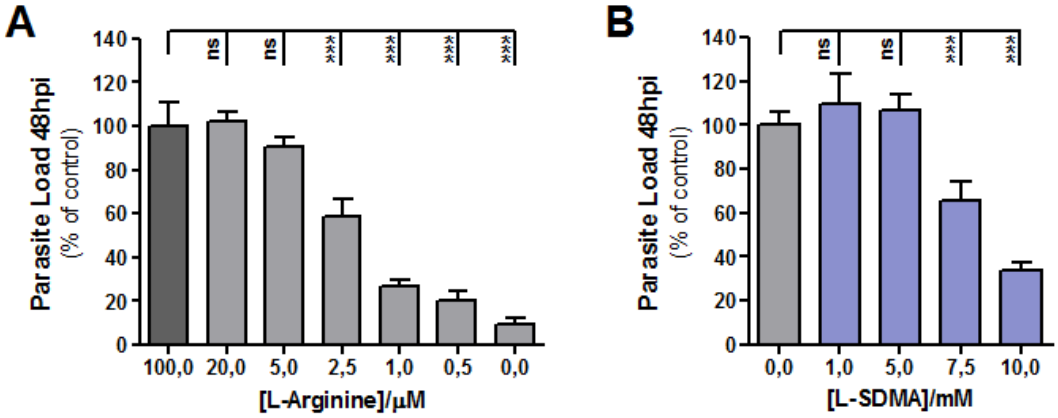

Figure 3.5 – Effect of Arg availability on *Plasmodium* hepatic infection. (A) Huh7 cells were infected with luciferase-expressing *P. berghei* sporozoites and cultured in medium with different concentrations of Arg. Parasite load was assessed by bioluminescence 48 hours after infection. Representative experiment out of 3 independent experiments. Error bars represent SD. **(B)** Huh7 cells were infected with luciferase-expressing *P. berghei* sporozoites and cultured in medium with increasing concentrations of the competitor L-SDMA. Parasite load was assessed 48 hours after infection by bioluminescence. Pool of 2 independent experiments. Error bars represent SD. Both panels: One-way ANOVA with post-test Dunnett. ns - not significant and *** $p < 0.001$.

SLC7A2 expression and function are not enhanced in *Plasmodium*-infected cells

Having established a role for *SLC7A2* and for the availability of Arg during *Plasmodium* hepatic infection, we decided to investigate if the expression of any of the splice variants of this transporter was altered in *Plasmodium*-infected cells, as was previously observed by microarray analysis [11]. To address this, we assessed their expression levels in sorted non-infected and infected Huh7 cells at 6, 18, 30 and 48 hpi with GFP-expressing *P. berghei* parasites. Our results show

that hepatoma cells express both the liver-expressed, low affinity variant 1 (that originates CAT2A), and the inducible, high affinity variant 2 (that encodes CAT2B) (Fig. 3.6A). However, no significant differences in expression were observed for any of the variants between infected and non-infected cells at the selected time points (Fig. 3.6A).

We then sought to determine whether *Plasmodium* infection influenced the uptake of Arg by the host cells via CAT2 transporters. To this end, we determined the specific uptake of [^{3}H] Arg by sorted *P. berghei*-infected and non-infected cells at 24 hpi. Huh7 cells with the knockdown of *SLC7A2* (the SLC7A2#02 cell line) were used as control for non-specific transport (in these cells, *SLC7A2* expression is very low and, therefore, their Arg uptake is mainly mediated by other transporters). Of note, in the conditions used, only CAT2A-mediated Arg transport can be assessed. Once again, no significant differences were observed, suggesting that although Arg is essential for *Plasmodium* hepatic infection, CAT2A-mediated Arg uptake is not increased in infected cells (Fig. 3.6B). Finally, we used [^{3}H] Arg uptake to assess the extent to which CAT2A and CAT2B contribute to the total uptake of Arg by Huh7 cells. Our data show that Arg uptake by the SLC7A2#02 cell line, which has a 90% knockdown of *SLC7A2* expression, is reduced by 50%, implying that CAT2A and CAT2B are responsible for at least half of the total Arg uptake by Huh7 cells (Fig. 3.6C).

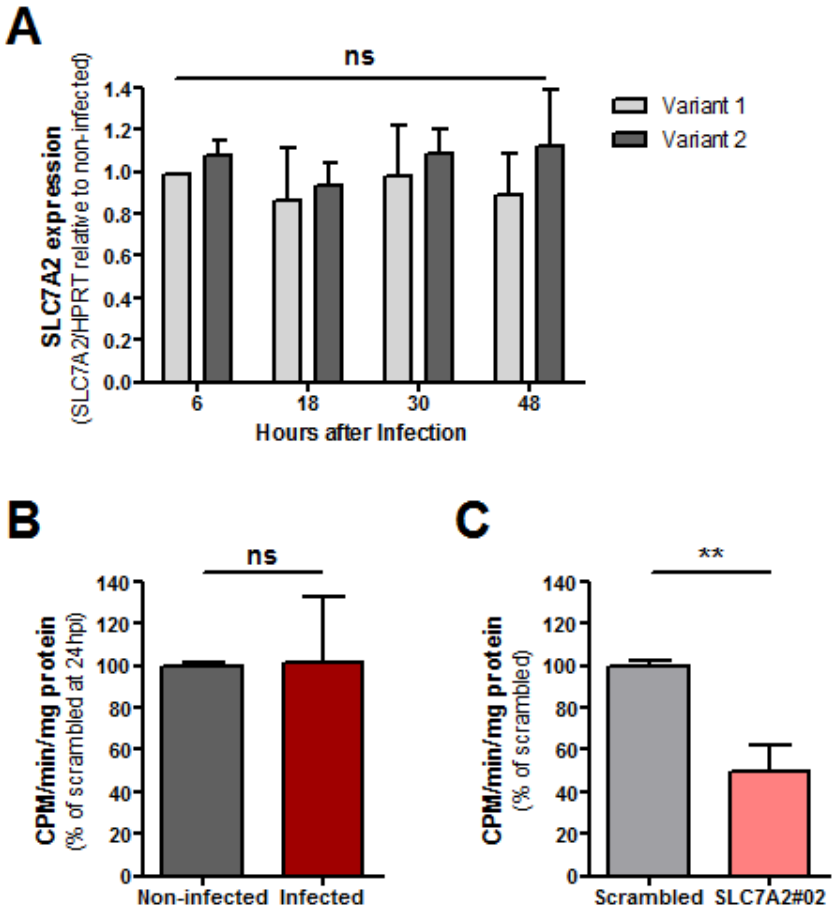

Figure 3.6 – *Plasmodium* infection does not alter *SLC7A2* expression and CAT2-mediated Arg uptake by infected cells. (A) Quantification of the transcriptional expression of both variants of *SLC7A2* on sorted infected and non-infected Huh7 cells by qPCR. Each time point corresponds to a pool of 2 independent sorting experiments. Error bars represent SD. Two-way ANOVA with Bonferroni. **(B)** Specific [^{3}H] Arg uptake by sorted *P. berghei*-infected cells and non-infected cells at 24 hpi. Pool of 2 independent experiments. Unpaired t-test. **(C)** [^{3}H] Arg uptake by control cells and cells with the stable knockdown of *SLC7A2*. Pool of 3 independent experiments. Mann-Whitney test. ns - not significant and ** $p < 0.01$.

Successful *Plasmodium* development depends on polyamine synthesis

A significant amount of the Arg taken up by the infected host cell will likely be employed in one of the two main metabolic pathways that have been described in the context of infections by other pathogens, the iNOS and the arginase pathways, which lead to the synthesis of NO and polyamines, respectively (Fig. 3.7) [22].

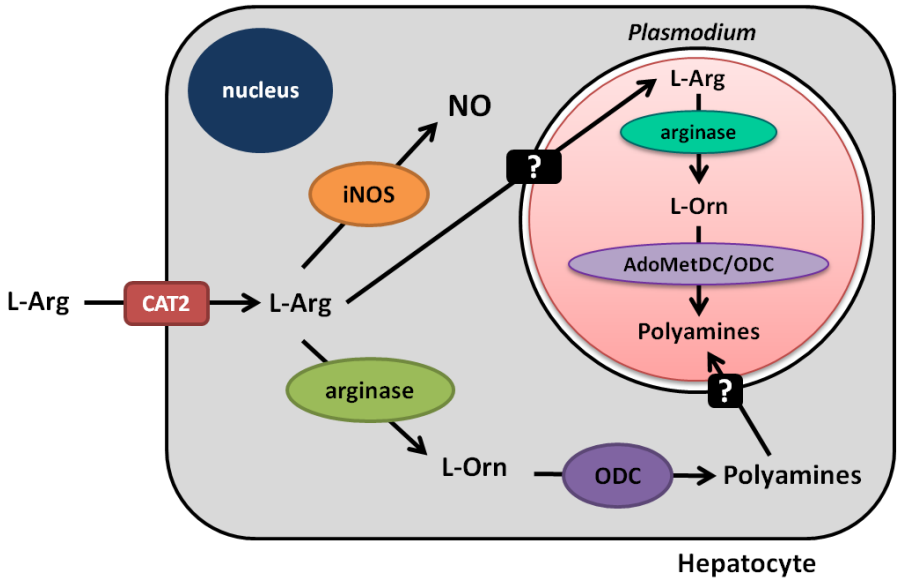

Figure 3.7 – Arg metabolic pathways and their influence on *Plasmodium* infection.

In a first attempt to uncover which pathway uses the Arg taken up by *Plasmodium*-infected cells, we assessed the expression levels of the key enzymes from both pathways in sorted non-infected and infected Huh7 cells at 6, 18, 30 and 48 hpi by qPCR, employing specific primers for each gene (see Table 3.2). No significant differences in expression of the enzymes were observed between infected and non-infected cells at the selected time points (Fig. 3.8).

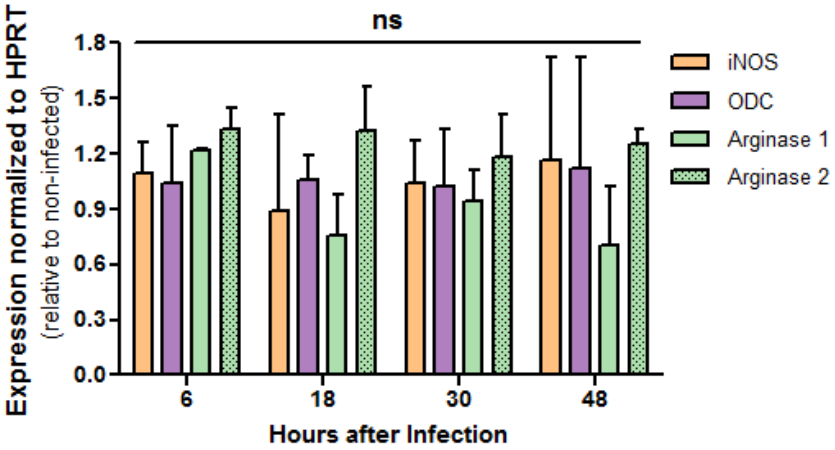

Figure 3.8 – Expression of the enzymes involved in Arg metabolism is not altered in *Plasmodium*-infected cells. Quantification of the transcriptional expression of iNOS, ODC, arginase 1 and arginase 2 on sorted infected and non-infected Huh7 cells by qPCR. Each time point corresponds to a pool of 2 independent sortings. Error bars represent SD. Two-way ANOVA with Bonferroni. ns – not significant.

We then investigated the role of the NO production pathway on *Plasmodium* liver stages. To this end, we assessed the impact of L-NAME, a well-known inhibitor of iNOS, on hepatic infection. Our *in vitro* and *ex vivo* results showed that inhibition of iNOS does not affect *Plasmodium* infection of hepatic cells (Fig. 3.9A, B). Similarly, the administration of L-NAME to mice did not have an impact on *in vivo P. berghei* liver load (Fig. 3.9C). These results are in agreement with published data employing the L-NAME inhibitor *in vivo* and with results of infection of iNOS-KO mice [232].

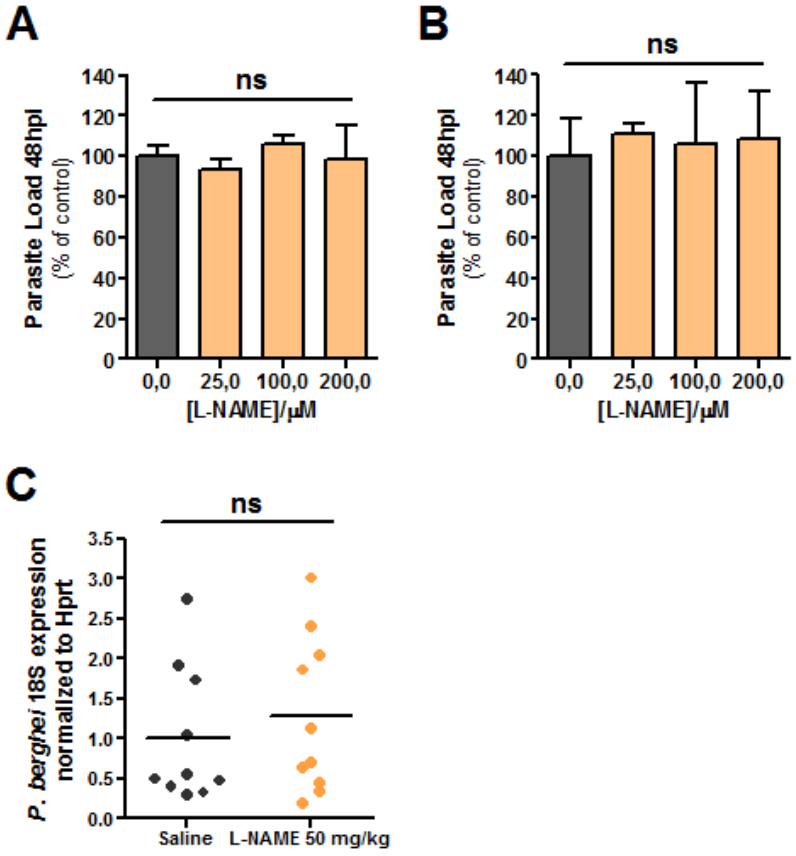

Figure 3.9 – Chemical inhibition of NO production does not impact *Plasmodium* hepatic infection. (A) Huh7 cells were infected with luciferase-expressing *P. berghei* sporozoites and 2 hours later the culture medium was replaced by medium with increasing concentrations of L-NAME. Parasite load (luminescence) was assessed at 48 hpi. Representative experiment out of 2 independent experiments. Error bars represent SD. One-way ANOVA with post-test Dunnett. **(B)** Mouse primary hepatocytes were infected with luciferase-expressing *P. berghei* sporozoites and 2 hours later the culture medium was replaced by medium with increasing concentrations of L-NAME. Parasite load (luminescence) was assessed at 48 hpi. Representative experiment out of 2 independent experiments. Error bars represent SD. One-way ANOVA with post-test Dunnett. **(C)**

C57BL/6 mice received four daily doses of 50 mg/kg of L-NAME i.p., starting 3 days before infection and until the day of sporozoite i.v. injection. Parasite load was assessed at 44 hpi by qPCR. Pool of 2 independent experiments. Saline: n = 10 mice; L-NAME-treated: n = 10 mice. Two-tailed Mann-Whitney test. ns - not significant.

Since the inhibition of NO production did not affect *Plasmodium* hepatic infection, we wondered if its stimulation would have any effect in this regard. Some studies of *Plasmodium*-infected mice reported that increasing the circulating levels of Arg enhances NO production [32, 33]. With this in mind, we attempted to stimulate NO production in hepatocytes by supplementing the drinking water of the mice with 2.5% Arg (w/v) for 4 weeks. Livers were then collected 44 hours after infection with *P. berghei* sporozoites and parasite load was determined by qPCR. No difference was observed between the group drinking the supplemented water and the group drinking normal water (Fig. 3.10). These results suggest that providing extra Arg might not be sufficient to stimulate NO production by hepatocytes and thereby affect *Plasmodium* infection, or that the extra Arg provided is being employed by other pathways.

Taking together the results of the inhibition of NO production by L-NAME and the attempt of its stimulation through Arg supplementation, it would seem that the Arg being taken up by *Plasmodium*-infected cells is not being used for NO production.

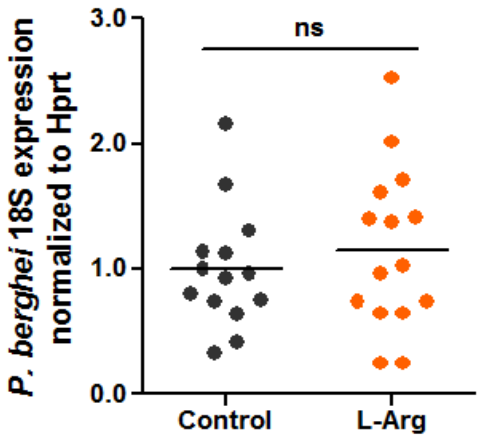

Figure 3.10 – Arg supplementation does not affect *Plasmodium* hepatic infection. Mice were allowed to drink a 2.5% (w/v) Arg solution *ad libitum* for 4 weeks before infection with *P. berghei* sporozoites. Parasite load was assessed at 44 hpi by qPCR. Pool of 3 independent experiments. Control: n = 14 mice; L-Arg: n = 15 mice. Two-tailed Mann-Whitney test. ns - not significant.

We then decided to investigate whether Arg is being used for polyamine synthesis. To this end, we inhibited the rate-limiting enzyme of this pathway, ODC, with the well-known inhibitor α-difluoromethylornithine (DFMO), by adding it to Huh7 cells 2

hours after infection with luciferase-expressing *P. berghei* sporozoites. Our results show that the addition of increasing concentrations of DFMO to the culture medium leads to a decrease in parasite load (Fig. 3.11A). Using GFP-expressing *P. berghei* parasites, we also observed by flow cytometry that a pre-treatment of the cells with DFMO inhibits cell invasion by these parasites, as shown by the significantly lower number of GFP^+ cells detected 2 hpi (Fig. 3.11B). Importantly, the development of *P. berghei* liver stage parasites is significantly affected by the addition of DFMO, in agreement with previous reports of a cytostatic effect of this compound on *P. falciparum* blood stages [340, 420]. Overall, these data suggest that polyamine synthesis plays an important role during *Plasmodium* hepatic growth.

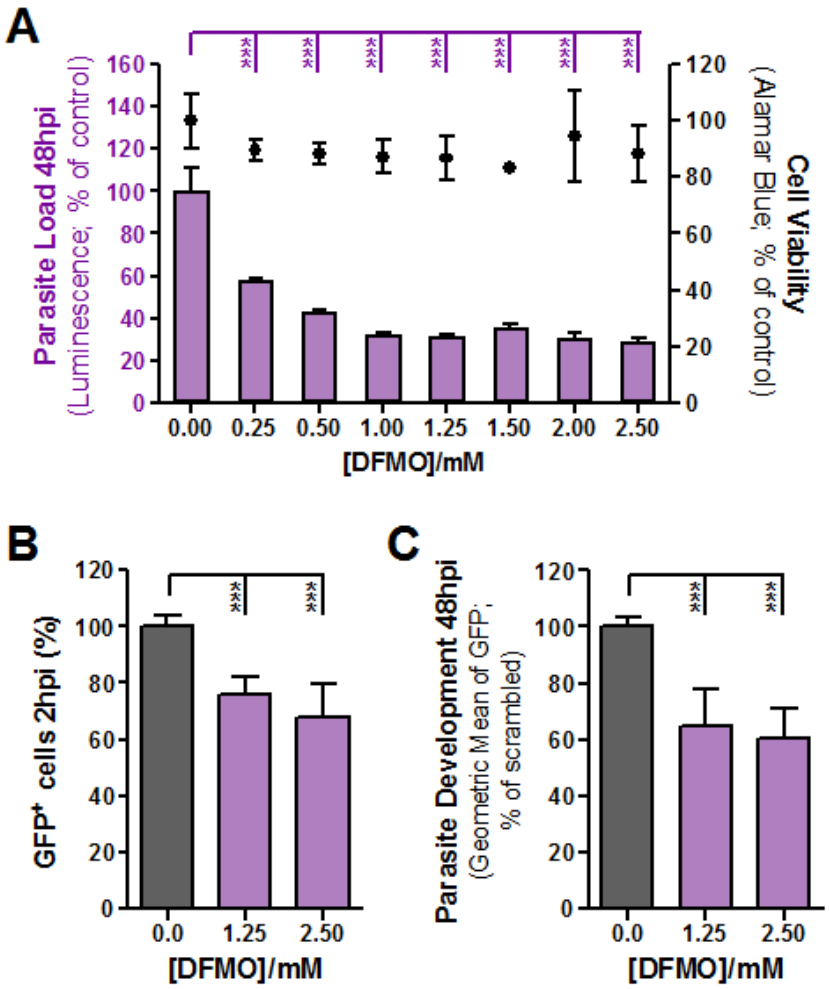

Figure 3.11 – ODC inhibition affects *P. berghei* invasion and development inside hepatoma cells. (A) Huh7 cells were infected with luciferase-expressing *P. berghei* sporozoites and 2 hours later the culture medium was replaced by medium with increasing concentrations of DFMO. Parasite load (bioluminescence) and cell viability were assessed

at 48 hpi. Representative experiment out of 2 independent experiments. Error bars represent SD. **(B)** The culture medium of Huh7 cells was replaced by medium with 1.25 or 2.50 mM of DFMO 1 hour prior to infection with GFP-expressing sporozoites. Cell invasion was quantified by determining the percentage of GFP^+ cells 2 hpi by flow cytometry. Pool of 3 independent experiments. Error bars represent SD. **(C)** Huh7 cells were infected with GFP-expressing *P. berghei* sporozoites and the culture medium was replaced 2 hpi by media with 1.25 or 2.50 mM of DFMO. Parasite development was assessed by flow cytometry by determining the fluorescence intensity of GFP^+ cells at 48 hpi. Pool of 3 independent experiments. Error bars represent SD. All panels: One-way ANOVA with post-test Dunnett. *** $p < 0.001$.

Both *Plasmodium* and the host cells express the enzymes of the polyamine synthesis pathways (Fig. 3.7). In addition, the ODC activity of *Plasmodium* AdoMetDC/ODC catalyzes the same reaction as mammalian ODC, and can also be inhibited by DFMO [340]. Therefore, we sought to deconvolute the effect of the host and parasite polyamine synthesis pathways on infection, using an RNAi approach to down-modulate the expression of ODC and arginase 1 in the host cell. Our results show that down-modulation of the expression of host ODC and arginase 1 has no impact on cell invasion and on *Plasmodium* development (Fig. 3.12A, B), suggesting that *Plasmodium* parasites rely mainly on their own pathway to synthesize polyamines. The efficiency of knockdown was confirmed by qPCR employing specific primers for these genes (Table 3.2).

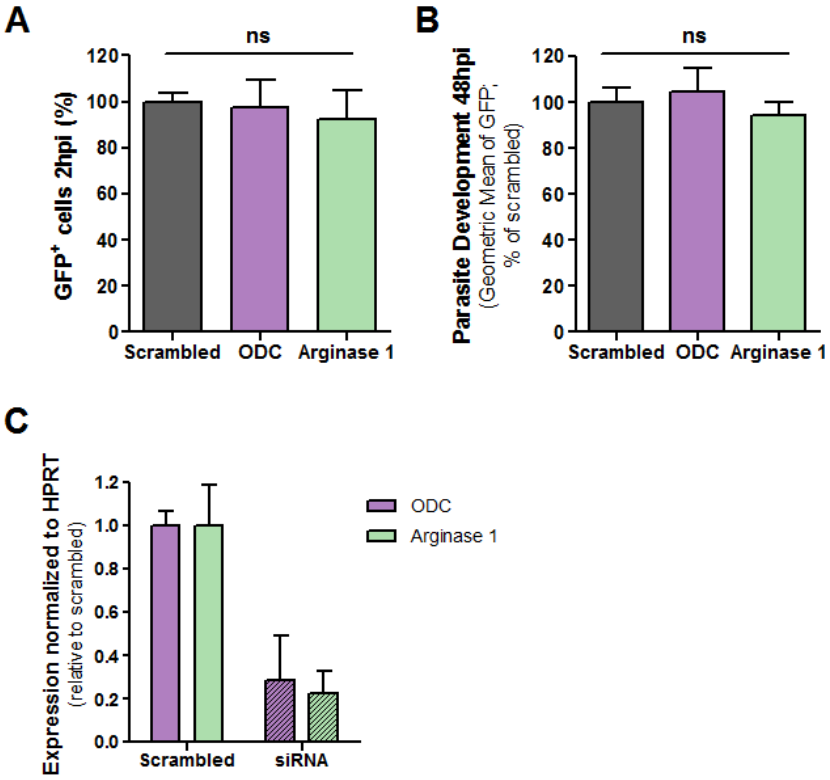

Figure 3.12 – Inhibition of polyamine synthesis by the host cell through down-modulation of its enzymes ODC and arginase 1 does not affect *P. berghei* invasion and development. (A) Huh7 cells with the knockdown of ODC and arginase 1 were infected with GFP-expressing *P. berghei* sporozoites and cell invasion was quantified by determining the percentage of GFP^+ cells 2 hpi by flow cytometry. Pool of 3 independent experiments. Error bars represent SD. One-way ANOVA with post-test Dunnett. **(B)** Huh7 cells with the knockdown of ODC and arginase 1 were infected with GFP-expressing *P. berghei* sporozoites and parasite development was assessed by flow cytometry at 48 hpi. Pool of 3 independent experiments. Error bars represent SD. One-way ANOVA with post-test Dunnett. **(C)** Knockdown efficiency upon transfection of Huh7 cells with the siRNAs targeting the host's ODC and arginase 1. Error bars represent SD. ns - not significant.

The unexpected behavior of the arginase-KO parasite

To further investigate the dependence of the parasite on its own polyamine synthesis pathway, we compared the *in vitro* and *in vivo* infectivity of an available arginase-KO *P. berghei* parasite with that of its WT counterpart. We observed that, of a total 6 independent experiments *in vitro*, the arginase-KO displayed a significantly lower infection in 3 of those experiments and a similar infection in the remaining 3 experiments (Fig. 3.13A, B). This bimodal pattern was also reproduced in an *in vivo* setting. We carried out 8 independent rodent infection

studies where we compared the liver parasite loads of mice infected with WT or arginase-KO *P. berghei* parasites and also found a drastically lower liver infection in 4 of them and no significant differences in the remaining 4 experiments (Fig. 3.13C, D).

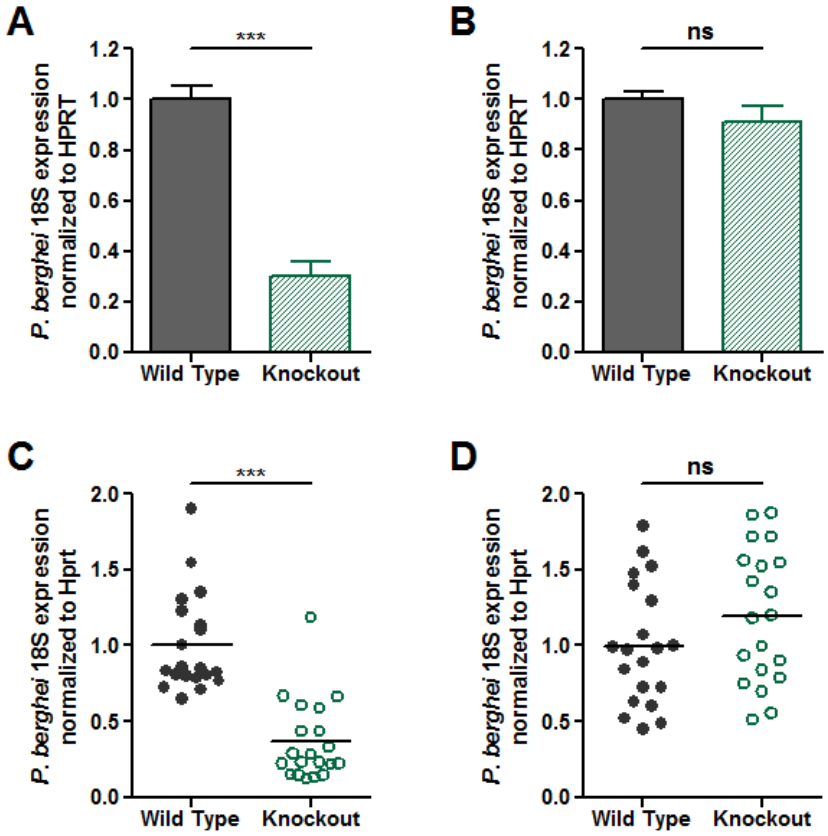

Figure 3.13 – The arginase-KO parasite displays a bimodal behavior both *in vitro* and *in vivo*. (A) Huh7 cells were infected with WT and arginase-KO *P. berghei* sporozoites and parasite load was assessed at 48 hpi by qPCR. In 3 out of 6 independent experiments, infection by the arginase-KO parasite was reduced by 70%. Error bars represent SEM. **(B)** In the remaining 3 out of 6 experiments, no difference was observed. Error bars represent SEM. **(C)** Mice were infected with WT and arginase-KO *P. berghei* sporozoites and parasite liver load was assessed at 44 hpi by qPCR. In 4 out of 8 independent experiments, infection by the arginase-KO was reduced by 65%. Wild Type: n = 20 mice; arginase-KO: n = 20 mice. **(D)** In the remaining 4 out of 8 experiments, no difference was observed. Wild Type: n = 20 mice; arginase-KO: n = 20 mice. All panels: Mann-Whitney test. ns - not significant and *** $p < 0.001$.

In the experiments in which the infection by the arginase-KO parasite is reduced we also investigated whether the effect was due to a reduction in the number of parasites or in their development. We found that the observed reduction in

parasite load 48 hpi can be fully explained by a reduction in the percentage of infected cells, suggesting that the survival of the arginase-KO parasite might be impaired (Fig. 3.14A). The surviving arginase-KO parasites do not show any impairment in their hepatic development, as confirmed by their similar average EEF size in comparison with the WT parasite (Fig. 3.14B).

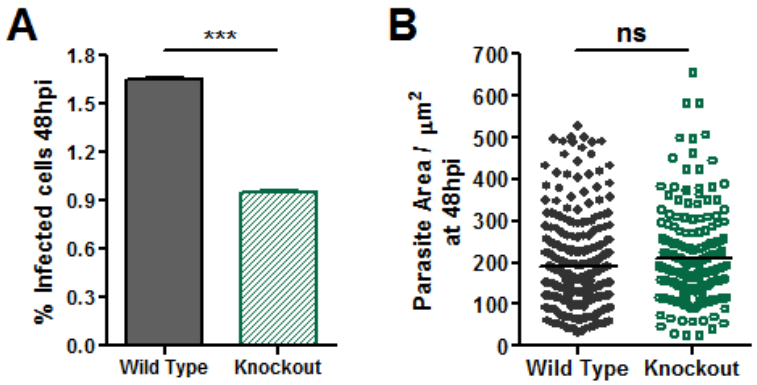

Figure 3.14 – The reduced infection by the arginase-KO parasite observed in half of the experiments is caused by a reduction in the percentage of infected cells and not by an impairment of parasite development. (A) Huh7 cells were infected with WT and arginase-KO *P. berghei* sporozoites and the percentage of infected cells was quantified by immunofluorescence microscopy 48 hpi. Representative experiment out of 2 independent experiments. Error bars represent SD. **(B)** Parasite size was determined by immunofluorescence microscopy at 48 hpi. Representative experiment out of 2 independent experiments. Both panels: Unpaired t-test. ns - not significant and *** $p < 0.001$.

Finally, in the experiments in which the infectivities of both parasites were similar, the knockdown of the expression of the host's ODC or arginase I led to a 30% decrease in parasite load (Fig. 3.15A). In the experiments in which the infection by the arginase-KO parasite is reduced, the knockdown of the host's enzymes did not have any further effect on the parasite (Fig. 3.15B).

Collectively, these results suggest that the parasite needs polyamines for its hepatic development and that it relies primarily on its own polyamine synthesis pathway, as the knockdown of the host's polyamine synthesis enzymes does not affect its development. However, the results obtained with the arginase-KO parasite suggest that, under some circumstances, the parasite might circumvent the absence of its own polyamine biosynthesis machinery by acquiring, at least partially, the polyamines it needs to develop from its host.

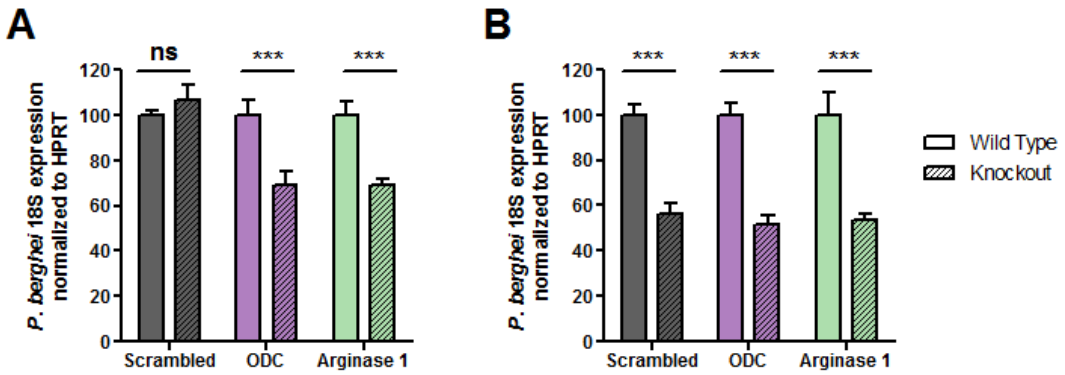

Figure 3.15 – The knockdown of the host's enzymes ODC and arginase 1 only affects the infection of the arginase-KO parasite when it behaves similarly to the WT. (A) Huh7 cells with or without the knockdown of host's ODC and arginase 1 were infected with WT and arginase-KO *P. berghei* sporozoites and parasite load was assessed at 48 hpi by qPCR. **(A)** In the experiments in which the arginase-KO parasite displayed a behavior similar to the WT parasite, ODC and arginase 1 knockdown led to a 30% reduction in parasite load. Pool of 4 independent experiments. Error bars represent SEM. **(B)** In the experiments in which the infection by the arginase-KO parasite was already reduced relative to the WT control, no further decrease was observed upon ODC and arginase 1 knockdown. Pool of 2 independent experiments. Error bars represent SEM. Both panels: Two-way ANOVA with post-test Bonferroni. ns - not significant and *** $p < 0.001$.

Discussion

Plasmodium parasites are incapable of *de novo* amino acid biosynthesis and, during the intraerythrocytic stage of their life cycle, obtain most of their supply of amino acids from the digestion of hemoglobin [305, 409]. Although Arg supplementation is unnecessary to support *P. falciparum* blood-stage growth, this amino acid was found to be significantly depleted during the parasite's trophozoite and schizont stages [24, 421]. The resulting hypoargininemia contributes to several aspects of disease severity, such as limited NO production, reduced RBC deformability and adherence of parasitized RBCs to endothelium [24, 410, 422, 423]. This Arg depletion has been attributed to the action of the parasite's arginase and results in the production of significant amounts of the polyamine synthesis precursor, ornithine [24]. As a result, it is not surprising that polyamines have been shown to be among the major metabolites present within *P. falciparum* blood-stage malaria parasites [334].

Hepatic *Plasmodium spp.* parasites cannot rely on hemoglobin degradation to obtain the amino acids they require and must, therefore, acquire them from the host hepatocyte. Here, we show that the normal developmental process of liver-stage *P. berghei* is dependent on Arg availability (Fig. 3.5). This Arg is acquired by the host cell mostly via the CAT2A and CAT2B transporters (Fig. 3.1, 3.2, 3.3 and 3.6C). Furthermore, it seems that the normal Arg uptake by the cells is sufficient to sustain *Plasmodium* development. This hypothesis is supported by the similar Arg uptake and *SLC7A2* expression observed in infected cells in comparison with non-infected (Fig. 3.6A, B).

Additionally, we show that the Arg taken up by the infected cell is mainly being used as a source of polyamines, to promote parasite growth (Fig. 3.11). The inhibition of polyamine production by the host cell alone, accomplished through the down-modulation of the expression of the host's arginase I or ODC enzymes, has no impact on *P. berghei* development in Huh7 cells. When the pathways from both the host and the parasite are inhibited simultaneously with the ODC inhibitor, DFMO, parasite development is significantly impaired (Fig. 3.11). These results suggested that the parasite relies mostly on its own polyamine synthesis pathway. To test this hypothesis, we used an arginase-KO *P. berghei* parasite, which displayed a clear bimodal behavior in terms of its hepatic infectivity (Fig. 3.13). In

half of the experiments (both *in vitro* and *in vivo*), the absence of the parasite's arginase led to a significant decrease in parasite load, due to a marked reduction in the percentage of infected cells at 48 hpi. In the remaining half of the experiments, no difference in infectivity could be detected between the arginase-KO parasite and its WT counterpart, unless there was a simultaneous impairment in the host's polyamine pathway (Fig. 3.15A). Collectively, these data suggest that the parasite preferentially uses its own biosynthesis pathway to obtain the polyamines it requires and when this pathway is compromised, if the parasites do not use some other compensatory mechanisms to guarantee their survival, most of them perish inside hepatocytes. Part of these compensatory mechanisms might involve the expression of transporters that will allow the uptake of polyamines and their precursors from the host cell (Fig. 3.15A). However, the existence of other compensatory mechanisms should also be expected, as the impairment of the host's polyamine synthesis pathway through the down-modulation of arginase 1 and ODC impacts *P. berghei* hepatic infection by only 30% (Fig. 3.15A). Finally, our results suggest that these compensatory mechanisms are induced during the parasite's life cycle in the mosquito vector. This notion is supported by our observation that each batch of arginase-KO parasites consistently displayed similar behaviors in *in vitro* and *in vivo* infections, which seems to exclude a host-dependent effect. However, further studies are clearly required to fully clarify this matter.

Acknowledgements

We are very grateful to Lesley G. Ellies (University of California, San Diego School of Medicine) for kindly providing the *Slc7a2*$^{+/-}$ breeding trio, to Vanessa Zuzarte-Luís for the protocol of extraction of mouse primary hepatocytes, to Ana Parreira and Filipa Teixeira for producing the various lines of *P. berghei*-infected mosquitoes and to the Bioimaging, Flow Cytometry and Rodent facilities of iMM Lisboa for technical support.

Inhibition of *Plasmodium* liver infection by amino acid supplementation and modulation of arginine metabolism

Patrícia Meireles[1], Carolina M. Andrade[1], António M. Mendes[1], Miguel Prudêncio[1]

[1] Instituto de Medicina Molecular, Faculdade de Medicina, Universidade de Lisboa, Avenida Professor Egas Moniz, 1649-028, Lisboa, Portugal

Author Contributions

PM and MP designed the experiments. PM performed all the experiments. CMA helped with one of the experiments evaluating the time of supplementation. AMM gave intellectual input to the work. PM wrote the chapter. MP supervised the work and revised the text.

Introduction

As described in the previous chapter, L-arginine (Arg) can be employed by cells as a precursor of both polyamines and nitric oxide (NO). Polyamines mediate several important cellular processes, including differentiation and proliferation, and assume particular importance for rapidly proliferating cells, such as cancer cells and protozoan parasites [323-329]. Most commonly, polyamine metabolism is targeted by preventing intracellular polyamine biosynthesis with enzyme inhibitors [324, 329, 424]. α-difluoromethylornithine (DFMO), an irreversible ornithine decarboxylase (ODC) inhibitor, is the most widely studied inhibitor of polyamine metabolism and it was approved by the Food and Drug Administration (FDA) for the treatment of African trypanosomiasis [424]. Its efficacy has been demonstrated against several tumors *in vitro* and *in vivo*, such as neuroblastoma, lung carcinoma and prostate cancer [424-426]. Clinical trials in cancer patients have shown that this inhibitor is well tolerated, even at high doses, with only the occasional occurrence of reversible ototoxicity, nausea and mild neutropenia. However, to date it has failed to translate to the clinic [324, 424, 426].

Inducible nitric oxide synthase (iNOS)-derived NO is involved in both the pathogenesis and control of several types of viral, bacterial and parasitic infections [427-429]. Bacterial lipopolysaccharides (LPS) and inflammatory cytokines, such as IFN-ɣ and TNF-α, are well-known stimulators of the production of NO via up-regulation of iNOS [429-433]. In malaria, increased NO production has been reported in both laboratory models of infection and human patients [434-436]. Early during a *Plasmodium* blood-stage infection, increased production of endogenous NO has been found to correlate with protection [437, 438]. Additionally, NO and NO donors have been shown to mediate *in vitro* killing of both hepatic and blood forms of malaria parasites [34-39]. However, controversy exists as to the role of NO in malaria because NO has also been reported to contribute to the development of cerebral malaria pathology [430, 439, 440].

It has been reported that an increase in the circulating levels of Arg in *Plasmodium*-infected mice leads to enhanced NO production [32, 33]. Yet, while in one of these studies Arg supplementation significantly decreased parasitaemia and improved survival of *P. yoelii*-infected Balb/c mice [33], none of these effects were observed in *P. berghei*-infected C57BL/6 mice [32]. In individuals with

moderately severe malaria, Arg infusion was shown to be safe, and effectively increased plasma Arg concentrations and NO production, leading to improved endothelial function [441, 442]. More recently, in a pilot study with patients with severe *P. falciparum* malaria in which Arg infusion was used as an adjunctive treatment, its safety was confirmed but no increase on NO bioavailability was observed [443].

Arg metabolism can be regulated by multiple factors that include dietary amino acids [407]. L-lysine (Lys), L-ornithine (Orn) and L-valine (Val) have been described as arginase inhibitors [30, 31]. Additionally, Lys and Orn also compete with Arg for entry into cells via cationic amino acid transporters [444]. Having shown in the previous chapter that Arg uptake via CAT2A and CAT2B and Arg-dependent polyamine synthesis play an important role on parasite hepatic development, we wondered whether *Plasmodium* infection could be impaired and NO production stimulated by appropriate amino acid supplementation.

Materials and Methods

Chemicals

RPMI 1640, William's E, PBS pH 7.4, trypsin, FBS, non-essential amino acids, penicillin/streptomycin, glutamine, HEPES pH 7, liver perfusion medium (LPM) and liver digestion medium (LDM) were purchased from Gibco/Invitrogen. All other chemicals were obtained from Sigma, unless otherwise specified.

Cells

Huh7 cells, a human hepatoma cell line, were cultured in RPMI 1640 medium supplemented with 10% FBS, 1% non-essential amino acids, 1% penicillin/streptomycin, 1% Glutamine and 1% HEPES, pH 7 and maintained at 37°C with 5% CO_2. Mouse primary hepatocytes were cultured in William's E medium supplemented with 4% FBS and 1% penicillin/streptomycin and maintained at 37°C with 5% CO_2.

Mice

C57BL/6 mice were purchased from Charles River and housed in the facilities of the Instituto de Medicina Molecular. All animal experiments were performed in strict compliance to the guidelines of our institution´s animal ethics committee and the Federation of European Laboratory Animal Science Associations (FELASA).

Parasites

GFP- or luciferase-expressing *P. berghei* ANKA sporozoites were dissected in non-supplemented RPMI medium from the salivary glands of infected female *A. stephensi* mosquitoes, bred at Instituto de Medicina Molecular (Lisbon, Portugal), prior to being employed for *in vitro, ex vivo* and *in vivo* infections [358, 359].

Overall *in vitro* infection by luminescence

Overall hepatic infection was determined by measuring the luminescence intensity in cells infected with a firefly luciferase-expressing *P. berghei* line, as previously described [358]. Briefly, Huh7 cells ($1.0x10^4$ per well) or mouse primary hepatocytes ($2.0x10^4$ per well) were seeded in 96-well plates the day before

infection. Sporozoite addition ($1.0x10^4$ per well) was followed by centrifugation at 1800xg for 5 minutes and the medium was replaced approximately 2 hours after infection by the appropriate medium. Parasite infection load was measured 48 hours after infection by a bioluminescence assay (Biotium) using a multiplate reader Infinite M200 (Tecan). The effect of the different treatments on the viability of the cells was assessed by the CellTiter-Blue assay (Promega) according to the manufacturer's protocol.

Isolation and infection of mouse primary hepatocytes

Mouse primary hepatocytes were isolated using a modified two-step perfusion protocol followed by a Percoll purification step [168, 413, 414]. Briefly, mice were euthanized by CO_2 inhalation and immediately processed for cannulation of the portal vein using a 26-gage needle. Upon successful cannulation, the inferior vena cava (IVC) was cut to allow fluid to drain. Liver perfusion medium (LPM) was perfused at 8–9 mL/min for 10 minutes followed by liver digestion medium (LDM) at the same rate. Intermittent clamping of the IVC (3 seconds clamp every 30 seconds) was performed during LDM perfusion to improve tissue digestion. After digestion, the liver was excised and the cells were liberated by tearing and shaking of the liver with forceps. The cell suspension was then sequentially filtered through a 100 µm and a 70 µm cell strainer and spun at 50xg for 3 min. The cell pellet was resuspended in Williams's E Medium with 10% of FBS and carefully overlaid on a 60% Percoll solution (1:1). The cell suspension was fractionated by centrifugation at 750xg for 20 minutes, without break, at 20 °C. Viable hepatocytes deposited in the pellet were washed with Williams's E Medium with 10% FBS, spun at 50xg for 3 minutes and resuspended in complete Williams's E Medium (supplemented with 4% FBS and 1% penicillin/streptomycin). Hepatocytes were then plated at a density of $2.0x10^4$ in 96-well plates and infected 16 hours later with $1.0x10^4$ *P. berghei* sporozoites. Viability and yield were assessed by trypan blue staining.

Quantification of the percentage of *P. berghei*-infected cells and parasite development by flow cytometry

The percentage of infected cells corresponds to the percentage of GFP^+ cells 48 hours after infection with a GFP-expressing parasite line. Intracellular parasite

development was assessed by measuring the intensity of the GFP signal of the infected cells 48 hours after infection, as previously described [163]. Huh7 cells ($5.0x10^4$ per well) were seeded in 24-well plates. On the following day, cells were infected with $3.0x10^4$ freshly dissected GFP-expressing *P. berghei* sporozoites. Culture medium was replaced by the appropriate medium 2 hours after infection. Cells were collected for flow cytometry analysis at 48 hpi and analyzed on a Becton Dickinson FACSCalibur. Data acquisition and analysis were carried out using the CELLQuest (version 3.1.1 f1, Becton Dickinson) and FlowJo (version 6.4.7, FlowJo) software packages, respectively.

I*n vivo* amino acid supplementation

The drinking water of 4 weeks old male C57BL/6 mice was replaced by sterilized water with 2.5% (w/v) L-arginine hydrochloride (Fisher Scientific), 2.5% (w/v) L-lysine (Sigma), 2.5% (w/v) L-valine (Sigma) or 2.5% (w/v) L-ornithine (Sigma) alone, in combinations of 2 amino acids, and a triple combination with Arg, Lys and Val. Control mice were provided with sterilized water alone. Mice were allowed to drink *ad libitu*m for 4 weeks, unless otherwise indicated, and then were infected as described on the following section.

P. berghei sporozoites *in vivo* infection and quantification of parasite liver load by qPCR

Mice were infected i.v., through retro-orbital injection, with $1.0x10^4$ *P. berghei* sporozoites. Livers were collected at 45 hpi and homogenized in 3 mL of denaturing solution (4 M guanidine thiocyanate; 25 mM sodium citrate pH 7, 0.5% *N*-lauroylsarcosine and 0.7% β mercaptoethanol in DEPC-treated water). Total liver RNA was extracted with the NZY Total RNA Isolation Kit (NZYTech), according to the manufacturer's protocol, and parasite load was quantified by qPCR using primers specific to *P. berghei* 18S RNA (Table 4.1). Mouse Hprt expression was used for normalization.

Immunohistochemical staining of liver sections

For microscopy, PFA-fixed liver lobes were cut in 50µm sections and were incubated in permeabilization/blocking solution (1% BSA, 0,5% Triton-X100 in

PBS) at room temperature for 1 hour. Parasites were stained with an anti-UIS4 antibody (dilution 1:500) for 90 minutes at room temperature, followed by three washes with permeabilization/blocking solution. Slices were further incubated in a 1:300 dilution of anti-goat Alexa-Fluor 568 (Life Technologies) in the presence of a 1:1000 dilution of Hoechst 33342 (Invitrogen) for nuclei staining. Additional washes were carried out with permeabilization/blocking solution and, finally, with PBS. Coverslips were mounted on microscope slides with Fluoromount (SouthernBiotech). Confocal images were acquired using a Zeiss LSM 710 confocal microscope. Widefield images for size and number determination were acquired in a Leica DM5000B microscope. Images were processed with ImageJ software (version 1.47).

RNA extraction, cDNA synthesis and qPCR

RNA was extracted from cultured Huh7 cells using the High Pure RNA Isolation kit (Roche) according to the manufacturer´s instructions. The amount of RNA in each sample was assessed with a NanoDrop® ND-1000 spectrophotometer.

Complementary DNA (cDNA) was synthesized from 1 µg of RNA using the Roche cDNA synthesis kit, according to the manufacturer´s instructions. The cDNA was synthesized employing the following thermocycling parameters: 25°C for 10 minutes, 55°C for 30 minutes, and 85°C for 5 minutes. qPCR reaction was performed in a total volume of 20 µL in a ABI Prism 7500 Fast system (Applied Biosystems) using the iTaq^{TM} Universal SYBR® Green kit (BioRad) as follows: 50°C for 2 minutes, 95°C for 10 minutes, 40 cycles at 95°C for 15 seconds and 60°C for 1 minute, melting stage was done at 95°C for 15 seconds, 60°C for 1 minute, and 95°C for 30 seconds. Primers for the housekeeping gene hypoxanthine-guanine phosphoribosyltransferase (*Hprt*) were used for normalization in all experiments (Table 4.1). The delta-delta CT relative quantification method was used for analysis of qPCR results.

Table 4.1 - List of primer sequences used.

Gene	forward primer (5' - 3')	reverse primer (5' - 3')
Pb18S	AAGCATTAAATAAAGCGAATACATCCTTAC	GGAGATTGGTTTTGACGTTTATGTG
Hprt	TTTGCTGACCTGCTGGATTAC	CAAGACATTCTTTCCAGTTAAAGTTG
Clec4f	TGAGTGGAATAAAGAGCCTCCC	TCATAGTCCCTAAGCCTCTGGA
CD68	AGCTGCCTGACAAGGGACACT	AGGAGGACCAGGCCAATGAT
F4/80	CCCCAGTGTCCTTACAGAGTG	GTGCCCAGAGTGGATGTCT

Statistical Analyses

Statistical analyses were performed using the GraphPad Prism 5 software. One-way ANOVA, Two-way ANOVA, Survival Test Gehan-Breslow-Wilcoxon, Mann-Whitney U test or Unpaired t-test were used for significance of the differences observed, as indicated in each figure. ns – not significant, * $p < 0.05$, ** $p < 0.01$ and *** $p < 0.001$.

Results

Amino acid supplementation impacts *Plasmodium* hepatic infection *in vitro* and *ex vivo*

Having demonstrated that Arg uptake via CAT2A and CAT2B, as well as Arg-dependent polyamine synthesis, are important for parasite hepatic development, we wondered whether *Plasmodium* infection could be impaired by appropriate amino acid supplementation. Lys, Orn and Val have been described as arginase inhibitors, suggesting they could be employed to inhibit the polyamine synthesis pathway [30, 31]. We also decided to evaluate the effect of Arg on infection because it has been described that increasing the amount of available Arg can enhance NO production, which was shown to kill malaria parasites *in vitro* [32-39].

We started by culturing Huh7 cells in RPMI and infecting them with luciferase-expressing *P. berghei* sporozoites. Two hours later, the medium was replaced by Arg-free medium supplemented with either 100 µM Arg, the physiological concentration of this amino acid, or 1 mM Arg, the approximate supraphysiological concentration of this amino acid present in RPMI. Additional supplementations with 20 mM Lys, 20 mM Val or both, which have been shown to completely inhibit arginase activity at physiological concentrations of Arg, were also assayed [31]. Parasite load was assessed 48 hours after sporozoite addition by luminescence. Our data show that supplementation of the medium with Lys or Lys and Val leads to a decrease in infection, particularly at physiological levels of Arg (Fig. 4.1A), suggesting an impairment of polyamine synthesis in these conditions due to arginase inhibition. Notably, infection was not affected when Arg concentration was increased in the absence of any additional supplementation. The supplementation with Lys or Lys and Val in the presence of supraphysiological concentrations of Arg led to a more moderate decrease in infection, possibly due to the competition of Arg and Lys for their transporters.

We then performed a similar experiment under *ex vivo* conditions, employing mouse primary hepatocytes as host cells (Fig. 4.1B). Similarly to what was observed for Huh7 cells, supplementation with Lys or with Lys and Val impacted *Plasmodium* infection the most, with a 99% decrease in parasite load in the case of supplementation with Lys alone, indicating that arginase inhibition by Lys or by

Lys and Val is also effective *ex vivo*. In agreement with our *in vitro* data, the observed effects are more pronounced if Arg is present at physiological concentrations. Finally, we observed a non-statistically significant tendency for increased parasite load in the presence of supraphysiological concentrations of Arg, which could suggest an increase in polyamine production by hepatocytes in this condition.

In order to further dissect how these amino acid supplementations influence hepatic infection, we employed an established flow cytometry-based approach that makes use of GFP-expressing *P. berghei* parasites to determine the number of infected cells and to measure parasite development [163]. Supplementation with Orn was also included in these experiments due to its reported ability to inhibit arginase activity [30]. We observed that, in mouse primary hepatocytes, Lys supplementation at physiological concentrations of Arg leads to a 65% reduction in the number of infected cells at 48 hpi (Fig. 4.1C). Supplementation with Lys and Val also impacts the number of infected cells at 48hpi, especially at physiological concentrations of Arg, but the effect is milder than with Lys alone. The number of infected cells was not significantly affected in any of the other conditions tested. Supplementation with Lys and supplementation with Lys and Val at physiological concentrations of Arg were also the most effective at reducing parasite development (Fig. 4.1D). On the other hand, supplementation with Orn significantly increased parasite development, at both Arg concentrations tested (Fig. 4.1D). This is not entirely surprising because even though Orn was described to have an inhibitory effect on arginase, it is also the product of Arg degradation by this enzyme and the substrate for polyamine synthesis. *Plasmodium* development was also highly enhanced at supraphysiological concentrations of Arg, suggesting that higher concentrations of Arg probably stimulate polyamine synthesis in mouse primary hepatocytes (Fig. 4.1D).

Overall, our data show that *Plasmodium* hepatic infection can be modulated *in vitro* and *ex vivo* by amino acid supplementation in the cell culture medium. More specifically, our results show that supplementation of the cell culture medium with Lys, Val, or a combination of both amino acids leads to a marked decrease in hepatic cell infection by the malaria parasite.

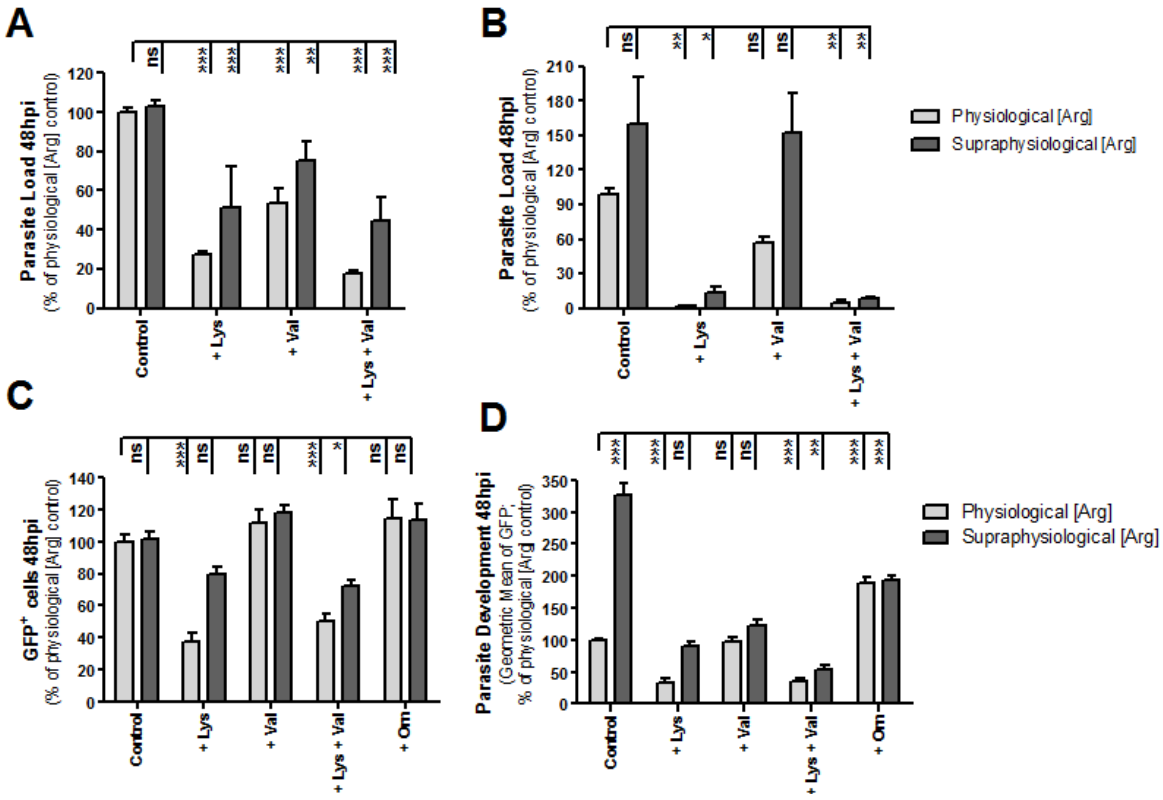

Figure 4.1 - Modulation of hepatic *Plasmodium* infection by amino acid supplementation *in vitro* (A) and *ex vivo* (B-D). (A) Huh7 cells were infected with luciferase-expressing *P. berghei* sporozoites and the culture medium was replaced 2 hpi by medium supplemented with 20 mM Lys, 20 mM Val or 20 mM Lys and 20 mM Val, at physiological (100 µM) or supraphysiological (1 mM) Arg concentrations. Parasite load (luminescence) was assessed 48 hpi. Pool of 2 independent experiments. **(B)** Similar experiments were performed in mouse primary hepatocytes. Parasite load (luminescence) was assessed 48 hpi. Pool of 3 independent experiments. **(C)** Mouse primary hepatocytes were infected with GFP-expressing sporozoites. Culture medium was replaced 2 hpi with the appropriate medium and the percentage of GFP^+ cells was quantified by flow cytometry 48 hpi. Pool of 3 independent experiments. **(D)** Parasite development in mouse primary hepatocytes was assessed by determining the fluorescence intensity of GFP^+ cells by flow cytometry at 48 hpi. Pool of 3 independent experiments. For all panels, results were normalized to the infection load of the control group with physiological Arg concentration (taken as 100% infection) and error bars represent SEM. One-way ANOVA with post-test Dunnett. ns - not significant, * $p < 0.05$, ** $p < 0.01$ and *** $p < 0.001$.

Amino acid supplementation impacts *Plasmodium* hepatic infection *in vivo*

We then sought to investigate whether the observed modulating effect of amino acids on *Plasmodium* infection *in vitro* and *ex vivo* could serve to inhibit

Plasmodium liver infection *in vivo*. To this end, the drinking water of C57Bl/6 mice was supplemented with Lys, Orn, Val or Lys and Val, in an attempt to inhibit arginase activity and, consequently, impair polyamine production *in* vivo. After 4 weeks of supplementation, mice were infected with *P. berghei* sporozoites and the parasite liver load was assessed 45 hours later by qPCR. Our data show that supplementation with Lys, Val or Lys and Val leads to a small and non-statistically significant decrease in *Plasmodium* liver load (Fig. 4.2A), which indicates that the inhibitory effect of these amino acids is not sufficient to significantly impair *Plasmodium* infection *in vivo*. Orn supplementation did not have any impact on *P. berghei* liver infection.

It has been described that, upon inhibition of arginase activity, Arg supplementation significantly increases NO production by hepatocytes [31]. Therefore, we wondered if we could further decrease *Plasmodium* liver infection by adding Arg to the Lys, Orn, Val or Lys and Val supplementations. Indeed, we observed that the impact on *Plasmodium* liver infection is enhanced when Arg is combined with these amino acids, with the exception of Val (Fig. 4.2B). Most notably, combining Arg with Lys and Val highly impacts *Plasmodium* infection, leading to a 70% decrease on parasite liver load.

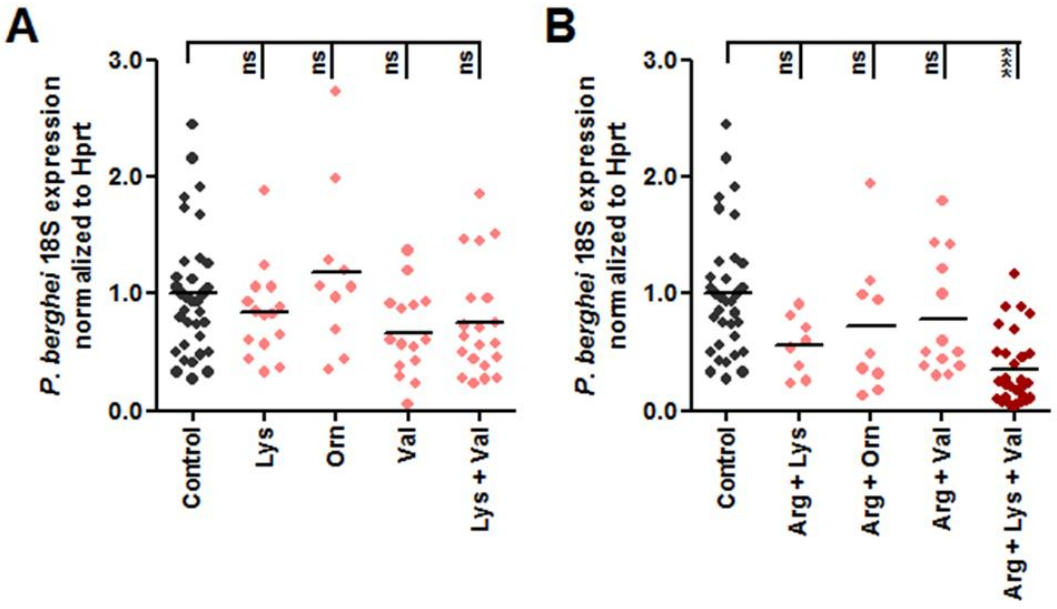

Figure 4.2 – Modulation of *Plasmodium* liver infection by amino acid supplementation *in vivo*. The drinking water of the mice was replaced by sterilized water supplemented with 2.5% (w/v) of each amino acid, individually or in combination, and the mice were allowed to drink *ad libitum* for 4 weeks. Mice were infected with *P. berghei*

sporozoites and parasite load was assessed by qPCR at 45 hpi. **(A)** Parasite liver load following infection of mice supplemented with arginase-inhibiting amino acids. **(B)** Parasite liver load following infection of mice supplemented with Lys, Orn, Val, and Lys and Val in combination with Arg, to stimulate NO production. Both panels: Pool of 2 to 7 independent experiments. Control: n = 34; Lys: n = 15; Orn: n = 10; Val: n = 15; Lys + Val: n = 20; Arg + Lys: n = 8; Arg + Orn: n = 9; Arg + Val: n = 13; Arg + Lys + Val: n = 29 mice. One-way ANOVA with post-test Dunnett. ns - not significant and *** $p < 0.001$.

In vivo supplementation with Lys, Val and Arg inhibits polyamine synthesis and stimulates NO production by hepatocytes

The results outlined above suggest that *in vivo Plasmodium* liver infection can be modulated by the concurrent inhibition of polyamine synthesis by supplementation with Lys and Val and stimulation of NO production by supplementation with Arg. To further clarify the effect of the Lys/Val/Arg supplementation on *Plasmodium* liver infection, 50µm liver sections were analyzed by fluorescence microscopy in order to compare the number and size of hepatic parasites in control and supplemented mice. The results obtained show a relatively small but clearly significant reduction on parasite size in the livers of supplemented mice, showing that the supplementation employed impairs parasite development (Fig. 4.3A). Crucially, however, a drastic reduction in the number of parasites per liver area is also observed in supplemented mice, suggesting parasite elimination in the livers of these mice (Fig. 4.3B). These results support our hypothesis that Lys and Val are inhibiting arginase and, consequently, the production of polyamines required for parasite growth, while the extra Arg supplied is being channeled to the production of NO, leading to parasite elimination.

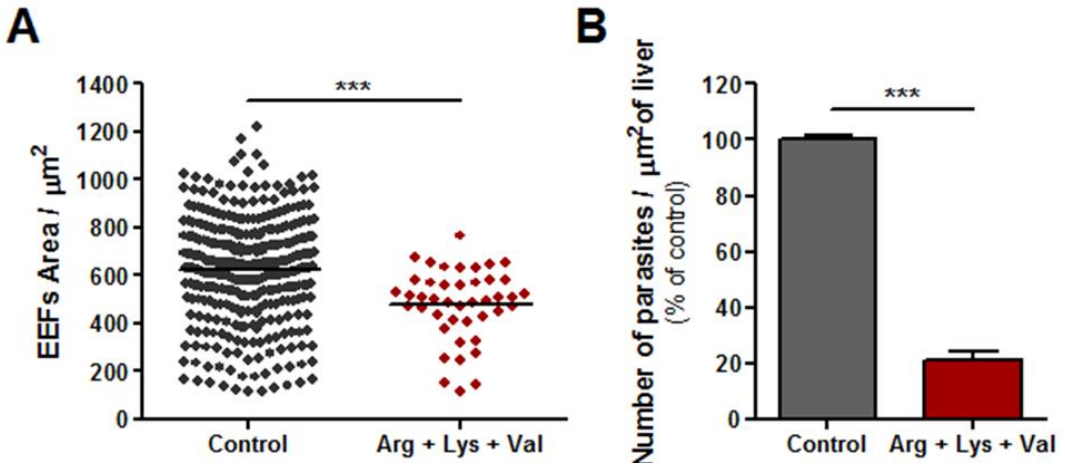

Figure 4.3 - *In vivo* dietary supplementation with Lys/Val/Arg decreases the number of *P. berghei* parasites in the liver of C57BL/6 mice. (A) Immunofluorescence microscopy quantification of EEF areas in the liver sections of control or supplemented mice. Two-tailed Mann-Whitney test. **(B)** Immunofluorescence microscopy quantification of the number of parasites per liver area of control or supplemented mice. Error bars represent SD. Unpaired t-test. Both panels: pool of 1 mouse per group from 2 independent experiments. *** $p < 0.001$.

In order to confirm that Lys and Val are indeed inhibiting arginase, a well-known arginase inhibitor, N^{ω}-hydroxy-nor-arginine (nor-NOHA) [445-448], was employed in combination with Arg supplementation. The drinking water of the mice was supplemented as previously described and, in the last week of supplementation, 200 µL of a 20 mg/kg nor-NOHA solution were injected i.p. every other day, starting on day 7 before infection and finishing one day after infection. Our results show that the administration of nor-NOHA to mice drinking Arg-supplemented water decreases liver parasite load to a very similar extent to that observed upon supplementation with Lys, Val and Arg (Fig. 4.4). The fact that the nor-NOHA/Arg treatment recapitulated the effect on infection of the Lys/Val/Arg supplementation strongly suggests that Lys and Val indeed function as arginase inhibitors in the latter supplementation. Additionally, when the Lys/Val/Arg supplementation was combined with the administration of nor-NOHA, a cumulative effect on infection was not observed, suggesting that Lys and Val might compete with nor-NOHA for the active site of the arginase enzyme.

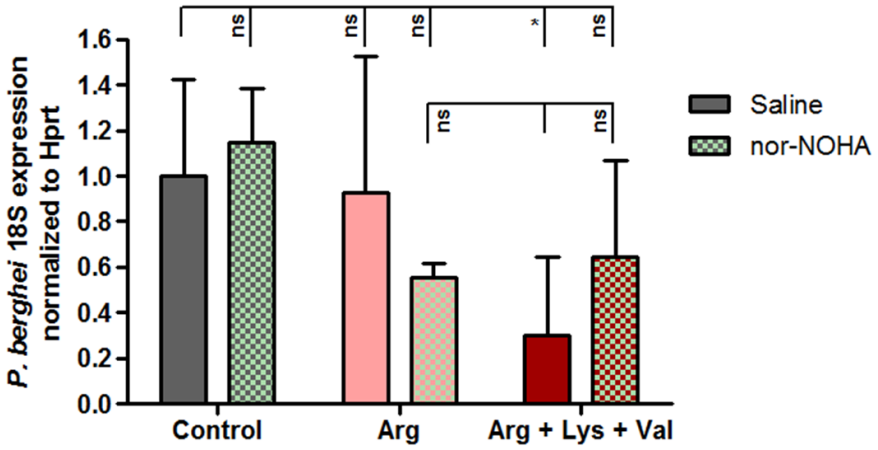

Figure 4.4 – Lys and Val function as arginase inhibitors in the Lys/Val/Arg supplementation. Mice received five doses of a 20 mg/kg nor-NOHA solution i.p. every other day for one week. Parasite load was assessed by qPCR at 45 hpi. One experiment with 5 mice per group. Error bars represent SD. One-way ANOVA with post-test Dunnett. ns - not significant and ** $p < 0.01$.

Having confirmed the role of Lys and Val on the Lys/Val/Arg supplementation, we then aimed at confirming that the supplemented Arg is indeed being employed for NO production by iNOS. To this end, we used N_{ω}-Nitro-L-arginine methyl ester (L-NAME), a well-known inhibitor of iNOS [445, 449, 450]. Mice were allowed to drink control water or water supplemented with Lys/Val/Arg for 4 weeks and 50 mg/kg of L-NAME or saline were injected daily i.p., starting 3 days before and until the day of i.v. injection of *P. berghei* sporozoites. Our results show that administration of L-NAME to mice on Lys/Val/Arg supplementation abolishes the decrease in parasite load observed in the livers of mice supplemented with Lys/Val/Arg and treated with saline (Fig. 4.5). This result supports the notion that the supplemented Arg is employed to produce NO that contributes to parasite death and elimination.

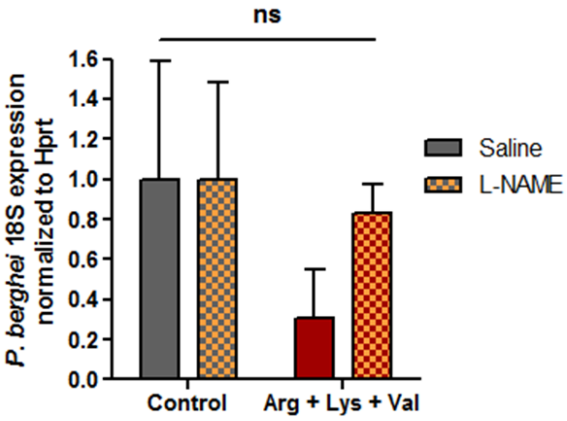

Figure 4.5 – Arg in the Lys/Val/Arg supplementation stimulates the iNOS pathway. Mice received 4 daily doses of a 50 mg/kg L-NAME solution i.p., starting 3 days before infection with *P. berghei* sporozoites. Parasite load was assessed by qPCR at 45 hpi. One experiment with 5 mice per group. Error bars represent SD. One-way ANOVA with post-test Dunnett. ns - not significant.

Finally, we sought to identify the cells where the iNOS pathway is stimulated by the Lys/Val/Arg supplementation. As described in the general introduction, the liver is composed by several types of cells. Among these, Kupffer cells, similarly to other phagocytic cells, are the main producers of NO. To investigate their role in the mechanism of action of the Lys/Val/Arg supplementation, Kupffer cells were depleted *in vivo* through the administration of clodronate-filled liposomes. Once delivered into phagocytic cells using liposomes as vehicles, clodronate is released and, because it cannot escape from the cell, it accumulates intracellularly leading to cell death [451]. Mice were allowed to drink control water or water supplemented with Lys/Val/Arg for 4 weeks and 200 µL of clodronate liposomes or PBS liposomes were then injected i.v. 48 hours before infection with *P. berghei* sporozoites. Liver parasite load was assessed by qPCR at 45 hpi. The efficiency of the depletion was assessed by quantifying the expression of three specific markers: Clec4f, which is specifically expressed by Kupffer cells; CD68, which is a marker of the macrophage lineage; and F4/80, which is expressed by mature macrophages (Fig. 4.6A). While Kupffer cells were completely eliminated by the administration of clodronate liposomes, as shown by the absence of expression of Clec4f, some expression of the CD68 and F4/80 markers could be detected, which probably results from monocytes and macrophages that were recruited to the liver because of *Plasmodium* infection. Importantly, our liver infection results show that depleting liver phagocytes does not abolish the reduction in parasite liver load typically observed with the Lys/Val/Arg supplementation (Fig. 4.6B). This result suggests that the stimulation of the iNOS pathway by the Lys/Val/Arg supplementation occurs in hepatocytes, which is in agreement with a previous

report in which immunofluorescence analysis of livers from Brown Norway rats infected with *P. berghei* showed that iNOS expression was found in infected hepatocytes, rather than on Kupffer or endothelial cells [452].

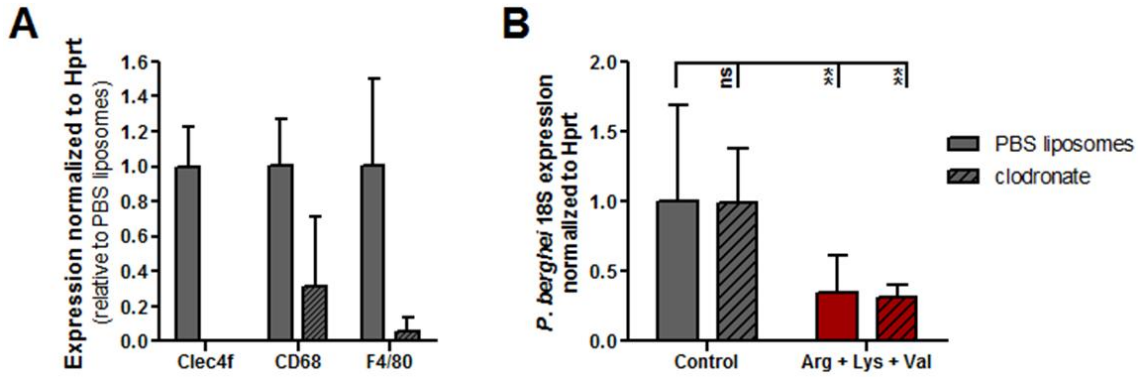

Figure 4.6 – Lys/Val/Arg supplementation stimulates the iNOS pathway of hepatocytes. Mice received 200 µL of the PBS- or clodronate-filled liposome formulation by i.v. injection 48 hours before infection with *P. berghei* sporozoites. **(A)** Assessment of hepatic phagocyte depletion by qPCR at 45 hpi. Clec4f is a specific marker for Kupffer cells, CD68 is a marker of the macrophage lineage, and F4/80 is a marker of mature macrophages. **(B)** Liver parasite load was assessed by qPCR at 45 hpi. One experiment with 5 mice per group. Error bars represent SD. One-way ANOVA with post-test Dunnett. ns - not significant and ** $p < 0.01$.

Effect of Lys/Val/Arg supplementation for different periods of time on *P. berghei* liver infection

Finally, we wondered whether the impact of the Lys/Val/Arg supplementation on liver *P. berghei* load would be dependent on the amount of time the mice were allowed to drink the supplemented water and, consequently, on the total amount of amino acids ingested. To assess this, we infected mice after 1, 2, 3, 4, 5 and 6 weeks of supplementation and quantified liver parasite load by qPCR at 45 hpi. Our results show that the effect on infection is similar for all the supplementation periods tested (Fig. 4.7), with no correlation being observed between liver parasite liver load and the duration of supplementation. These results suggest that the duration of Lys/Val/Arg supplementation can be decreased from 4 weeks in future experiments, without any significant loss of impact on the infection impairment phenotype.

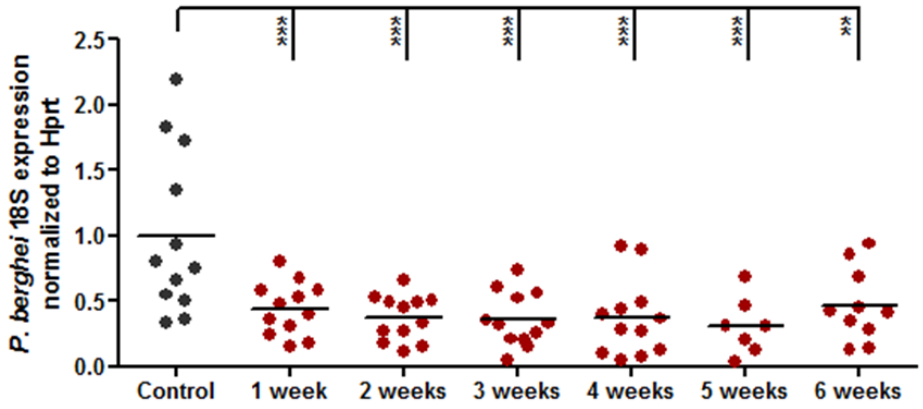

Figure 4.7 – Effect of the length of Lys/Val/Arg supplementation on *P. berghei* liver load. Mice were infected through i.v. injection of *P. berghei* sporozoites after drinking control or supplemented water for 1, 2, 3, 4, 5 and 6 weeks. Liver load was determined by qPCR at 45 hpi. Pool of 2-3 independent experiments. n = 12 mice in all groups except 5 weeks (n = 7) and 6 weeks (n = 10). One-way ANOVA with Dunnett. ** $p < 0.01$ and *** $p < 0.001$.

Discussion

Dietary amino acid supplementation has been employed in several clinical and non-clinical applications. In some instances, amino acid supplementation is used solely to balance nutritional needs or deficiencies. In other cases, amino acids or their metabolic products can be used to interfere with the function of enzymes or receptors, modulating those pathways.

Lysine can be found as a dietary supplement in the form of L-lysine-HCl. This amino acid has an anxiolytic action through its effects on serotonin receptors in the intestinal tract, and through serotonin regulation in the amygdale [453-455]. Lysine supplementation exerts positive effects in patients with ornithine aminotransferase (OAT) deficiency [456, 457], with lysinuric protein intolerance (LPI) [458-461], and has been proposed for hyperammonaemia-hyperornithinaemia-homocitrullinuria (HHH) syndrome treatment, but its benefits are unclear [462]. On the other hand, this amino acid should be avoided in cases of glutaric aciduria type I (GA-I) [463]. High doses of lysine have been associated with some side-effects, such as abdominal cramps and diarrhea [458, 459].

Valine is an essential, branched-chain amino acid (BCAA) and is always used in combination with leucine and isoleucine, the other two BCAAs. Dietary BCAA supplementation has been suggested to aid in the recovery of burn victims [464] and has beneficial effects before and after exercise for decreasing exercise-induced muscle damage and promoting muscle-protein synthesis [465, 466]. Valine supplementation, usually in combination with isoleucine, is also used in some aminoacidopathies, such as methylmalonic acidemia (MMA) [467], propionic acidemia (PA) [468] and maple syrup urine disease (MSUD) [469-471], to ameliorate the effects of the dietary protein restriction imposed to these patients.

Arginine is becoming an increasingly popular ingredient in dietary supplements and is generally recognized as safe at intakes of up to 20 g/day [472]. As a precursor of nitric oxide (NO), arginine supplementation is effective in the treatment of some conditions where vasodilation is required, such as hypertension [473, 474], erectile dysfunction [475, 476] and high blood pressure as part of pre-eclampsia in pregnant women [477]. Supplementation with this amino acid is employed for the treatment of some aminoacidopathies, such as GA-I [478, 479], homocystinuria (HCU) [480, 481], LPI [482-485] and HHH syndrome [462, 486-

488]. However, it should be avoided in cases of OAT and guanidinoacetate methyltransferase (GAMT) deficiencies [489], worsening such conditions. Interestingly, arginine was also shown to stimulate the secretion of growth hormone when administered i.v. [490, 491].

Arg supplements are the only amino acid-based supplementation that has been employed in malaria infection. Arg administration was reported to increase the circulating levels of Arg in *Plasmodium*-infected mice, leading to enhanced NO production [32, 33]. Yet, while in one of these studies Arg supplementation significantly decreased parasitaemia and improved survival of *P. yoelii*-infected Balb/c mice [33], none of these effects were observed in *P. berghei*-infected C57BL/6 mice [32]. In individuals with moderately severe malaria, Arg infusion was shown to be safe, and effectively increased plasma Arg concentrations and NO production, leading to improved endothelial function [441, 442].

Having established an important role for Arg metabolism and polyamine production during *Plasmodium* hepatic development in the previous chapter, we wondered whether we could employ adequate amino acid supplementations as an alternative, drugless approach to inhibit *Plasmodium* liver infection. We decided to study the effect of supplementation with Lys, Orn and Val due to their described role as arginase inhibitors [30, 31]. Furthermore, we employed Arg supplementation to increase the amount of Arg available in circulation and enhance NO production [32-39].

Both our *in vitro* and *ex vivo* data showed that supplementing the medium with Lys or Lys and Val, at physiological concentrations of Arg, markedly impacts *P. berghei* infection (Fig. 4.1A, B). The observed decrease in parasite load is mainly due to an impaired *P. berghei* development (Fig. 4.1D), which is consistent with an inhibition of polyamine synthesis. In fact, a previous report showed that these concentrations of Lys or Val almost completely abolish arginase activity in rat hepatocytes [31]. As human arginase 1 and arginase 2 inhibitors have also been shown to inhibit *Plasmodium* arginase [25, 492], it is possible that Lys and Val are also hindering polyamine production by the parasite itself. Interestingly, Arg supplementation in mouse primary hepatocytes highly increases parasite development, suggesting that, in these cells, the extra Arg might be used for polyamine production. Supporting this hypothesis is the fact that hepatocytes abundantly express arginase 1 and that, in mammalian cells, Arg is mainly

catabolized by the arginase pathway rather than by the iNOS pathway [407, 493, 494].

We then evaluated if we would be able to modulate *Plasmodium* liver infection *in vivo* through supplementation of the drinking water of mice. Our data shows that supplementation with Lys, Val or Lys and Val leads to a small and non-statistically significant decrease in *Plasmodium* liver load (Fig. 4.2A), which indicates that supplying the mice with these amino acids is not sufficient to impair *Plasmodium* infection *in vivo*. This can be explained by a lower amount of amino acids that actually reach the hepatocytes. The bioavailability of amino acids provided orally might be lower than that achieved by cell culture medium supplementation, and therefore their effective concentration in hepatocytes might not be enough to inhibit arginase activity. Alternatively, it might be that inhibiting polyamine synthesis alone *in vivo* is not sufficient to impact *Plasmodium* infection. In fact, α-difluoromethylornithine (DFMO) has been shown to be more effective at inhibiting *P. falciparum* AdoMetDC/ODC enzyme than the mammalian ODC; however, it has only a cytostatic effect on the parasite, slowing down parasite growth but not leading to parasite death [340].

It has been described that, upon inhibition of arginase activity, Arg supplementation significantly increases NO production by hepatocytes [31]. Therefore, in order to try to further impact *Plasmodium* infection, we decided to add Arg to Lys, Orn, Val, and Lys and Val supplementations. We observed that combining Arg with Lys and Val leads to a striking decrease in *Plasmodium* liver infection (Fig 4.2B), which is due to an impairment in parasite development (Fig. 4.3A) and to a decrease in the number of *P. berghei*-infected hepatocytes (Fig. 4.3B). To confirm the inhibitory effect of Lys and Val in the Lys/Val/Arg supplementation, a similar effect on *Plasmodium* liver infection was recapitulated by combining a well-known arginase inhibitor, nor-NOHA, with Arg alone (Fig. 4.4). Additionally, the administration of an iNOS inhibitor following Lys/Val/Arg supplementation reverted the characteristic decrease in *P. berghei* liver load, directly implicating iNOS-mediated NO production on infection inhibition (Fig. 4.5). Finally, we excluded Kupffer cells and other phagocytic cells as the producers of NO, as the depletion of liver phagocytic cells did not abolish the reduction obtained with the Lys/Val/Arg supplementation (Fig. 4.6), suggesting that NO production might be stimulated in hepatocytes themselves. These results are in agreement

with a previous report in Brown Norway rats infected with *P. berghei* that showed that iNOS expression was found in infected hepatocytes, not Kupffer or endothelial cells [452]. However, it is possible that NO production by hepatocytes is being stimulated by cytokines produced by immune cells. This hypothesis is supported by our *ex vivo* data that shows that supplementation with Lys and Val in the presence of supraphysiological concentrations of Arg leads to only 20% decrease in the number of infected hepatocytes, while we observed a 80% reduction with the Lys/Val/Arg supplementation *in vivo*. Future experiments will aim at identifying the immune cells and cytokines involved in the stimulation of NO production by hepatocytes.

Overall, our results support a model in which the Lys/Val/Arg supplementation blocks polyamine synthesis by inhibiting arginase activity and, concurrently, stimulates NO production by iNOS, contributing to parasite elimination (Fig. 4.8). Adequate amino acid supplementation may therefore constitute a novel, drugless approach to modulate liver-stage of *Plasmodium* infection, which could be employed as a prophylactic strategy against malaria.

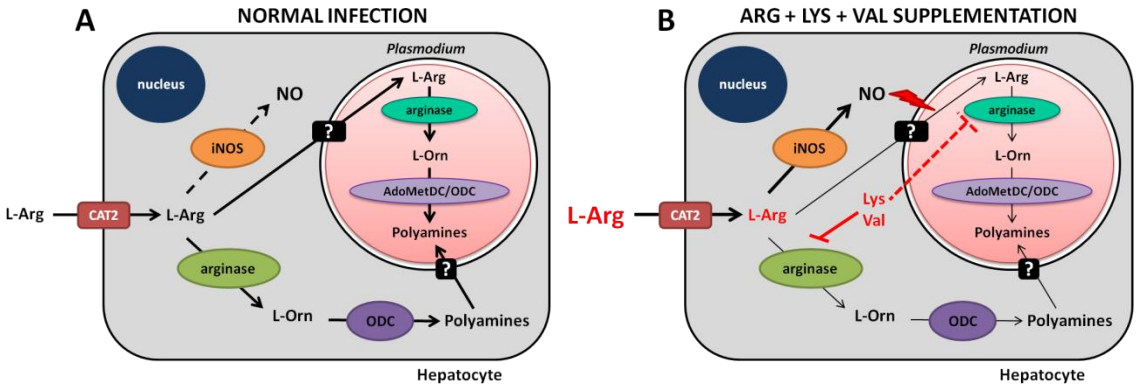

Figure 4.8 – Model of the Lys/Val/Arg supplementation-mediated modulation of Arg metabolism in *Plasmodium*-infected hepatocytes. (A) In a normal infection, the Arg taken up via CAT2A and CAT2B by the infected hepatocyte is used for the production of polyamines, both by the host cell and by the parasite, contributing to parasite development. **(B)** Upon Lys/Val/Arg supplementation, Lys and Val inhibit arginase and, therefore, block polyamine synthesis. The extra arginine provided is then channeled to the NO production pathway, leading to parasite killing.

General Discussion

General Discussion

Plasmodium parasites are obligate intracellular pathogens within their mammalian hosts, infecting and replicating inside hepatocytes during the asymptomatic stage of the infection and, later, inside red blood cells (RBCs), originating the symptoms of malaria. Despite its asymptomatic nature, the intrahepatic stage of infection is an obligatory step of *Plasmodium* life cycle and involves a massive multiplication of each parasite, with 10^4- to 10^5-fold replication of its genome, while the erythrocytic stage typically only involves 4 rounds of replication [5, 6, 495]. This remarkable cellular and genomic expansion inside hepatocytes is possible because the parasite takes advantage of the extremely metabolite- and nutrient-rich environment of these cells. *Plasmodium* parasites scavenge nutrients from the host hepatocyte both by passive diffusion through pores in the parasitophorous vacuole membrane (PVM) and by active processes, such as those that take up glucose, fatty acids and cholesterol [7-10]. Parasite utilization of host cell nutrients makes them unavailable for the host cell and leads to a metabolic adaptation of the latter in order to ensure its own survival. Indeed, microarrays of *P. berghei*-infected hepatoma cells and *P. yoelii*-infected mouse hepatocytes revealed that the transcriptome of an infected cell favors biosynthetic pathways including carbohydrate and fatty acid metabolism [11].

Several nutrients derived by the parasite from the host hepatocyte have already been identified. These include phosphatidylcholine [228], phosphatidylinositol 3,5-bisphosphate ($PI(3,5)P_2$) [229-231], iron [232], fatty acids [9], cholesterol [10] and glucose [7, 8, 322]. With this work, we deepened our understanding on the role of glucose for *Plasmodium* liver-stage development and added another essential nutrient to this list, the amino acid L-arginine (Arg).

Glucose is the main carbon source for *Plasmodium* blood stage parasites [296, 297]. Therefore, it is not surprising that it plays a similar role in the liver stage of infection. However, while the glucose consumption rate of an infected RBC is estimated to be up to 100-fold higher than that of a non-infected RBC [297, 298], our results show a modest 2-fold increase in glucose uptake by *P. berghei*-infected hepatoma cells. As these cells are rapidly proliferating cancer cells, they already have a very high glucose uptake and, therefore, only need to double their glucose uptake to meet the needs of the dividing parasite and their own. Interestingly, we

were able to link the increased glucose uptake by infected cells to parasite replication because the former is only observed from 30 hpi onwards, when schizogony is occurring, and is not observed in cells containing non-developing parasites.

We also showed that glucose transporter 1 (GLUT1), which is the most abundant glucose transporter on the RBC membrane [315, 316], is also responsible for the increased glucose uptake by infected hepatoma cells. The extensive parasite replication inside these cells promotes the depletion of intracellular glucose levels, ultimately leading to a phosphoinositide 3-kinase (PI3K)-independent translocation of GLUT1 to the plasma membrane to re-establish the energy status of the cell.

GLUT2 is the major glucose transporter in hepatocytes, being involved in both glucose uptake and release. On the other hand, despite being expressed by all hepatocytes, GLUT1 is only localized at the membrane of perivenous hepatocytes [12, 349, 350, 390, 391]. Nevertheless, we showed that *in vivo* chemical inhibition of GLUT1-mediated glucose uptake has a substantial impact on the number of *P. berghei*-infected hepatocytes. There are two possible explanations for this observation. The first is that the inhibitor will only inhibit GLUT1-mediated glucose on perivenous hepatocytes and, therefore, will only have an effect on the parasites inside these hepatocytes. In a liver cell plate, which contains 15–25 hepatocytes, only around 10% are hypoxic, perivenous hepatocytes and have membranar GLUT1 [245]. However, it has been reported that the survival of parasites inside hypoxic hepatocytes is improved up to three times in comparison with non-hypoxic hepatocytes and that these parasites also develop considerably more than the ones in non-hypoxic conditions [394]. Thus, inhibition of GLUT1-mediated glucose uptake by these hepatocytes only would be enough to explain the 40% reduction in liver parasite load observed. Another possible explanation stems from our *in vitro* results that show that *Plasmodium* development inside hepatoma cells leads to GLUT1 translocation to the plasma membrane. After reaching the liver, sporozoites invade hepatocytes randomly, without preference for periportal or perivenous hepatocytes [496]. This means that a significant proportion of parasites will invade periportal hepatocytes, which have GLUT2 at the membrane but also express GLUT1, although it is kept in their endosomal compartments. The replication of the parasite inside these hepatocytes could lead to a depletion of the cellular glucose pool and trigger the translocation of GLUT1 to the plasma

membrane, as has been described in other cell types [497-499]. This would increase the percentage of infected hepatocytes with GLUT1 at the plasma membrane and, therefore, the percentage of cells targeted by the inhibitor.

Overall, our results establish glucose as an essential nutrient for *Plasmodium* intrahepatic development and survival *in vitro* and *in vivo,* and unveil GLUT1 as an important player in hepatic infection by providing the glucose necessary for both the parasite and the host cell.

Whereas glucose appears to be key for energy production by *Plasmodium*-infected cells, amino acids are also likely to play a pivotal role during the parasite's intracellular development process. Thus, besides glucose-transporting molecules, several amino acid transporters were also included in our RNAi study aimed at identifying host cell membrane transporters with a role during the liver stage of the parasite's life cycle. This approach led to the identification of the CAT2 transporter of Arg, a precursor of the biosynthesis of polyamines, which constitute key nutrients for replicating cells.

Polyamines are synthesized from Arg by all cells but occur in particularly high concentrations in rapidly proliferating cells, such as cancer cells and protozoan parasites [323-325]. In the case of *Plasmodium* parasites, polyamines account for 14% of the total metabolome of isolated intraerythrocytic parasites and their availability was proven essential for the parasite's survival and rapid proliferation [328, 329, 334]. As *Plasmodium* parasites are incapable of amino acid biosynthesis, they were shown to rely on hemoglobin catabolism and amino acid uptake from the host cell [305, 421] and to have developed a mechanism to respond to low amino acid availability by entering into a hibernation state [500]. Arginine, the precursor of polyamines, was shown to be depleted to almost undetectable levels from the extracellular medium during the erythrocytic development of *Plasmodium* parasites, with the concomitant accumulation of its product, ornithine, due to the action of the parasite's arginase [24]. In fact, hypoargininemia is one of the hallmarks of malaria pathogenesis and several clinical studies have demonstrated a correlation between reduced plasma arginine levels and advanced malaria in malaria patients [410, 441, 501]. However, the growth rate of blood stage *Plasmodium* parasites *in vitro* is not affected by the absence of Arg in the culture medium [421]. Additionally, the vast majority of the ornithine is excreted into the extracellular environment, suggesting that the

parasite might deplete the host arginine pool in order to decrease NO production by the host's iNOS and, therefore, avoid being eliminated [24].

Our results show that arginine uptake and metabolism are also pivotal for *Plasmodium* liver stage development. Arg uptake into cells is mainly mediated by the cationic amino acid transporter (CAT) family of proteins, a subfamily of the solute carrier family 7 (SLC7) [18, 19]. The four members of the CAT family are the nearly-ubiquitous CAT1, encoded by *SLC7A1*, the two products of *SLC7A2*, the gene that encodes through alternative splicing the low affinity CAT2A and the high affinity CAT2B transporters, the brain-specific CAT3, encoded by *SLC7A3*, and CAT4, encoded by *SLC7A4*, whose function is still unknown [19, 403-406]. In hepatocytes, basal Arg uptake is mainly mediated by the low-affinity CAT2A transporter, but they are also able to express the cytokine-inducible, high affinity variant CAT2B [19, 403-406]. The knockdown of the expression of the *SLC7A2* gene decreases the amount of Arg taken up by hepatoma cells by around 50%. When these cells are infected with *P. berghei* sporozoites, parasite development is significantly decreased, suggesting that the reduced Arg availability in these cells is impairing the normal parasite development. In agreement with these data, when Arg concentration in the culture medium is decreased or a competitor for Arg transport is employed, *P. berghei* infection is significantly decreased. However, and contrarily to what was reported for blood stage infection [421], our results suggest that *P. bergh*ei-infected hepatic cells do not uptake more Arg than non-infected cells. This is in agreement with the fact that the expression of CAT2A and CAT2B is not increased in infected cells relative to non-infected cells. Altogether, these results suggest that the amount of Arg that is normally taken up by hepatic cells is sufficient to sustain the polyamine needs of both the parasite and the host cell, so there is no need to increase the expression of the transporters and Arg uptake.

Once inside hepatocytes, which abundantly express arginase 1, Arg is mainly catabolized by the arginase pathway rather than the iNOS pathway [407, 493, 494]. This seems to also be true for infected hepatocytes as neither inhibition nor stimulation of NO production via iNOS appear to have an impact on *P. berghei* hepatic infection. As arginase and iNOS compete for the same substrate, if most Arg is being metabolized by the arginase pathway, it becomes unavailable for iNOS thereby limiting NO production [24, 25, 502]. Several pathogens, including

Trypanosoma spp., *Leishmania spp.*, *Toxoplasma gondii*, *Shistosoma mansoni*, *Candida albicans*, and *Helicobacter pylori* ([416-419, 503] and reviewed in [22, 504]), take advantage of this competition to limit NO production and escape elimination.

In an infected hepatocyte, Arg can be converted into polyamines by both the host cell and the parasite pathways. Our results show that the RNAi-mediated impairment of the host cell polyamine synthesis pathway alone has no effect on *Plasmodium* hepatic infection. Only when both pathways are inhibited simultaneously, by employing a well-known host's ODC and parasite's AdoMetDC/ODC inhibitor, is *P. berghei* development significantly impaired. Thus, it seems that the parasite relies preferentially on its own polyamine synthesis pathway rather than on the host's. Interestingly, an arginase-KO *P. berghei* parasite, whose polyamine synthesis pathway is compromised, displays a clear bimodal behavior in terms of its hepatic infectivity. Either most of the parasites perish inside hepatocytes or, through some unknown compensatory mechanism, they overcome the lack of this pathway and are able to survive and develop normally.

In the blood stage of *Plasmodium* infection, arginase-KO parasites exhibit a slight delay in ascending parasitaemia but eventually develop high blood parasitaemias comparable to those of WT parasites, and exhibit no difference in the onset of morbidity [24]. A possible explanation for this blood stage behavior is that arginase-KO parasites may acquire sufficient amounts of ornithine and polyamines either from the plasma or through the activity of the host cell arginase [24, 328, 329]. Indeed, both putrescine and spermidine have been shown to be taken up by the parasite via a saturable process, dependent on pH and temperature but independent of extracellular Na^+ concentration, with competition between different polyamines, the ornithine precursor, and other basic amino acids [346]. Interestingly, it has been reported that *P. falciparum* encodes 6 putative amino acid transporters; among them, three are members of the amino acid/auxin permease (AAAP) family and mediate H^+- and/or Na^+-dependent amino acid transport [505]. It is possible that one or more of these transporters might be involved in the compensatory mechanism proposed for the arginase-KO parasite during the blood stage of infection and be responsible for the bimodal behavior displayed by the parasite in the liver stage of infection.

Overall, we have established the crucial role of Arg uptake and metabolism for *Plasmodium* liver-stage development, which can be explored to find new prophylactic approaches for the control of *Plasmodium* infection. Most commonly, Arg metabolism and, more specifically, polyamine synthesis can be modulated by interfering with enzymatic activity through the use of appropriate inhibitors [324, 329, 424]. α-difluoromethylornithine (DFMO), an irreversible ODC inhibitor, is the most widely studied inhibitor of polyamine metabolism and was approved by the Food and Drug Administration (FDA) for the treatment of African trypanosomiasis [424]. However, DFMO was shown to only have a cytostatic effect on *P. falciparum* proliferation *in vitro,* and is not curative of *in vivo P. berghei* infection [26, 328, 340, 341]. Additionally, our results show that inhibition of ODC by DFMO decreases parasite development but does not lead to parasite elimination.

Our results suggest that inhibition of polyamine synthesis alone is not sufficient to eliminate *Plasmodium* parasites. However, combining the inhibition of polyamine synthesis with the stimulation of NO production might constitute an efficacious strategy to impair hepatic infection. Ideally this would be achieved without resorting to the use of drugs or drug-like compounds. We thus wondered whether appropriate amino acid supplementation could be employed to suppress liver stage infection by the *Plasmodium* parasite, as such an approach might constitute an appealing prophylactic strategy.

Dietary amino acid supplementation is commonly employed to balance nutritional needs or deficiencies, especially in individuals with metabolic diseases that require a protein restrictive diet. Amino acids or their metabolic products can also be used to interfere with the function of enzymes or receptors, modulating the pathways in which they intervene. Arg metabolism has been shown to be regulated by dietary amino acids, such as Lys, Orn and Val, which have been described as arginase inhibitors [30, 31, 407]. On the other hand, Arg administration leads to enhanced NO production in *Plasmodium*-infected mice and malaria patients [32, 33, 441, 442]. Our results show that a Lys/Val/Arg supplementation is effective at blocking polyamine synthesis through the inhibition of arginase activity, while simultaneously stimulating NO production by iNOS, contributing to parasite elimination by hepatocytes. Adequate amino acid supplementation may therefore constitute a novel, drugless approach to modulate liver-stage of *Plasmodium* infection, which could be employed as a prophylactic strategy against malaria.

In this dissertation, we established the pivotal role of glucose and Arg uptake by GLUT1 and CAT2 transporters, respectively, and of their downstream metabolic pathways in *Plasmodium* infection of hepatic cells. Additionally, we explored dietary amino acid supplementation as a new drugless approach to modulate *Plasmodium* development and survival during the hepatic stage of the parasite's life cycle. Our results provide new insights into the host-parasite interactions at play during liver-stage infection by malaria parasites and pave the way for the development of novel intervention strategies against this disease.

References

1. WHO, World Malaria Report. 2015.
2. Lopez Del Prado, G.R., et al., Malaria in developing countries. J Infect Dev Ctries, 2014. 8(1): p. 1-4.
3. Mota M.M., P.G., Vanderberg J., Frevert U., Hafalla JCR., Nussenzweig R., Rodriguez A., Migration of *Plasmodium* sporozoites through cells before infection., in Science. 2001. p. 141-144.
4. Prudêncio M, R.A., Mota MM, The silent path to thousands of merozoites: the *Plasmodium* liver stage, in Nat. Rev. Microbiol. 2006. p. 849-856.
5. Lindner, S.E., J.L. Miller, and S.H. Kappe, Malaria parasite pre-erythrocytic infection: preparation meets opportunity. Cell Microbiol, 2012. 14(3): p. 316-24.
6. Kaushansky, A. and S.H. Kappe, Selection and refinement: the malaria parasite's infection and exploitation of host hepatocytes. Curr Opin Microbiol, 2015. 26: p. 71-8.
7. Blume, M., et al., A constitutive pan-hexose permease for the *Plasmodium* life cycle and transgenic models for screening of antimalarial sugar analogs. FASEB J, 2011. 25(4): p. 1218-29.
8. Slavic, K., et al., Use of a selective inhibitor to define the chemotherapeutic potential of the plasmodial hexose transporter in different stages of the parasite's life cycle. Antimicrob Agents Chemother, 2011. 55(6): p. 2824-30.
9. Mikolajczak, S.A., et al., L-FABP is a critical host factor for successful malaria liver stage development. Int J Parasitol, 2007. 37(5): p. 483-9.
10. Labaied, M., et al., *Plasmodium* salvages cholesterol internalized by LDL and synthesized de novo in the liver. Cell Microbiol, 2011. 13(4): p. 569-86.
11. Albuquerque, S.S., et al., Host cell transcriptional profiling during malaria liver stage infection reveals a coordinated and sequential set of biological events. BMC Genomics, 2009. 10: p. 270.
12. Tal, M., et al., Restricted expression of the erythroid/brain glucose transporter isoform to perivenous hepatocytes in rats. Modulation by glucose. J Clin Invest, 1990. 86(3): p. 986-92.
13. Smith, T.A., Facilitative glucose transporter expression in human cancer tissue. Br J Biomed Sci, 1999. 56(4): p. 285-92.
14. Hellwig, B. and H.G. Joost, Differentiation of erythrocyte-(GLUT1), liver-(GLUT2), and adipocyte-type (GLUT4) glucose transporters by binding of the inhibitory ligands cytochalasin B, forskolin, dipyridamole, and isobutylmethylxanthine. Mol Pharmacol, 1991. 40(3): p. 383-9.

15. Woodrow, C.J., R.J. Burchmore, and S. Krishna, Hexose permeation pathways in *Plasmodium falciparum*-infected erythrocytes. Proc Natl Acad Sci U S A, 2000. 97(18): p. 9931-6.
16. Joet, T., et al., Validation of the hexose transporter of *Plasmodium falciparum* as a novel drug target. Proc Natl Acad Sci U S A, 2003. 100(13): p. 7476-9.
17. Slavic, K., et al., Life cycle studies of the hexose transporter of *Plasmodium* species and genetic validation of their essentiality. Mol Microbiol, 2010. 75(6): p. 1402-13.
18. Verrey, F., et al., CATs and HATs: the SLC7 family of amino acid transporters. Pflugers Arch, 2004. 447(5): p. 532-42.
19. Fotiadis, D., Y. Kanai, and M. Palacin, The SLC3 and SLC7 families of amino acid transporters. Mol Aspects Med, 2013. 34(2-3): p. 139-58.
20. Closs EI, S.A., Vekony N, Rotmann A, Plasma membrane transporters for arginine, in J Nutr. 2004. p. 2752S–9S.
21. Wanasen N, S.L., L-arginine metabolism and its impact on host immunity against Leishmania infection, in Immunol Res. 2008. p. 15–25.
22. Das, P., A. Lahiri, and D. Chakravortty, Modulation of the arginase pathway in the context of microbial pathogenesis: a metabolic enzyme moonlighting as an immune modulator. PLoS Pathog, 2010. 6(6): p. e1000899.
23. Muller, I.B., R.D. Walter, and C. Wrenger, Structural metal dependency of the arginase from the human malaria parasite *Plasmodium falciparum*. Biol Chem, 2005. 386(2): p. 117-26.
24. Olszewski, K.L., et al., Host-parasite interactions revealed by *Plasmodium falciparum* metabolomics. Cell Host Microbe, 2009. 5(2): p. 191-9.
25. Dowling, D.P., et al., Crystal structure of arginase from *Plasmodium falciparum* and implications for L-arginine depletion in malarial infection. Biochemistry, 2010. 49(26): p. 5600-8.
26. Das Gupta, R., et al., 3-Aminooxy-1-aminopropane and derivatives have an antiproliferative effect on cultured *Plasmodium falciparum* by decreasing intracellular polyamine concentrations. Antimicrob Agents Chemother, 2005. 49(7): p. 2857-64.
27. Clark, K., et al., Transcriptional responses of *Plasmodium falciparum* to alpha-difluoromethylornithine-induced polyamine depletion. Biol Chem, 2008. 389(2): p. 111-25.
28. Becker, J.V., et al., *Plasmodium falciparum* spermidine synthase inhibition results in unique perturbation-specific effects observed on transcript, protein and metabolite levels. BMC Genomics, 2010. 11: p. 235.

29. Wanasen N, M.C., Ellies LG, Soong L, L-Arginine and Cationic Amino Acid Transporter 2B Regulate Growth and Survival Of *Leishmania amazonensis* Amastigotes in Macrophages, in Infection and Immunity. 2007. p. 2802-2810.
30. Hunter, A.a.D., C.E., The inhibition of arginase by amino acids. The Journal of Biological Chemistry, 1945. 157: p. 427-446.
31. Lerzynski, G., C.V. Suschek, and V. Kolb-Bachofen, In hepatocytes the regulation of NOS-2 activity at physiological L-arginine levels suggests a close link to the urea cycle. Nitric Oxide, 2006. 14(4): p. 300-8.
32. Martins, Y.C., et al., Efficacy of different nitric oxide-based strategies in preventing experimental cerebral malaria by *Plasmodium berghei* ANKA. PLoS One, 2012. 7(2): p. e32048.
33. Zhu, X., et al., Supplement of L-Arg improves protective immunity during early-stage *Plasmodium yoelii* 17XL infection. Parasite Immunol, 2012. 34(8-9): p. 412-20.
34. Rockett, K.A., et al., Killing of *Plasmodium falciparum* in vitro by nitric oxide derivatives. Infect Immun, 1991. 59(9): p. 3280-3.
35. Hollenstein, U., et al., Serum procalcitonin levels in severe *Plasmodium falciparum* malaria. Am J Trop Med Hyg, 1998. 59(6): p. 860-3.
36. Venturini, G., et al., Nitric oxide inhibits falcipain, the *Plasmodium falciparum* trophozoite cysteine protease. Biochem Biophys Res Commun, 2000. 267(1): p. 190-3.
37. Balmer, P., et al., The effect of nitric oxide on the growth of *Plasmodium falciparum*, *P. chabaudi* and *P. berghei in vitro*. Parasite Immunol, 2000. 22(2): p. 97-106.
38. Gyan, B., et al., Human monocytes cultured with and without interferon-gamma inhibit *Plasmodium falciparum* parasite growth in vitro via secretion of reactive nitrogen intermediates. Parasite Immunol, 1994. 16(7): p. 371-5.
39. Sedegah, M., F. Finkelman, and S.L. Hoffman, Interleukin 12 induction of interferon gamma-dependent protection against malaria. Proc Natl Acad Sci U S A, 1994. 91(22): p. 10700-2.
40. Zuzarte-Luis, V., M.M. Mota, and A.M. Vigario, Malaria infections: what and how can mice teach us. J Immunol Methods, 2014. 410: p. 113-22.
41. Prudencio, M., M.M. Mota, and A.M. Mendes, A toolbox to study liver stage malaria. Trends Parasitol, 2011. 27(12): p. 565-74.
42. Jones, R.A., S.S. Panda, and C.D. Hall, Quinine conjugates and quinine analogues as potential antimalarial agents. Eur J Med Chem, 2015. 97: p. 335-55.
43. Kantele, A. and T.S. Jokiranta, Review of cases with the emerging fifth human malaria parasite, *Plasmodium knowlesi*. Clin Infect Dis, 2011. 52(11): p. 1356-62.

44. Kevin Baird, J., Malaria caused by *Plasmodium vivax*: recurrent, difficult to treat, disabling, and threatening to life--the infectious bite preempts these hazards. Pathog Glob Health, 2013. 107(8): p. 475-9.
45. Mendis, K., et al., The neglected burden of *Plasmodium vivax* malaria. Am J Trop Med Hyg, 2001. 64(1-2 Suppl): p. 97-106.
46. Ngassa Mbenda, H.G. and A. Das, Molecular evidence of *Plasmodium vivax* mono and mixed malaria parasite infections in Duffy-negative native Cameroonians. PLoS One, 2014. 9(8): p. e103262.
47. Mendes, C., et al., Duffy negative antigen is no longer a barrier to *Plasmodium vivax*--molecular evidences from the African West Coast (Angola and Equatorial Guinea). PLoS Negl Trop Dis, 2011. 5(6): p. e1192.
48. Wurtz, N., et al., Vivax malaria in Mauritania includes infection of a Duffy-negative individual. Malar J, 2011. 10: p. 336.
49. Carvalho, T.A., et al., *Plasmodium vivax* infection in Anajas, State of Para: no differential resistance profile among Duffy-negative and Duffy-positive individuals. Malar J, 2012. 11: p. 430.
50. Lo, E., et al., Molecular epidemiology of *Plasmodium vivax* and *Plasmodium falciparum* malaria among Duffy-positive and Duffy-negative populations in Ethiopia. Malar J, 2015. 14: p. 84.
51. Sadanand, S., Malaria: an evaluation of the current state of research on pathogenesis and antimalarial drugs. Yale J Biol Med, 2010. 83(4): p. 185-91.
52. van Vugt, M., et al., Malaria treatment and prophylaxis in endemic and nonendemic countries: evidence on strategies and their cost-effectiveness. Future Microbiol, 2011. 6(12): p. 1485-500.
53. Neghina, R., et al., Malaria, a journey in time: in search of the lost myths and forgotten stories. Am J Med Sci, 2010. 340(6): p. 492-8.
54. Buonsenso, D. and L. Cataldi, Watch out for malaria: still a leading cause of child death worldwide. Ital J Pediatr, 2010. 36: p. 58.
55. Cox, F.E., History of the discovery of the malaria parasites and their vectors. Parasit Vectors, 2010. 3(1): p. 5.
56. Cunha, C.B. and B.A. Cunha, Brief history of the clinical diagnosis of malaria: from Hippocrates to Osler. J Vector Borne Dis, 2008. 45(3): p. 194-9.
57. Hempelmann, E. and K. Krafts, Bad air, amulets and mosquitoes: 2,000 years of changing perspectives on malaria. Malar J, 2013. 12: p. 232.
58. Nobelprize.org. Available from: http://www.nobelprize.org/.

59. Krafts, K., E. Hempelmann, and A. Skorska-Stania, From methylene blue to chloroquine: a brief review of the development of an antimalarial therapy. Parasitol Res, 2012. 111(1): p. 1-6.
60. Bynum, W.F., Ronald Ross and the malaria-mosquito cycle. Parassitologia, 1999. 41(1-3): p. 49-52.
61. Dutta, A., Where Ronald Ross (1857-1932) worked: the discovery of malarial transmission and the *Plasmodium* life cycle. J Med Biogr, 2009. 17(2): p. 120-2.
62. Fantini, B., The concept of specificity and the Italian contribution to the discovery of the malaria transmission cycle. Parassitologia, 1999. 41(1-3): p. 39-47.
63. James S., T.P., Exo-erythrocytic schizogony in *Plasmodium gallinaceum* Brumpt. Parasitology, 1938. 30(01): p. 128-138.
64. Shortt, H.E. and P.C. Garnham, Pre-erythrocytic stage in mammalian malaria parasites. Nature, 1948. 161(4082): p. 126.
65. Garnham, P.C., The developmental cycle of *Hepatocystes (Plasmodium) kochi* in the monkey host. Trans R Soc Trop Med Hyg, 1948. 41(5): p. 601-16.
66. Shortt, H.E. and P.C. Garnham, The pre-erythrocytic development of *Plasmodium cynomolgi* and *Plasmodium vivax*. Trans R Soc Trop Med Hyg, 1948. 41(6): p. 785-95.
67. Shortt, H.E., N.H. Fairley, and et al., The pre-erythrocytic stage of *Plasmodium falciparum*; a preliminary note. Br Med J, 1949. 2(4635): p. 1006-8, illust.
68. Shortt, H.E., P.C. Garnham, and et al., The pre-erythrocytic stage of human malaria, *Plasmodium vivax*. Br Med J, 1948. 1(4550): p. 547.
69. Garnham, P.C., et al., Pre-erythrocytic Stages of Human Malaria: *Plasmodium Ovale*. Br Med J, 1954. 1(4856): p. 257.
70. Bray, R.S., Studies on malaria in chimpanzees. VIII. The experimental transmission and pre-erythrocytic phase of *Plasmodium malariae*, with a note on the host-range of the parasite. Am J Trop Med Hyg, 1960. 9: p. 455-65.
71. Krotoski, W.A., et al., Demonstration of hypnozoites in sporozoite-transmitted *Plasmodium vivax* infection. Am J Trop Med Hyg, 1982. 31(6): p. 1291-3.
72. Majori, G., Short history of malaria and its eradication in Italy with short notes on the fight against the infection in the mediterranean basin. Mediterr J Hematol Infect Dis, 2012. 4(1): p. e2012016.
73. Bruce-Chwatt, L.J., Malaria eradication in Portugal. Trans R Soc Trop Med Hyg, 1977. 71(3): p. 232-40.
74. Fonseca, A.G., et al., The burden of imported malaria in Portugal 2003 to 2012. J Travel Med, 2014. 21(5): p. 354-6.

75. de Villiers, K.A., J. Gildenhuys, and T. le Roex, Iron(III) protoporphyrin IX complexes of the antimalarial Cinchona alkaloids quinine and quinidine. ACS Chem Biol, 2012. 7(4): p. 666-71.
76. Egan, T.J., et al., Fate of haem iron in the malaria parasite *Plasmodium falciparum*. Biochem J, 2002. 365(Pt 2): p. 343-7.
77. Coatney, G.R., Pitfalls in a discovery: the chronicle of chloroquine. Am J Trop Med Hyg, 1963. 12: p. 121-8.
78. Ecker, A., et al., PfCRT and its role in antimalarial drug resistance. Trends Parasitol, 2012. 28(11): p. 504-14.
79. Roepe, P.D., Molecular and physiologic basis of quinoline drug resistance in *Plasmodium falciparum* malaria. Future Microbiol, 2009. 4(4): p. 441-55.
80. Bray, P.G., et al., PfCRT and the trans-vacuolar proton electrochemical gradient: regulating the access of chloroquine to ferriprotoporphyrin IX. Mol Microbiol, 2006. 62(1): p. 238-51.
81. Slater, A.F. and A. Cerami, Inhibition by chloroquine of a novel haem polymerase enzyme activity in malaria trophozoites. Nature, 1992. 355(6356): p. 167-9.
82. Hempelmann, E., Hemozoin biocrystallization in *Plasmodium falciparum* and the antimalarial activity of crystallization inhibitors. Parasitol Res, 2007. 100(4): p. 671-6.
83. Fidock, D.A., et al., Mutations in the *P. falciparum* digestive vacuole transmembrane protein PfCRT and evidence for their role in chloroquine resistance. Mol Cell, 2000. 6(4): p. 861-71.
84. Ashley, E.A., J. Recht, and N.J. White, Primaquine: the risks and the benefits. Malar J, 2014. 13: p. 418.
85. Alving, A.S., et al., Mitigation of the haemolytic effect of primaquine and enhancement of its action against exoerythrocytic forms of the Chesson strain of *Plasmodium vivax* by intermittent regimens of drug administration: a preliminary report. Bull World Health Organ, 1960. 22: p. 621-31.
86. Greenwood, B., Anti-malarial drugs and the prevention of malaria in the population of malaria endemic areas. Malar J, 2010. 9 Suppl 3: p. S2.
87. Tekwani, B.L. and L.A. Walker, 8-Aminoquinolines: future role as antiprotozoal drugs. Curr Opin Infect Dis, 2006. 19(6): p. 623-31.
88. White, N.J., et al., Rationale for recommending a lower dose of primaquine as a *Plasmodium falciparum* gametocytocide in populations where G6PD deficiency is common. Malar J, 2012. 11: p. 418.
89. White, N.J., Primaquine to prevent transmission of falciparum malaria. Lancet Infect Dis, 2013. 13(2): p. 175-81.

90. Mihaly, G.W., et al., Pharmacokinetics of primaquine in man: identification of the carboxylic acid derivative as a major plasma metabolite. Br J Clin Pharmacol, 1984. 17(4): p. 441-6.
91. Bennett, J.W., et al., Primaquine failure and cytochrome P-450 2D6 in *Plasmodium vivax* malaria. N Engl J Med, 2013. 369(14): p. 1381-2.
92. O'Neill, P.M., V.E. Barton, and S.A. Ward, The molecular mechanism of action of artemisinin--the debate continues. Molecules, 2010. 15(3): p. 1705-21.
93. Lin, A.J., D.L. Klayman, and W.K. Milhous, Antimalarial activity of new water-soluble dihydroartemisinin derivatives. J Med Chem, 1987. 30(11): p. 2147-50.
94. Brossi, A., et al., Arteether, a new antimalarial drug: synthesis and antimalarial properties. J Med Chem, 1988. 31(3): p. 645-50.
95. Davis, T.M., H.A. Karunajeewa, and K.F. Ilett, Artemisinin-based combination therapies for uncomplicated malaria. Med J Aust, 2005. 182(4): p. 181-5.
96. ter Kuile, F., et al., *Plasmodium falciparum*: *in vitro* studies of the pharmacodynamic properties of drugs used for the treatment of severe malaria. Exp Parasitol, 1993. 76(1): p. 85-95.
97. Kumar, N. and H. Zheng, Stage-specific gametocytocidal effect *in vitro* of the antimalaria drug qinghaosu on *Plasmodium falciparum*. Parasitol Res, 1990. 76(3): p. 214-8.
98. Nosten, F. and N.J. White, Artemisinin-based combination treatment of falciparum malaria. Am J Trop Med Hyg, 2007. 77(6 Suppl): p. 181-92.
99. Wells, T.N., P.L. Alonso, and W.E. Gutteridge, New medicines to improve control and contribute to the eradication of malaria. Nat Rev Drug Discov, 2009. 8(11): p. 879-91.
100. Asenso-Okyere K., A.F.A., Tarekegn J., Andam K.S., A review of the economic impact of malaria in agricultural development. Agricultural Economics, 2011. 42: p. 293–304.
101. Sachs, J. and P. Malaney, The economic and social burden of malaria. Nature, 2002. 415(6872): p. 680-5.
102. Mia M.S., B.R.A., Er A., Abidin R.D.Z.R.Z., Pereira J.J., Malaria and Climate Change: Discussion on Economic Impacts. American Journal of Environmental Sciences, 2011. 7(1): p. 73-82.
103. Russell, S., The economic burden of illness for households in developing countries: a review of studies focusing on malaria, tuberculosis, and human immunodeficiency virus/acquired immunodeficiency syndrome. Am J Trop Med Hyg, 2004. 71(2 Suppl): p. 147-55.

104. Holding, P.A. and P.K. Kitsao-Wekulo, Describing the burden of malaria on child development: what should we be measuring and how should we be measuring it? Am J Trop Med Hyg, 2004. 71(2 Suppl): p. 71-9.
105. Greenwood, B.M., et al., Malaria. Lancet, 2005. 365(9469): p. 1487-98.
106. Okumu, F.O. and S.J. Moore, Combining indoor residual spraying and insecticide-treated nets for malaria control in Africa: a review of possible outcomes and an outline of suggestions for the future. Malar J, 2011. 10: p. 208.
107. Pluess, B., et al., Indoor residual spraying for preventing malaria. Cochrane Database Syst Rev, 2010(4): p. CD006657.
108. Fane, M., et al., *Anopheles gambiae* resistance to pyrethroid-treated nets in cotton versus rice areas in Mali. Acta Trop, 2012. 122(1): p. 1-6.
109. Temu, E.A., et al., Pyrethroid resistance in *Anopheles gambiae*, in Bomi County, Liberia, compromises malaria vector control. PLoS One, 2012. 7(9): p. e44986.
110. Qin, Q., et al., Insecticide resistance of *Anopheles sinensis* and An. vagus in Hainan Island, a malaria-endemic area of China. Parasit Vectors, 2014. 7: p. 92.
111. Mawejje, H.D., et al., Insecticide resistance monitoring of field-collected *Anopheles gambiae* s.l. populations from Jinja, eastern Uganda, identifies high levels of pyrethroid resistance. Med Vet Entomol, 2013. 27(3): p. 276-83.
112. Vatandoost, H. and A.A. Hanafi-Bojd, Indication of pyrethroid resistance in the main malaria vector, *Anopheles stephensi* from Iran. Asian Pac J Trop Med, 2012. 5(9): p. 722-6.
113. Toe, K.H., et al., Increased pyrethroid resistance in malaria vectors and decreased bed net effectiveness, Burkina Faso. Emerg Infect Dis, 2014. 20(10): p. 1691-6.
114. Bigoga, J.D., et al., Pyrethroid resistance in *Anopheles gambiae* from the rubber cultivated area of Niete, South Region of Cameroon. Acta Trop, 2012. 124(3): p. 210-4.
115. Protopopoff, N., et al., High level of resistance in the mosquito *Anopheles gambiae* to pyrethroid insecticides and reduced susceptibility to bendiocarb in north-western Tanzania. Malar J, 2013. 12: p. 149.
116. Mulamba, C., et al., Widespread pyrethroid and DDT resistance in the major malaria vector *Anopheles funestus* in East Africa is driven by metabolic resistance mechanisms. PLoS One, 2014. 9(10): p. e110058.
117. Kabula, B., et al., Distribution and spread of pyrethroid and DDT resistance among the *Anopheles gambiae* complex in Tanzania. Med Vet Entomol, 2014. 28(3): p. 244-52.
118. Jones, C.M., et al., The dynamics of pyrethroid resistance in *Anopheles arabiensis* from Zanzibar and an assessment of the underlying genetic basis. Parasit Vectors, 2013. 6: p. 343.

119. Kalanda, G.C., et al., Comparative efficacy of chloroquine and sulphadoxine--pyrimethamine in pregnant women and children: a meta-analysis. Trop Med Int Health, 2006. 11(5): p. 569-77.
120. Choosing a Drug to Prevent Malaria; Centers for Disease Control and Prevention. November 9, 2012; Available from: http://www.cdc.gov/malaria/travelers/drugs.html.
121. Guidelines for malaria prevention in travellers from the UK 2015; Public Health England; Department of Health. 2015.
122. Hoffman, S.L., et al., The March Toward Malaria Vaccines. Am J Prev Med, 2015. 49(6 Suppl 4): p. S319-33.
123. Efficacy and safety of RTS,S/AS01 malaria vaccine with or without a booster dose in infants and children in Africa: final results of a phase 3, individually randomised, controlled trial. Lancet, 2015. 386(9988): p. 31-45.
124. Moorthy, V.S. and J.M. Okwo-Bele, Final results from a pivotal phase 3 malaria vaccine trial. Lancet, 2015. 386(9988): p. 5-7.
125. Mosquirix™ Assessment Report; European Medicines Agency. 23 July 2015.
126. Pilot implementation of first malaria vaccine recommended by WHO advisory groups; World Health Organization. 23 October 2015; Available from: http://www.who.int/mediacentre/news/releases/2015/sage/en/.
127. Kattenberg, J.H., et al., Systematic review and meta-analysis: rapid diagnostic tests versus placental histology, microscopy and PCR for malaria in pregnant women. Malar J, 2011. 10: p. 321.
128. Chiodini, P.L., et al., The heat stability of *Plasmodium* lactate dehydrogenase-based and histidine-rich protein 2-based malaria rapid diagnostic tests. Trans R Soc Trop Med Hyg, 2007. 101(4): p. 331-7.
129. Snounou, G. and H.P. Beck, The use of PCR genotyping in the assessment of recrudescence or reinfection after antimalarial drug treatment. Parasitol Today, 1998. 14(11): p. 462-7.
130. Uneke, C.J., Diagnosis of *Plasmodium falciparum* malaria in pregnancy in sub-Saharan Africa: the challenges and public health implications. Parasitol Res, 2008. 102(3): p. 333-42.
131. Omo-Aghoja, L.O., et al., The challenges of diagnosis and treatment of malaria in pregnancy in low resource settings. Acta Obstet Gynecol Scand, 2008. 87(7): p. 693-6.
132. Dondorp, A.M., et al., Artesunate versus quinine in the treatment of severe falciparum malaria in African children (AQUAMAT): an open-label, randomised trial. Lancet, 2010. 376(9753): p. 1647-57.
133. Ashley, E.A., et al., Spread of artemisinin resistance in *Plasmodium falciparum* malaria. N Engl J Med, 2014. 371(5): p. 411-23.

134. Snow, R.W., J.F. Trape, and K. Marsh, The past, present and future of childhood malaria mortality in Africa. Trends Parasitol, 2001. 17(12): p. 593-7.
135. Noedl, H., et al., Evidence of artemisinin-resistant malaria in western Cambodia. N Engl J Med, 2008. 359(24): p. 2619-20.
136. Dondorp, A.M., et al., Artemisinin resistance in *Plasmodium falciparum* malaria. N Engl J Med, 2009. 361(5): p. 455-67.
137. Witkowski, B., et al., Reduced artemisinin susceptibility of *Plasmodium falciparum* ring stages in western Cambodia. Antimicrob Agents Chemother, 2013. 57(2): p. 914-23.
138. Saralamba, S., et al., Intrahost modeling of artemisinin resistance in *Plasmodium falciparum*. Proc Natl Acad Sci U S A, 2011. 108(1): p. 397-402.
139. Mok, S., et al., Artemisinin resistance in *Plasmodium falciparum* is associated with an altered temporal pattern of transcription. BMC Genomics, 2011. 12: p. 391.
140. Witkowski, B., et al., Novel phenotypic assays for the detection of artemisinin-resistant *Plasmodium falciparum* malaria in Cambodia: *in vitro* and *ex vivo* drug-response studies. Lancet Infect Dis, 2013. 13(12): p. 1043-9.
141. Chotivanich, K., et al., Laboratory detection of artemisinin-resistant *Plasmodium falciparum*. Antimicrob Agents Chemother, 2014. 58(6): p. 3157-61.
142. Phyo, A.P., et al., Emergence of artemisinin-resistant malaria on the western border of Thailand: a longitudinal study. Lancet, 2012. 379(9830): p. 1960-6.
143. Tun, K.M., et al., Spread of artemisinin-resistant *Plasmodium falciparum* in Myanmar: a cross-sectional survey of the K13 molecular marker. Lancet Infect Dis, 2015. 15(4): p. 415-21.
144. Ariey, F., et al., A molecular marker of artemisinin-resistant *Plasmodium falciparum* malaria. Nature, 2014. 505(7481): p. 50-5.
145. Mota, M.M., et al., Migration of *Plasmodium* sporozoites through cells before infection. Science, 2001. 291(5501): p. 141-4.
146. Menard, R., et al., Looking under the skin: the first steps in malarial infection and immunity. Nat Rev Microbiol, 2013. 11(10): p. 701-12.
147. Sinnis, P. and F. Zavala, The skin: where malaria infection and the host immune response begin. Semin Immunopathol, 2012. 34(6): p. 787-92.
148. Risco-Castillo, V., et al., Malaria Sporozoites Traverse Host Cells within Transient Vacuoles. Cell Host Microbe, 2015.
149. Prudencio, M., A. Rodriguez, and M.M. Mota, The silent path to thousands of merozoites: the *Plasmodium* liver stage. Nat Rev Microbiol, 2006. 4(11): p. 849-56.
150. Baer, K., et al., Release of hepatic *Plasmodium yoelii* merozoites into the pulmonary microvasculature. PLoS Pathog, 2007. 3(11): p. e171.

151. Siu, E. and A. Ploss, Modeling malaria in humanized mice: opportunities and challenges. Ann N Y Acad Sci, 2015. 1342: p. 29-36.

152. Josling, G.A. and M. Llinas, Sexual development in *Plasmodium* parasites: knowing when it's time to commit. Nat Rev Microbiol, 2015. 13(9): p. 573-87.

153. Trager, W., M.A. Rudzinska, and P.C. Bradbury, The fine structure of *Plasmodium falciparum* and its host erythrocytes in natural malarial infections in man. Bull World Health Organ, 1966. 35(6): p. 883-5.

154. Akinyi, S., et al., A 95 kDa protein of *Plasmodium vivax* and *P. cynomolgi* visualized by three-dimensional tomography in the caveola-vesicle complexes (Schuffner's dots) of infected erythrocytes is a member of the PHIST family. Mol Microbiol, 2012. 84(5): p. 816-31.

155. Kulzer, S., et al., Parasite-encoded Hsp40 proteins define novel mobile structures in the cytosol of the *P. falciparum*-infected erythrocyte. Cell Microbiol, 2010. 12(10): p. 1398-420.

156. Tamez, P.A., et al., An erythrocyte vesicle protein exported by the malaria parasite promotes tubovesicular lipid import from the host cell surface. PLoS Pathog, 2008. 4(8): p. e1000118.

157. Smith, J.D., The role of PfEMP1 adhesion domain classification in Plasmodium falciparum pathogenesis research. Mol Biochem Parasitol, 2014. 195(2): p. 82-7.

158. Taylor, L.H. and A.F. Read, Why so few transmission stages? Reproductive restraint by malaria parasites. Parasitol Today, 1997. 13(4): p. 135-40.

159. Billker, O., et al., Identification of xanthurenic acid as the putative inducer of malaria development in the mosquito. Nature, 1998. 392(6673): p. 289-92.

160. Sinden, R.E., *Plasmodium* differentiation in the mosquito. Parassitologia, 1999. 41(1-3): p. 139-48.

161. Kaushansky, A., et al., Of men in mice: the success and promise of humanized mouse models for human malaria parasite infections. Cell Microbiol, 2014. 16(5): p. 602-11.

162. Hollingdale, M.R., P. Leland, and A.L. Schwartz, In vitro cultivation of the exoerythrocytic stage of *Plasmodium berghei* in a hepatoma cell line. Am J Trop Med Hyg, 1983. 32(4): p. 682-4.

163. Prudencio, M., et al., Dissecting in vitro host cell infection by *Plasmodium* sporozoites using flow cytometry. Cell Microbiol, 2008. 10(1): p. 218-24.

164. Mota, M.M. and A. Rodriguez, *Plasmodium yoelii*: efficient in vitro invasion and complete development of sporozoites in mouse hepatic cell lines. Exp Parasitol, 2000. 96(4): p. 257-9.

165. Hollingdale, M.R., et al., *In vitro* culture of two populations (dividing and nondividing) of exoerythrocytic parasites of *Plasmodium vivax*. Am J Trop Med Hyg, 1985. 34(2): p. 216-22.

166. Sattabongkot, J., et al., Establishment of a human hepatocyte line that supports in vitro development of the exo-erythrocytic stages of the malaria parasites *Plasmodium falciparum* and *P. vivax*. Am J Trop Med Hyg, 2006. 74(5): p. 708-15.

167. Khetani, S.R. and S.N. Bhatia, Microscale culture of human liver cells for drug development. Nat Biotechnol, 2008. 26(1): p. 120-6.

168. Goncalves, L.A., A.M. Vigario, and C. Penha-Goncalves, Improved isolation of murine hepatocytes for *in vitro* malaria liver stage studies. Malar J, 2007. 6: p. 169.

169. Langhorne, J., et al., The relevance of non-human primate and rodent malaria models for humans. Malar J, 2011. 10: p. 23.

170. Craig, A.G., et al., The role of animal models for research on severe malaria. PLoS Pathog, 2012. 8(2): p. e1002401.

171. Vaughan, A.M., et al., Development of humanized mouse models to study human malaria parasite infection. Future Microbiol, 2012. 7(5): p. 657-65.

172. Vaughan, A.M., et al., Complete *Plasmodium falciparum* liver-stage development in liver-chimeric mice. J Clin Invest, 2012. 122(10): p. 3618-28.

173. Matsuoka, H., et al., A rodent malaria, *Plasmodium berghei*, is experimentally transmitted to mice by merely probing of infective mosquito, *Anopheles stephensi*. Parasitol Int, 2002. 51(1): p. 17-23.

174. Sidjanski, S. and J.P. Vanderberg, Delayed migration of *Plasmodium* sporozoites from the mosquito bite site to the blood. Am J Trop Med Hyg, 1997. 57(4): p. 426-9.

175. Vanderberg, J.P. and U. Frevert, Intravital microscopy demonstrating antibody-mediated immobilisation of *Plasmodium berghei* sporozoites injected into skin by mosquitoes. Int J Parasitol, 2004. 34(9): p. 991-6.

176. Medica, D.L. and P. Sinnis, Quantitative dynamics of *Plasmodium yoelii* sporozoite transmission by infected anopheline mosquitoes. Infect Immun, 2005. 73(7): p. 4363-9.

177. Rosenberg, R., et al., An estimation of the number of malaria sporozoites ejected by a feeding mosquito. Trans R Soc Trop Med Hyg, 1990. 84(2): p. 209-12.

178. Beier, J.C., et al., Quantitation of malaria sporozoites transmitted *in vitro* during salivation by wild Afrotropical *Anopheles*. Med Vet Entomol, 1991. 5(1): p. 71-9.

179. Amino, R., et al., Quantitative imaging of *Plasmodium* transmission from mosquito to mammal. Nat Med, 2006. 12(2): p. 220-4.

180. Frischknecht, F., The skin as interface in the transmission of arthropod-borne pathogens. Cell Microbiol, 2007. 9(7): p. 1630-40.

181. Yamauchi, L.M., et al., *Plasmodium* sporozoites trickle out of the injection site. Cell Microbiol, 2007. 9(5): p. 1215-22.

182. Chakravarty, S., et al., $CD8^+$ T lymphocytes protective against malaria liver stages are primed in skin-draining lymph nodes. Nat Med, 2007. 13(9): p. 1035-41.

183. Gueirard, P., et al., Development of the malaria parasite in the skin of the mammalian host. Proc Natl Acad Sci U S A, 2010. 107(43): p. 18640-5.

184. Voza, T., et al., Extrahepatic exoerythrocytic forms of rodent malaria parasites at the site of inoculation: clearance after immunization, susceptibility to primaquine, and contribution to blood-stage infection. Infect Immun, 2012. 80(6): p. 2158-64.

185. Leitner, W.W., E.S. Bergmann-Leitner, and E. Angov, Comparison of Plasmodium berghei challenge models for the evaluation of pre-erythrocytic malaria vaccines and their effect on perceived vaccine efficacy. Malar J, 2010. 9: p. 145.

186. Conteh, S., et al., *Plasmodium yoelii*-infected *A. stephensi* inefficiently transmit malaria compared to intravenous route. PLoS One, 2010. 5(1): p. e8947.

187. Baer, K., et al., Kupffer cells are obligatory for *Plasmodium yoelii* sporozoite infection of the liver. Cell Microbiol, 2007. 9(2): p. 397-412.

188. Frevert, U., et al., Intravital observation of *Plasmodium berghei* sporozoite infection of the liver. PLoS Biol, 2005. 3(6): p. e192.

189. Tavares, J., et al., Role of host cell traversal by the malaria sporozoite during liver infection. J Exp Med, 2013. 210(5): p. 905-15.

190. Klotz, C. and U. Frevert, *Plasmodium yoelii* sporozoites modulate cytokine profile and induce apoptosis in murine Kupffer cells. Int J Parasitol, 2008. 38(14): p. 1639-50.

191. Mota, M.M., J.C. Hafalla, and A. Rodriguez, Migration through host cells activates *Plasmodium* sporozoites for infection. Nat Med, 2002. 8(11): p. 1318-22.

192. Kumar, K.A., et al., Exposure of *Plasmodium* sporozoites to the intracellular concentration of potassium enhances infectivity and reduces cell passage activity. Mol Biochem Parasitol, 2007. 156(1): p. 32-40.

193. Carrolo, M., et al., Hepatocyte growth factor and its receptor are required for malaria infection. Nat Med, 2003. 9(11): p. 1363-9.

194. Ejigiri, I. and P. Sinnis, *Plasmodium* sporozoite-host interactions from the dermis to the hepatocyte. Curr Opin Microbiol, 2009. 12(4): p. 401-7.

195. Ishino, T., et al., Cell-passage activity is required for the malarial parasite to cross the liver sinusoidal cell layer. PLoS Biol, 2004. 2(1): p. E4.

196. Ishino, T., Y. Chinzei, and M. Yuda, A *Plasmodium* sporozoite protein with a membrane attack complex domain is required for breaching the liver sinusoidal cell layer prior to hepatocyte infection. Cell Microbiol, 2005. 7(2): p. 199-208.

197. Kaiser, K., et al., A member of a conserved *Plasmodium* protein family with membrane-attack complex/perforin (MACPF)-like domains localizes to the micronemes of sporozoites. Mol Biochem Parasitol, 2004. 133(1): p. 15-26.
198. Kariu, T., et al., CelTOS, a novel malarial protein that mediates transmission to mosquito and vertebrate hosts. Mol Microbiol, 2006. 59(5): p. 1369-79.
199. Bhanot, P., et al., A surface phospholipase is involved in the migration of *Plasmodium* sporozoites through cells. J Biol Chem, 2005. 280(8): p. 6752-60.
200. Coppi, A., et al., Heparan sulfate proteoglycans provide a signal to *Plasmodium* sporozoites to stop migrating and productively invade host cells. Cell Host Microbe, 2007. 2(5): p. 316-27.
201. Coppi, A., et al., The malaria circumsporozoite protein has two functional domains, each with distinct roles as sporozoites journey from mosquito to mammalian host. J Exp Med, 2011. 208(2): p. 341-56.
202. Morahan, B.J., L. Wang, and R.L. Coppel, No TRAP, no invasion. Trends Parasitol, 2009. 25(2): p. 77-84.
203. Sultan, A.A., et al., TRAP is necessary for gliding motility and infectivity of plasmodium sporozoites. Cell, 1997. 90(3): p. 511-22.
204. Gaur, D. and C.E. Chitnis, Molecular interactions and signaling mechanisms during erythrocyte invasion by malaria parasites. Curr Opin Microbiol, 2011. 14(4): p. 422-8.
205. Gonzalez, V., et al., Host cell entry by apicomplexa parasites requires actin polymerization in the host cell. Cell Host Microbe, 2009. 5(3): p. 259-72.
206. Silvie, O., et al., Cholesterol contributes to the organization of tetraspanin-enriched microdomains and to CD81-dependent infection by malaria sporozoites. J Cell Sci, 2006. 119(Pt 10): p. 1992-2002.
207. Silvie, O., et al., Alternative invasion pathways for *Plasmodium berghei* sporozoites. Int J Parasitol, 2007. 37(2): p. 173-82.
208. Silvie, O., et al., Expression of human CD81 differently affects host cell susceptibility to malaria sporozoites depending on the *Plasmodium* species. Cell Microbiol, 2006. 8(7): p. 1134-46.
209. Foquet, L., et al., Anti-CD81 but not anti-SR-BI blocks *Plasmodium falciparum* liver infection in a humanized mouse model. J Antimicrob Chemother, 2015. 70(6): p. 1784-7.
210. Rodrigues, C.D., et al., Host scavenger receptor SR-BI plays a dual role in the establishment of malaria parasite liver infection. Cell Host Microbe, 2008. 4(3): p. 271-82.
211. Yalaoui, S., et al., Scavenger receptor BI boosts hepatocyte permissiveness to *Plasmodium* infection. Cell Host Microbe, 2008. 4(3): p. 283-92.

212. Kaushansky, A. and S.H. Kappe, The crucial role of hepatocyte growth factor receptor during liver-stage infection is not conserved among *Plasmodium* species. Nat Med, 2011. 17(10): p. 1180-1; author reply 1181.

213. van Dijk, M.R., et al., Genetically attenuated, P36p-deficient malarial sporozoites induce protective immunity and apoptosis of infected liver cells. Proc Natl Acad Sci U S A, 2005. 102(34): p. 12194-9.

214. Kaushansky, A., et al., Malaria parasite liver stages render host hepatocytes susceptible to mitochondria-initiated apoptosis. Cell Death Dis, 2013. 4: p. e762.

215. van de Sand, C., et al., The liver stage of *Plasmodium berghei* inhibits host cell apoptosis. Mol Microbiol, 2005. 58(3): p. 731-42.

216. Bano, N., et al., Cellular interactions of *Plasmodium* liver stage with its host mammalian cell. Int J Parasitol, 2007. 37(12): p. 1329-41.

217. Labaied, M., et al., *Plasmodium yoelii* sporozoites with simultaneous deletion of P52 and P36 are completely attenuated and confer sterile immunity against infection. Infect Immun, 2007. 75(8): p. 3758-68.

218. van Schaijk, B.C., et al., Gene disruption of *Plasmodium falciparum* p52 results in attenuation of malaria liver stage development in cultured primary human hepatocytes. PLoS One, 2008. 3(10): p. e3549.

219. Kaushansky, A., et al., Malaria parasites target the hepatocyte receptor EphA2 for successful host infection. Science, 2015. 350(6264): p. 1089-92.

220. Vera, I.M., et al., *Plasmodium* protease ROM1 is important for proper formation of the parasitophorous vacuole. PLoS Pathog, 2011. 7(9): p. e1002197.

221. Doolan, D.L., et al., Identification and characterization of the protective hepatocyte erythrocyte protein 17 kDa gene of *Plasmodium yoelii*, homolog of *Plasmodium falciparum* exported protein 1. J Biol Chem, 1996. 271(30): p. 17861-8.

222. Mueller, A.K., et al., *Plasmodium* liver stage developmental arrest by depletion of a protein at the parasite-host interface. Proc Natl Acad Sci U S A, 2005. 102(8): p. 3022-7.

223. MacKellar, D.C., et al., A systematic analysis of the early transcribed membrane protein family throughout the life cycle of *Plasmodium yoelii*. Cell Microbiol, 2011. 13(11): p. 1755-67.

224. Jayabalasingham, B., N. Bano, and I. Coppens, Metamorphosis of the malaria parasite in the liver is associated with organelle clearance. Cell Res, 2010. 20(9): p. 1043-59.

225. Hegge, S., et al., Key factors regulating *Plasmodium berghei* sporozoite survival and transformation revealed by an automated visual assay. FASEB J, 2010. 24(12): p. 5003-12.

226. Doi, Y., et al., Calcium signal regulates temperature-dependent transformation of sporozoites in malaria parasite development. Exp Parasitol, 2011. 128(2): p. 176-80.
227. Stanway, R.R., et al., Organelle segregation into *Plasmodium* liver stage merozoites. Cell Microbiol, 2011. 13(11): p. 1768-82.
228. Itoe, M.A., et al., Host cell phosphatidylcholine is a key mediator of malaria parasite survival during liver stage infection. Cell Host Microbe, 2014. 16(6): p. 778-86.
229. Thieleke-Matos, C., et al., Host PI(3,5)P2 activity is required for *Plasmodium berghei* growth during liver stage infection. Traffic, 2014. 15(10): p. 1066-82.
230. Lopes da Silva, M., et al., The host endocytic pathway is essential for *Plasmodium berghei* late liver stage development. Traffic, 2012. 13(10): p. 1351-63.
231. Grutzke, J., et al., The spatiotemporal dynamics and membranous features of the *Plasmodium* liver stage tubovesicular network. Traffic, 2014. 15(4): p. 362-82.
232. Portugal, S., et al., Host-mediated regulation of superinfection in malaria. Nat Med, 2011. 17(6): p. 732-7.
233. Tarun, A.S., et al., A combined transcriptome and proteome survey of malaria parasite liver stages. Proc Natl Acad Sci U S A, 2008. 105(1): p. 305-10.
234. Vaughan, A.M., et al., Type II fatty acid synthesis is essential only for malaria parasite late liver stage development. Cell Microbiol, 2009. 11(3): p. 506-20.
235. Yu, M., et al., The fatty acid biosynthesis enzyme FabI plays a key role in the development of liver-stage malarial parasites. Cell Host Microbe, 2008. 4(6): p. 567-78.
236. Haussig, J.M., K. Matuschewski, and T.W. Kooij, Inactivation of a *Plasmodium* apicoplast protein attenuates formation of liver merozoites. Mol Microbiol, 2011. 81(6): p. 1511-25.
237. Sturm, A., et al., Manipulation of host hepatocytes by the malaria parasite for delivery into liver sinusoids. Science, 2006. 313(5791): p. 1287-90.
238. Blackman, M.J., Malarial proteases and host cell egress: an 'emerging' cascade. Cell Microbiol, 2008. 10(10): p. 1925-34.
239. Putrianti, E.D., et al., The *Plasmodium* serine-type SERA proteases display distinct expression patterns and non-essential in vivo roles during life cycle progression of the malaria parasite. Cell Microbiol, 2010. 12(6): p. 725-39.
240. Schmidt-Christensen, A., et al., Expression and processing of *Plasmodium berghei* SERA3 during liver stages. Cell Microbiol, 2008. 10(8): p. 1723-34.
241. Tarun, A.S., et al., Quantitative isolation and in vivo imaging of malaria parasite liver stages. Int J Parasitol, 2006. 36(12): p. 1283-93.
242. Graewe, S., et al., Hostile takeover by *Plasmodium*: reorganization of parasite and host cell membranes during liver stage egress. PLoS Pathog, 2011. 7(9): p. e1002224.

243. Bhatia, S.N., et al., Cell and tissue engineering for liver disease. Sci Transl Med, 2014. 6(245): p. 245sr2.

244. Juza, R.M. and E.M. Pauli, Clinical and surgical anatomy of the liver: a review for clinicians. Clin Anat, 2014. 27(5): p. 764-9.

245. Monga, S.P.S., Molecular Pathology of Liver Diseases. Molecular Pathology Library Series, ed. P.T. Cagle. 2011: Springer.

246. Rui, L., Energy metabolism in the liver. Compr Physiol, 2014. 4(1): p. 177-97.

247. Gissen, P. and I.M. Arias, Structural and functional hepatocyte polarity and liver disease. J Hepatol, 2015. 63(4): p. 1023-37.

248. Naito, M., G. Hasegawa, and K. Takahashi, Development, differentiation, and maturation of Kupffer cells. Microsc Res Tech, 1997. 39(4): p. 350-64.

249. Tietz, P.S. and N.F. Larusso, Cholangiocyte biology. Curr Opin Gastroenterol, 2006. 22(3): p. 279-87.

250. Geerts, A., History, heterogeneity, developmental biology, and functions of quiescent hepatic stellate cells. Semin Liver Dis, 2001. 21(3): p. 311-35.

251. Blomhoff, R., et al., Transport and storage of vitamin A. Science, 1990. 250(4979): p. 399-404.

252. Si-Tayeb, K., F.P. Lemaigre, and S.A. Duncan, Organogenesis and development of the liver. Dev Cell, 2010. 18(2): p. 175-89.

253. Gebhardt, R. and M. Matz-Soja, Liver zonation: Novel aspects of its regulation and its impact on homeostasis. World J Gastroenterol, 2014. 20(26): p. 8491-504.

254. Malarkey, D.E., et al., New insights into functional aspects of liver morphology. Toxicol Pathol, 2005. 33(1): p. 27-34.

255. Gordillo, M., T. Evans, and V. Gouon-Evans, Orchestrating liver development. Development, 2015. 142(12): p. 2094-108.

256. Katz, N., et al., Heterogeneous reciprocal localization of fructose-1,6-bisphosphatase and of glucokinase in microdissected periportal and perivenous rat liver tissue. FEBS Lett, 1977. 83(2): p. 272-6.

257. Jungermann, K. and T. Kietzmann, Zonation of parenchymal and nonparenchymal metabolism in liver. Annu Rev Nutr, 1996. 16: p. 179-203.

258. Gebhardt, R., et al., Hepatocellular heterogeneity in ammonia metabolism: demonstration of limited colocalization of carbamoylphosphate synthetase and glutamine synthetase. Eur J Cell Biol, 1991. 56(2): p. 464-7.

259. Haussinger, D., W.H. Lamers, and A.F. Moorman, Hepatocyte heterogeneity in the metabolism of amino acids and ammonia. Enzyme, 1992. 46(1-3): p. 72-93.

260. Braeuning, A., et al., Differential gene expression in periportal and perivenous mouse hepatocytes. FEBS J, 2006. 273(22): p. 5051-61.

261. Benhamouche, S., et al., Apc tumor suppressor gene is the "zonation-keeper" of mouse liver. Dev Cell, 2006. 10(6): p. 759-70.

262. Hailfinger, S., et al., Zonal gene expression in murine liver: lessons from tumors. Hepatology, 2006. 43(3): p. 407-14.

263. Sekine, S., et al., Liver-specific loss of beta-catenin blocks glutamine synthesis pathway activity and cytochrome p450 expression in mice. Hepatology, 2006. 43(4): p. 817-25.

264. Colletti, M., et al., Convergence of Wnt signaling on the HNF4alpha-driven transcription in controlling liver zonation. Gastroenterology, 2009. 137(2): p. 660-72.

265. Roden, M., K.F. Petersen, and G.I. Shulman, Nuclear magnetic resonance studies of hepatic glucose metabolism in humans. Recent Prog Horm Res, 2001. 56: p. 219-37.

266. Gardemann, A., H. Strulik, and K. Jungermann, A portal-arterial glucose concentration gradient as a signal for an insulin-dependent net glucose uptake in perfused rat liver. FEBS Lett, 1986. 202(2): p. 255-9.

267. Seyer, P., et al., Hepatic glucose sensing is required to preserve beta cell glucose competence. J Clin Invest, 2013. 123(4): p. 1662-76.

268. Valera, A. and F. Bosch, Glucokinase expression in rat hepatoma cells induces glucose uptake and is rate limiting in glucose utilization. Eur J Biochem, 1994. 222(2): p. 533-9.

269. Agius, L., Glucokinase and molecular aspects of liver glycogen metabolism. Biochem J, 2008. 414(1): p. 1-18.

270. Zhang, T., et al., Acetylation negatively regulates glycogen phosphorylase by recruiting protein phosphatase 1. Cell Metab, 2012. 15(1): p. 75-87.

271. Kir, S., et al., FGF19 as a postprandial, insulin-independent activator of hepatic protein and glycogen synthesis. Science, 2011. 331(6024): p. 1621-4.

272. Kuo T. , M.A., Chen T. , Wang J.-C., Glucocorticoid Signaling, Advances in Experimental Medicine and Biology, ed. C.H. J.-C. Wang. Vol. 872. 2015, New York: Springer Science+Business Media.

273. Oosterveer, M.H. and K. Schoonjans, Hepatic glucose sensing and integrative pathways in the liver. Cell Mol Life Sci, 2014. 71(8): p. 1453-67.

274. Kim, H.S., et al., Hepatic-specific disruption of SIRT6 in mice results in fatty liver formation due to enhanced glycolysis and triglyceride synthesis. Cell Metab, 2010. 12(3): p. 224-36.

275. Okar, D.A., et al., PFK-2/FBPase-2: maker and breaker of the essential biofactor fructose-2,6-bisphosphate. Trends Biochem Sci, 2001. 26(1): p. 30-5.

276. Rider, M.H., et al., 6-phosphofructo-2-kinase/fructose-2,6-bisphosphatase: head-to-head with a bifunctional enzyme that controls glycolysis. Biochem J, 2004. 381(Pt 3): p. 561-79.
277. Patra, K.C. and N. Hay, The pentose phosphate pathway and cancer. Trends Biochem Sci, 2014. 39(8): p. 347-54.
278. Horecker, B.L., The pentose phosphate pathway. J Biol Chem, 2002. 277(50): p. 47965-71.
279. Kruger, N.J. and A. von Schaewen, The oxidative pentose phosphate pathway: structure and organisation. Curr Opin Plant Biol, 2003. 6(3): p. 236-46.
280. Michael, M.D., et al., Loss of insulin signaling in hepatocytes leads to severe insulin resistance and progressive hepatic dysfunction. Mol Cell, 2000. 6(1): p. 87-97.
281. Wasserman, D.H., et al., Glucagon is a primary controller of hepatic glycogenolysis and gluconeogenesis during muscular work. Am J Physiol, 1989. 257(1 Pt 1): p. E108-17.
282. Potthoff, M.J., et al., FGF15/19 regulates hepatic glucose metabolism by inhibiting the CREB-PGC-1alpha pathway. Cell Metab, 2011. 13(6): p. 729-38.
283. Sumara, G., et al., Gut-derived serotonin is a multifunctional determinant to fasting adaptation. Cell Metab, 2012. 16(5): p. 588-600.
284. Lopez, H.W., et al., Opposite fluxes of glutamine and alanine in the splanchnic area are an efficient mechanism for nitrogen sparing in rats. J Nutr, 1998. 128(9): p. 1487-94.
285. Hamberg, O., K. Nielsen, and H. Vilstrup, Effects of an increase in protein intake on hepatic efficacy for urea synthesis in healthy subjects and in patients with cirrhosis. J Hepatol, 1992. 14(2-3): p. 237-43.
286. Petersen, K.F., H. Vilstrup, and N. Tygstrup, Effect of dietary protein on the capacity of urea synthesis in rats. Horm Metab Res, 1990. 22(12): p. 612-5.
287. Young, V.R., et al., Rates of urea production and hydrolysis and leucine oxidation change linearly over widely varying protein intakes in healthy adults. J Nutr, 2000. 130(4): p. 761-6.
288. Matthews, D.E. and R.S. Downey, Measurement of urea kinetics in humans: a validation of stable isotope tracer methods. Am J Physiol, 1984. 246(6 Pt 1): p. E519-27.
289. Long, C.L., M. Jeevanandam, and J.M. Kinney, Metabolism and recycling of urea in man. Am J Clin Nutr, 1978. 31(8): p. 1367-82.
290. Metges, C.C., Contribution of microbial amino acids to amino acid homeostasis of the host. J Nutr, 2000. 130(7): p. 1857S-64S.

291. Danielsen, M. and A.A. Jackson, Limits of adaptation to a diet low in protein in normal man: urea kinetics. Clin Sci (Lond), 1992. 83(1): p. 103-8.
292. Nissim, I., et al., Role of the glutamate dehydrogenase reaction in furnishing aspartate nitrogen for urea synthesis: studies in perfused rat liver with 15N. Biochem J, 2003. 376(Pt 1): p. 179-88.
293. Brosnan, J.T., et al., Alanine metabolism in the perfused rat liver. Studies with (15)N. J Biol Chem, 2001. 276(34): p. 31876-82.
294. Dingemanse, M.A., et al., Development of the ornithine cycle in rat liver: zonation of a metabolic pathway. Hepatology, 1996. 24(2): p. 407-11.
295. Gebhardt, R. and D. Mecke, Heterogeneous distribution of glutamine synthetase among rat liver parenchymal cells in situ and in primary culture. EMBO J, 1983. 2(4): p. 567-70.
296. Lakshmanan, V., K.Y. Rhee, and J.P. Daily, Metabolomics and malaria biology. Mol Biochem Parasitol, 2011. 175(2): p. 104-11.
297. Olszewski, K.L. and M. Llinas, Central carbon metabolism of *Plasmodium* parasites. Mol Biochem Parasitol, 2011. 175(2): p. 95-103.
298. Roth, E., Jr., *Plasmodium falciparum* carbohydrate metabolism: a connection between host cell and parasite. Blood Cells, 1990. 16(2-3): p. 453-60; discussion 461-6.
299. Lian, L.Y., et al., Glycerol: an unexpected major metabolite of energy metabolism by the human malaria parasite. Malar J, 2009. 8: p. 38.
300. Jensen, M.D., M. Conley, and L.D. Helstowski, Culture of *Plasmodium falciparum*: the role of pH, glucose, and lactate. J Parasitol, 1983. 69(6): p. 1060-7.
301. Hammond, D.J., R.A. Aman, and C.C. Wang, The role of compartmentation and glycerol kinase in the synthesis of ATP within the glycosome of *Trypanosoma brucei*. J Biol Chem, 1985. 260(29): p. 15646-54.
302. Scheibel, L.W. and J. Miller, Glycolytic and cytochrome oxidase activity in *Plasmodia*. Mil Med, 1969. 134(10): p. 1074-80.
303. Bowman, I.B., et al., The metabolism of *Plasmodium berghei*, the malaria parasite of rodents. 2. An effect of mepacrine on the metabolism of glucose by the parasite separated from its host cell. Biochem J, 1961. 78(3): p. 472-8.
304. Buckwitz, D., et al., Glucose-6-phosphate dehydrogenase from *Plasmodium berghei*: kinetic and electrophoretic characterization. Biomed Biochim Acta, 1990. 49(2-3): p. S295-300.
305. Gardner, M.J., et al., Genome sequence of the human malaria parasite *Plasmodium falciparum*. Nature, 2002. 419(6906): p. 498-511.

306. Bozdech, Z., et al., The transcriptome of the intraerythrocytic developmental cycle of *Plasmodium falciparum*. PLoS Biol, 2003. 1(1): p. E5.

307. Kurdi-Haidar, B. and L. Luzzatto, Expression and characterization of glucose-6-phosphate dehydrogenase of *Plasmodium falciparum*. Mol Biochem Parasitol, 1990. 41(1): p. 83-91.

308. Geary, T.G., et al., Nutritional requirements of *Plasmodium falciparum* in culture. III. Further observations on essential nutrients and antimetabolites. J Protozool, 1985. 32(4): p. 608-13.

309. Cobbold, S.A., et al., Kinetic flux profiling elucidates two independent acetyl-CoA biosynthetic pathways in *Plasmodium falciparum*. J Biol Chem, 2013. 288(51): p. 36338-50.

310. MacRae, J.I., et al., Mitochondrial metabolism of sexual and asexual blood stages of the malaria parasite *Plasmodium falciparum*. BMC Biol, 2013. 11: p. 67.

311. Storm, J., et al., Phosphoenolpyruvate carboxylase identified as a key enzyme in erythrocytic *Plasmodium falciparum* carbon metabolism. PLoS Pathog, 2014. 10(1): p. e1003876.

312. von Itzstein, M., et al., Hot, sweet and sticky: the glycobiology of *Plasmodium falciparum*. Trends Parasitol, 2008. 24(5): p. 210-8.

313. Ke, H., et al., Genetic investigation of tricarboxylic acid metabolism during the *Plasmodium falciparum* life cycle. Cell Rep, 2015. 11(1): p. 164-74.

314. Dasgupta, B., Polysaccharides in the different stages of the life-cycles of certain sporozoa. Parasitology, 1960. 50: p. 509-14.

315. Kirk, K., H.A. Horner, and J. Kirk, Glucose uptake in *Plasmodium falciparum*-infected erythrocytes is an equilibrative not an active process. Mol Biochem Parasitol, 1996. 82(2): p. 195-205.

316. Slavic, K., et al., Plasmodial sugar transporters as anti-malarial drug targets and comparisons with other protozoa. Malar J, 2011. 10: p. 165.

317. Desai, S.A., D.J. Krogstad, and E.W. McCleskey, A nutrient-permeable channel on the intraerythrocytic malaria parasite. Nature, 1993. 362(6421): p. 643-6.

318. Woodrow, C.J., J.I. Penny, and S. Krishna, Intraerythrocytic *Plasmodium falciparum* expresses a high affinity facilitative hexose transporter. J Biol Chem, 1999. 274(11): p. 7272-7.

319. Mack, S.R., S. Samuels, and J.P. Vanderberg, Hemolymph of *Anopheles stephensi* from noninfected and *Plasmodium berghei*-infected mosquitoes. 3. Carbohydrates. J Parasitol, 1979. 65(2): p. 217-21.

320. Hall, N., et al., A comprehensive survey of the *Plasmodium* life cycle by genomic, transcriptomic, and proteomic analyses. Science, 2005. 307(5706): p. 82-6.

321. Florens, L., et al., A proteomic view of the *Plasmodium falciparum* life cycle. Nature, 2002. 419(6906): p. 520-6.

322. Itani, S., M. Torii, and T. Ishino, D-Glucose concentration is the key factor facilitating liver stage maturation of *Plasmodium*. Parasitol Int, 2014. 63(4): p. 584-90.

323. Gerner, E.W. and F.L. Meyskens, Jr., Polyamines and cancer: old molecules, new understanding. Nat Rev Cancer, 2004. 4(10): p. 781-92.

324. Casero, R.A., Jr. and L.J. Marton, Targeting polyamine metabolism and function in cancer and other hyperproliferative diseases. Nat Rev Drug Discov, 2007. 6(5): p. 373-90.

325. Heby, O., L. Persson, and M. Rentala, Targeting the polyamine biosynthetic enzymes: a promising approach to therapy of African sleeping sickness, Chagas' disease, and leishmaniasis. Amino Acids, 2007. 33(2): p. 359-66.

326. Muller, S., G.H. Coombs, and R.D. Walter, Targeting polyamines of parasitic protozoa in chemotherapy. Trends Parasitol, 2001. 17(5): p. 242-9.

327. Kusano, T., et al., Polyamines: essential factors for growth and survival. Planta, 2008. 228(3): p. 367-81.

328. Birkholtz, L.M., et al., Polyamine homoeostasis as a drug target in pathogenic protozoa: peculiarities and possibilities. Biochem J, 2011. 438(2): p. 229-44.

329. Clark, K., et al., Functional consequences of perturbing polyamine metabolism in the malaria parasite, *Plasmodium falciparum*. Amino Acids, 2010. 38(2): p. 633-44.

330. Pegg, A.E., Regulation of ornithine decarboxylase. J Biol Chem, 2006. 281(21): p. 14529-32.

331. Pegg, A.E., S-Adenosylmethionine decarboxylase. Essays Biochem, 2009. 46: p. 25-45.

332. Bale, S. and S.E. Ealick, Structural biology of S-adenosylmethionine decarboxylase. Amino Acids, 2010. 38(2): p. 451-60.

333. Ikeguchi, Y., M.C. Bewley, and A.E. Pegg, Aminopropyltransferases: function, structure and genetics. J Biochem, 2006. 139(1): p. 1-9.

334. Teng, R., et al., Metabolite profiling of the intraerythrocytic malaria parasite *Plasmodium falciparum* by (1)H NMR spectroscopy. NMR Biomed, 2009. 22(3): p. 292-302.

335. Haider, N., et al., The spermidine synthase of the malaria parasite *Plasmodium falciparum*: molecular and biochemical characterisation of the polyamine synthesis enzyme. Mol Biochem Parasitol, 2005. 142(2): p. 224-36.

336. Muller, S., et al., In the human malaria parasite *Plasmodium falciparum*, polyamines are synthesized by a bifunctional ornithine decarboxylase, S-adenosylmethionine decarboxylase. J Biol Chem, 2000. 275(11): p. 8097-102.

337. Birkholtz, L.M., et al., Parasite-specific inserts in the bifunctional S-adenosylmethionine decarboxylase/ornithine decarboxylase of *Plasmodium falciparum* modulate catalytic activities and domain interactions. Biochem J, 2004. 377(Pt 2): p. 439-48.

338. Wrenger, C., et al., The *Plasmodium falciparum* bifunctional ornithine decarboxylase, S-adenosyl-L-methionine decarboxylase, enables a well balanced polyamine synthesis without domain-domain interaction. J Biol Chem, 2001. 276(32): p. 29651-6.

339. Krause, T., et al., The ornithine decarboxylase domain of the bifunctional ornithine decarboxylase/S-adenosylmethionine decarboxylase of *Plasmodium falciparum*: recombinant expression and catalytic properties of two different constructs. Biochem J, 2000. 352 Pt 2: p. 287-92.

340. Assaraf, Y.G., et al., Cytostatic effect of DL-alpha-difluoromethylornithine against *Plasmodium falciparum* and its reversal by diamines and spermidine. Parasitol Res, 1987. 73(4): p. 313-8.

341. Bitonti, A.J., P.P. McCann, and A. Sjoerdsma, *Plasmodium falciparum* and *Plasmodium berghei*: effects of ornithine decarboxylase inhibitors on erythrocytic schizogony. Exp Parasitol, 1987. 64(2): p. 237-43.

342. Wright, P.S., et al., Irreversible inhibition of S-adenosylmethionine decarboxylase in *Plasmodium falciparum*-infected erythrocytes: growth inhibition in vitro. Biochem Pharmacol, 1991. 41(11): p. 1713-8.

343. Bitonti, A.J., et al., Bis(benzyl)polyamine analogs inhibit the growth of chloroquine-resistant human malaria parasites (*Plasmodium falciparum*) in vitro and in combination with alpha-difluoromethylornithine cure murine malaria. Proc Natl Acad Sci U S A, 1989. 86(2): p. 651-5.

344. Klenke, B., et al., Antiplasmodial activity of a series of 1,3,5-triazine-substituted polyamines. J Antimicrob Chemother, 2003. 52(2): p. 290-3.

345. Liew, L.P., et al., Synthesis and *in vitro* and *in vivo* evaluation of antimalarial polyamines. Eur J Med Chem, 2013. 69: p. 22-31.

346. Niemand, J., et al., Polyamine uptake by the intraerythrocytic malaria parasite, *Plasmodium falciparum*. Int J Parasitol, 2012. 42(10): p. 921-9.

347. Hollingdale, M.R., P.P. McCann, and A. Sjoerdsma, *Plasmodium berghei*: inhibitors of ornithine decarboxylase block exoerythrocytic schizogony. Exp Parasitol, 1985. 60(1): p. 111-7.

348. Gillet, J.M., et al., *Plasmodium berghei*: inhibition of the sporogonous cycle by alpha-difluoromethylornithine. Exp Parasitol, 1983. 56(2): p. 190-3.

349. Karim, S., D.H. Adams, and P.F. Lalor, Hepatic expression and cellular distribution of the glucose transporter family. World J Gastroenterol, 2012. 18(46): p. 6771-81.

350. Mueckler, M. and B. Thorens, The SLC2 (GLUT) family of membrane transporters. Mol Aspects Med, 2013. 34(2-3): p. 121-38.
351. Koranyi, L., et al., Glucose transporter gene expression in rat brain: Pretranslational changes associated with chronic insulin-induced hypoglycemia, fasting, and diabetes. Mol Cell Neurosci, 1991. 2(3): p. 244-52.
352. Manel, N., et al., The ubiquitous glucose transporter GLUT-1 is a receptor for HTLV. Cell, 2003. 115(4): p. 449-59.
353. Loisel-Meyer, S., et al., Glut1-mediated glucose transport regulates HIV infection. Proc Natl Acad Sci U S A, 2012. 109(7): p. 2549-54.
354. Vander Jagt, D.L., et al., D-lactate production in erythrocytes infected with *Plasmodium falciparum*. Mol Biochem Parasitol, 1990. 42(2): p. 277-84.
355. Pfaller, M.A., et al., *Plasmodium falciparum*: stage-specific lactate production in synchronized cultures. Exp Parasitol, 1982. 54(3): p. 391-6.
356. Penkler, G., et al., Construction and validation of a detailed kinetic model of glycolysis in *Plasmodium falciparum*. FEBS J, 2015. 282(8): p. 1481-511.
357. Feistel, T., et al., An expression system to screen for inhibitors of parasite glucose transporters. Mol Biochem Parasitol, 2008. 162(1): p. 71-6.
358. Ploemen, I.H., et al., Visualisation and quantitative analysis of the rodent malaria liver stage by real time imaging. PLoS One, 2009. 4(11): p. e7881.
359. Franke-Fayard, B., et al., A *Plasmodium berghei* reference line that constitutively expresses GFP at a high level throughout the complete life cycle. Mol Biochem Parasitol, 2004. 137(1): p. 23-33.
360. O'Neil, R.G., L. Wu, and N. Mullani, Uptake of a fluorescent deoxyglucose analog (2-NBDG) in tumor cells. Mol Imaging Biol, 2005. 7(6): p. 388-92.
361. Yamada, K., et al., A real-time method of imaging glucose uptake in single, living mammalian cells. Nat Protoc, 2007. 2(3): p. 753-62.
362. Fujita, J., Cold shock response in mammalian cells. J Mol Microbiol Biotechnol, 1999. 1(2): p. 243-55.
363. Sun, L., et al., Transcriptome response to heat stress in a chicken hepatocellular carcinoma cell line. Cell Stress Chaperones, 2015. 20(6): p. 939-50.
364. Sergent, O., et al., Role for membrane fluidity in ethanol-induced oxidative stress of primary rat hepatocytes. J Pharmacol Exp Ther, 2005. 313(1): p. 104-11.
365. Nourissat, P., et al., Ethanol induces oxidative stress in primary rat hepatocytes through the early involvement of lipid raft clustering. Hepatology, 2008. 47(1): p. 59-70.
366. Collins, C.M., J.M. Boss, and S.H. Speck, Identification of infected B-cell populations by using a recombinant murine gammaherpesvirus 68 expressing a fluorescent protein. J Virol, 2009. 83(13): p. 6484-93.

367. Liu, Y., et al., A small-molecule inhibitor of glucose transporter 1 downregulates glycolysis, induces cell-cycle arrest, and inhibits cancer cell growth in vitro and in vivo. Mol Cancer Ther, 2012. 11(8): p. 1672-82.

368. Imamura, H., et al., Visualization of ATP levels inside single living cells with fluorescence resonance energy transfer-based genetically encoded indicators. Proc Natl Acad Sci U S A, 2009. 106(37): p. 15651-6.

369. Ando, T., et al., Visualization and measurement of ATP levels in living cells replicating hepatitis C virus genome RNA. PLoS Pathog, 2012. 8(3): p. e1002561.

370. Kinet, S., et al., Isolated receptor binding domains of HTLV-1 and HTLV-2 envelopes bind Glut-1 on activated $CD4^+$ and $CD8^+$ T cells. Retrovirology, 2007. 4: p. 31.

371. Koseoglu, M.H. and F.I. Beigi, Mechanism of stimulation of glucose transport in response to inhibition of oxidative phosphorylation: analysis with myc-tagged Glut1. Mol Cell Biochem, 1999. 194(1-2): p. 109-16.

372. Shrayyef, M.Z., Gerich, JE, Normal Glucose Homeostasis, in Principles of Diabetes Mellitus, L. Poretsky, Editor. 2010, Springer.

373. Vidyashankar, S., et al., Liv.52 up-regulates cellular antioxidants and increase glucose uptake to circumvent oleic acid induced hepatic steatosis in HepG2 cells. Phytomedicine, 2012. 19(13): p. 1156-65.

374. Moore, M.C., et al., Regulation of hepatic glucose uptake and storage *in vivo*. Adv Nutr, 2012. 3(3): p. 286-94.

375. Cunningham, J.J., et al., Enhanced hepatic insulin sensitivity and peripheral glucose uptake in cold acclimating rats. Endocrinology, 1985. 117(4): p. 1585-9.

376. Pencek, R.R., et al., Exercise-induced changes in insulin and glucagon are not required for enhanced hepatic glucose uptake after exercise but influence the fate of glucose within the liver. Diabetes, 2004. 53(12): p. 3041-7.

377. Bitar, M.S., E. Al-Saleh, and F. Al-Mulla, Oxidative stress--mediated alterations in glucose dynamics in a genetic animal model of type II diabetes. Life Sci, 2005. 77(20): p. 2552-73.

378. Bechmann, L.P., et al., The interaction of hepatic lipid and glucose metabolism in liver diseases. J Hepatol, 2012. 56(4): p. 952-64.

379. Yu, J.W., et al., Hepatitis C virus core protein induces hepatic metabolism disorders through down-regulation of the SIRT1-AMPK signaling pathway. Int J Infect Dis, 2013. 17(7): p. e539-45.

380. Takanaga, H., B. Chaudhuri, and W.B. Frommer, GLUT1 and GLUT9 as major contributors to glucose influx in HepG2 cells identified by a high sensitivity intramolecular FRET glucose sensor. Biochim Biophys Acta, 2008. 1778(4): p. 1091-9.

381. Cloherty, E.K., et al., Regulation of GLUT1-mediated sugar transport by an antiport/uniport switch mechanism. Biochemistry, 1996. 35(40): p. 13231-9.
382. Levine, K.B., et al., Structural and physiologic determinants of human erythrocyte sugar transport regulation by adenosine triphosphate. Biochemistry, 1998. 37(35): p. 12221-32.
383. Blodgett, D.M., et al., Structural basis of GLUT1 inhibition by cytoplasmic ATP. J Gen Physiol, 2007. 130(2): p. 157-68.
384. Brunton, J., et al., Feeding uninvited guests: mTOR and AMPK set the table for intracellular pathogens. PLoS Pathog, 2013. 9(10): p. e1003552.
385. Abbud, W., et al., Stimulation of AMP-activated protein kinase (AMPK) is associated with enhancement of Glut1-mediated glucose transport. Arch Biochem Biophys, 2000. 380(2): p. 347-52.
386. Barnes, K., et al., Activation of GLUT1 by metabolic and osmotic stress: potential involvement of AMP-activated protein kinase (AMPK). J Cell Sci, 2002. 115(Pt 11): p. 2433-42.
387. Perrini, S., et al., Dehydroepiandrosterone stimulates glucose uptake in human and murine adipocytes by inducing GLUT1 and GLUT4 translocation to the plasma membrane. Diabetes, 2004. 53(1): p. 41-52.
388. Egert, S., N. Nguyen, and M. Schwaiger, Myocardial glucose transporter GLUT1: translocation induced by insulin and ischemia. J Mol Cell Cardiol, 1999. 31(7): p. 1337-44.
389. Mueckler, M., Facilitative glucose transporters. Eur J Biochem, 1994. 219(3): p. 713-25.
390. Thorens, B., et al., Liver glucose transporter: a basolateral protein in hepatocytes and intestine and kidney cells. Am J Physiol, 1990. 259(6 Pt 1): p. C279-85.
391. Bilir, B.M., et al., Novel control of the position-dependent expression of genes in hepatocytes. The GLUT-1 transporter. J Biol Chem, 1993. 268(26): p. 19776-84.
392. Simpson, I.A., et al., Blood-brain barrier glucose transporter: effects of hypo- and hyperglycemia revisited. J Neurochem, 1999. 72(1): p. 238-47.
393. Ebert, B.L., J.D. Firth, and P.J. Ratcliffe, Hypoxia and mitochondrial inhibitors regulate expression of glucose transporter-1 via distinct Cis-acting sequences. J Biol Chem, 1995. 270(49): p. 29083-9.
394. Ng, S., et al., Hypoxia promotes liver-stage malaria infection in primary human hepatocytes *in vitro*. Dis Model Mech, 2014. 7(2): p. 215-24.
395. Chen, C., et al., Regulation of glut1 mRNA by hypoxia-inducible factor-1. Interaction between H-ras and hypoxia. J Biol Chem, 2001. 276(12): p. 9519-25.

396. Dasgupta, S., et al., Proteasome inhibitors alter levels of intracellular peptides in HEK293T and SH-SY5Y cells. PLoS One, 2014. 9(7): p. e103604.

397. Prudencio, M., et al., Kinome-wide RNAi screen implicates at least 5 host hepatocyte kinases in *Plasmodium* sporozoite infection. PLoS Pathog, 2008. 4(11): p. e1000201.

398. Lee, E.E., et al., A Protein Kinase C Phosphorylation Motif in GLUT1 Affects Glucose Transport and is Mutated in GLUT1 Deficiency Syndrome. Mol Cell, 2015. 58(5): p. 845-53.

399. Pagliassotti, M.J. and A.D. Cherrington, Regulation of net hepatic glucose uptake in vivo. Annu Rev Physiol, 1992. 54: p. 847-60.

400. Danquah, I., G. Bedu-Addo, and F.P. Mockenhaupt, Type 2 diabetes mellitus and increased risk for malaria infection. Emerg Infect Dis, 2010. 16(10): p. 1601-4.

401. Wild, S., et al., Global prevalence of diabetes: estimates for the year 2000 and projections for 2030. Diabetes Care, 2004. 27(5): p. 1047-53.

402. Palacin, M., et al., Molecular biology of mammalian plasma membrane amino acid transporters. Physiol Rev, 1998. 78(4): p. 969-1054.

403. Closs, E.I., et al., Human cationic amino acid transporters hCAT-1, hCAT-2A, and hCAT-2B: three related carriers with distinct transport properties. Biochemistry, 1997. 36(21): p. 6462-8.

404. Closs, E.I., et al., Identification of a low affinity, high capacity transporter of cationic amino acids in mouse liver. J Biol Chem, 1993. 268(10): p. 7538-44.

405. Kim, J.W., et al., Transport of cationic amino acids by the mouse ecotropic retrovirus receptor. Nature, 1991. 352(6337): p. 725-8.

406. Hosokawa, H., et al., Cloning and characterization of a brain-specific cationic amino acid transporter. J Biol Chem, 1997. 272(13): p. 8717-22.

407. Wu, G., et al., Arginine metabolism and nutrition in growth, health and disease. Amino Acids, 2009. 37(1): p. 153-68.

408. Vockley, J.G., et al., Cloning and characterization of the human type II arginase gene. Genomics, 1996. 38(2): p. 118-23.

409. Krugliak, M., J. Zhang, and H. Ginsburg, Intraerythrocytic *Plasmodium falciparum* utilizes only a fraction of the amino acids derived from the digestion of host cell cytosol for the biosynthesis of its proteins. Mol Biochem Parasitol, 2002. 119(2): p. 249-56.

410. Lopansri, B.K., et al., Low plasma arginine concentrations in children with cerebral malaria and decreased nitric oxide production. Lancet, 2003. 361(9358): p. 676-8.

411. Nicholson, B., et al., Sustained nitric oxide production in macrophages requires the arginine transporter CAT2. J Biol Chem, 2001. 276(19): p. 15881-5.

412. Zuzarte-Luis, V., J. Sales-Dias, and M.M. Mota, Simple, sensitive and quantitative bioluminescence assay for determination of malaria pre-patent period. Malar J, 2014. 13: p. 15.

413. Liehl, P., et al., Host-cell sensors for *Plasmodium* activate innate immunity against liver-stage infection. Nat Med, 2014. 20(1): p. 47-53.

414. Zhang, W., et al., PCB 126 and other dioxin-like PCBs specifically suppress hepatic PEPCK expression via the aryl hydrocarbon receptor. PLoS One, 2012. 7(5): p. e37103.

415. Aroeira, R.I., A.M. Sebastiao, and C.A. Valente, BDNF, via truncated TrkB receptor, modulates GlyT1 and GlyT2 in astrocytes. Glia, 2015. 63(12): p. 2181-97.

416. Barry, D.P., et al., Cationic amino acid transporter 2 enhances innate immunity during *Helicobacter pylori* infection. PLoS One, 2011. 6(12): p. e29046.

417. Sans-Fons, M.G., et al., Arginine transport is impaired in C57Bl/6 mouse macrophages as a result of a deletion in the promoter of *Slc7a2* (CAT2), and susceptibility to *Leishmania* infection is reduced. J Infect Dis, 2013. 207(11): p. 1684-93.

418. Thompson, R.W., et al., Cationic amino acid transporter-2 regulates immunity by modulating arginase activity. PLoS Pathog, 2008. 4(3): p. e1000023.

419. Wanasen, N., et al., L-arginine and cationic amino acid transporter 2B regulate growth and survival of *Leishmania amazonensis* amastigotes in macrophages. Infect Immun, 2007. 75(6): p. 2802-10.

420. Assaraf, Y.G., et al., *Plasmodium falciparum*: synchronization of cultures with DL-alpha-difluoromethylornithine, an inhibitor of polyamine biosynthesis. Exp Parasitol, 1986. 61(2): p. 229-35.

421. Liu, J., et al., *Plasmodium falciparum* ensures its amino acid supply with multiple acquisition pathways and redundant proteolytic enzyme systems. Proc Natl Acad Sci U S A, 2006. 103(23): p. 8840-5.

422. Rey, J., et al., Reduced erythrocyte deformability associated with hypoargininemia during *Plasmodium falciparum* malaria. Sci Rep, 2014. 4: p. 3767.

423. Weinberg, J.B., et al., Arginine, nitric oxide, carbon monoxide, and endothelial function in severe malaria. Curr Opin Infect Dis, 2008. 21(5): p. 468-75.

424. Gamble, L.D., et al., Polyamine pathway inhibition as a novel therapeutic approach to treating neuroblastoma. Front Oncol, 2012. 2: p. 162.

425. Samoilenko capital O, C.A.C., et al., Effect of polyamine metabolism inhibitors on Lewis lung carcinoma growth and metastasis. Exp Oncol, 2015. 37(2): p. 151-3.

426. Meyskens, F.L., Jr., A.R. Simoneau, and E.W. Gerner, Chemoprevention of prostate cancer with the polyamine synthesis inhibitor difluoromethylornithine. Recent Results Cancer Res, 2014. 202: p. 115-20.

427. Legorreta-Herrera, M., et al., Nitric oxide is involved in the upregulation of IFN-gamma and IL-10 mRNA expression by CD8(+) T cells during the blood stages of *P. chabaudi AS* infection in CBA/Ca mice. Int J Biol Sci, 2011. 7(9): p. 1401-11.

428. Bogdan, C., Nitric oxide and the immune response. Nat Immunol, 2001. 2(10): p. 907-16.

429. Skorokhod, O.A., et al., Malarial pigment haemozoin, IFN-gamma, TNF-alpha, IL-1beta and LPS do not stimulate expression of inducible nitric oxide synthase and production of nitric oxide in immuno-purified human monocytes. Malar J, 2007. 6: p. 73.

430. Nahrevanian, H., Immune effector mechanisms of the nitric oxide pathway in malaria: cytotoxicity versus cytoprotection. Braz J Infect Dis, 2006. 10(4): p. 283-92.

431. Geller, D.A., et al., Cytokines, endotoxin, and glucocorticoids regulate the expression of inducible nitric oxide synthase in hepatocytes. Proc Natl Acad Sci U S A, 1993. 90(2): p. 522-6.

432. Nussler, A.K., et al., Stimulation of the nitric oxide synthase pathway in human hepatocytes by cytokines and endotoxin. J Exp Med, 1992. 176(1): p. 261-4.

433. Dascombe, M.J. and H. Nahrevanian, Pharmacological assessment of the role of nitric oxide in mice infected with lethal and nonlethal species of malaria. Parasite Immunol, 2003. 25(3): p. 149-59.

434. Taylor-Robinson, A.W., et al., The role of TH1 and TH2 cells in a rodent malaria infection. Science, 1993. 260(5116): p. 1931-4.

435. Kremsner, P.G., et al., High plasma levels of nitrogen oxides are associated with severe disease and correlate with rapid parasitological and clinical cure in *Plasmodium falciparum* malaria. Trans R Soc Trop Med Hyg, 1996. 90(1): p. 44-7.

436. Chiwakata, C.B., C.J. Hemmer, and M. Dietrich, High levels of inducible nitric oxide synthase mRNA are associated with increased monocyte counts in blood and have a beneficial role in *Plasmodium falciparum* malaria. Infect Immun, 2000. 68(1): p. 394-9.

437. Legorreta-Herrera, M., R.O. Meza, and L. Moreno-Fierros, Pretreatment with Cry1Ac protoxin modulates the immune response, and increases the survival of *Plasmodium*-infected CBA/Ca mice. J Biomed Biotechnol, 2010. 2010: p. 198921.

438. Jacobs, P., D. Radzioch, and M.M. Stevenson, Nitric oxide expression in the spleen, but not in the liver, correlates with resistance to blood-stage malaria in mice. J Immunol, 1995. 155(11): p. 5306-13.

439. Asensio, V.C., H. Oshima, and P.B. Falanga, *Plasmodium berghei*: is nitric oxide involved in the pathogenesis of mouse cerebral malaria? Exp Parasitol, 1993. 77(1): p. 111-7.

440. Newton, C.R., et al., Intracranial pressure in African children with cerebral malaria. Lancet, 1991. 337(8741): p. 573-6.

441. Yeo, T.W., et al., Impaired nitric oxide bioavailability and L-arginine reversible endothelial dysfunction in adults with falciparum malaria. J Exp Med, 2007. 204(11): p. 2693-704.

442. Yeo, T.W., et al., Safety profile of L-arginine infusion in moderately severe falciparum malaria. PLoS One, 2008. 3(6): p. e2347.

443. Yeo, T.W., et al., A randomized pilot study of L-arginine infusion in severe falciparum malaria: preliminary safety, efficacy and pharmacokinetics. PLoS One, 2013. 8(7): p. e69587.

444. Bogle, R.G., et al., Identification of inhibitors of nitric oxide synthase that do not interact with the endothelial cell L-arginine transporter. Br J Pharmacol, 1992. 105(4): p. 768-70.

445. Woods, S., et al., MAP kinase phosphatase-2 plays a key role in the control of infection with *Toxoplasma gondii* by modulating iNOS and arginase-1 activities in mice. PLoS Pathog, 2013. 9(8): p. e1003535.

446. Morris, S.M., Jr., Recent advances in arginine metabolism: roles and regulation of the arginases. Br J Pharmacol, 2009. 157(6): p. 922-30.

447. Kropf, P., et al., Arginase and polyamine synthesis are key factors in the regulation of experimental leishmaniasis in vivo. FASEB J, 2005. 19(8): p. 1000-2.

448. Al-Mutairi, M.S., et al., MAP kinase phosphatase-2 plays a critical role in response to infection by *Leishmania mexicana*. PLoS Pathog, 2010. 6(11): p. e1001192.

449. Wang, T. and Y. Xia, Inducible nitric oxide synthase aggresome formation is mediated by nitric oxide. Biochem Biophys Res Commun, 2012. 426(3): p. 386-9.

450. Roberts, F., et al., Inhibition of nitric oxide production exacerbates chronic ocular toxoplasmosis. Parasite Immunol, 2000. 22(1): p. 1-5.

451. van Rooijen, N., A. Sanders, and T.K. van den Berg, Apoptosis of macrophages induced by liposome-mediated intracellular delivery of clodronate and propamidine. J Immunol Methods, 1996. 193(1): p. 93-9.

452. Klotz, F.W., et al., Co-localization of inducible-nitric oxide synthase and *Plasmodium berghei* in hepatocytes from rats immunized with irradiated sporozoites. J Immunol, 1995. 154(7): p. 3391-5.

453. Smriga, M., et al., Dietary L-lysine deficiency increases stress-induced anxiety and fecal excretion in rats. J Nutr, 2002. 132(12): p. 3744-6.

454. Smriga, M. and K. Torii, L-Lysine acts like a partial serotonin receptor 4 antagonist and inhibits serotonin-mediated intestinal pathologies and anxiety in rats. Proc Natl Acad Sci U S A, 2003. 100(26): p. 15370-5.

455. Smriga, M., et al., Lysine fortification reduces anxiety and lessens stress in family members in economically weak communities in Northwest Syria. Proc Natl Acad Sci U S A, 2004. 101(22): p. 8285-8.

456. Peltola, K., et al., Oral lysine feeding in gyrate atrophy with hyperornithinaemia--a pilot study. J Inherit Metab Dis, 2000. 23(4): p. 305-7.

457. Elpeleg, N. and S.H. Korman, Sustained oral lysine supplementation in ornithine delta-aminotransferase deficiency. J Inherit Metab Dis, 2001. 24(3): p. 423-4.

458. Rajantie, J., et al., Lysinuric protein intolerance: a two-year trial of dietary supplementation therapy with citrulline and lysine. J Pediatr, 1980. 97(6): p. 927-32.

459. Lukkarinen, M., et al., Oral supplementation corrects plasma lysine concentrations in lysinuric protein intolerance. Metabolism, 2003. 52(7): p. 935-8.

460. Lukkarinen, M., et al., Effect of lysine infusion on urea cycle in lysinuric protein intolerance. Metabolism, 2000. 49(5): p. 621-5.

461. Tanner, L.M., et al., Long-term oral lysine supplementation in lysinuric protein intolerance. Metabolism, 2007. 56(2): p. 185-9.

462. Fell, V., et al., Ornithinemia, hyperammonemia, and homocitrullinuria. A disease associated with mental retardation and possibly caused by defective mitochondrial transport. Am J Dis Child, 1974. 127(5): p. 752-6.

463. Kolker, S., et al., Diagnosis and management of glutaric aciduria type I--revised recommendations. J Inherit Metab Dis, 2011. 34(3): p. 677-94.

464. De Bandt, J.P. and L. Cynober, Therapeutic use of branched-chain amino acids in burn, trauma, and sepsis. J Nutr, 2006. 136(1 Suppl): p. 308S-13S.

465. Shimomura, Y., et al., Exercise promotes BCAA catabolism: effects of BCAA supplementation on skeletal muscle during exercise. J Nutr, 2004. 134(6 Suppl): p. 1583S-1587S.

466. Shimomura, Y., et al., Nutraceutical effects of branched-chain amino acids on skeletal muscle. J Nutr, 2006. 136(2): p. 529S-532S.

467. Hauser, N.S., et al., Variable dietary management of methylmalonic acidemia: metabolic and energetic correlations. Am J Clin Nutr, 2011. 93(1): p. 47-56.

468. Lane, T.N., M.K. Spraker, and S.S. Parker, Propionic acidemia manifesting with low isoleucine generalized exfoliative dermatosis. Pediatr Dermatol, 2007. 24(5): p. 508-10.

469. Morton, D.H., et al., Diagnosis and treatment of maple syrup disease: a study of 36 patients. Pediatrics, 2002. 109(6): p. 999-1008.

470. Parini, R., et al., Nasogastric drip feeding as the only treatment of neonatal maple syrup urine disease. Pediatrics, 1993. 92(2): p. 280-3.
471. Nyhan, W.L., et al., Treatment of the acute crisis in maple syrup urine disease. Arch Pediatr Adolesc Med, 1998. 152(6): p. 593-8.
472. Shao, A. and J.N. Hathcock, Risk assessment for the amino acids taurine, L-glutamine and L-arginine. Regul Toxicol Pharmacol, 2008. 50(3): p. 376-99.
473. Tapiero, H., et al., I. Arginine. Biomed Pharmacother, 2002. 56(9): p. 439-45.
474. Nakaki, T., et al., L-arginine-induced hypotension. Lancet, 1990. 336(8716): p. 696.
475. Un, O., et al., L-arginine and tetrahydrobiopterin, but not sodium nitrite partially restored erectile dysfunction in aged rats. Aging Male, 2014. 17(4): p. 248-55.
476. Moody, J.A., et al., Effects of long-term oral administration of L-arginine on the rat erectile response. J Urol, 1997. 158(3 Pt 1): p. 942-7.
477. Gui, S., et al., Arginine supplementation for improving maternal and neonatal outcomes in hypertensive disorder of pregnancy: a systematic review. J Renin Angiotensin Aldosterone Syst, 2014. 15(1): p. 88-96.
478. Zinnanti, W.J. and J. Lazovic, Mouse model of encephalopathy and novel treatment strategies with substrate competition in glutaric aciduria type I. Mol Genet Metab, 2010. 100 Suppl 1: p. S88-91.
479. Strauss, K.A., et al., Safety, efficacy and physiological actions of a lysine-free, arginine-rich formula to treat glutaryl-CoA dehydrogenase deficiency: focus on cerebral amino acid influx. Mol Genet Metab, 2011. 104(1-2): p. 93-106.
480. Sydow, K., et al., ADMA and oxidative stress are responsible for endothelial dysfunction in hyperhomocyst(e)inemia: effects of L-arginine and B vitamins. Cardiovasc Res, 2003. 57(1): p. 244-52.
481. Cusworth, D.C. and A. Gattereau, Inhibition of renal tubular reabsorption of homocystine by lysine and arginine. Lancet, 1968. 2(7574): p. 916-7.
482. Mizutani, N., et al., Oral administration of arginine and citrulline in the treatment of lysinuric protein intolerance. Tohoku J Exp Med, 1984. 142(1): p. 15-24.
483. Rajantie, J., Orotic aciduria in lysinuric protein intolerance: dependence on the urea cycle intermediates. Pediatr Res, 1981. 15(2): p. 115-9.
484. Kekomaki, M., et al., Familial protein intolerance with deficient transport of basic amino acids. An analysis of 10 patients. Acta Paediatr Scand, 1967. 56(6): p. 617-30.
485. Oyanagi, K., et al., The mechanism of hyperammonemia in congenital lysinuria. J Pediatr, 1979. 94(2): p. 255-7.
486. Simell, O., et al., Ornithine loading did not prevent induced hyperammonemia in a patient with hyperornithinemia-hyperammonemia-homocitrullinuria syndrome. Pediatr Res, 1985. 19(12): p. 1283-7.

487. Oyanagi, K., et al., The mechanism of hyperammonaemia and hyperornithinaemia in the syndrome of hyperornithinaemia, hyperammonaemia with homocitrullinuria. J Inherit Metab Dis, 1983. 6(3): p. 133-4.

488. Dionisi Vici, C., et al., Hyperornithinemia-hyperammonemia-homocitrullinuria syndrome: low creatine excretion and effect of citrulline, arginine, or ornithine supplement. Pediatr Res, 1987. 22(3): p. 364-7.

489. van Vliet, D., et al., Single amino acid supplementation in aminoacidopathies: a systematic review. Orphanet J Rare Dis, 2014. 9: p. 7.

490. Alba-Roth, J., et al., Arginine stimulates growth hormone secretion by suppressing endogenous somatostatin secretion. J Clin Endocrinol Metab, 1988. 67(6): p. 1186-9.

491. Collier, S.R., D.P. Casey, and J.A. Kanaley, Growth hormone responses to varying doses of oral arginine. Growth Horm IGF Res, 2005. 15(2): p. 136-9.

492. Ilies, M., et al., Binding of alpha,alpha-disubstituted amino acids to arginase suggests new avenues for inhibitor design. J Med Chem, 2011. 54(15): p. 5432-43.

493. Wu, G. and S.M. Morris, Jr., Arginine metabolism: nitric oxide and beyond. Biochem J, 1998. 336 (Pt 1): p. 1-17.

494. Morris, S.M., Jr., Arginine metabolism: boundaries of our knowledge. J Nutr, 2007. 137(6 Suppl 2): p. 1602S-1609S.

495. Borrmann, S. and K. Matuschewski, Targeting *Plasmodium* liver stages: better late than never. Trends Mol Med, 2011. 17(9): p. 527-36.

496. Austin, L.S., A. Kaushansky, and S.H. Kappe, Susceptibility to *Plasmodium* liver stage infection is altered by hepatocyte polyploidy. Cell Microbiol, 2014. 16(5): p. 784-95.

497. Roelofs, B., et al., Acute activation of glucose uptake by glucose deprivation in L929 fibroblast cells. Biochimie, 2006. 88(12): p. 1941-6.

498. Kitzman, H.H., Jr., et al., Effect of glucose deprivation of GLUT 1 expression in 3T3-L1 adipocytes. J Biol Chem, 1993. 268(2): p. 1320-5.

499. Tordjman, K.M., K.A. Leingang, and M. Mueckler, Differential regulation of the HepG2 and adipocyte/muscle glucose transporters in 3T3L1 adipocytes. Effect of chronic glucose deprivation. Biochem J, 1990. 271(1): p. 201-7.

500. Babbitt, S.E., et al., *Plasmodium falciparum* responds to amino acid starvation by entering into a hibernatory state. Proc Natl Acad Sci U S A, 2012. 109(47): p. E3278-87.

501. Mackintosh, C.L., J.G. Beeson, and K. Marsh, Clinical features and pathogenesis of severe malaria. Trends Parasitol, 2004. 20(12): p. 597-603.

502. Munder, M., et al., Th1/Th2-regulated expression of arginase isoforms in murine macrophages and dendritic cells. J Immunol, 1999. 163(7): p. 3771-7.

503. Wanasen, N. and L. Soong, L-arginine metabolism and its impact on host immunity against *Leishmania* infection. Immunol Res, 2008. 41(1): p. 15-25.

504. Landfear, S.M., Nutrient transport and pathogenesis in selected parasitic protozoa. Eukaryot Cell, 2011. 10(4): p. 483-93.

505. Martin, R.E., et al., The 'permeome' of the malaria parasite: an overview of the membrane transport proteins of *Plasmodium falciparum*. Genome Biol, 2005. 6(3): p. R26.

Curriculum Vitae and Publications

Curriculum Vitae

PERSONAL DATA

Name: Patrícia dos Santos Meireles

Name in scientific papers: Meireles, P.

Birth Date: 05-02-1987

Nationality: Portuguese

Address: Travessa da Belavista, nº21, Sanfins de Ferreira, 4595-362 Paços de Ferreira, Portugal

E-mail: pmeireles@medicina.ulisboa.pt

SCIENTIFIC/PROFESSIONAL ACTIVITIES

Date: April 2011 to present

Position: PhD Student

Main activities: Study nutrient uptake and metabolism in *Plasmodium*-infected hepatic cells

Institution: Prudêncio Lab, Instituto de Medicina Molecular (IMM), Lisboa, Portugal

Date: September 2009 to November 2010

Position: Master Student

Main activities: Study the role of the protein Myrip on secretory vesicle recruitment to the plasma membrane

Institution: Laboratoire de dynamique membranaire et maladies neurologiques, Institut de Biologie Physico-Chimique (IBPC), Paris, France

EDUCATION AND TRAINING

Date: 2008-2010

Degree: MSc in Biochemistry

Final grade: 17 / B

Degree granting institution: Faculty of Sciences , University of Porto, Portugal

Thesis title: Role of the protein Myrip on secretory vesicle recruitment to the plasma membrane

Supervisor: Claire Desnos, PhD

Institution: Laboratoire de dynamique membranaire et maladies neurologiques, Institut de Biologie Physico-Chimique (IBPC), Paris, France

Date: 2005-2008

Degree: BSc Biochemistry

Final grade: 16 / B

Degree granting institution: Faculty of Sciences , University of Porto, Portugal

Thesis title: Study of the induced immune response in mice experimentally infected with strains of *Candida albicans* deficient in the production of secreted aspartic proteases

Supervisor: Manuel Vilanova, PhD

Institution: Immunobiology Laboratory, Instituto de Biologia Molecular e Celular (IBMC)/ Instituto de Ciências Biomédicas Abel Salazar (ICBAS), Porto, Portugal

RESEARCH INTERESTS

Biochemistry, cell biology, microbiology, infection, immune responses, interactions host-pathogen, nutrient uptake, transporters, metabolism, malaria.

PUBLICATIONS

Meireles P, Andrade CM, Aroeira RI, Staines HM, Mendes AM, Prudêncio M. Inhibition of *Plasmodium* liver infection by amino acid supplementation and modulation of polyamine synthesis. (manuscript in preparation)

Meireles P, Sales-Dias J, Andrade CM, Mancio-Silva L, Simas JP, Staines HM, Prudêncio M. GLUT1-mediated glucose uptake during *Plasmodium* hepatic infection. (manuscript submitted)

Ruivo MTG, Vera IM, Sales-Dias J, Meireles P, Mota MM, Mancio-Silva L. Host AMPK is a key modulator of *Plasmodium* liver infection. (under revision at Cell Reports)

Liehl P, Meireles P, Albuquerque IS, Pinkevych M, Baptista F, Mota MM, Davenport MP, Prudêncio M. Innate immunity induced by *Plasmodium* liver infection inhibits malaria reinfections. Infect Immun. 2015 Mar; 83(3):1172-80.

Oliveira R, Guedes RC, Meireles P, Albuquerque IS, Gonçalves LM, Pires E, Bronze MR, Gut J, Rosenthal PJ, Prudêncio M, Moreira R, O'Neill PM, Lopes F. Tetraoxane-pyrimidine nitrile hybrids as dual stage antimalarials. J Med Chem. 2014 Jun 12; 57(11):4916-23.

Miranda D, Capela R, Albuquerque IS, Meireles P, Paiva I, Nogueira F, Amewu R, Gut J, Rosenthal PJ, Oliveira R, Mota MM, Moreira R, Marti F, Prudêncio M, O'Neill PM, Lopes F. Novel endoperoxide-based transmission-blocking antimalarials with liver- and blood-schizontocidal activities. ACS Med Chem Lett. 2013 Dec 20; 5(2):108-12.

Lin JW, Meireles P, Prudêncio M, Engelmann S, Annoura T, Sajid M, Chevalley-Maurel S, Ramesar J, Nahar C, Avramut CM, Koster AJ, Matuschewski K, Waters AP, Janse CJ, Mair GR, Khan SM. Loss-of-function analyses defines vital and redundant functions of the *Plasmodium* rhomboid protease family. Mol Microbiol. 2013 Apr; 88(2):318-38.

Huet S, Fanget I, Jouannot O, Meireles P, Zeiske T, Larochette N, Darchen F, Desnos C. Myrip couples the capture of secretory granules by the actin-rich cell cortex and their attachment to the plasma membrane. J Neurosci. 2012 Feb 15; 32(7):2564-77.

FELLOWSHIPS AND AWARDS

April 2011 to present

Doctoral grant from Fundação para a Ciência e Tecnologia (FCT)

May 2015

11th Annual BioMalPar/EVIMalaR Conference, EMBL Advanced Training Centre, Heidelberg, Germany. *Best Student Oral Presentation.*

November 2012

VI PhD Students Meeting IMM/CAML, 29-30 November 2012, Lisbon. *Best Poster Presentation.*

COURSES AND MEETINGS

Courses:

Biostatistics, 23 February-13 April 2011, IMM, Lisbon, Portugal

Nanomedicine, 28 February-2 March 2011, IMM, Lisbon, Portugal

Launching your research career, 30 May-1 June 2012, IMM, Lisbon, Portugal

Small RNAs in Cell Biology and Human Disease, 13-14 October 2011, IMM, Lisbon, Portugal

Bioimaging nanocourse in microscopy, 5-6 December 2011 IMM, Lisbon, Portugal

Use of large data sets to study parasite biology, 25-26 June 2012, IMM, Lisbon, Portugal

Laboratory Animal Science, February-March 2013, IMM, Lisbon, Portugal

Curso Livre de Língua e Cultura Japonesa, September 2012-July 2013, Instituto Oriental, Faculdade de Ciências Sociais e Humanas, Universidade Nova de Lisboa, Lisboa, Portugal

Curso Intensivo de Francês (A1 e A2), June-July 2009, Faculdade de Letras da Universidade do Porto, Porto, Portugal

Curso de Iniciação à Medicina Legal, November 2007-March 2008, Instituto de Ciências Biomédicas Abel Salazar (ICBAS), Porto, Portugal

Curso Livre de Inglês (C1.1 and C1.2), September 2006-July 2007, Faculdade de Letras da Universidade do Porto, Porto, Portugal

Meetings:

11th Annual BioMalPar/EVIMalaR Conference, 11-13 May 2015, EMBL Advanced Training Centre, Heidelberg, Germany.

IX PhD Students Meeting IMM/CAML, 26-27 March 2015, Lisbon, Portugal.

1st Lisbon Immunology & Infection Meeting (LIIM), 26 March 2015, Instituto Gulbenkian de Ciência (IGC), Oeiras, Portugal.

VII PhD Students Meeting IMM/CAML, 5-6 December 2013, Lisbon, Portugal.

10th Annual BioMalPar/EVIMalaR Conference, 12-15 May 2014, EMBL Advanced Training Centre, Heidelberg, Germany.

VI PhD Students Meeting IMM/CAML, 29-30 November 2012, Lisbon, Portugal.

V PhD Students Meeting IMM/CAML, 17-18 October 2011, Lisbon, Portugal.

3rd Plataforma Ibérica da Malária, June 2011, Lisbon, Portugal.

PRESENTATIONS AT INTERNATIONAL MEETINGS

Oral Communication: 11th Annual BioMalPar/EVIMalaR Conference, 11-13 May 2015, EMBL Advanced Training Centre, Heidelberg, Germany. Patrícia Meireles, Rita Aroeira, António Mendes, Miguel Prudêncio. "Inhibition of *Plasmodium* liver infection by amino acid supplementation and modulation of polyamine synthesis."

Poster: 10th Annual BioMalPar/EVIMalaR Conference, 12-15 May 2014, EMBL Advanced Training Centre, Heidelberg, Germany. Patrícia Meireles, Joana Sales-Dias, Liliana Mâncio, Maria M. Mota, Miguel Prudêncio. "The role of D-glucose uptake by Glucose Transporter 1 during the liver stage of Plasmodium infection."

PRESENTATIONS AT NATIONAL MEETINGS

Poster: 1st Lisbon Immunology & Infection Meeting (LIIM), 26 March 2015, Instituto Gulbenkian de Ciência (IGC), Oeiras, Portugal. Patrícia Meireles, Rita Aroeira, António Mendes, Miguel Prudêncio. "Inhibition of *Plasmodium* liver infection by amino acid supplementation and modulation of polyamine synthesis."

Oral Communication: IX PhD Students Meeting IMM/CAML, 26-27 March 2015, Lisbon. Patrícia Meireles, Rita Aroeira, António Mendes, Miguel Prudêncio. "The role of L-arginine uptake and polyamine production during liver stage infection by the malaria parasite."

Oral Communication: VII PhD Students Meeting IMM/CAML, 5-6 December 2013, Lisbon. Patrícia Meireles, Joana Dias, Liliana Mâncio, Maria M. Mota, Miguel Prudêncio. “The role of D-glucose uptake by glucose transporter 1 during the liver stage of *Plasmodium* infection.”

Poster: VI PhD Students Meeting IMM/CAML, 29-30 November 2012, Lisbon. Patrícia Meireles, Maria M. Mota, Miguel Prudêncio. “Nutrient uptake and transport by the malaria parasite in the liver.”

Poster: V PhD Students Meeting IMM/CAML, 17-18 October 2011, Lisbon. Patrícia Meireles, Maria M. Mota, Miguel Prudêncio. “Nutrient uptake and transport by the malaria parasite in the liver.”

IAI Journals.ASM.org

Innate Immunity Induced by *Plasmodium* Liver Infection Inhibits Malaria Reinfections

Peter Liehl,[a] Patrícia Meireles,[a] Inês S. Albuquerque,[a] Mykola Pinkevych,[b] Fernanda Baptista,[a] Maria M. Mota,[a] Miles P. Davenport,[b] Miguel Prudêncio[a]

Instituto de Medicina Molecular, Faculdade de Medicina, Universidade de Lisboa, Lisbon, Portugal[a]; Centre for Vascular Research, UNSW Australia, Sydney, NSW, Australia[b]

Following transmission through a mosquito bite to the mammalian host, *Plasmodium* parasites first invade and replicate inside hepatocytes before infecting erythrocytes and causing malaria. The mechanisms limiting *Plasmodium* reinfections in humans living in regions of malaria endemicity have mainly been explored by studying the resistance induced by the blood stage of infection. However, epidemiologic studies have suggested that in high-transmission areas, preerythrocytic stages also activate host resistance to reinfection. This, along with the recent discovery that liver infections trigger a specific and effective type I interferon (IFN) response, prompted us to hypothesize that this pre-erythrocyte-stage-induced resistance is linked to liver innate immunity. Here, we combined experimental approaches and mathematical modeling to recapitulate field studies and understand the molecular basis behind such resistance. We present a newly established mouse reinfection model and demonstrate that rodent malaria liver-stage infection inhibits reinfection. This protection relies on the activation of innate immunity and involves the type I IFN response and the antimicrobial cytokine gamma IFN (IFN-γ). Importantly, mathematical simulations indicate that the predictions based on our experimental murine reinfection model fit available epidemiological data. Overall, our study revealed that liver-stage-induced innate immunity may contribute to the preerythrocytic resistance observed in humans in regions of malaria hyperendemicity.

Malaria accounts for over half a million deaths per year and is thus the most prevalent parasitic human disease worldwide (1). The disease is caused by an intracellular protozoan parasite of the genus *Plasmodium* that infects multiple hosts, such as *Anopheles* mosquitoes and humans and other mammalians (2). Infection begins with a bite of a female mosquito that injects a few *Plasmodium* sporozoites, which represent the mosquito-transmitted parasite form, into the skin of the mammalian host. After migrating through skin cells (3), sporozoites enter the bloodstream and are then rapidly and specifically retained in the liver sinusoids. Sporozoites then cross the sinusoidal barrier (4) and traverse several liver cells until individual parasites invade a final hepatocyte with the formation of a parasitophorous vacuole (5). Inside this vacuolar niche, sporozoites asymptomatically develop and replicate into thousands of erythrocyte-infective parasites, termed merozoites (6). Finally, merozoites are released into the bloodstream and rapidly infect erythrocytes, initiating the blood stage and the clinical phase of infection (7).

Malaria reinfections are common, especially in regions of high malaria transmission. *Plasmodium* parasites present an extraordinarily high rate of polymorphism; consequently, the host can be reinfected by different parasites that repeatedly escape the immune response (8). Therefore, efficient immunity to reinfection in one individual is obtained only after many years of facing recurrent infections with many different parasite strains (9, 10). Most of our knowledge of immune defense mechanisms acting against *Plasmodium* reinfection relies on studies focusing on the blood stage of infection. These studies have revealed that host resistance to blood-stage infection is complex and mediated by both the innate immune system, which limits the initial growth of all blood-stage parasites, irrespective of *Plasmodium* species or strain, and adaptive immunity, which is genotype specific (reviewed in references 9, 10, and 11). In addition, recent studies have suggested that high levels of blood-stage parasitemia protect the host from secondary or superinfection, by inhibiting liver-stage reinfection (12, 13). In mice, this increased resistance seems to be mediated by the iron-regulatory hormone hepcidin, which impairs parasite growth by restricting iron availability in the liver (12). Thus, antimalarial host responses induced during the erythrocytic stage of infection are effective against reinfection of both the blood and the liver.

Interestingly, epidemiological and mathematical modeling studies have also suggested that, in addition to these blood-stage-induced defenses, resistance mechanisms must exist which are triggered by infection stages that precede blood-stage infection (14–16). However, the immune responses raised during these initial stages of infection remain poorly explored (reviewed in references 17 and 18). Recently, we have shown that *Plasmodium* liver-stage parasites are sensed by the host and specifically activate a type I interferon (IFN) response (19). This response controls par-

Received 16 October 2014 **Returned for modification** 24 November 2014
Accepted 2 January 2015

Accepted manuscript posted online 12 January 2015

Citation Liehl P, Meireles P, Albuquerque IS, Pinkevych M, Baptista F, Mota MM, Davenport MP, Prudêncio M. 2015. Innate immunity induced by *Plasmodium* liver infection inhibits malaria reinfections. Infect Immun 83:1172–1180. doi:10.1128/IAI.02796-14.

Editor: J. H. Adams

Address correspondence to Peter Liehl, pliehl@medicina.ulisboa.pt, or Miguel Prudêncio, mprudencio@medicina.ulisboa.pt.

P.L. and P.M. contributed equally to this article.

Supplemental material for this article may be found at http://dx.doi.org/10.1128/IAI.02796-14.

doi:10.1128/IAI.02796-14

The authors have paid a fee to allow immediate free access to this article.

asite load during this first obligatory step of infection and mediates host resistance when experimentally induced prior to infection (19). In regions of hyperendemicity, the entomological inoculation rate (EIR), which indicates the number of infective mosquito bites within a given time interval (20), can reach several hundred infective bites per person per year (21–24). Since liver-stage infection lasts 7 to 13 days in humans (25, 26), a person living in these regions of hyperendemicity is likely to be reinfected while parasites from a previous infection are still in the liver. On the basis of our recent results, we speculated that this reinfection is less efficient than the primary infection as it occurs in the context of a type I IFN response triggered by the first infection and that this effect could participate in the resistance mechanism observed in epidemiological studies.

To test this hypothesis, we have established a mouse reinfection model. We show that innate immunity induced by a primary *Plasmodium berghei* liver-stage infection contributes significantly to host resistance to reinfection, not only after intravenous injections of high sporozoite doses but, crucially, also following mosquito bite infections. Our data indicate that the mechanisms of inhibition of a secondary infection depend on the activation of type I IFN signaling and gamma IFN (IFN-γ) expression. Last, we utilized a mathematical modeling approach to understand whether the resistance observed in the murine model might explain epidemiological observations of the rates of *P. falciparum* infection. We showed that the host resistance observed in our murine model is consistent with the observed changes in infection rates seen in epidemiological studies of human infection with *P. falciparum*.

MATERIALS AND METHODS

Supplemental experimental information is available in the supplemental material.

Ethics statement. All *in vivo* protocols were approved by the internal animal care committee of the Instituto de Medicina Molecular (IMM) and performed according to national and European regulations (project license AEC_2010_034_MP_Rdt_General).

Mice. Mice were housed in the facilities of the IMM. C57BL/6J wild-type (WT) mice were purchased from Charles River Breeding Laboratories. *Ifnar1*$^{-/-}$ mice were bred in specific-pathogen-free facilities at the Instituto Gulbenkian de Ciência. *Ifn*-γ$^{-/-}$ mice were purchased from The Jackson Laboratories (27). Mice used in this work were in the C57BL/6J background and had been backcrossed at least 10 times.

Parasite strains, liver infection, and blood parasitemia. Green fluorescent protein (GFP)-expressing *P. berghei* ANKA (28) sporozoites were obtained by dissection of *Anopheles stephensi*-infected mosquitoes bred at the IMM. Mice were injected intravenously with 50,000 sporozoites. Mosquito bite infection was performed with 10 mosquitoes per mouse. Parasite liver load was quantified by quantitative real-time PCR (qRT-PCR) in extracts of total livers. The presence of erythrocyte-stage parasites was monitored by flow cytometry. Measurements were performed on a Fortessa (BD Biosciences) flow cytometer. A drop of blood in 1× phosphate-buffered saline (PBS) was used to measure the blood parasitemia of GFP-expressing parasites. Flow cytometry data were analyzed using FlowJo software (version 9.0.2, Tree Star Inc., OR, USA).

RNA isolation of total livers and qRT-PCR quantification. For mouse liver RNA extraction, whole livers were homogenized in 3 ml denaturing solution (4 M guanidine thiocyanate, 25 mM sodium citrate [pH 7], 0.5% *N*-lauroylsarcosine, 0.7% mercaptoethanol, diethyl pyrocarbonate [DEPC]-treated water). RNA was extracted using an RNeasy minikit (Qiagen). cDNA was synthesized using a Transcriptor first-strand cDNA synthesis kit (Roche). Gene expression analysis was performed using Bio-Rad kits. For analysis, the expression levels of all target genes were normalized against the hypoxanthine guanine phosphoribosyltransferase (*Hprt*) housekeeping gene using the delta threshold cycle (ΔC_T) method. Changes in gene expression values were calculated using the Pfaffl method (29). We used the following oligonucleotide primer pairs to detect target gene transcripts: *Hprt*-F (CATTATGCCGAGGATTTGGA) and *Hprt*-R (AATCCAGCAGGTCAGCAAAG), *Ifit1*-F (CCTTTACAGCAACCATGGGAGA) and *Ifit1*-R (GCAGCTTCCATGTGAAGTGAC), *Ifi44*-F (TCGATTCCATGAAACCAATCAC) and *Ifi44*-R (CAAATGCAGAATGCCATGTTTT), *Usp18*-F (CGTGCTTGAGAGGGTCATTTG) and *Usp18*-R (GGTCGGGAGTCCACAACTTC), *Ifit3*-F (CTGAACTGCTCAGCCCACAC) and *Ifit3*-R (TGGACATACTTCCTTCCCTGA), *Irf7*-F (CTTCAGCACTTTCTTCCGAGA) and *Irf7*-R (TGTAGTGTGGTGACCCTTGC), *Ifn*-γ-F (CACACTGCATCTTGGCTTTG) and *Ifn*-γ-R (TCTGGCTCTGCAGGATTTTC), and *P. berghei* 18S rRNA-F (AAGCATTAAATAAAGCGAATACATCCTTAC) and *P. berghei* 18S rRNA-R (GGAGATTGGTTTTGACGTTTATGTG).

Statistical analyses. Data are expressed as means ± standard errors of the means (SEM). Statistically significant differences between two different groups were analyzed using the Mann-Whitney test. Statistical tests involving three groups or more were analyzed using the nonparametric Kruskal-Wallis test with posterior Dunn's multiple comparison tests. Results with a P value of <0.05 were considered statistically significant. Significances are represented in the figures as follows: *, $P < 0.05$; **, $P < 0.01$; ***, $P < 0.001$. All statistic tests were performed using Graph Prism 5.0 software.

Mathematical simulations. (i) Estimating the maximum "blocking" of the liver stage. In order to estimate the extent to which prior liver-stage infection is able to block subsequent liver stages, we analyzed the data from our murine experiments. There are two ways to estimate the level of blocking. First, we might consider simply the reduction in liver infection load in the second infection (Fig. 1B and C). However, this may underestimate the reduction in subsequent blood-stage infection because, although liver cells may contain *Plasmodium* DNA, this may not result in fully infectious merozoites. Therefore, the most direct way to estimate the reduction in release of infectious merozoites from the liver is to estimate the delay in infection dynamics in a second infection compared to a first infection (Fig. 2B). In order to estimate the initial number of infectious merozoites that were released from liver, we fitted the logistic growth function to the mean level of parasitemia observed in the experimental data. This function is a good approximation of the growth of the concentration of parasites over time (threshold cycle [C_T]) in blood until the concentration reaches a maximal value:

$$C(t) = \frac{MPe^{rt}}{M + P(e^{rt} - 1)} \quad (1)$$

where P is the initial concentration of parasites in blood, M is the asymptotic maximum of the concentration of parasites in blood, and r is the initial growth rate of parasites. We used GraphPad Prism 6.04 (GraphPad Software Inc. La Jolla, CA), to fit function 1 to the mean of experimental data. We assumed that the only parameter that is different in groups with single and repeated infections is the initial concentration of parasites (P); let us call the concentrations P_1 and P_2, respectively. Parameters M and r are shared between groups. The graphs of the best-fit function (equation 1) to the data are shown in Fig. S2A in the supplemental material, and the best-fit parameters are as follows: $P_1 = 2.28\% \times 10^{-5}$ infected red blood cells (RBC), $P_2 = 9.1\% \times 10^{-7}$ infected RBC, $M = 3.296\%$ infected RBC, and $r = 2.345$ parasites per day. Comparing P_1 and P_2, we find the concentration of merozoites released from the liver after reinfection is approximately 25-fold less than after the single infection.

(ii) Deterministic model of the impact of the innate liver-stage immunity on the force of infection. We developed a mathematical model in order to investigate whether the effects of innate immunity blocking subsequent liver-stage infections could contribute to the relationship between the entomological inoculation rate (EIR) and the force of infection (FOI) that was observed in field studies. In the absence of induced resistance, we would expect that the proportion of infected bites reaching the

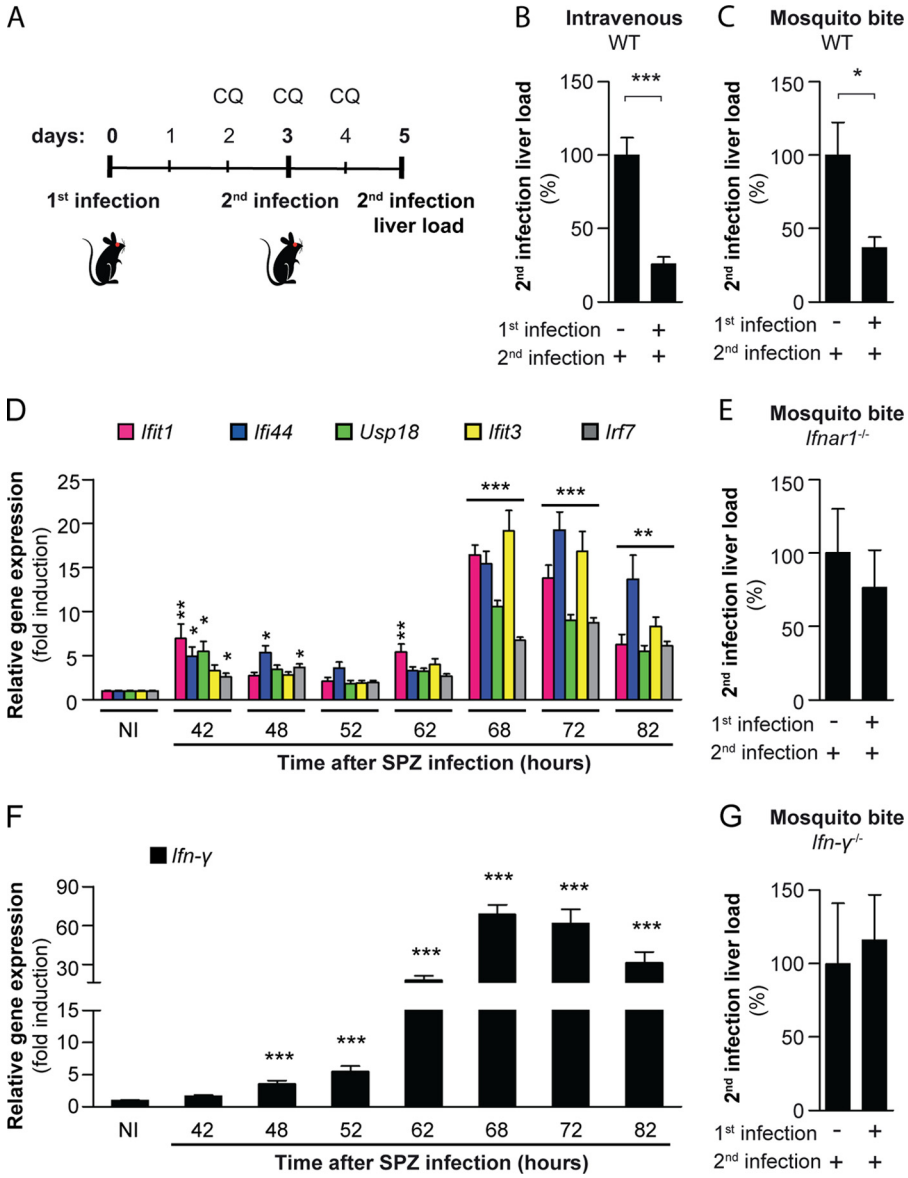

FIG 1 Role of type I IFN and IFN-γ in a *P. berghei* liver-stage reinfection model. (A) Schematic representation of the reinfection protocol. Mice were injected intravenously (i.v.) with 50,000 *P. berghei* sporozoites or an equivalent amount of noninfected (NI) salivary glands on day 0. Both groups of animals were treated with 700 μg of chloroquine (CQ) on days 2, 3, and 4 after injection. On day 3, mice were reinfected by the i.v. injection of 50,000 *P. berghei* sporozoites. Alternatively, mice were subjected to bites of infected *Anopheles* mosquitoes or an equivalent number of noninfected mosquitoes, treated with CQ on days 2, 3, and 4 after inoculation, and infected or reinfected on day 3 by mosquito bite. The amount of parasite 18S ribosomal small-subunit transcripts (18S rRNA), corresponding to the parasite liver load of the second infection, was measured by qRT-PCR 44 h after reinfection. (B) Parasite liver loads in reinfected WT mice, measured by qRT-PCR of *P. berghei* 18S rRNA 44 h after the second infection with *P. berghei* sporozoites and plotted as the percentages of the *P. berghei* 18S rRNA levels in control WT mice. The results shown represent the means and SEM of the results of two independent experiments (single infection, $n = 14$; reinfection, $n = 14$). The Mann-Whitney test demonstrated a statistically significant difference between control and reinfected mice ($P < 0.001$). (C) Parasite liver loads in reinfected WT mice, measured by qRT-PCR of *P. berghei* 18S rRNA, 44 h after two consecutive mosquito bite infections (10 mosquitoes/mouse) plotted as percentages of the levels in control WT mice. The results shown represent the means and SEM of the results of three independent experiments (single infection, $n = 16$; reinfection, $n = 18$). The Mann-Whitney test demonstrated a statistically significant difference between control and reinfected mice ($P < 0.05$). (D) Expression of genes *Ifit1*, *Ifi44*, *Usp18*, *Ifit3*, and *Irf7* in total liver extracts of WT mice collected at multiple time points after infection with 50,000 *P. berghei* sporozoites (SPZ). For each time point, the values shown are the means and SEM of the results of two independent experiments (NI, $n = 10$; 42 h, $n = 8$; 48 h, $n = 8$; 52 h, $n = 16$; 62 h, $n = 11$; 68 h, $n = 10$; 72 h, $n = 10$; 82 h, $n = 10$). The Kruskal-Wallis test followed by Dunn's multiple-comparison test revealed statistically significant differences between uninfected control samples and liver samples 42 h, 68 h, 72 h, and 82 h after infection ($P < 0.05$). (E) Parasite liver loads in reinfected *Ifnar1*$^{-/-}$ mice, measured by qRT-PCR of *P. berghei* 18S rRNA, 44 h after two consecutive mosquito bite infections (10 mosquitoes/mouse) plotted as percentages of the levels in control *Ifnar1*$^{-/-}$ mice. The results shown represent the means and SEM of the results of two independent experiments (single infection, $n = 14$; reinfection, $n = 13$). The Mann-Whitney test demonstrated no statistically significant difference between control and reinfected *Ifnar1*$^{-/-}$ mice. (F) *Ifn*-γ gene expression in whole livers of WT mice collected at multiple time points after infection with 50,000 *P. berghei* sporozoites. For each time point, the values represented are the means and SEM of the results of four (42 h, 48 h, and 52 h) and two (62 h, 72 h, and 82 h) independent experiments (NI, $n = 38$; 42 h, $n = 20$; 48 h, $n = 37$; 52 h, $n = 20$; 62 h, $n = 10$; 68 h, $n = 10$; 72 h, $n = 10$; 82 h, $n = 10$). The Kruskal-Wallis test followed by Dunn's multiple-comparison test revealed statistically significant differences between uninfected control samples and liver samples 48 h, 52 h, 62 h, 72 h, and 82 h after infection ($P < 0.001$). (G) Parasite liver loads in reinfected *Ifn*-γ$^{-/-}$ mice, measured by qRT-PCR of *P. berghei* 18S rRNA, 44 h after two consecutive mosquito bite infections (10 mosquitoes/mouse), plotted as percentages of the levels in control *Ifn*-γ$^{-/-}$ mice. The results shown represent the means and SEM of the results of two independent experiments (single infection, $n = 8$; reinfection, $n = 8$). The Mann-Whitney test demonstrated no statistically significant difference between control and reinfected *Ifn*-γ$^{-/-}$ mice.

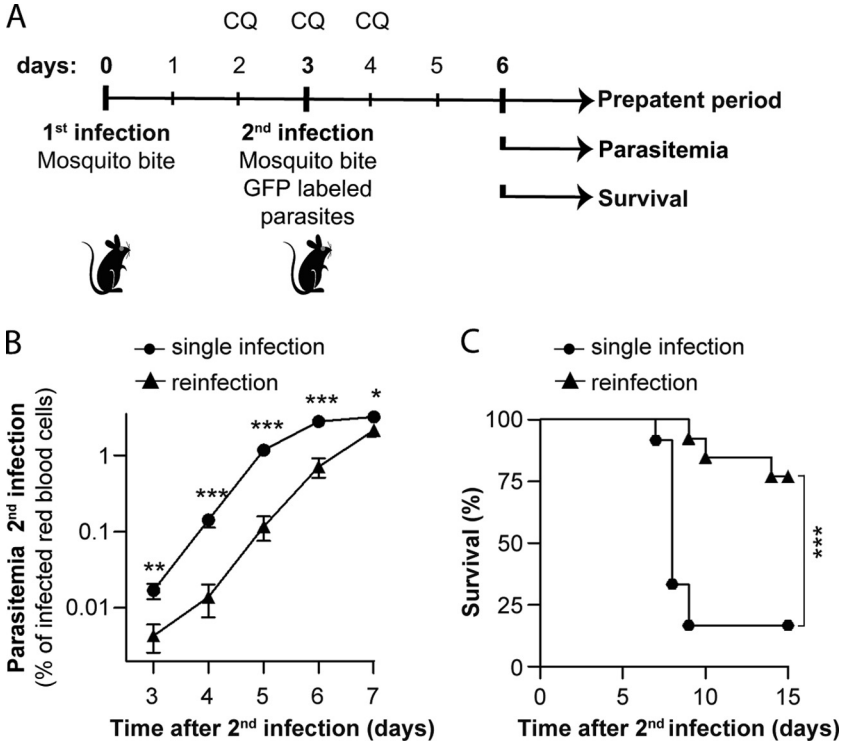

FIG 2 Effect of a primary *P. berghei* liver infection on the blood stage of a subsequent sporozoite-initiated reinfection. (A) Schematic representation of the reinfection protocol. Mice were injected with 50,000 *P. berghei* sporozoites or noninfected salivary glands on day 0. Both groups of animals were treated with 700 μg of chloroquine (CQ) on days 2, 3, and 4 after injection. On day 3, mice were reinfected with 50,000 *P. berghei* GFP-expressing sporozoites. Parasitemia (percentage of red blood cells infected with GFP-expressing parasites) was measured by flow cytometry starting at day 3 after the second infection. Survival was monitored daily. (B and C) Parasitemia and survival in reinfected WT mice after mosquito bite infection (10 mosquitoes/mouse). The results shown represent the means and SEM of the results of two independent experiments (single infection, $n = 11$; reinfection, $n = 12$). The Mann-Whitney test demonstrated a statistically significant difference in parasitemia levels between control and reinfected mice ($P < 0.01$). The log-rank test demonstrated a statistically significant difference in survival rates between control and reinfected mice ($P < 0.001$).

liver would be constant at different biting rates and that the slope of this would be determined by the baseline success rate of an infected bite reaching the blood stage (r). In this case, the relation between EIR and FOI would be a straight line:

$$y = rx \tag{2}$$

where x represents EIR and y represents FOI.

In the case of induced immunity that blocks infections from subsequent bites, we can also find the expected relationship between EIR and FOI. For a given EIR, the waiting times between infected bites have an exponential distribution. If we again assume a baseline success of an infection from a bite reaching the blood stage of r, then the waiting time between instances of "successful" liver-stage infection is rx. Therefore, the cumulative distribution function (CDF) of an exponential distribution with parameter rx at point T gives us the probability that next bite would occur during the period T from a previous infection—and would be blocked by the innate immune response. Thus, the relation between EIR and FOI can be expressed by the following formula:

$$y = rx[1 - p\,\mathrm{CDF}_{\mathrm{exp}}(rx,\ T)] \tag{3}$$

where p is the probability that a liver-stage infection will be blocked by the innate immune response induced by a previous bite, given that it occurred during the period T of the active immunity response. We then fitted model 2 and model 3 to the experimental data and compared the fits using the Akaike information criterion (AIC).

(iii) Stochastic model of the impact of the innate liver-stage immunity on the force of infection. We also developed a stochastic model that is able to take into account a more complex infection kinetics than the deterministic model, such as multiple consecutive bites and gradual acquisition and loss of immunity. This allows us to investigate whether the effects of innate immunity blocking subsequent liver-stage infections would produce the same relationship between entomological inoculation rate (EIR) and force of infection (FOI) as that predicted by the deterministic model and observed in field studies (30–33). This model simulated biting at different rates and the proportion of infectious bites that successfully initiated blood-stage infections.

(iv) Modeling infection. The simulation takes into account 3 possible types of infection: (i) infections that survive the liver stage and pass on to the blood stage, which induce strong innate liver stage resistance to subsequent liver-stage infections (with the maximal level of $R_s = 1$); (ii) infections that are cleared at the liver stage by the innate liver-stage immunity induced by previous infections—we assume that they would induce a lower level of resistance than completed liver-stage infections (at a level of R_p, which we assume to be 25% of the maximal inhibition [i.e., $R_p = 0.25 \times R_s$]); and (iii) bite infections that do not reach the liver stage. We assume that there is a baseline probability (R_b) that infectious bites would fail to result in liver-stage infection. They do not induce liver-stage immunity. According to model 2, R_b is equal to 0.93 (rate of progression to blood-stage infection $r = 0.07$).

(v) Simulation of biting rates. The model assumes that for a given EIR, infective bites arrive randomly with exponentially distributed waiting times (13, 34, 35). Each bite infection then has a probability of reaching the blood stage, which is determined by the baseline probability of success (R_b) and the level of induced resistance at a given time [$R(t)$]. After a successful bite infection, the level of induced resistance rises to its max-

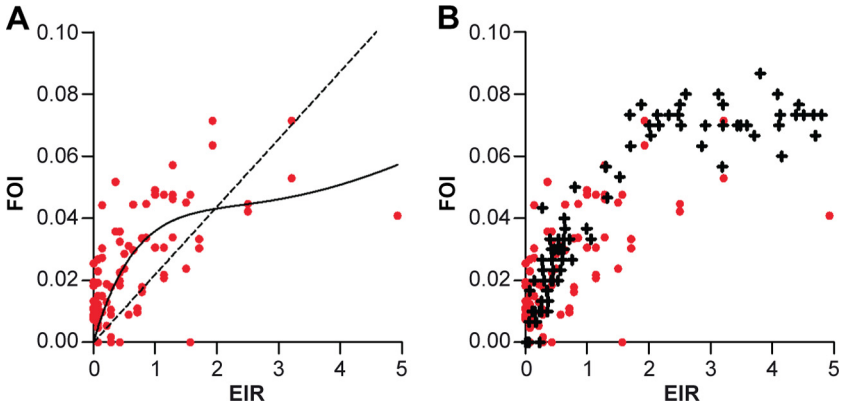

FIG 3 Linking murine reinfection data to epidemiological observations. (A) Deterministic modeling of the experimental relationship between the EIR (entomological inoculation rate; average number of infectious bites per person per unit time) and the FOI (force of infection; number of infections per person per unit of time). Using published data on EIR and FOI from a field study in western Kenya (extracted from Table 2 of reference 30; red dots), we fitted either a baseline model (fixed proportion of infectious bites progressing to blood stage) (dashed line) or a model with induced liver-stage immunity (solid line). The model of induced liver-stage immunity showed a better fit to the experimental data compared by AIC. The best-fit parameters for the models are as follows: for model 2, $r = 0.022$; for model 3, $r = 0.069$, $p = 0.85$, $t = 12.2$ days. (B) Results of the stochastic simulation of the relation between EIR and FOI in the presence of induced resistance. Red dots represent the field study data (extracted from Table 2 of reference 30); crosses represent the estimates from the simulation.

imum and then falls over time (see formula 4 below). Thus, for each simulated bite, a uniformly distributed random number α is assigned to it. The value of this number and the current level of induced resistance determine which of categories 1 to 3 this infection belongs to as follows. (i) If $R(t)$ plus R_b is $<\alpha$, where $R(t)$ is the current level of the liver stage resistance, then the infection is considered of type 1 and induces subsequent resistance to infection. (ii) If R_b is less than α and α is less than $R(t)$ plus R_b, where $R(t)$ is the current level of liver stage resistance, then the infection is considered of type 2. (iii) If α is less than R_b, then the infection does not reach the liver stage and the infection is considered of type 3 and does not contribute to the innate liver-stage immunity.

(vi) Modeling changes in induced resistance. The dynamics of induced resistance to liver-stage infection in humans is unknown. However, we can estimate the likely duration of resistance using the data from the studies in *P. berghei* and scaling for the longer duration of the intrahepatic stage of infection in *P. falciparum*. We assume that resistance in *P. falciparum* infection has a duration of 12 days and is induced over time during liver-stage infection (peaking at d_1 days after the initial infection; we assume $d_1 = 6$ days) and then decays over some period (for d_2 days after the peak; we assume $d_2 = 6$ days). We chose the logistic growth function to describe the growth and decay of liver stage resistance over time. For this function, we need an initial level of resistance immediately after initiation of the liver stage ($R_0 = 0.05$) and a peak level of resistance (M, the asymptotic maximum resistance [which will never be attained], which we assume to be slightly larger than the maximum resistance $M = R_{\max}/0.98$). The function that describes both the growth and decay is defined by formula 4.

$$f(t) = \begin{cases} \dfrac{MR_0e^{r_1(t-t_0)}}{M + R_0(e^{r_1(t-t_0)} - 1)}, & t_0 \le t < t_0 + d_1, \\ \dfrac{MR_{\max}e^{-r_2(t-t_0-d_1)}}{M + R_{\max}(e^{-r_2(t-t_0-d_1)} - 1)}, & t_0 + d_1 \le t < t_0 + d_1 + d_2, \\ 0, & t \ge t_0 + d_1 + d_2 \end{cases} \quad (4)$$

where $r_i = \ln[(R_0R_{\max}) + MR_{\max})/R_0(M - R_{\max})]/d_i$, $i = 1, 2$, and $R_{\max}$ is the maximal level of induced liver-stage immunity, which can take a value of R_s or R_p, depending on conditions i to iii as described above. Fig. S2B in the supplemental material shows the trajectory of resistance over time after a successful bite.

The total level of induced resistance $R(t)$ induced by all previous infections is calculated using formula 5.

$$R(t) = \mathrm{Min}\left[\sum_{i=1}^{n} f_i(t),\ R_{\max}\right] \quad (5)$$

where function $f_i(t)$ is the immunity induced by the i-th infection ($i = 1, \ldots, n$).

Using this stochastic model, we can then simulate different biting rates and analyze the observed FOI that we obtain in the simulation. We compared the relationship of EIR to FOI predicted by the simulations with that observed in a published field study presented in Table 2 in a study by Beier et al. (30). We ran simulations with EIR values ranging from 0.01 to 5 infective bites/day and observed the rate of infection expected. The stochastic simulation showed the same relationship between EIR and FOI as in model 3, namely, as the EIR increases, infections from an increasing proportion of bites are blocked by induced resistance, and we see a decreasing proportion of infections from bites making it to the blood. This is shown in Fig. 3B. A sample of the simulation calculated with an EIR of 1 is shown in Fig. S2C in the supplemental material.

RESULTS

Induction of type I IFN and IFN-γ by a first *P. berghei* liver infection protects against reinfection. To test the hypothesis that a primary *Plasmodium* liver infection induces protection from reinfection, we set up an assay in which mice were first injected with *P. berghei* parasites or, for control animals, with an equivalent amount of salivary gland material from noninfected mosquitoes. Three days later, mice were reinfected and the liver parasite burden 42 h after the rechallenge was monitored by quantitative real-time PCR, targeting the parasite 18S ribosomal small-subunit transcripts (Fig. 1A). Since a primary liver-stage infection lasts 2 to 3 days in our rodent model (see Fig. S1 in the supplemental material), we were able to attribute the measured liver parasite burden to the second infection. To minimize the influence of blood-stage-induced immune responses, mice were treated with chloroquine from day 2 to day 5 after the primary infection, effectively killing developing erythrocyte-stage parasites without affecting the liver stages (36–38) (Fig. 1A). This was also confirmed by the absence of blood-stage parasitemia on day 2 after the second sporozoite infection, when any blood-stage parasites would likely have resulted from the first infection (observation of Giemsa-stained blood smears; data not shown). When mice were

infected by intravenous injection of 50,000 sporozoites, we found that primed mice were significantly more resistant to a second challenge with 50,000 sporozoites than control animals (Fig. 1B). Thus, our data indicate that, within 3 days, a primary exposure to a high number of sporozoites activates a significant host resistance to a malaria liver-stage reinfection. We next carried out a similar experiment in which mice were infected by mosquito bites. A significant 2-fold decrease of liver parasite load in reinfected mice was also observed when infections were performed via this natural route (Fig. 1C). Overall, our data show that, 3 days after an initial liver-stage infection, the host benefits from increased defenses against *Plasmodium* sporozoite reinfection. Notably, this protection is observed not only after a primary infection by intravenous injection with (nonphysiologically) high numbers of sporozoites but also when sporozoites are delivered by mosquito bites.

We next sought to understand the molecular mechanisms underlying this phenomenon. Recently, we have shown that a primary liver-stage infection induces a hepatic type I IFN signature (19). The recognition mechanism relies on the detection of *Plasmodium* RNA by the cytosolic RNA sensor MDA5 and likely other as-yet-unidentified receptors. The signaling cascade involves the mitochondrial antiviral signaling protein (MAVS) adapter molecule and transcription factors interferon regulatory factor 3 (IRF3) and IRF7. Our data further suggested a model in which released type I IFN binds, in both an autocrine manner and a paracrine manner, to the heterodimeric alpha interferon receptor (IFNAR, composed of IFNAR1 and IFNAR2), activating transcription of IFN-inducible genes, with a peak of expression at 42 h after infection (19, 39). Here we have extended our analysis of the liver type I IFN response to later time points. We challenged mice with 50,000 *P. berghei* sporozoites and treated them with chloroquine on the second, third, and fourth days after infection. We first confirmed a significant expression of several type I IFN-inducible genes (*Ifit1*, *Ifi44*, *Usp18*, *Ifit3*, and *Irf7*) at 42 h after infection, followed by a progressive decline of the response (Fig. 1D). Strikingly, we found another significant and strong induction at 68 and 72 h after infection, which suggests that the liver reinitiates *de novo* type I IFN signaling at those later time points (Fig. 1D). To analyze the *in vivo* contribution of type I IFN-dependent signaling to host resistance to sporozoite reinfection, we monitored the liver parasite load in reinfected IFNAR1-deficient (*Ifnar1*$^{-/-}$) mice following infections by mosquito bites. In contrast to wild-type (WT) mice, preinfected *Ifnar1*$^{-/-}$ mice did not display a decreased liver parasite load after a secondary challenge by *P. berghei* sporozoites (Fig. 1E). This result demonstrates that the type I IFN response in the liver is physiologically relevant in host defense against sporozoite reinfection in mice.

Next, we sought to approach the effector mechanisms that are involved in the observed phenotype downstream of the type I IFN response. Previously, we have provided evidence that the hepatocyte-mediated type I IFN response *per se* is not able to eliminate the parasite during a primary infection. However, this response is critical for the recruitment of immune cells to the infected hepatocyte, which leads to *Plasmodium* elimination (19). As IFN-γ has been identified as a cytokine that is able to mediate the killing of intrahepatic *Plasmodium* parasites (40–42), we hypothesized that the mechanism of parasite elimination in the liver after reinfection is IFN-γ dependent. We monitored transcript expression of the gene encoding this cytokine in whole-liver extracts at different time points after infection, using the previously established infection protocol and chloroquine treatment. *Ifn*-γ expression started to be induced by 48 h after *P. berghei* liver infection, followed by a slow but steady increase in transcript levels until 52 h postchallenge. Interestingly, and similarly to the observation of the type I IFN response, we observed a peak of *Ifn*-γ gene induction at 68 h after infection (Fig. 1F). To assess the functional role of IFN-γ in innate immunity to *Plasmodium* reinfection, IFN-γ-deficient (*Ifn*-γ$^{-/-}$) mice were reinfected by mosquito bites after a primary mosquito bite infection. We found that, in contrast to WT animals but similarly to *Ifnar1*$^{-/-}$ mice, *Ifn*-γ$^{-/-}$ mutants lost their protection against sporozoite reinfection (Fig. 1G). Taken together, our data suggest that liver-stage infection by *P. berghei* first stimulates type I IFN pathway activation and later stimulates IFN-γ expression, both of which play a critical role in host defense against reinfection.

A primary liver infection affects the blood stage of a sporozoite reinfection. In contrast to the liver stage, which is asymptomatic, the blood stage of infection is responsible for all the symptoms associated with malaria. Thus, we next investigated whether *P. berghei*-induced host protection also impacts the development of the subsequent blood-stage infection and the associated pathogenesis. We performed both primary and secondary infections by mosquito bites, following the same protocol as previously described, and used *P. berghei* parasites expressing green fluorescence protein (GFP) for reinfection (Fig. 2A). First, we measured the length of the prepatent period, i.e., the time between sporozoite injection and the appearance of blood-stage parasites, by observing Giemsa-stained blood smears under a light-field microscope. Strikingly, we observed that 50% of the reinfected mice demonstrated a 1-day delay in the appearance of blood-stage parasites from the secondary infection compared to primary-infected controls (data not shown). As the prepatent period is a good indicator of the number of infective merozoites produced in the liver (43), this result suggests that fewer merozoites are released from reinfected mice than from control mice. Next, we measured the percentage of GFP-expressing infected red blood cells (blood-stage parasitemia of the second infection) by flow cytometry. Our results indicate that growth of blood-stage parasites from a secondary infection in primed mice was significantly delayed compared to that seen in nonprimed, control animals (Fig. 2B). Moreover, reinfected mice presented a delay in malaria-associated mortality compared to control animals (Fig. 2C). These data indicate that the host resistance activated by a primary sporozoite liver infection is physiologically relevant as it not only inhibits liver infection but also delays blood-stage patency, resulting in a decrease in the associated mortality.

Mathematical modeling of murine reinfection correlates with epidemiological data. Several studies carried out in low-, medium-, and high-transmission areas have measured the time required for *Plasmodium* parasites to reappear in the blood of individuals after parasitemia has been cleared with blood-stage-specific antimalarial compounds (14, 15, 21, 30, 44–47). Interestingly, these and other modeling studies have revealed a discrepancy between the estimated number of infective bites per human per time unit (i.e., the EIR) and the resulting force of infection (FOI; i.e., the rate of new blood-stage infections) (16, 33). These data indicate that, first, even at a low EIR, not all infective bites translate into subsequent infections, and second, as the transmission rate increases (i.e., when EIR increases), the proportion of infective bites that result in blood-stage infection progressively

decreases (33). Thus, the observed FOI is lower than what would be expected if it remained proportional to the rate of infective bites. These data suggest that a high proportion of sporozoite reinfections are blocked under high-transmission conditions and that the preerythrocytic stage and/or early blood stage of infection may activate effective host defenses. Therefore, we decided to test whether our experimental data could explain the increased preerythrocytic resistance with increasing FOI observed in humans (33).

We created two models linking FOI to EIR, one with a constant proportion of infections from bites reaching the blood stage and another in which infections from bites could be blocked by innate liver-stage immunity. The reduction in the infection that would be induced by a prior liver-stage infection was estimated based on the analysis of the reduction in the numbers of blood-stage parasites observed after primary and secondary murine infections (for more details, see Materials and Methods; also see Fig. S2A in the supplemental material). In order to determine which model better explains the field study data, we compared the results of the fitting of the two models to experimental data on *P. falciparum* EIR and FOI from a field trial in western Kenya published in reference 30. The results of fitting are shown in Fig. 3A. Using the Akaike information criterion (AIC) to compare the two models, we found that the model taking into account induced liver-stage immunity provided a significantly better fit to the field data (the AICs for constant-proportion model 2 and for innate-immunity model 3 are −660 and −700, respectively).

This deterministic model assumed a constant level of blocking of new infections for a fixed period after the first infection. However, it is likely that innate immunity is induced and subsequently decays over time. To take these dynamics into consideration, we developed a stochastic model of malaria infection that takes into account more-complex factors such as multiple consecutive bites and gradual acquisition and loss of immunity. Our model is based on four assumptions: (i) infective bites arrive randomly at a given biting rate (13, 34, 35); (ii) only a proportion of bites result in infection (e.g., in a number of cases, mosquito injection of sporozoites is unsuccessful or sporozoites remain in the skin); (iii) a successful liver-stage infection (i.e., an infection that progresses to the blood stage) induces strong host resistance and thus inhibits the establishment of a subsequent liver-stage infection; and (iv) a liver-stage infection that is blocked by innate immunity and does not progress to a blood-stage infection nonetheless induces a small amount of resistance to subsequent infections.

To parameterize the model, we estimated the baseline proportion of infectious bites that result in blood-stage infection (baseline FOI/EIR ratio) at 7%, based on the best-fit parameters of deterministic model 2. Finally, we estimated how the reduction in infectivity (or increase in host resistance) changes over time after infection. Fig. S2B in the supplemental material illustrates how the probability of success of a reinfection changes with time after a preceding successful infective bite, based on our assumptions. Full details of the parameters and mathematical formalism of the model are provided in Materials and Methods.

Based on this model, we were able to simulate different rates of infectious biting (the EIR) and observed the expected number of blood-stage infections arising from this (the FOI). We then overlaid our simulated data onto the EIR and FOI relationship observed in field studies. We found that the stochastic simulation predicts that, similarly to the deterministic model of the inhibitory effect of prior liver-stage infection, the number of infections per bite does not remain proportional to EIR but instead reduces with increasing biting rates, as was observed in regions of hyperendemicity (Fig. 3B). Overall, our combined modeling and experimental data suggest for the first time that inhibition of reinfection in high-transmission areas can be at least partly explained by the activation of innate immunity in the liver.

DISCUSSION

We have established a mouse reinfection model and shown that the innate immunity induced by a primary *P. berghei* liver-stage infection impairs a second sporozoite reinfection. Importantly, we also observed a significant inhibition of reinfection when both infections were initiated by mosquito bites, as well as a delay in blood-stage parasitemia and in malaria-associated mortality. Using an interdisciplinary approach, we incorporated our experimental data into a mathematical model and were able to show that the predictions based on our experimental results are sufficient to explain the available epidemiological data.

The issue treated in this study deals with a situation experienced daily by the populations living in areas of high malaria transmission, which face regular and repeated reinfections. Interestingly, in regions of malaria hyperendemicity, individuals in whom blood parasitemia has been cleared with blood stage-specific antimalarial compounds resist a large number of consecutive mosquito bite infections before parasites become detectable in the blood smears compared to individuals living in areas of medium or low transmission (14–16, 21, 33). Several attempts have been made to explain this phenomenon, including genetic factors and heterogeneous mosquito biting preferences that would result in a few people receiving most of the infective bites (33). However, the observed resistance could also be the consequence of human immune defenses triggered by the preerythrocyte stage and/or early blood stage of infection. As this resistance was also associated with the age of study participants, a role for acquired adaptive immunity has been suggested (18), although an explanation of how it would participate in this protection remains elusive (9, 18). Our murine reinfection model, combined with mathematical simulations, suggests for the first time that liver innate immunity induced by hepatic *Plasmodium* infection can also account for these observed protective effects. Our data show that this kind of interdisciplinary approach can improve the mechanistic understanding of the antimalarial resistance operating in humans.

Importantly, our findings seem to extend to other *Plasmodium* species, as another recent study with another rodent parasite strain, *P. yoelii*, showed that a first liver infection inhibits a second reinfection (48). In regions of malaria endemicity, the prevalence of multiple distinct genetic *Plasmodium* variants and species is the norm (49) and humans can be successively infected with several different genotypes (50, 51) or even with different parasite species (52, 53) at one time. A major problem in fighting malaria is the poor cross-reactivity of adaptive immune responses to different *Plasmodium* species (54). Dissecting the level of cross-protective effects of innate immune responses between different parasite strains and species would contribute to a better understanding of the relevance of innate immunity during liver-stage reinfections in the field and could be of medical interest as this knowledge could be exploited to improve the efficiency of currently available antimalarial therapies.

Our report provides genetic evidence of an important role for

the type I IFN response and IFN-γ in the host defense against malaria liver-stage reinfection. IFN-γ treatment is known to efficiently kill intrahepatic parasites (40–42), but we provide the first evidence of a biologically relevant IFN-γ response *in vivo* after mosquito bite-transmitted malaria infection (*P. berghei*). Our data are in accordance with the recent report of an IFN-γ response in mice injected intravenously with high numbers of *P. yoelii* sporozoites (48). As hepatocytes are not substantial producers of IFN-γ (55), we hypothesize that the type I IFN response likely recruits myeloid cells, in particular, NK and NK-T cells, which are known to secrete large amounts of IFN-γ, to the infected hepatocytes (56). Interestingly, Miller et al. have shown that NK-T cells constitute the only effector cell population that is crucial for host resistance to sporozoite reinfection (48). However, more data will be critical to gain further insight into the effector molecules mediating the IFN-γ-dependent host resistance to reinfections and to pinpoint when exactly these defense mechanisms are most effective in eliminating parasites during liver reinfection. Indeed, the decrease in parasite load we observed in comparisons of reinfected mice to nonprimed animals was of considerably higher magnitude at the early blood stage (~10-fold decrease) than at the liver stage (2- to 3-fold decrease at 44 h after infection). This suggests that the observed resistance could be linked to a more efficient elimination of parasites in their last maturation steps in the liver, i.e., when they start to egress from hepatocytes and transition to blood-stage infection. Taken together, our data strongly suggest that the liver-stage-induced type I IFN and IFN-γ response is a major host defense mechanism against sporozoite reinfection in our mouse model. A detailed characterization of the mechanisms by which the host detects and kills intrahepatic parasites will be helpful to pave the way for innovative strategies in the development of effective preerythrocyte-based vaccines and prophylactic immunotherapies.

ACKNOWLEDGMENTS

We thank A. Parreira for *Anopheles stephensi* production and infection and A. Zaidman-Rémy for critical reading of the manuscript.

This work was supported by Fundação para a Ciência e Tecnologia (FCT, Portugal) grants PTDC-SAU-MIC-117060-2010 (to Miguel Prudêncio) and EXCL/IMI-MIC/0056/2012 (to M.M.M.). P.L. was supported by Fondation pour la Recherche Médicale and FCT (fellowship SFRH/BPD/41547/2007). P.M. was supported by FCT (fellowship SFRH/BD/71098/2010). Miguel Prudêncio and M.P.D. are supported by an Australian Research Council Discovery Grant (DP120100064). M.P.D. is an NHMRC Senior Research Fellow.

REFERENCES

1. **Murray CJ, Rosenfeld LC, Lim SS, Andrews KG, Foreman KJ, Haring D, Fullman N, Naghavi M, Lozano R, Lopez AD.** 2012. Global malaria mortality between 1980 and 2010: a systematic analysis. Lancet **379:**413–431. http://dx.doi.org/10.1016/S0140-6736(12)60034-8.
2. **Prudêncio M, Rodriguez A, Mota MM.** 2006. The silent path to thousands of merozoites: the Plasmodium liver stage. Nat Rev Microbiol **4:**849–856. http://dx.doi.org/10.1038/nrmicro1529.
3. **Amino R, Giovannini D, Thiberge S, Gueirard P, Boisson B, Dubremetz JF, Prevost MC, Ishino T, Yuda M, Menard R.** 2008. Host cell traversal is important for progression of the malaria parasite through the dermis to the liver. Cell Host Microbe **3:**88–96. http://dx.doi.org/10.1016/j.chom.2007.12.007.
4. **Tavares J, Formaglio P, Thiberge S, Mordelet E, Van Rooijen N, Medvinsky A, Menard R, Amino R.** 2013. Role of host cell traversal by the malaria sporozoite during liver infection. J Exp Med **210:**905–915. http://dx.doi.org/10.1084/jem.20121130.
5. **Mota MM, Pradel G, Vanderberg JP, Hafalla JC, Frevert U, Nussenzweig RS, Nussenzweig V, Rodriguez A.** 2001. Migration of Plasmodium sporozoites through cells before infection. Science **291:**141–144. http://dx.doi.org/10.1126/science.291.5501.141.
6. **Sturm A, Amino R, van de Sand C, Regen T, Retzlaff S, Rennenberg A, Krueger A, Pollok JM, Menard R, Heussler VT.** 2006. Manipulation of host hepatocytes by the malaria parasite for delivery into liver sinusoids. Science **313:**1287–1290. http://dx.doi.org/10.1126/science.1129720.
7. **Haldar K, Murphy SC, Milner DA, Taylor TE.** 2007. Malaria: mechanisms of erythrocytic infection and pathological correlates of severe disease. Annu Rev Pathol **2:**217–249. http://dx.doi.org/10.1146/annurev.pathol.2.010506.091913.
8. **Takala SL, Plowe CV.** 2009. Genetic diversity and malaria vaccine design, testing and efficacy: preventing and overcoming 'vaccine resistant malaria'. Parasite Immunol **31:**560–573. http://dx.doi.org/10.1111/j.1365-3024.2009.01138.x.
9. **Marsh K, Kinyanjui S.** 2006. Immune effector mechanisms in malaria. Parasite Immunol **28:**51–60. http://dx.doi.org/10.1111/j.1365-3024.2006.00808.x.
10. **Langhorne J, Ndungu FM, Sponaas AM, Marsh K.** 2008. Immunity to malaria: more questions than answers. Nat Immunol **9:**725–732. http://dx.doi.org/10.1038/ni.f.205.
11. **Stevenson MM, Riley EM.** 2004. Innate immunity to malaria. Nat Rev Immunol **4:**169–180. http://dx.doi.org/10.1038/nri1311.
12. **Portugal S, Carret C, Recker M, Armitage AE, Goncalves LA, Epiphanio S, Sullivan D, Roy C, Newbold CI, Drakesmith H, Mota MM.** 2011. Host-mediated regulation of superinfection in malaria. Nat Med **17:**732–737. http://dx.doi.org/10.1038/nm.2368.
13. **Pinkevych M, Petravic J, Chelimo K, Vulule J, Kazura JW, Moormann AM, Davenport MP.** 9 September 2013, posting date. Density-dependent blood stage Plasmodium falciparum suppresses malaria super-infection in a malaria holoendemic population. Am J Trop Med Hyg http://dx.doi.org/10.4269/ajtmh.13-0049.
14. **Sokhna CS, Rogier C, Dieye A, Trape JF.** 2000. Host factors affecting the delay of reappearance of Plasmodium falciparum after radical treatment among a semi-immune population exposed to intense perennial transmission. Am J Trop Med Hyg **62:**266–270.
15. **Tall A, Sokhna C, Perraut R, Fontenille D, Marrama L, Ly AB, Sarr FD, Toure A, Trape JF, Spiegel A, Rogier C, Druilhe P.** 2009. Assessment of the relative success of sporozoite inoculations in individuals exposed to moderate seasonal transmission. Malar J **8:**161. http://dx.doi.org/10.1186/1475-2875-8-161.
16. **Smith T, Maire N, Dietz K, Killeen GF, Vounatsou P, Molineaux L, Tanner M.** 2006. Relationship between the entomologic inoculation rate and the force of infection for Plasmodium falciparum malaria. Am J Trop Med Hyg **75**(2 Suppl)**:**11–18.
17. **Liehl P, Mota MM.** 2012. Innate recognition of malarial parasites by mammalian hosts. Int J Parasitol **42:**557–566. http://dx.doi.org/10.1016/j.ijpara.2012.04.006.
18. **Offeddu V, Thathy V, Marsh K, Matuschewski K.** 2012. Naturally acquired immune responses against Plasmodium falciparum sporozoites and liver infection. Int J Parasitol **42:**535–548. http://dx.doi.org/10.1016/j.ijpara.2012.03.011.
19. **Liehl P, Zuzarte-Luis V, Chan J, Zillinger T, Baptista F, Carapau D, Konert M, Hanson KK, Carret C, Lassnig C, Muller M, Kalinke U, Saeed M, Chora AF, Golenbock DT, Strobl B, Prudencio M, Coelho LP, Kappe SH, Superti-Furga G, Pichlmair A, Vigario AM, Rice CM, Fitzgerald KA, Barchet W, Mota MM.** 2014. Host-cell sensors for Plasmodium activate innate immunity against liver-stage infection. Nat Med **20:**47–53. http://dx.doi.org/10.1038/nm.3424.
20. **Macdonald G.** 1956. Epidemiological basis of malaria control. Bull World Health Organ **15:**613–626.
21. **Charlwood JD, Smith T, Lyimo E, Kitua AY, Masanja H, Booth M, Alonso PL, Tanner M.** 1998. Incidence of Plasmodium falciparum infection in infants in relation to exposure to sporozoite-infected anophelines. Am J Trop Med Hyg **59:**243–251.
22. **Beier JC, Killeen GF, Githure JI.** 1999. Short report: entomologic inoculation rates and Plasmodium falciparum malaria prevalence in Africa. Am J Trop Med Hyg **61:**109–113.
23. **Rogier C, Tall A, Diagne N, Fontenille D, Spiegel A, Trape JF.** 1999. Plasmodium falciparum clinical malaria: lessons from longitudinal studies in Senegal. Parassitologia **41:**255–259.
24. **Bloland PB, Boriga DA, Ruebush TK, McCormick JB, Roberts JM, Oloo AJ, Hawley W, Lal A, Nahlen B, Campbell CC.** 1999. Longitudinal

cohort study of the epidemiology of malaria infections in an area of intense malaria transmission II. Descriptive epidemiology of malaria infection and disease among children. Am J Trop Med Hyg **60:**641–648.
25. **Epstein JE, Rao S, Williams F, Freilich D, Luke T, Sedegah M, de la Vega P, Sacci J, Richie TL, Hoffman SL.** 2007. Safety and clinical outcome of experimental challenge of human volunteers with Plasmodium falciparum-infected mosquitoes: an update. J Infect Dis **196:**145–154. http://dx.doi.org/10.1086/518510.
26. **Verhage DF, Telgt DS, Bousema JT, Hermsen CC, van Gemert GJ, van der Meer JW, Sauerwein RW.** 2005. Clinical outcome of experimental human malaria induced by Plasmodium falciparum-infected mosquitoes. Neth J Med **63:**52–58.
27. **Dalton DK, Pitts-Meek S, Keshav S, Figari IS, Bradley A, Stewart TA.** 1993. Multiple defects of immune cell function in mice with disrupted interferon-gamma genes. Science **259:**1739–1742. http://dx.doi.org/10.1126/science.8456300.
28. **Franke-Fayard B, Trueman H, Ramesar J, Mendoza J, van der Keur M, van der Linden R, Sinden RE, Waters AP, Janse CJ.** 2004. A Plasmodium berghei reference line that constitutively expresses GFP at a high level throughout the complete life cycle. Mol Biochem Parasitol **137:**23–33. http://dx.doi.org/10.1016/j.molbiopara.2004.04.007.
29. **Pfaffl MW.** 2001. A new mathematical model for relative quantification in real-time RT-PCR. Nucleic Acids Res **29:**e45. http://dx.doi.org/10.1093/nar/29.9.e45.
30. **Beier JC, Oster CN, Onyango FK, Bales JD, Sherwood JA, Perkins PV, Chumo DK, Koech DV, Whitmire RE, Roberts CR, Diggs CL, Hoffman SL.** 1994. Plasmodium falciparum incidence relative to entomologic inoculation rates at a site proposed for testing malaria vaccines in western Kenya. Am J Trop Med Hyg **50:**529–536.
31. **Bekessy A, Molineaux L, Storey J.** 1976. Estimation of incidence and recovery rates of Plasmodium falciparum parasitaemia from longitudinal data. Bull World Health Organ **54:**685–693.
32. **Pull JH, Grab B.** 1974. A simple epidemiological model for evaluating the malaria inoculation rate and the risk of infection in infants. Bull World Health Organ **51:**507–516.
33. **Smith DL, Drakeley CJ, Chiyaka C, Hay SI.** 2010. A quantitative analysis of transmission efficiency versus intensity for malaria. Nat Commun **1:**108. http://dx.doi.org/10.1038/ncomms1107.
34. **Pinkevych M, Petravic J, Chelimo K, Kazura JW, Moormann AM, Davenport MP.** 2012. The dynamics of naturally acquired immunity to Plasmodium falciparum infection. PLoS Comput Biol **8:**e1002729. http://dx.doi.org/10.1371/journal.pcbi.1002729.
35. **Pinkevych M, Petravic J, Chelimo K, Vulule J, Kazura JW, Moormann AM, Davenport MP.** 2014. Decreased growth rate of P. falciparum blood stage parasitemia with age in a holoendemic population. J Infect Dis **209:**1136–1143. http://dx.doi.org/10.1093/infdis/jit613.
36. **Peters W.** 1974. Recent advances in antimalarial chemotherapy and drug resistance. Adv Parasitol **12:**69–114. http://dx.doi.org/10.1016/S0065-308X(08)60387-5.
37. **Yayon A, Vande Waa JA, Yayon M, Geary TG, Jensen JB.** 1983. Stage-dependent effects of chloroquine on Plasmodium falciparum in vitro. J Protozool **30:**642–647. http://dx.doi.org/10.1111/j.1550-7408.1983.tb05336.x.
38. **Belnoue E, Costa FT, Frankenberg T, Vigario AM, Voza T, Leroy N, Rodrigues MM, Landau I, Snounou G, Renia L.** 2004. Protective T cell immunity against malaria liver stage after vaccination with live sporozoites under chloroquine treatment. J Immunol **172:**2487–2495. http://dx.doi.org/10.4049/jimmunol.172.4.2487.
39. **Decker T, Muller M, Stockinger S.** 2005. The yin and yang of type I interferon activity in bacterial infection. Nat Rev Immunol **5:**675–687. http://dx.doi.org/10.1038/nri1684.
40. **Schofield L, Ferreira A, Altszuler R, Nussenzweig V, Nussenzweig RS.** 1987. Interferon-gamma inhibits the intrahepatocytic development of malaria parasites in vitro. J Immunol **139:**2020–2025.
41. **Vergara U, Ferreira A, Schellekens H, Nussenzweig V.** 1987. Mechanism of escape of exoerythrocytic forms (EEF) of malaria parasites from the inhibitory effects of interferon-gamma. J Immunol **138:**4447–4449.
42. **Mellouk S, Green SJ, Nacy CA, Hoffman SL.** 1991. IFN-gamma inhibits development of Plasmodium berghei exoerythrocytic stages in hepatocytes by an L-arginine-dependent effector mechanism. J Immunol **146:**3971–3976.
43. **Zuzarte-Luis V, Sales-Dias J, Mota MM.** 2014. Simple, sensitive and quantitative bioluminescence assay for determination of malaria prepatent period. Malar J **13:**15. http://dx.doi.org/10.1186/1475-2875-13-15.
44. **Owusu-Agyei S, Koram KA, Baird JK, Utz GC, Binka FN, Nkrumah FK, Fryauff DJ, Hoffman SL.** 2001. Incidence of symptomatic and asymptomatic Plasmodium falciparum infection following curative therapy in adult residents of northern Ghana. Am J Trop Med Hyg **65:**197–203.
45. **Moormann AM, Sumba PO, Chelimo K, Fang H, Tisch DJ, Dent AE, John CC, Long CA, Vulule J, Kazura JW.** 2013. Humoral and cellular immunity to Plasmodium falciparum merozoite surface protein 1 and protection from infection with blood-stage parasites. J Infect Dis **208:**149–158. http://dx.doi.org/10.1093/infdis/jit134.
46. **Sokhna CS, Faye FBK, Spiegel A, Dieng H, Trape JF.** 2001. Rapid reappearance of Plasmodium falciparum after drug treatment among Senegalese adults exposed to moderate seasonal transmission. Am J Trop Med Hyg **65:**167–170.
47. **Sagara I, Sangare D, Dolo G, Guindo A, Sissoko M, Sogoba M, Niambele MB, Yalcoue D, Kaslow DC, Dicko A, Klion AD, Diallo D, Miller LH, Toure Y, Doumbo O.** 2002. A high malaria reinfection rate in children and young adults living under a low entomological inoculation rate in a periurban area of Bamako, Mali. Am J Trop Med Hyg **66:**310–313.
48. **Miller JL, Sack BK, Baldwin M, Vaughan AM, Kappe SH.** 3 April 2014, posting date. Interferon-mediated innate immune responses against malaria parasite liver stages. Cell Rep http://dx.doi.org/10.1016/j.celrep.2014.03.018.
49. **Richie TL.** 1988. Interactions between malaria parasites infecting the same vertebrate host. Parasitology **96**(Pt 3)**:**607–639.
50. **Greenhouse B, Myrick A, Dokomajilar C, Woo JM, Carlson EJ, Rosenthal PJ, Dorsey G.** 2006. Validation of microsatellite markers for use in genotyping polyclonal Plasmodium falciparum infections. Am J Trop Med Hyg **75:**836–842.
51. **Juliano JJ, Porter K, Mwapasa V, Sem R, Rogers WO, Ariey F, Wongsrichanalai C, Read A, Meshnick SR.** 2010. Exposing malaria in-host diversity and estimating population diversity by capture-recapture using massively parallel pyrosequencing. Proc Natl Acad Sci U S A **107:**20138–20143. http://dx.doi.org/10.1073/pnas.1007068107.
52. **Black J, Hommel M, Snounou G, Pinder M.** 1994. Mixed infections with Plasmodium falciparum and P malariae and fever in malaria. Lancet **343:**1095.
53. **Bruce MC, Macheso A, Kelly-Hope LA, Nkhoma S, McConnachie A, Molyneux ME.** 2008. Effect of transmission setting and mixed species infections on clinical measures of malaria in Malawi. PLoS One **3:**e2775. http://dx.doi.org/10.1371/journal.pone.0002775.
54. **Doolan DL, Dobano C, Baird JK.** 2009. Acquired immunity to malaria. Clin Microbiol Rev **22:**13–36, table of contents. http://dx.doi.org/10.1128/CMR.00025-08.
55. **Horras CJ, Lamb CL, Mitchell KA.** 2011. Regulation of hepatocyte fate by interferon-gamma. Cytokine Growth Factor Rev **22:**35–43. http://dx.doi.org/10.1016/j.cytogfr.2011.01.001.
56. **Schoenborn JR, Wilson CB.** 2007. Regulation of interferon-gamma during innate and adaptive immune responses. Adv Immunol **96:**41–101. http://dx.doi.org/10.1016/S0065-2776(07)96002-2.

Molecular Microbiology (2013) 88(2), 318–338 ■
doi:10.1111/mmi.12187
First published online 12 March 2013

Loss-of-function analyses defines vital and redundant functions of the *Plasmodium* rhomboid protease family

Jing-wen Lin,[1] Patrícia Meireles,[3] Miguel Prudêncio,[3] Sabine Engelmann,[5] Takeshi Annoura,[1] Mohammed Sajid,[1] Séverine Chevalley-Maurel,[1] Jai Ramesar,[1] Carolin Nahar,[6] Cristina M. C. Avramut,[2] Abraham J. Koster,[2] Kai Matuschewski,[5,6] Andrew P. Waters,[7] Chris J. Janse,[1] Gunnar R. Mair[4] and Shahid M. Khan[1]***

[1]*Leiden Malaria Research Group (Parasitology), and* [2]*Section Electron Microscopy (Molecular Cell Biology), Leiden University Medical Centre, Leiden, The Netherlands.*

[3]*Malaria Unit, and* [4]*Molecular Parasitology Unit, Instituto de Medicina Molecular, Faculdade de Medicina, Universidade de Lisboa, Lisboa, Portugal.*

[5]*Parasitology, Department of Infectious Diseases, University of Heidelberg Medical School, Heidelberg, Germany.*

[6]*Max Planck Institute for Infection Biology, Parasitology Unit, Berlin, Germany.*

[7]*Division of Infection and Immunity, Institute of Biomedical Life Sciences & Wellcome Centre for Molecular Parasitology, Glasgow Biomedical Research Centre, University of Glasgow, Glasgow, UK.*

Summary

Rhomboid-like proteases cleave membrane-anchored proteins within their transmembrane domains. In apicomplexan parasites substrates include molecules that function in parasite motility and host cell invasion. While two *Plasmodium* rhomboids, ROM1 and ROM4, have been examined, the roles of the remaining six rhomboids during the malaria parasite's life cycle are unknown. We present systematic gene deletion analyses of all eight *Plasmodium* rhomboid-like proteins as a means to discover stage-specific phenotypes and potential functions in the rodent malaria model, *P. berghei*. Four rhomboids (ROM4, 6, 7 and 8) are refractory to gene deletion, suggesting an essential role during asexual blood stage development. In contrast ROM1, 3, 9 and 10 were dispensable for blood stage development and exhibited no, subtle or severe defects in mosquito or liver development. Parasites lacking ROM9 and ROM10 showed no major phenotypic defects. Parasites lacking ROM1 presented a delay in blood stage patency following liver infection, but in contrast to a previous study blood stage parasites had similar growth and virulence characteristics as wild type parasites. Parasites lacking ROM3 in mosquitoes readily established oocysts but failed to produce sporozoites. ROM3 is the first apicomplexan rhomboid identified to play a vital role in sporogony.

Accepted 13 February, 2013. For correspondence. *E-mail s.m.khan@lumc.nl; Tel. (+31) 715261405; Fax (+31) 715266907; **E-mail gmair@fm.ul.pt; Tel. (+351) 217999513; Fax (+351) 217999500.

Introduction

Rhomboid-like proteins are intramembrane serine proteases that hydrolyse a substrate within its transmembrane (TM) spanning domain (Freeman, 2004). The first rhomboid protease described was *Drosophila melanogaster* Rhomboid-1 that initiates cell signalling by cleaving the membrane-resident Spitz, an epidermal growth factor (EGF)-like ligand precursor, releasing it as an activated molecule from the membrane and promoting subsequent EGF-receptor signalling (Urban *et al.*, 2001). With the exception of viruses, rhomboid-like proteins are found in all kingdoms of life and share a conserved core structure of six TM domains that contains the catalytic serine-histidine diad (Koonin *et al.*, 2003; Wang *et al.*, 2006; Wu *et al.*, 2006; Ben-Shem *et al.*, 2007; Lemberg and Freeman, 2007). Interestingly, as a family of proteins, they share only around 5% sequence identity in the core region (Urban *et al.*, 2002b) and have highly variable amino termini. Some members have additional TM domains at either N- or C-termini of the core six, but their precise functions are unknown. Rhomboids function in cell–cell signalling in metazoans (Urban *et al.*, 2002a; Sundaram, 2004), quorum sensing between bacteria (Stevenson *et al.*, 2007), facilitate mitochondrial membrane fusion in yeast (McQuibban *et al.*, 2003) and regulate apoptosis (Cipolat *et al.*, 2006).

Many eukaryotic organisms contain large rhomboid gene families. Multiple rhomboid-like enzymes are also found in the genomes of apicomplexan parasites such as *Toxoplasma gondii*, *Plasmodium spp.*, *Eimeria tenella*, *Cryptosporidium spp.*, *Theileria spp.* and *Babesia bovis*.

Based on a phylogenetic clustering of rhomboid-like proteins, a nomenclature has been defined according to the initial assignment of *T. gondii rhomboids* (Dowse and Soldati, 2005) which expresses six rhomboid-like proteins *Tg*ROM1–6. Only four TgROMs (i.e. ROM1, 3, 4 and 6) have direct *Plasmodium* homologues (Dowse and Soldati, 2005); there are no direct homologues of TgROM2 and TgROM5 in *Plasmodium* and ROM7–10 are only present in *Plasmodium* but not in *T. gondii*. Although *Plasmodium* species do not have a direct TgROM5 homologue, *P. falciparum* ROM1 and ROM4 share substrate specificities with TgROM5 (Baker *et al*., 2006). Apicomplexan ROM6 is most likely an evolutionarily ancient mitochondrial PARL-like rhomboid, whereas all the others seem to be unique to apicomplexan parasites (Dowse and Soldati, 2005). Interestingly, *Plasmodium* ROM9 also has a putative mitochondrial-targeting sequence and clusters with PARL-like rhomboids (Santos *et al*., 2011b).

Although *in vitro* certain rhomboids of apicomplexan parasites can cleave adhesins that are known to mediate recognition of, and attachment to host cells, their *in vivo* substrate specificities are largely unknown (Freeman, 2009; Santos *et al*., 2011b). Understanding the biological functions of apicomplexan rhomboids is an active area of research because of the critical roles identified for several of these molecules in host cell invasion and pathogenesis (Freeman, 2009; Buguliskis *et al*., 2010; Santos *et al*., 2011b). In *T. gondii*, TgROM4 has been shown to process surface adhesins including MIC 2, 3 (microneme proteins) and apical membrane antigen 1 [AMA1 (Buguliskis *et al*., 2010)]; this TgROM4-mediated AMA1 cleavage critically regulates the parasite's switch from an invasive to a replicative mode (Santos *et al*., 2011a). TgROM1 is localized in micronemes (Brossier *et al*., 2005) and although it is critical for parasite growth, TgROM1 is not essential for parasite invasion (Brossier *et al*., 2008). From the eight *Plasmodium* rhomboids, only ROM1 and ROM4 have been analysed in more detail. *In vitro* substrates of the *P. falciparum* proteins include the merozoite-specific proteins AMA1 and proteins of the EBL (erythrocyte binding ligands) and RBL (reticulocyte binding ligands) families as well as several proteins of the invasive ookinete- and sporozoite-stages, such as TRAP (thrombospondin-related anonymous protein), CTRP (circumsporozoite- and TRAP-related protein) and MAEBL (merozoite adhesive erythrocytic binding protein) (Baker *et al*., 2006). Structural analysis of the RBL protein EBA175 (Erythrocyte-binding antigen 175) and TRAP provided evidence for shedding of these proteins by a rhomboid-like protease (O'Donnell *et al*., 2006) and indeed both proteins are cleaved *in vitro* by ROM4 (O'Donnell *et al*., 2006; Ejigiri *et al*., 2012). In *P. falciparum* only a small fraction of AMA1 is shed by ROM1 and the intramembrane cleavage can be reduced to undetectable levels by mutagenesis without discernible phenotypic consequences (Olivieri *et al*., 2011). The successful generation of *P. berghei* and *P. yoelii* mutants that lack expression of ROM1 also demonstrated that ROM1 is not essential for blood stage multiplication (Srinivasan *et al*., 2009; Vera *et al*., 2011). Blood stages of these mutants suffer only from a minor reduction in growth, again indicating that intramembrane cleavage of AMA1 by ROM1 is not essential for invasion of erythrocytes. ROM1 mutants in *P. yoelii* also showed a slight growth defect during liver stage development which has been attributed to reduced cleavage of the parasitophorous vacuole protein UIS4 (upregulated in sporozoites 4) by ROM1 (Vera *et al*., 2011). Whether additional proteins are processed by *Plasmodium* ROM4 or ROM1 *in vivo* is still unknown. The non-essential nature of ROM1 during the complete life cycle indicates that other rhomboids or proteases from other families can cleave substrates of ROM1. ROM4 on the other hand has been reported to be essential for blood stage growth as attempts to mutate the *rom4* gene of *P. falciparum* failed (O'Donnell *et al*., 2006). However, differences in cellular localization and *in vitro* substrate specificities of ROM1 and ROM4 (Baker *et al*., 2006; O'Donnell *et al*., 2006) raise questions as to whether these rhomboids cleave the same substrates *in vivo*. In blood stage *P. falciparum* ROM1 is located in micronemes of merozoites and ROM4 is embedded into the merozoite plasma membrane (O'Donnell *et al*., 2006).

Due to the absence of data defining *Plasmodium* rhomboid expression, cellular localization, or importance during the parasite's life cycle, it is largely unknown which, if any rhomboids are biologically essential, redundant or perhaps share overlapping functions. We therefore undertook a genetic screen of all eight rhomboids by targeting each gene for deletion by homologous recombination using the genetically most tractable malaria parasite, *P. berghei*. Multiple attempts to disrupt genes encoding ROM4, ROM6, ROM7 and ROM8 failed, suggesting that these proteins have essential, non-redundant functions during blood stage development. We show that in addition to ROM1, three other rhomboid-like proteases – ROM3, ROM9 and ROM10 – are redundant for asexual blood stage development in mice. Parasites lacking ROM9 and ROM10 showed no major phenotypic defects during the entire life cycle; however, parasites lacking ROM1 were slightly compromised with respect to their ability to develop in the liver. Although already transcribed strongly in the female gametocyte, ROM3 is crucial during oocyst development inside the mosquito. Parasites lacking ROM3 produce normal numbers of ookinetes that readily establish oocysts in the mosquito. Although normal in size and number, oocysts fail to sporulate, suggesting that ROM3 plays a key role in the regulation of cytokinesis and production of individual sporozoites.

Table 1. Expression profile of *Plasmodium rhomboids*.

Protein	Gene ID	mRNA				Protein			
P. berghei		**As[a,b]**	**Gct[a,b]**	**Ook[a]**	**Sp[a,b]**	**As[c]**	**Gct[d]**		**Sp[c]**
ROM1	PBANKA_093350	+ (–)	+ (–)	++	+ (++)	– (+[e])	±		– (+[e])
ROM3	PBANKA_070270	– (++)	+ (–)	–	– (–)	–	–		–
ROM4	PBANKA_110650	+ (++)	+ (–)	++	+ (++)	– (+[f])	–		– (+[f])
ROM6	PBANKA_135810	+ (–)	+ (–)	–	– (+)	–	–		–
ROM7	PBANKA_113460	+ (–)	– (–)	–	– (+)	–	–		–
ROM8	PBANKA_103130	+ (–)	– (–)	–	– (–)	–	–		–
ROM9	PBANKA_111470	± (–)	± (–)	–	+ (–)	–	–		–
ROM10	PBANKA_111780	+ (++)	± (–)	+	– (–)	–	–		–
P. falciparum		**As[g]**	**Gct[g]**		**Sp[h]**	**As[c]**	**Gct[c]**	**Ooc[c]**	**Sp[c]**
ROM1	PF3D7_1114100	+	±		+	+	–	–	–
ROM3	PF3D7_0828000	±	++		±	±	–	–	–
ROM4	PF3D7_0506900	+	++		+	++	–	–	+
ROM6	PF3D7_1345200	±	±		±	–	±	–	–
ROM7	PF3D7_1358300	±	–		–	–	–	–	–
ROM8	PF3D7_1411200	+	+		+	–	–	–	–
ROM9	PF3D7_0515100	±	±		±	–	±	–	–
ROM10	PF3D7_0618600	+	±		±	±	+	–	–

a. RT-PCR results in this study (see Fig. S1).
b. PlasmoDB EST data in parentheses (–, no data; +, 1 EST; ++, 2–7 ESTs).
c. PlasmoDB proteome data (–, no data; ±, 1–2; +, 3–10; ++, > 10).
d. PbANKA Male vs female gametocyte proteome (Khan *et al.*, 2005).
e. IFA evidence using anti-PbROM1 serum (Srinivasan *et al.*, 2009).
f. Western and IFA evidence using anti-PbROM4 serum (Ejigiri *et al.*, 2012).
g. PlasmoDB RNAseq data (–, no data; ±, 0–6; +, 6–10) RPKM (log2).
h. PlasmoDB oligo array (–, no data; ±, 1–100; +, 100–1000; ++, > 1000) RMA value.
AS, asexual stages; Gct, gametocytes; Ook, ookinetes; Ooc, oocysts; Sp, sporozoites.

Results

The gene expression profiles of rhomboids across the parasite life cycle

The genome of the rodent malaria parasite *P. berghei* contains eight genes encoding rhomboid proteases (Dowse and Soldati, 2005) (Gene IDs are shown in Table 1). Each member shows a high level of sequence identity (70–85%) with its rhomboid orthologue from the human malaria parasite *P. falciparum* and shares a syntenic location in the genome (http://www.plasmodb.org) with an identical exon/intron gene structure.

We compared expression data of all rhomboid genes in *P. berghei* and *P. falciparum* in publicly available literature as well as transcriptome and proteome datasets across the life cycle (Table 1) (http://www.plasmodb.org and Khan *et al.*, 2005). Immunofluorescence assays (IFA) on HA-tagged ROM1 and ROM4 show expression of these proteins in dividing schizonts and merozoites in *P. falciparum* (O'Donnell *et al.*, 2006). A similar pattern of expression of *P. berghei* and *P. yoelii* ROM1 has been shown in schizonts and merozoites by IFA (Srinivasan *et al.*, 2009; Vera *et al.*, 2011). In both *P. berghei* and *P. falciparum* ROM1 is located in the micronemes. *P. berghei* ROM1 and ROM4 of *P. falciparum* and *P. berghei* have been detected in the sporozoite stage (Srinivasan *et al.*, 2009; Ejigiri *et al.*, 2012) (Table 1). Our RT-PCR analyses (Fig. S1) demonstrate transcription of *P. berghei rom1* and *rom4* in blood stages and sporozoites. These different observations indicate that both ROM1 and ROM4 of human and rodent parasites have comparable patterns of expression and cellular location. For other rhomboids the information on stage-specific expression is much more limited. Proteome analyses indicate that ROM6, ROM9 and ROM10 are expressed in *P. falciparum* gametocytes (Table 1); however, proteome evidence for expression of these proteins in *P. berghei* gametocytes or other blood stages is absent. ROM7 and ROM8 are absent in all *P. falciparum* and *P. berghei* proteomes and ROM3 is only detected in *P. falciparum* blood stages. EST, RNAseq (Table 1) and RT-PCR analyses (Fig. S1), however, indicate that ROM3, ROM7 and ROM8 are expressed in blood stages and therefore the absence in proteomes may suggest that rhomboids are relatively low abundant proteins, although we have to take into account the difficulties of proteomic sequencing multi-pass TM proteins. *P. falciparum* RNAseq analyses indicate that transcription of *rom3* and *rom4* is upregulated in gametocytes compared with asexual stages (Table 1). RNAseq analyses of different *P. berghei* blood stages also showed strongly increased transcripts levels of *rom3* and *rom4* in gametocytes (W.A.M. Hoeijmakers, A. Religa, C.J. Janse, A.P. Waters and H.G. Stunnenberg, unpubl. data). We con-

firmed transcription of these rhomboids in *P. berghei* gametocytes by RT-PCR (Fig. S1).

The similarities between the eight rhomboid genes of *P. falciparum* and *P. berghei* and similarities in expression patterns and cellular locations of several rhomboids point towards a conserved function between rhomboid orthologues across the parasites' life cycle in both species. Since most rhomboids appear to be expressed in multiple life cycle stages, the expression pattern is, however, not a good indicator for a putative role at a distinct life cycle stage.

Evidence for an essential role of ROM4, 6, 7 and 8 in asexual blood stage parasites – ROM1, 3, 9 and 10 are dispensable

As a first step towards understanding the roles of rhomboid proteases during the *Plasmodium* life cycle, we undertook a systematic, individual gene deletion approach for each of the eight *P. berghei* rhomboid genes and provide here a detailed analysis of the growth characteristics of gene deletion mutants for four rhomboids. Using well-established standard assays, the following phenotypes of the gene deletion mutants were characterized throughout the complete life cycle including blood, mosquito and liver stages: *in vivo* asexual blood stage multiplication rate, *in vivo* gametocyte production, *in vitro* ookinete formation, oocyst and sporozoite development in *Anopheles stephensi* mosquitoes and the prepatent period in mice after injection of sporozoites. The prepatent period is defined as the time taken to achieve a 0.5–2% blood stage parasitemia in mice after intravenous inoculation of 10^4 sporozoites.

Standard genetic modification technologies used to replace entire *rhomboid* genes by double cross-over integration with a drug resistant marker resulted in gene deletion mutants for *rom1*, *3*, *9* and *10*, while multiple attempts to disrupt *rom4*, *6*, *7* and *8* were unsuccessful (see Tables S1, S2 and S3 for details of these unsuccessful gene-deletion attempts including primers used to amplify the targeting sequences, generate the gene-deletion constructs and genotype). We demonstrated by RT-PCR that *rom4*, *6*, *7* and *8* are transcribed in blood stages (Fig. S1) and the multiple unsuccessful attempts to disrupt *rom4*, *6*, *7* and *8* may indicate that these genes have a critical function for asexual blood stage growth and multiplication. While a failure to disrupt a gene is not an unequivocal proof that the encoded protein is essential for blood stage growth/multiplication for *rom4* we show that the failure of disruption is not due to refractoriness of the genetic locus to genetic modification by creating a transgenic mutant (*rom4::mCherry*) that expresses a C-terminally mCherry-tagged ROM4 (Fig. S2). Genotype analysis of the *rom4::mCherry* parasites and analysis of ROM4::mCherry expression (Fig. S2) demonstrates that correct genetic modification of the *rom4* locus is possible. Immunofluorescence analysis of ROM4::mCherry revealed its expression in gametocytes (Fig. S2); however, the very weak fluorescence signals in asexual blood stages prevented confirmation of merozoite surface location observed in *P. falciparum* (Fig. S2). The normal asexual multiplication rate (Table 2) indicates that the mCherry-tagged ROM4 functions normally during blood stage development. All information on the failed attempts to disrupt *rom4*, *6*, *7* and *8*, including DNA constructs and primers have been submitted to the RMgmDB database of genetically modified rodent malaria parasites (http://www.pberghei.eu).

The correct integration of the constructs and successful disruption of the other *rhomboids*, *rom1*, *3*, *9 and 10*, were confirmed by diagnostic PCR and Southern analysis of separated chromosomes (Figs 1 and 2). Northern analyses showed transcription of all four genes in blood stages of wild type *P. berghei* ANKA parasites and confirmed the lack of transcription in the blood stages of the respective gene-deletion mutants (Figs 1 and 2). The clonal lines of the gene-deletion mutants Δ*rom1*, Δ*rom3*, Δ*rom9* and Δ*rom10* showed no change in asexual growth rates *in vivo* (Table 2). Despite the evidence for transcription and protein expression of ROM1, 9 and 10 in asexual blood stages (Figs 1, 2 and S1; Table 1) this indicates a non-essential, redundant function for these proteins during asexual blood stage multiplication.

ROM9 and ROM10 are dispensable for the entire life cycle

Two independent gene-deletion mutants were generated for *rom9*: Δ*rom9*-a and Δ*rom9*-b (Fig. 2C). Asexual blood stage multiplication, gametocyte production and ookinete production of both Δ*rom9* mutants were similar to that of wild type *P. berghei* parasites.

We analysed Δ*rom9*-a parasites during development in mosquitoes and in hepatocytes. The Δ*rom9* parasites produced wild type levels of oocysts (Table 2). Although we showed that *rom9* is transcribed in salivary gland sporozoites (Fig. S1), we found no significant differences between Δ*rom9* parasites and wild type parasites with respect to the production of sporozoites, their gliding motility (data not shown), traversal and invasion of hepatocytes and in the prepatent period in mice after injection of sporozoites (Table 2). Immunofluorescence analyses of liver stage parasites stained with antibodies against markers for parasite development (HSP70), parasitophorous vacuole membrane (PVM) (UIS4 and EXP1) and merozoite formation (MSP1), also revealed no distinct differences in morphology between Δ*rom9* and wild type liver stage parasites at 24 h or 48 h after sporozoite invasion (Fig. 3A). However, Δ*rom9* parasite loads between 53 and 57 h after

Table 2. Phenotypes of *P. berghei* mutants lacking expression of rhomboids.

Lines	Asexual multiplication rate[a] (s.d.)	Gametocyte production[b] % (s.d.)	Ookinete production[c] % (s.d.)	Oocyst production[d] (s.d.)	Sporozoite production[e] × 10^3 (s.d.)	Sporozoite traversal[f] % (s.d.)	Sporozoite invasion rate[g] % (s.d.)	Prepatent period compared with wt[h]
Mutants								
Δ*rom1-p*	10 (0) $n = 2$	16.4 (0.5)	56.6 (1.8)	156.3 (151.8)	ND	ND	ND	ND
Δ*rom1-c*	10 (0) $n = 3$	17.3 (1.0)	68.9 (9.5)	155.6 (118.9)	35.9 (3.3)	27.3 (7.6)	23.3 (8.5)[j]	+1 ($n = 3$)
				220.0 (70.3)	49.0 (1.6)	ND	35.6 (10.6)[j]	+1 ($n = 3$)
				ND	ND	ND	58.5 (6.8)	ND
Δ*rom3-a*	10 (0) $n = 3$	17.9 (1.3)	61.3 (5.9)	148.4 (136.8)	NA	NA	NA	NA
Δ*rom3-b*	10 (0) $n = 2$	18.9 (3.0)	71.0 (6.1)	259.7 (155.8)	NA	NA	NA	NA
Δ*rom9-a*	10 (0) $n = 4$	18.9 (4.1)	74.3 (11.0)	145.8 (123.8)	43.2 (6.5)	21.1 (2.1)	51.7 (9.2)	+0 ($n = 5$)
Δ*rom9-b*	10 (0) $n = 4$	19.0 (2,7)	74.2 (4.6)	ND	ND	ND	ND	ND
Δ*rom10*	10 (0) $n = 4$	18.1 (2.6)	63.8 (7.4)	191.8 (147.2)	44.7 (8.0)	ND	53.3 (4.5)	+0 ($n = 3$)
Tagging mutants								
rom3::gfp	10 (0) $n = 3$	18.0 (2.7)	66.5 (4.7)	298.2 (110.7)	51.4 (8.9)	ND	ND	ND
rom4::mCherry	10 (0) $n = 7$	ND	ND	ND	ND	ND	ND	ND
wt[i]	10 (0) $n > 10$	15–25	50–90	120–290	35–80	19.3–25.7	53.0 –61.8	+0

a. The multiplication rate per 24 h of blood stage parasites in mice infected with a single parasite.
b. The percentage of blood stage parasites developing into gametocytes *in vivo*.
c. The percentage of female gametes developing into mature ookinetes *in vitro*.
d. The mean number of oocysts per mosquito (days 11–14).
e. The mean number of salivary gland sporozoites per mosquito (days 19–22).
f. Percentage of Dextran positive cells in Huh7 cell cultures 2 h after post-infection.
g. The percentage of intracellular sporozoites at 3 h post-infection of Huh7 cell cultures.
h. The prepatent period (measured in days post sporozoite infection) is defined as the day when a blood stage infection with a parasitemia of 0.5–2% is observed (+0 = similar to wild type; +1 = 1 day delay compared with wild type).
i. The developmental data for wild type parasites are shown as the range of mean values of > 10 experiments.
j. $P < 0.05$, determined by Student's *t*-test as compared with wild type control run in parallel.
ND, not done; NA, not applicable.

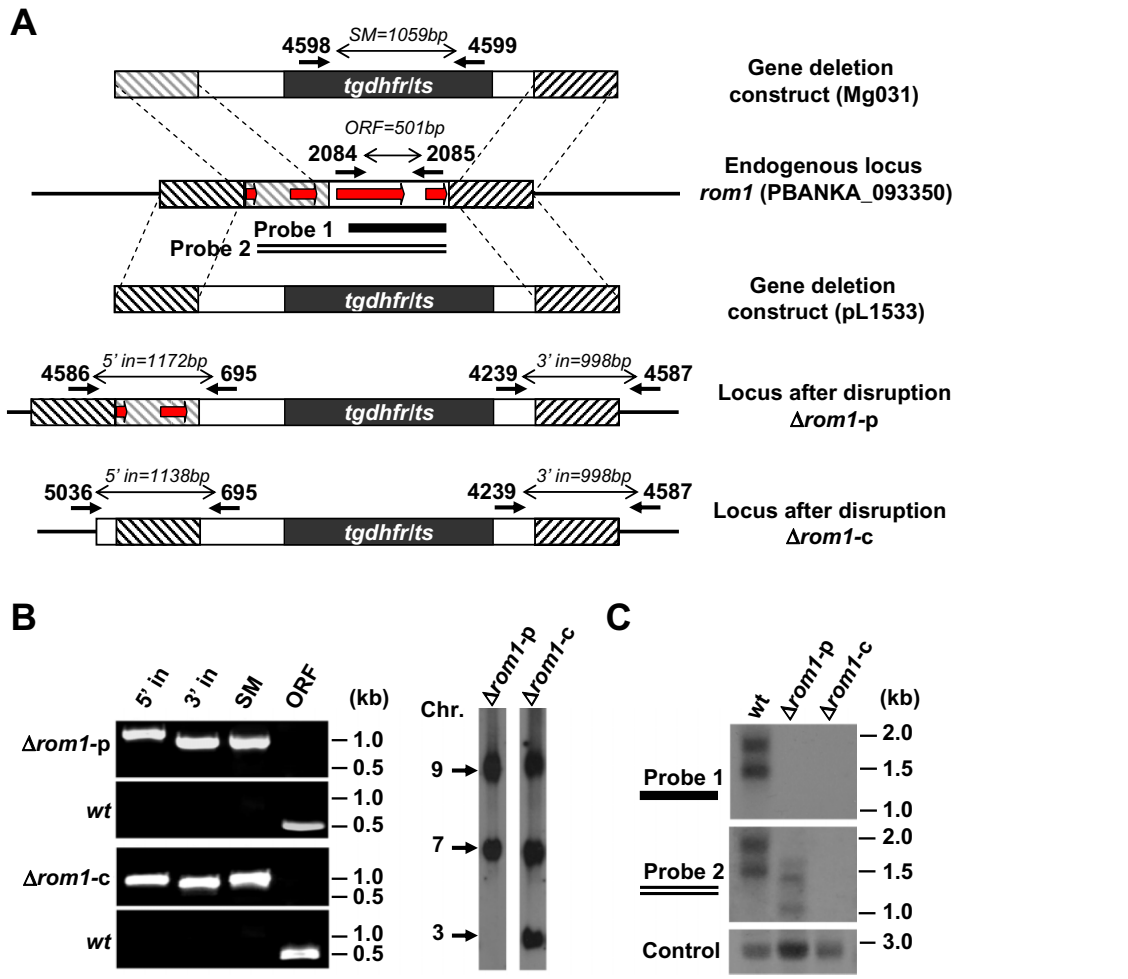

Fig. 1. Generation of mutants lacking expression of *P. berghei* rhomboid 1.
A. Schematic representation of the constructs Mg031 and pL1533 targeting *rhomboid-1* for gene deletion by double cross-over homologous recombination at the target regions (hatched boxes), and the locus before and after disruption. Each construct contains the *tgdhfr/ts* selection cassette (black box). Mg031 replaces the 3rd and 4th exons (red arrows) of the ORF but retains 1st and 2nd exons in mutant Δ*rom1*-p. pL1533 replaces the complete ORF in Δ*rom1*-c. Primer positions for diagnostic PCRs, amplicon sizes and the location of two PCR probes for the Northern blot analyses are shown (see Table S3 for primer sequences).
B. Diagnostic PCRs (left) and Southern analyses of separated chromosomes (right) confirm the correct integration of the constructs in Δ*rom1*-p and Δ*rom1*-c. Primer pairs and amplicon sizes are shown in A: 5′/3′ in, integration PCR; SM, amplification of the *tgdhfr/ts* selection cassette; ORF, deleted ORF. For Southern analyses, pulsed field gel-separated chromosomes were hybridized with a 3′UTR *pbdhfr* probe that recognizes the constructs integrated into *rom1* locus on chromosome 9 and the endogenous *dhfr/ts* locus on chromosome 7; in the Δ*rom1*-c line, the probe also hybridizes to the GFP-luciferase reporter cassette in the *230p* locus on chromosome 3.
C. Northern blot analyses of mRNA from mixed blood stage parasites confirm the loss of wild type *rom1* transcripts in Δ*rom1*-p and Δ*rom1*-c. Locations of the PCR probes used for hybridization were shown in A (PCR probes were generated by PCR-amplification from wild type *P. berghei* genomic DNA using primers 2084/2085 for Probe 1, and primers 2082/2085 for Probe 2; see Table S3 for primer sequences). In blood stages of Δ*rom1*-p, truncated transcripts were detected with Probe 2, recognizing exons 1 and 2 of *rom1*. In Δ*rom1*-c, no transcripts were detected. As a loading control, hybridization was performed with probe L644R that recognizes the large subunit ribosomal RNA. wt, wild-type *P. berghei* ANKA.

infection (measured by RT-PCR, FACS and luciferase assay) were consistently lower both *in vitro* and *in vivo* (Fig. 3B and C) which may indicate that this enzyme plays a (minor) role during liver stage development.

We generated one gene deletion mutant for *rom10* and analysed this mutant throughout the entire life cycle. The phenotype of Δ*rom10* parasites was similar to that of wild type parasites in all developmental assays (Table 2), specifically *in vivo* asexual multiplication rate, *in vivo* gametocyte production, *in vitro* ookinete production, oocyst and sporozoite production and *in vivo* liver stage development. In addition, Δ*rom10* sporozoites showed normal rates of gliding (data not shown), *in vitro* hepatocyte invasion rate and prepatent period (Table 2). These results indicate that this protein is redundant and/or that its function can be fulfilled by other (rhomboid) proteases.

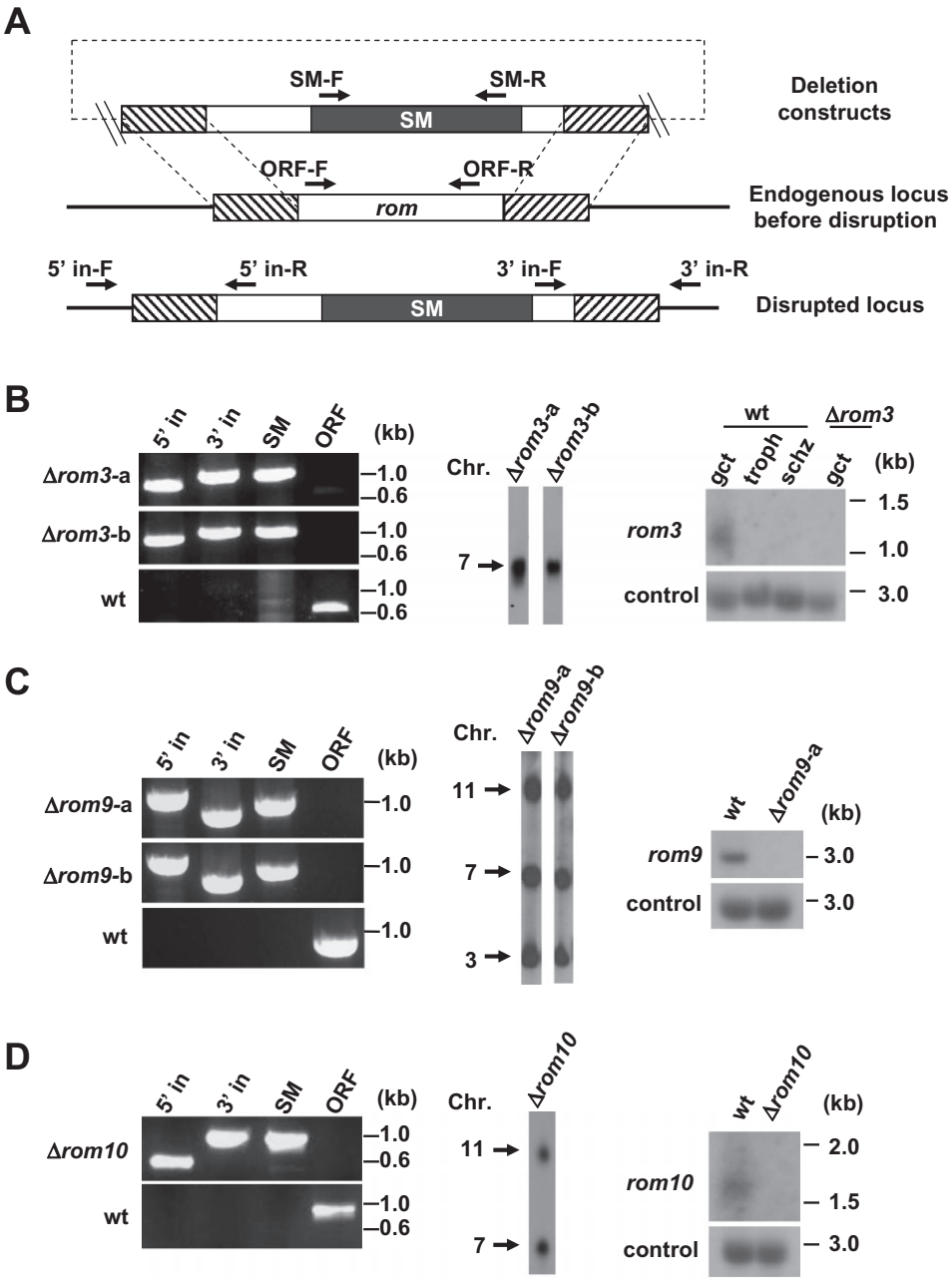

Δrom1 parasites have wild type blood stage growth and virulence characteristics, but show delayed liver stage development

In the course of this study we generated two independent *P. berghei* Δ*rom1* mutants; the first mutant Δ*rom1*-p is a partial gene deletion lacking the 3rd and 4th exons of *rom1* that contain the catalytic diad (Fig. 1A and B); the second mutant Δ*rom1*-c lacks the entire open reading frame (ORF) (Fig. 1A and B). Northern analyses of *rom1* transcripts in blood stages using two PCR-amplified probes specific to 3rd and 4th exons, or to the whole ORF, showed that Δ*rom1*-p lacks transcripts containing the 3rd and 4th exons but still produces stable, truncated transcripts consisting of the 1st and 2nd exons. As expected, Δ*rom1*-c had no detectable *rom1* transcripts (Fig. 1C). Both Δ*rom1*-p and Δ*rom1*-c showed *in vivo* multiplication rates that were similar to wild type *P. berghei* parasites when analysed in the cloning-assay (Table 2). To determine possible differences in growth rate and virulence during prolonged infections in mice, we analysed the growth rate of Δ*rom1* and wild type parasites in C57BL/6 and in BALB/c mice (Fig. 4A and B). C57BL/6 mice are sensitive to experimental cerebral malaria (ECM) and cer-

Fig. 2. Generation of mutants lacking expression of *P. berghei* rhomboid 3, 9 and 10.
A. Schematic representation of the DNA construct used for targeting rhomboid genes for deletion and the gene locus before and after disruption. The constructs which contain a drug-selectable marker cassette (SM; black box) disrupt the genes by double cross-over homologous recombination at the target regions (hatched boxes). The locations of primers for diagnostic PCRs are shown.
B. Diagnostic PCRs, Southern and Northern analyses confirm correct disruption of *rhomboid 3* (*rom3*) in 2 independent mutants, Δ*rom3*-a and Δ*rom3*-b. For diagnostic PCRs (left), the following primers were used: 5′ integration (5′ in): 2389/695; 3′ integration: (3′ in) 4239/1886; amplification of the *tgdhfr/ts* selection cassette (SM): 4598/4599; deleted ORF (ORF): 1812/1813. For Southern analyses of separated chromosomes (middle), pulsed field gel-separated chromosome were hybridized using a *tgdhfr/ts* probe that recognizes the construct integrated into *rom3* locus on chromosome 7. Northern blot analysis (right) of mRNA of different blood stages shows transcripts only present in wild type gametocytes (gct). No transcripts are detected in trophozoites (troph) or schizonts (schz). The analysis also confirms the loss of *rom3* transcripts in gct of Δ*rom3*. Hybridization was performed using a PCR probe recognizing *rom3* ORF (primers 1812/1813). As a loading control, hybridization was performed with probe L644R that recognizes the large subunit ribosomal RNA.
C. Analysis of two independent mutants, Δ*rom9*-a and Δ*rom9*-b, lacking expression of ROM9. For diagnostic PCRs (left), the following primers were used: 5′ in: 7083/4906; 3′ in: 4239/7084; SM (h*dfhr::*y*fcu*): 4698/4699; ORF: 7085/7086. For Southern analyses (middle), chromosomes were hybridized using a 3′UTR *pbdhfr* probe that recognizes the construct integrated into *rom9* on chromosome 11, the *dhfr/ts* on chromosome 7 and the GFP-luciferase reporter cassette in the *230p* locus on chromosome 3. Northern blot was hybridized with a PCR probe recognizing *rom9* ORF (primers 7085/7086) (right).
D. Analysis of Δ*rom10* lacking expression of ROM10. For diagnostic PCRs (left), the following primers were used: 5′ in: 6939/4179; 3′ in: 4239/2088; SM (*tgdhfr/ts*): 4598/4599; ORF: 6940/2066. Chromosomes were hybridized using a 3′UTR *pbdhfr* probe that recognizes the construct integrated into *rom10* on chromosome 11 and the *dhfr/ts* on chromosome 7 (middle). Northern blot was hybridized with a PCR probe recognizing *rom10* ORF (primers 6940/2066) (right). See Table S3 for all primer sequences and product sizes.

ebral complications develop 6–8 days post-infection with *P. berghei* ANKA parasites, whereas BALB/c mice are ECM-resistant and develop fulminating (and lethal) parasitemias peaking 2–3 weeks after infection. In both C57BL/6 and BALB/c mice Δ*rom1* parasites showed infection patterns that were highly similar to infections initiated with wild parasites (Fig. 4A and B); all Δ*rom1* infected C57BL/6 mice developed ECM symptoms at day 6 or 7 after infection (Fig. 4A).

Δ*rom1* parasites were next examined during mosquito and liver stage development. These parasites produced numbers of ookinetes, oocysts and salivary gland sporozoites similar to those of wild type parasites (Table 2). However, liver-stage development was reduced as shown by a 1-day extension of the prepatent period in mice following the inoculation with 10^4 purified sporozoites. While gliding motility (data not shown) and the rate of cell traversal of sporozoites were similar to wild type parasites (Table 2), we observed in two out of three experiments a reduction in sporozoite *in vitro* invasion rates (Table 2) that could explain (in part) the delay in the prepatent period. Immunofluorescence analyses of liver stage parasites stained with antibodies against markers for parasite development (HSP70), PVM (UIS4 and EXP1) and merozoite formation (MSP1), revealed no distinct differences in morphology and size between Δ*rom1* and wild type liver stages at 24 h or 48 h after sporozoite invasion (Fig. 4C). Although a significant reduction in parasite loads and expression of UIS4 have been reported for liver stages of *P. yoelii* mutants lacking expression of ROM1 (Vera *et al.*, 2011), we only observed a slight, but not significant, reduction in numbers of liver stages as determined by anti-UIS4 antibody staining (Fig. 4D) and we did not observe that these mutants had unusual PVM morphology. Liver stages of Δ*rom1* and wild-type parasites were also comparable in size at 48 h post-infection (Fig. 4D).

Δ*rom3 parasites establish oocysts but fail to produce sporozoites*

Two independent gene-deletion mutants, Δ*rom3*-a and Δ*rom3*-b, were generated (Fig. 2B). Asexual blood stage multiplication rates of both mutants determined in the cloning assay were normal and Δ*rom3* parasites produced wild type levels of gametocytes, ookinetes and oocysts (Table 2). By light microscopy, Δ*rom3* ookinetes have the characteristics of fully mature wild-type ookinetes such as an elongated ‘banana’ shape, hemozoin clusters and a centrally located, enlarged nucleus and the Δ*rom3* and wild type ookinetes show a similar (tetraploid) DNA content (Fig. S3). In addition, by electron microscopy analyses we were unable to detect differences in the ultrastructural morphology of wild-type and Δ*rom3* ookinetes, with respect to the nucleus, crystalloid body and the structure of the apical complex (Fig. S5). All membranes of these organelles exhibit a normal structure and the apical complex of Δ*rom3* ookinetes had the characteristic features of abundant micronemes, and the presence of microtubules and the inner membrane complex.

However, no sporozoites were detected in salivary glands of mosquitoes infected with Δ*rom3*-a or Δ*rom3*-b in three independent experiments. Inspection of Δ*rom3* oocysts by light-microscopy revealed normal oocyst production but a complete absence of sporozoite formation; mature oocysts had clearly vacuolated cytoplasm and there were no signs of sporulation (Fig. 5A). Western analysis of circumsporozoite protein (CSP) expression using anti-CSP antibody in oocysts-containing midguts at day 10 after infection, showed that CSP is almost absent in the Δ*rom3* oocysts (Fig. 5B). An indirect IFA on wild type and Δ*rom3* oocysts confirmed the strongly reduced CSP levels in Δ*rom3* oocysts (Fig. 5C). There was also

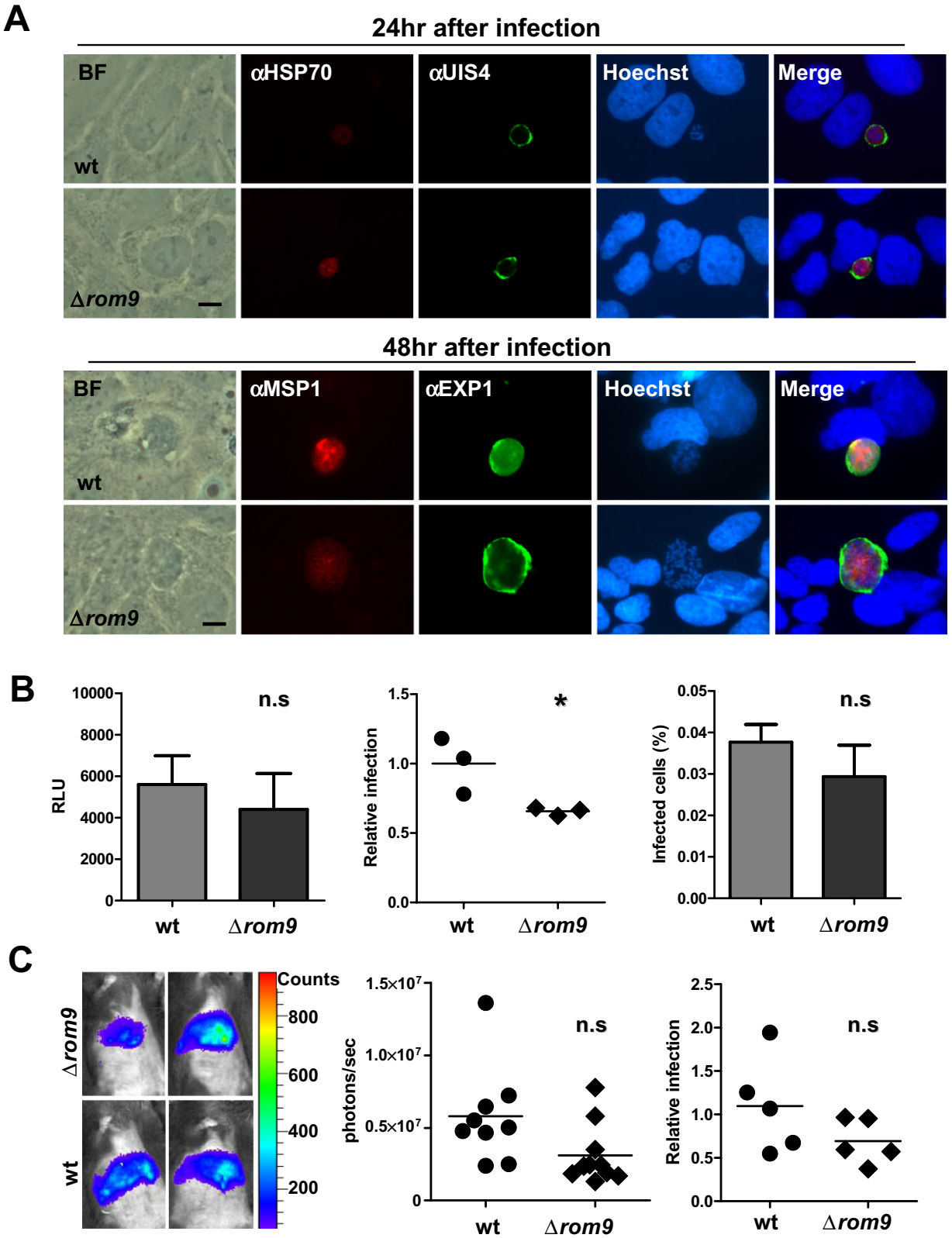
A
24hr after infection
BF
αHSP70
αUIS4
Hoechst
Merge
wt
Δrom9
48hr after infection
BF
αMSP1
αEXP1
Hoechst
Merge
wt
Δrom9
B
RLU
10000
8000
6000
4000
2000
0
n.s
wt
Δrom9
Relative infection
1.5
1.0
0.5
0.0
*
wt
Δrom9
Infected cells (%)
0.05
0.04
0.03
0.02
0.01
0.00
n.s
wt
Δrom9
C
Δrom9
wt
Counts
800
600
400
200
photons/sec
1.5×10^7
1.0×10^7
0.5×10^7
0
n.s
wt
Δrom9
Relative infection
2.5
2.0
1.5
1.0
0.5
0.0
n.s
wt
Δrom9

Fig. 3. Liver stage development of Δ*rom9* parasites.
A. Immunofluorescence assays of liver stages of Δ*rom9* and the wild type (wt) control *Pb*GFP-Luc$_{schz}$ at 24 h and 48 h after sporozoite infection of cultured Huh7 cells show a comparable morphology of Δ*rom9* and wild type parasites. Anti-HSP70 (red) antibody highlights the parasite's cytoplasm while anti-UIS4 (green) antibody decorates the PVM. Anti-MSP1 (red) antibody recognizes developing merozoites and anti-EXP1 (green) antibody the PVM. Nuclei were stained with Hoechst-33342 (Blue). BF, bright field; scale bars equals 10 μm.
B. Parasite loads at 57 h in cultured Huh7 cells after infection with 5×10^4 Δ*rom9* or wild type control *Pb*GFP-Luc$_{schz}$ sporozoites as determined by luciferase assay (left), qRT-PCR (middle) and FACS (right). All assays show a slight reduction of mutant parasite loads, however, only the relative infection value determined by qRT-PCR shows significant reduction (Student's *t*-test: n.s: not significant; $*P < 0.5$).
C. Parasite loads in C57BL/6 mice at 53 h after injection of 1×10^4 Δ*rom9* sporozoites or wild type control *Pb*GFP-Luc$_{schz}$ sporozoites as determined by *in vivo* imaging (left and middle) and qRT-PCR (right). Representative rainbow images of luminescence in livers of live mice (left) and the corresponding luminescence levels (photons s^{-1}) of livers in whole mice (middle) are shown (Student's *t*-test: n.s: not significant). The lines indicate mean values and the error bars indicate standard deviations. This figure is available in colour online at wileyonlinelibrary.com.

reduced intensity of Hoechst DNA-staining indicating decreased DNA replication in these oocysts (Fig. 5C). The crucial role of ROM3 in oocyst maturation/sporogony is unexpected given the high transcript levels detected in gametocytes (Table 1, Fig. S1B). When we analysed ROM3::GFP expression in *rom3*::*gfp* parasites (with the endogenous rom3 C-terminally tagged with GFP), we observed GFP signal in all female gametocytes (but not in male gametocytes) that persisted into mature ookinetes but was undetectable in oocysts (days 6–17) and sporozoites (Fig. 5D).

The normal development throughout the life cycle (Fig. 5D, Table 2) indicates that the C-terminal GFP-tag does not affect the essential function of ROM3 during sporozoite formation. We attempted to use the *rom3*::*gfp* parasites to gain a better understanding of the localization of ROM3 in female gametocytes and ookinetes. Specifically, we extracted soluble and insoluble protein fractions of *rom3*::*gfp* gametocytes and ookinetes and then examined the presence of ROM3 protein using antibodies against the GFP tag. Unfortunately, we were unable to unambiguously identify ROM::GFP in either fraction, presumably due to the very low expression of ROM3 in these stages (data not shown).

Discussion

The discovery of critical roles for certain rhomboid proteins in motility, host cell invasion and pathogenesis of apicomplexan parasites has attracted considerable attention. However, 10 years after their initial discovery, only two of the eight rhomboids of malaria parasites, ROM1 and ROM4, have been analysed in more detail. Multiple roles have been suggested for ROM1 and ROM4: invasion of red blood cells (RBC) (O'Donnell *et al*., 2006), sporozoite gliding motility (Ejigiri *et al*., 2012) and the formation of the PVM in infected hepatocytes (Vera *et al*., 2011). In this study, we investigated expression patterns of all eight *P. berghei* rhomboids and examined the effects of rhomboid gene deletion across the entire life cycle of the parasite in order to pinpoint additional, new role for this intramembrane protease family. In line with previously published work, our studies support the observations that ROM1 is dispensable for parasite development throughout the life cycle (Srinivasan *et al*., 2009; Vera *et al*., 2011) and that ROM4 is essential for asexual blood stage development (O'Donnell *et al*., 2006). We identified three more rhomboids that are dispensable for asexual blood stage development: ROM3, ROM9 and ROM10. Mutants lacking expression of ROM9 and ROM10 can complete the entire life cycle without major developmental defects. These observations indicate functional redundancy for several rhomboids (ROM1, 9 and 10) and suggest that processing of essential substrates may be fulfilled by more than one protease. ROM4 and ROM1 are targeted to different cellular locations in the merozoite – surface and microneme (O'Donnell *et al*., 2006) – making it unlikely that they process identical substrates that would allow ROM4 to compensate for ROM1 in the Δ*rom1* mutant, and clearly not vice versa.

The repeated failure to delete ROM4, ROM6, ROM7 and ROM8 genes indicate that these rhomboids play key and most likely independent roles during blood stage development that cannot be met by other proteins. Located on the merozoite surface, *P. falciparum* ROM4 is strongly implicated in the shedding of the erythrocyte binding antigen 175 (EBA175) during merozoite invasion (O'Donnell *et al*., 2006). Rodent malaria parasites lack EBA175 but express a homologue of EBA140 (BAEBL) which also belongs to the same EBL (erythrocyte-binding-like) TM protein family. Similar to EBA175, *P. falciparum* EBA140 is also an *in vitro* substrate of ROM4 (Baker *et al*., 2006), and in *P. yoelii* EBA140 (PY04764) is essential for RBC invasion (Otsuki *et al*., 2009). Interestingly, in *P. berghei* the related protein, PBANKA_133270, also contains a putative cleavage site, similar to the one found in EBA140. Our successful C-terminal tagging of *P. berghei* ROM4 strengthens the notion that the failure to disrupt *rom4* is not due to inaccessibility of this specific locus to genetic modification, but is due to its key role in the enzymatic processing of surface molecules like EBA140. Combined these data suggest that ROM4 shares essential roles in both human and rodent malaria parasites through cleavage of one or more merozoite surface proteins involved in RBC invasion, which cannot be compensated by other rhomboid or non-rhomboid

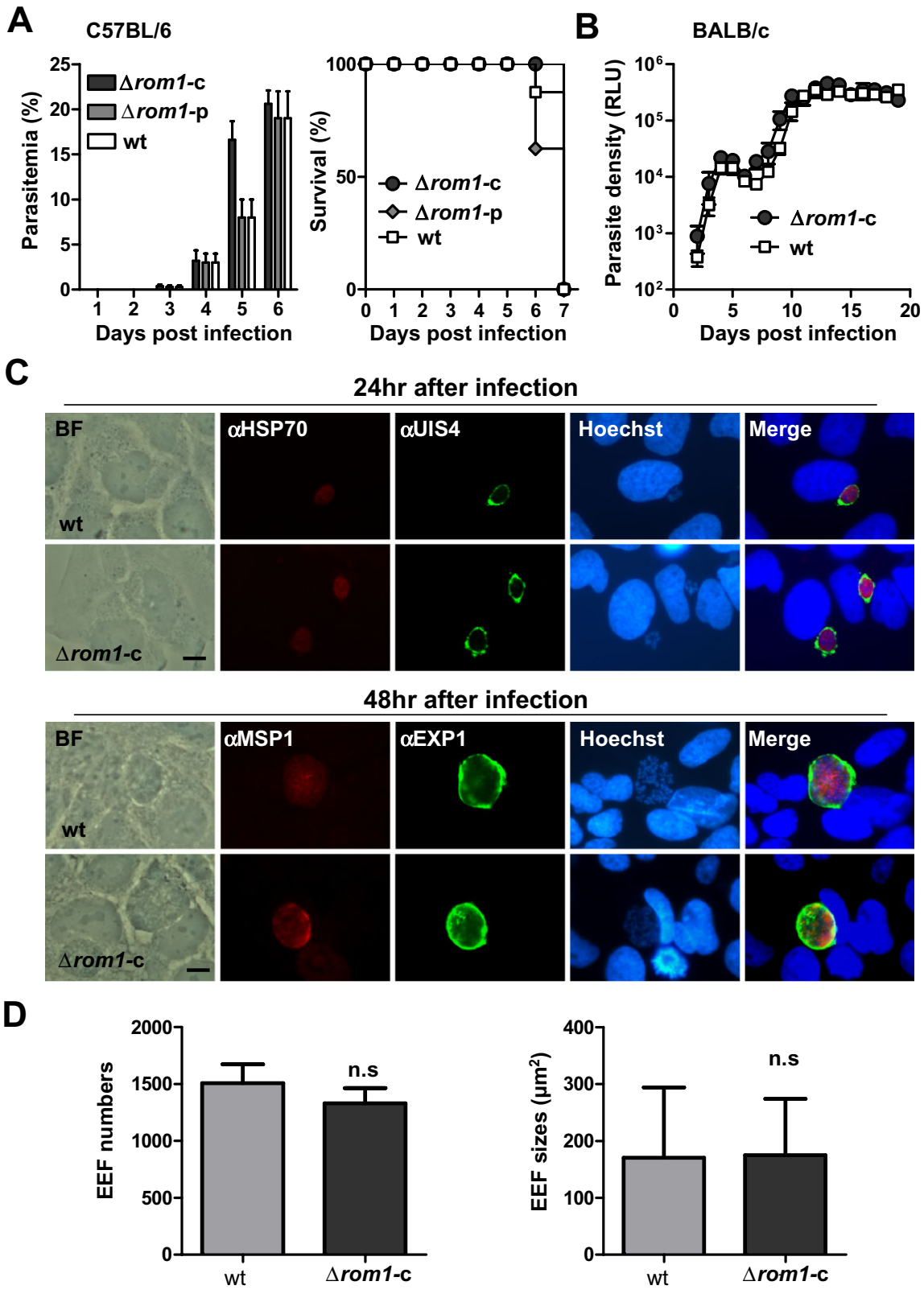
A
C57BL/6
Parasitemia (%)
Δrom1-c
Δrom1-p
wt
Days post infection
Survival (%)
Δrom1-c
Δrom1-p
wt
Days post infection
B
BALB/c
Parasite density (RLU)
Δrom1-c
wt
Days post infection
C
24hr after infection
BF
αHSP70
αUIS4
Hoechst
Merge
wt
Δrom1-c
48hr after infection
BF
αMSP1
αEXP1
Hoechst
Merge
wt
Δrom1-c
D
EEF numbers
n.s
wt
Δrom1-c
EEF sizes (μm²)
n.s
wt
Δrom1-c

Fig. 4. Blood and liver stage development of Δ*rom1* parasites.
A. The course of infection (left panel) and survival curve (right panel) in C57BL/6 mice ($n = 6$) infected with 10^5 wild-type (wt, cl15cy1), Δ*rom1*-p or Δ*rom1*-c. The parasitemia developed in mice infected with wt, Δ*rom1*-p and Δ*rom1*-c parasites are highly comparable during the whole course of infection (left). All C57BL/6 mice infected with wild-type (wt, cl15cy1), Δ*rom1*-p and Δ*rom1*-c parasites developed ECM complications on day 6–7 as indicated by a drop in body temperature below 34°C; mice were sacrificed at this point (right).
B. The course of infection in BALB/c mice ($n = 6$) infected with 10^4 parasites of wild-type (wt, GPF-luc$_{con}$) or Δ*rom1*-c parasites. Parasite densities were determined by measuring luciferase activity indicated as relative light unit (RLU) in the IVDL-assay. Error bars indicate standard deviations in A and B.
C. Immunofluorescence analyses of Δ*rom1*-c and the wild type (wt, GFP-Luc$_{con}$) exo-erythrocytic forms (EEF) at 24 h and 48 h after infection with 1×10^4 Δ*rom1*-c or wild type (GFP-Luc$_{con}$) parasites show normal development of Δ*rom1*-c parasites compared with wild type control. Anti-HSP70 (red) and anti-UIS4 (green) antibodies recognize the parasite's cytoplasm and the PVM. Anti-MSP1 (red) antibodies recognize developing merozoites and anti-EXP1 (green) antibodies stain the PVM. Nuclei were stained with Hoechst-33342 (Blue). BF, bright field; scale bars equals 10 μm.
D. EEF numbers per well of cultured Huh7 cells at 24 h (left) and the sizes of EEFs at 48 h (right) after sporozoite infection. The numbers of EEFs were determined by counting anti-UIS4 staining positive EEFs in the immunofluorescence assay, and the EEF sizes were determined by measuring the sizes of anti-Hsp70 staining positive parasites. The lines indicate mean values and the error bars indicate standard deviations. This figure is available in colour online at wileyonlinelibrary.com.

proteases. ROM4 from another apicomplexan parasite, *T. gondii*, has been established as a sheddase during gliding motility and invasion (Parussini *et al*., 2012). In addition to ROM1 and ROM4, *P. falciparum* ROM7 and ROM8 are also expressed in merozoites (Baker *et al*., 2006). It is, however, unlikely that these proteins process the same TM spanning proteins as ROM1 or ROM4, because they do not show the same *in vitro* substrate specificities as ROM1 or ROM4 (Baker *et al*., 2006). *Plasmodium* ROM7 only has orthologues in the apicomplexan parasites, *Babesia bovis* and *Theileria annulata*, while ROM8 does not cluster with any other apicomplexan rhomboids (Santos *et al*., 2011b).

Plasmodium ROM6 is the orthologue of *T. gondii* ROM6, which clusters with the PARL-like mitochondrial rhomboids and localizes to the single mitochondrion (Santos *et al*., 2011b); however, a mitochondrial location in *Plasmodium* has yet to be confirmed. These ROM6 proteins share common features in their TM domains and catalytic sites, which are characteristic for PARL-type rhomboids (Lemberg and Freeman, 2007), and contain predicted mitochondrial-targeting sequence (Verma *et al*., 2010). Known conserved substrates of PARL-type rhomboids are dynamin-related proteins (McQuibban *et al*., 2003; Dowse and Soldati, 2005). *Plasmodium* species express two conserved dynamins: DYN1 (PBANKA_090360) and DYN2 (PBANKA_052040). Interestingly, phylogenetic analyses show that *Plasmodium* DYN2 clusters with dynamins of other species that are mainly implicated in the division of the mitochondrial outer membrane (Charneau *et al*., 2007). Attempts to disrupt the *dyn2* gene were unsuccessful (Gunnar R. Mair and Chris J. Janse, unpubl. data; http://www.pberghei.eu/index.php?rmgm=765), suggesting its essential role in asexual stage parasites. Further research is needed to determine whether DYN2 is the substrate of ROM6 and protein localization studies with tagged proteins or antibodies may reveal whether both proteins are indeed located in the mitochondria in blood stages.

Although ROM1 is not essential for blood stage parasites, it has been reported that *P. berghei* and *P. yoelii* mutants lacking ROM1 exhibit a slight growth delay and appear less virulent in mice than wild type parasites (Srinivasan *et al*., 2009; Vera *et al*., 2011). In contrast, we were unable to detect either a growth or virulence-attenuation phenotype in experiments conducted with two independent *P. berghei* Δ*rom1* lines. The cause for these discrepancies in blood stage phenotypes between our and the *P. berghei* mutant reported by Srinivasan *et al*. (2009) is unknown. In the study of Srinivasan *et al*. (2009), the mutant clone examined was derived from a single transfection experiment that generated a 3′ end truncation of the gene encoding ROM1, preserving a large part of the ROM1 protein. We were able to detect a stable, although truncated, transcript transcribed from the 5′ end of the gene in the Δ*rom1*-p mutant; whether these are translated into stable, truncated proteins that are inserted into the membrane exerting a dominant-negative effect is unknown. Cloned lines of wild type *P. berghei* ANKA parasites are known to differ in growth and virulence characteristics (Amani *et al*., 1998) and environmental factors have been shown to influence the course of infections in mice (Levander *et al*., 1995); such differences between laboratories may influence the outcome of phenotypic analyses of genetically identical mutants. Therefore, the reported growth and virulence phenotype may be unrelated to the disruption of *rom1*.

In contrast to normal blood stage infections of the mutants reported in this study, we found that Δ*rom1* parasites have a slight defect in liver stage development with a consistent delay of 1 day in blood stage patency following sporozoite infection. A prolonged prepatent period was also observed by Srinivasan *et al*. (2009). This finding was confirmed by a twofold reduction in liver stage development of *P. yoelii* Δ*rom1* parasites (Vera *et al*., 2011). It has been suggested that this reduction in *P. yoelii* liver development results from reduced cleavage of the PVM protein UIS4 (upregulated in sporozoites 4) (Vera *et al*.,

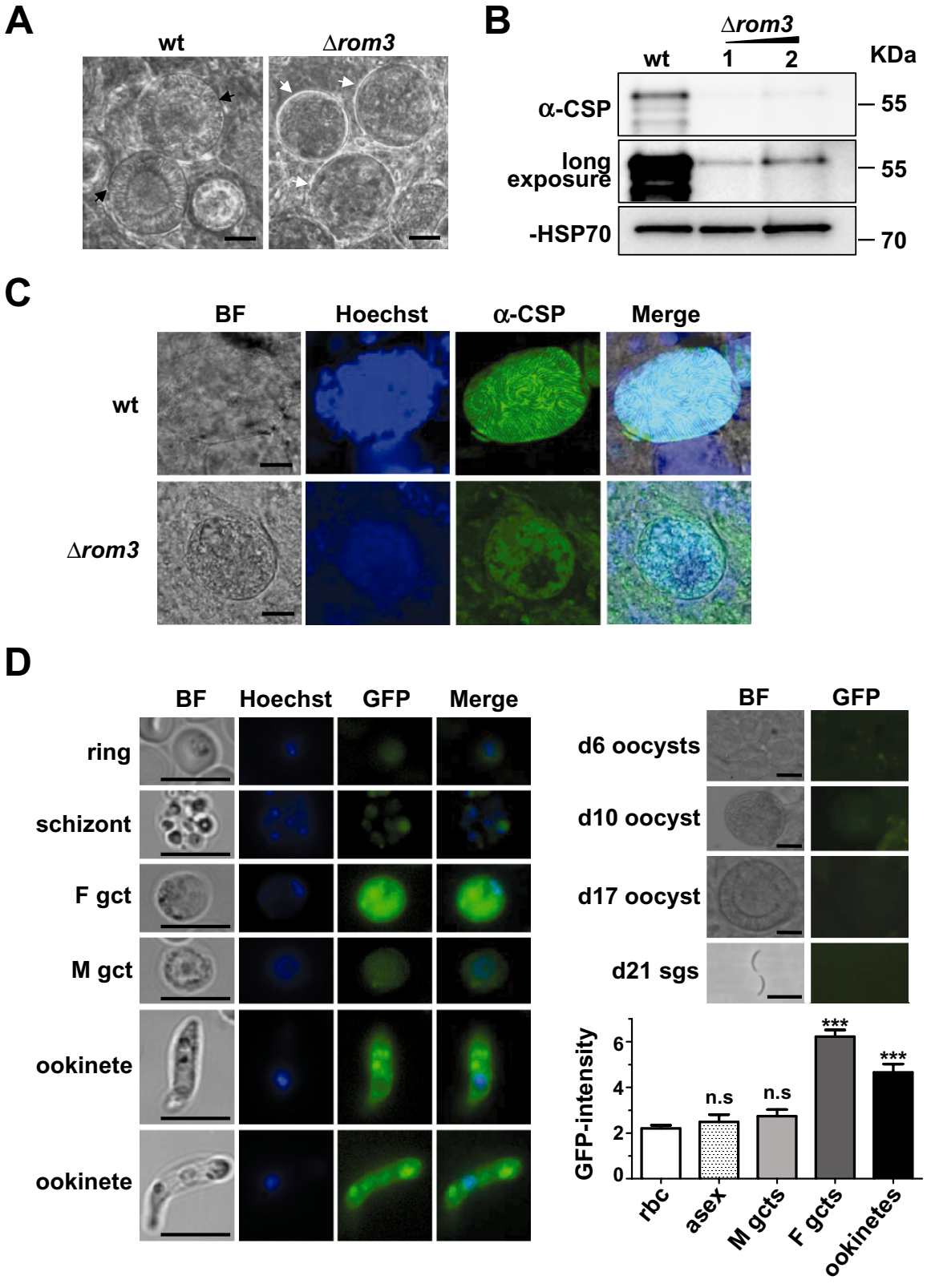
A
wt
Δrom3
B
Δrom3
wt
1
2
KDa
α-CSP
55
long exposure
55
-HSP70
70
C
BF
Hoechst
α-CSP
Merge
wt
Δrom3
D
BF
Hoechst
GFP
Merge
ring
schizont
F gct
M gct
ookinete
ookinete
BF
GFP
d6 oocysts
d10 oocyst
d17 oocyst
d21 sgs
GFP-intensity
0
2
4
6
n.s
n.s
***
***
rbc
asex
M gcts
F gcts
ookinetes

Fig. 5. Rhomboid 3 is essential for sporozoite formation in oocysts.
A. Phase contrast microscopy of wild type and aberrant, vacuolated Δ*rom3* oocysts on day 12 after mosquito infection. Mutants lack any signs of sporozoite formation (white arrow) whereas wild type (wt) oocysts collected on the same day show clear sporulation (black arrow). Scale bar 10 μm.
B. Western blot analysis of midguts from infected mosquitoes. Midguts from mosquitoes infected with Δ*rom3* (1 or 2 midguts, day 10) and wild-type (wt, day 10) were separated on SDS-PAGE and stained with anti-CSP and anti-HSP70 antibodies. A longer exposure of the anti-CSP blot is also shown.
C. Developmental defects of Δ*rom3* parasites examined by immunofluorescence assays. Compared with wild-type (wt), Δ*rom3* oocyst show decreased CSP expression as shown by staining oocysts with anti-CSP (green) antibody and reduced staining with the DNA-specific dye Hoechst-33342 (blue), indicating less DNA replication. BF, bright field. Scale bar 10 μm.
D. All *rom3::gfp* female gametocytes (F gct; $n = 50$) and ookinetes ($n > 100$) exhibited a GFP signal that was significantly above background values (***$P < 0.0001$, Student's *t*-test). No GFP signals above background were detected in either male gametocyte (M gct; $n = 30$) or asexual blood stages. In the mosquito vector no GFP signals were detected in either *rom3::gfp* oocysts (6–17 days after mosquito infection) or in salivary gland sporozoites (sgs, day 21). Nuclei are stained with Hoechst-33342 (blue). BF, bright field. Scale bar 10 μm. n.s, not significant, Student's *t*-test. This figure is available in colour online at wileyonlinelibrary.com.

2011). However, when we analysed liver stage development of *P. berghei* Δ*rom1* parasites, we did not find evidence for the aborted liver stage development or parasites with unusual PVM morphology. In addition to the prolonged prepatent period, we did observe a decrease in sporozoite invasion rate in two out of three experiments. However, since there are discrepancies in Δ*rom1-c* sporozoite-hepatocyte invasion rates, we cannot conclude that a reduction in invasion is responsible for the delay in the prepatent period. Altogether, the phenotypic observations of different Δ*rom1* parasites prove that ROM1 is not essential throughout the complete life cycle in both *P. berghei* and *P. yoelii*. In addition to ROM1, our loss-of-function analyses indicate that there is large degree of functional redundancy of *Plasmodium* rhomboids. We identified two other rhomboids, ROM9 and ROM10, which are dispensable throughout the complete life cycle. Both rhomboids are exclusive to *Plasmodium* (Santos *et al*., 2011b). Interestingly, ROM9 carries a mitochondrial targeting sequence (MitoProtII http://ihg.gsf.de/ihg/mitoprot.html) but its predicted topology is atypical of mitochondrial PARL-like rhomboids (Lemberg and Freeman, 2007). ROM10 lacks key residues predicted to be critical to rhomboid proteolysis (Baker *et al*., 2006; Lemberg and Freeman, 2007) and is therefore likely an inactive rhomboid. Although the expression of ROM10 was detected in multiple stages in *P. falciparum*, and our RT-PCR and Northern analyses also confirmed its expression in blood stage, the gene-deletion mutant showed no phenotypic defect throughout the entire life cycle.

In contrast to the Δ*rom1*, Δ*rom9* and Δ*rom10* parasites, mutants lacking ROM3 expression exhibit a strong and distinct phenotype. The gene encoding ROM3 is highly transcribed in gametocytes and in the *rom3*::*gfp* mutant, the GFP signal was clearly observed in female gametocytes through to the ookinete stage but was absent from developing oocysts and sporozoites. *P. berghei* mutants lacking ROM3 are capable of producing normal numbers of oocysts; however, these oocysts show a complete absence of sporozoite formation. This is the first apicomplexan rhomboid identified to play such a vital role in sporogony. Mutant oocysts show clear signs of stalled DNA replication and a failure to form individual sporozoites, and remain highly vacuolated. This 'delayed phenotype' in mutants which lack proteins normally expressed in female gametocytes/gametes but only manifest the consequences of the loss-of-function in maturing oocysts is not unique. Examples include several members of the LCCL/lectin adhesive-like protein (CCp/LAP) family with their distinct Lgl1(LCCL)-lectin adhesive domains (Raine *et al*., 2007). Deletion of these also female gametocyte expressed genes produces a phenotype in maturing oocysts comparable to the one observed in the Δ*rom3* parasites; vacuolated oocysts and absence of sporozoite formation (Raine *et al*., 2007; Ecker *et al*., 2008; Lavazec *et al*., 2009). CCp/LAP proteins have no TM domains and therefore are unlikely ROM3 substrates. They are localized to the crystalloid body in ookinetes which has been postulated to constitute a reservoir of proteins synthesized by the gametocyte to be used during oocyst growth and sporozoite development (Garnham *et al*., 1962; 1969; Saeed *et al*., 2010). However, ultrastructure analysis of the Δ*rom3* and wild-type ookinetes revealed no distinct differences with respect to their crystalloid bodies. In addition, although we observed a punctate location of ROM3::GFP in ookinetes, we did not observe the crystalloid-type location that was shown for LAP2 and LAP3 (Saeed *et al*., 2010). A failure of oocysts to sporulate also occurs in the absence of three other membrane-bound proteins: glycosyl phosphatidyl inositol (GPI) anchored CSP (PBANKA_040320) (Menard *et al*., 1997), or TM domain containing plasmepsin VI (PBANKA_040970) (Ecker *et al*., 2008) and PBANKA_130960 (Lasonder *et al*., 2008). CSP is localized on the oocyst plasma membrane and on the inner surface of the oocyst capsule; when budding begins, large amounts of CSP cover the surface of sporoblasts and sporozoites (Thathy *et al*., 2002). Our analyses of CSP expression and processing in Δ*rom3* parasites show that although CSP expression is strongly reduced (Figs 5B and S4), process-

ing appears to be normal (Fig. S4). Given that CSP contains a GPI anchor it is unlikely to be processed by ROM3. As most identified natural substrates of rhomboid proteases contain only a single TM domain, it is questionable if PBANKA_130960 is a substrate since it has several putative TM domains (http://www.plasmodb.org). In Table S5 we provide a list of putative substrates of ROM3, based on the published proteome data of oocysts and sporozoite proteins (http://www.plasmoDB.org), which are predicted to contain a single TM domain and encode a signal peptide. Whether plasmepsin VI is the substrate of ROM3 and contributes to the phenotype observed in ROM3-deficient mutants remains to be investigated. Since we observe expression of ROM3 in gametocytes and ookinetes and not in developing and mature oocysts, it is very much possible that the ROM3 substrate(s) is (are) also present and cleaved in gametocytes/ookinetes.

In this study we have examined all eight rhomboid proteases encoded by *P. berghei* and found four of them (ROM4, 6, 7 and 8) to be critical for asexual development, and one (ROM3) essential for mosquito development. While some member of these rhomboids may govern processes common to a large number of eukaryotic species (for example, the mitochondrial PARL-like rhomboid ROM6), most of them are unique to Apicomplexa and some unique to *Plasmodium*. These specific rhomboids and their substrates offer themselves as targets for anti-parasite interventions. While the exact nature of the function of most rhomboids and their substrate range remain to be elucidated, this study helps provide a clear framework of expression, function in parasite development and the specific and redundant enzymatic activities of this important class of proteases.

Experimental procedures

Experimental animals and P. berghei *ANKA reference lines*

Female C57BL/6, BALB/c and Swiss OF1 mice (6–8 weeks) and male C57BL/6 (6–8 weeks) from Charles River were used. All animal experiments performed at the LUMC were approved by the Animal Experiments Committee of the Leiden University Medical Center (DEC 07171; DEC 10099). The Dutch Experiments on Animal Act is established under European guidelines (EU directive no. 86/609/EEC regarding the Protection of Animals used for Experimental and Other Scientific Purposes). Animals used at the Instituto de Medicina Molecular, Faculdade de Medicina, Universidade de Lisboa, were housed in the Specific Pathogen Free facilities of the Institute. All experimental procedures were carried strictly within the rules of the Portuguese official Veterinary Directorate (Direcção Geral de Veterinária), which complies with the European Guideline 86/609/EC and follows the FELASA (Federation of European Laboratory Animal Science Associations) guidelines and recommendations concerning laboratory animal welfare.

Three reference *P. berghei* ANKA parasite lines were used for generation of the gene-deletion mutants and the transgenic parasites: the 'wild type' (wt) line cl15cy1 (Janse *et al.*, 2006b) and two reporter lines, i.e. *Pb*GFP-LUC$_{con}$ (line 676m1cl1; mutant RMgm-29; http://www.pberghei.eu) and *Pb*GFP-Luc$_{schz}$ (line 1037cl1; mutant RMgm-32; http://www.pberghei.eu). Both reporter lines were generated in the cl15cy1 parent line and express the fusion protein GFP-Luciferase either under the control of the constitutive *eef1*α promoter or the schizont-specific *ama1* promoter respectively. The *gfp-luc* expression cassette is stably integrated into the *pb230p* locus without introduction of a drug-selectable marker (Janse *et al.*, 2006a; Spaccapelo *et al.*, 2010).

RT-PCR analyses

To investigate the transcription pattern of the different rhomboid genes, RT-PCR was performed for each gene using cDNA from (i) asexual blood stages of a non-gametocyte producer *P. berghei* ANKA parasite line (HPE) (Janse *et al.*, 1989), (ii) purified gametocytes of wild type *P. berghei* ANKA (cl15cy1) parasites and (iii) salivary gland sporozoites of wild type *P. berghei* ANKA (cl15cy1). Primers were designed specific to the ORF of each gene and across introns when possible in order to distinguish amplicons from gDNA and cDNA. Details of the primers and expected sizes are shown in Table S4.

Generation of gene deletion mutants

To disrupt the *rhomboid* genes, the following replacement constructs were generated. Plasmid constructs targeting *rom1*, *3*, *4*, and *10* were constructed in the generic plasmid pL0001 (http://www.mr4.com) which contains the pyrimethamine resistant *Toxoplasma gondii* (*tg*) dihydrofolate reductase-thymidylate synthase (*dhfr/ts*) as a selectable marker (SM) under the control of *P. berghei dhfr/ts* promoter. Targeting regions for homologous recombination were PCR-amplified from *P. berghei* ANKA (cl15cy1) genomic DNA using primers specific for the 5′ or 3′ ends of each *rhomboid* gene (see Table S2 for the primer sequences) and cloned in upstream and downstream, respectively of the SM; this allows integration of the construct into the targeting regions by double cross-over homologous recombination and complete replacement of the ORF. For transfection the gene-deletion constructs were linearized with the appropriate restriction enzymes (Table S2).

Constructs targeting *rom6*, *8* and *9* were generated using a modified two-step PCR method (Lin *et al.*, 2011). Briefly, in the first PCR reaction two fragments of 5′ and 3′ targeting regions (TR) were amplified from *P. berghei* ANKA (cl15cy1) genomic DNA with the primer sets shown in Table S2. The reverse primers of 5′TR and the forward primers of 3′TR have 5′ extensions homologous to the h*dhfr*::y*fcu* selectable marker cassette from pL0048. In the second PCR reaction, the 5′TR and 3′TR were annealed to either side of the selectable marker cassette, and the joint fragment was amplified by the external anchor-tag primers 4661/4662, resulting in the PCR-based targeting constructs. Before transfection,

the PCR-based constructs were digested with *Nru*I (as indicated in primer sequences in Table S2) to remove the 'anchor-tag' and with *Dpn*I that digests any residual uncut pL0048 plasmid.

Transfection and selection of transformed parasites with pyrimethamine was performed using standard technology for the genetic modification of *P. berghei* (Janse *et al*., 2006b). All information on the generation of gene-deletion mutants (as well as unsuccessful disruption attempts), such as DNA constructs and primers, has been submitted to the RMgmDB database of genetically modified rodent malaria parasites (http://www.pberghei.eu).

Clonal parasite lines were obtained from all gene-deletion mutants by the method of limiting dilution. Correct integration of DNA constructs and disruption of the genes was verified by diagnostic PCR analyses (see Table S3 for primers used) and Southern analyses of chromosomes separated by pulsed-field gel electrophoresis hybridized with probes specific for the selectable maker (see Table S3 for primers used) (Janse *et al*., 2006b).

Generation and analyses of parasites expressing ROM3::GFP and ROM4::mCherry

To tag ROM3 C-terminally with GFP, 1.6 kb upstream of the stop codon of *rom3* containing the entire ORF were PCR-amplified from wild-type *P. berghei* ANKA genomic DNA, TOPO-cloned and sequence analysed (see Table S2 for the primers). The fragment was released from pCR2.1-TOPO (Invitrogen) through digestion with *EcoR*V and *BamH*I and ligated into the generic GFP-tagging plasmid pL1200 (Mair *et al*., 2010), resulting in construct pL1079 containing the pyrimethamine resistant *tgdhfr/ts* as a selectable marker. To tag ROM4 with mCherry, the complete ORF of *rom4* (except the stop codon) was PCR-amplified from wild type *P. berghei* ANKA genomic DNA (see Table S2 for the primers used). This ORF was digested with *Spe*I and *Bgl*II, and ligated into *Spe*I/*BamH*I digested vector pL1646 (containing a C-terminal mCherry tag and the *tgdhfr/ts* selectable marker cassette), resulting in construct pL1920. Before transfection, pL1709 was linearized with *Spe*I, and pL1920 was linearized with *BamH*I. Transfection, selection and cloning of transgenic parasites with pyrimethamine was carried out as described above, generating the following transgenic lines, *rom3::gfp* (line 654cl1) and *rom4::mCherry* (line 2143cl1) that express endogenous C-terminally tagged ROM3 and ROM4 respectively. The live GFP or mCherry signals of parasites of the transgenic mutants were examined by fluorescence microscopy (Leica DM-IRBE Flu) after staining with Hoechst-33342 (2 μmol l^{-1}, Sigma, NL) for 15 min at room temperature. The fluorescence intensity was measured using ImageJ software.

Analysis of transcription of rhomboid genes in blood stages of wild type and gene-deletion parasites

Transcript levels were analysed by standard Northern blot analyses. Total RNA was isolated from mixed blood stages or different stages of wild type *P. berghei* ANKA (cl15cy1), non-gametocyte producer line (HPE) and the different gene-deletion mutant lines. Northern blots were hybridized with probes specific for each rhomboid ORF, which had been PCR-amplified from wild-type *P. berghei* ANKA genomic DNA (primers shown in Table S3). As a loading control, Northern blots were hybridized with the oligonucleotide probe L644R that recognizes the large subunit ribosomal RNA (van Spaendonk *et al*., 2001).

In vivo *multiplication rate of asexual blood stages*

The multiplication rate of asexual blood stages in mice is determined during the cloning procedure of each gene-deletion mutant (Spaccapelo *et al*., 2010) and is calculated as follows: the percentage of infected erythrocytes in Swiss OF1 mice injected with a single parasite is quantified at days 8–11 on Giemsa-stained blood films. The mean asexual multiplication rate per 24 h is then calculated assuming a total of 1.2×10^{10} erythrocytes per mouse (2 ml of blood). The percentage of infected erythrocytes in mice infected with reference lines of the *P. berghei* ANKA strain consistently ranges between 0.5 and 2% at day 8 after infection, resulting in a mean multiplication rate of 10 per 24 h (Janse *et al*., 2003; Spaccapelo *et al*., 2010).

Course of parasitemia, virulence and experimental cerebral malaria in mice infected with Δrom1 parasites

The course of parasitemia was determined in BALB/c mice. Groups of six mice were intraperitoneally (i.p) infected with 10^4 Δ*rom1*-c parasites or equal numbers of the parental reporter line *Pb*GFP-LUC_{con}. The course of parasitemia was determined in a luciferase assay (IVDL-assay) (Franke-Fayard *et al*., 2008); *in vivo* parasite growth in mice is quantified by measuring the luciferase activity of GFP-Luciferase expressing parasites in tail blood. The IVDL-assay generates growth-curves that are identical to those obtained by manual counting of parasites in Giemsa-stained smears. In brief, 10 μl tail blood was collected daily from all mice using heparinized capillaries. Samples were stored at −80°C in Eppendorf tubes till further processing for the luciferase assay. Luciferase activity (luminescence) in the samples was measured as described (Franke-Fayard *et al*., 2008; Lin *et al*., 2013).

The capacity of Δ*rom1* to induce features of ECM was analysed in C57BL/6 mice. Groups of six mice were infected with 10^5 *P. berghei* ANKA (cl15cy1), Δ*rom1*-p or Δ*rom1*-c parasites. Onset of ECM in *P. berghei* infection was determined by measurement of a drop in body temperature below 34°C (Spaccapelo *et al*., 2010). The body temperature of infected mice was measured twice a day from day 5 to day 8 after infection using a laboratory thermometer (model BAT-12, Physitemp Instruments, Clifton, NJ) with a rectal probe (RET-2) for mice. When infected mice showed a drop in temperature (below 34°C) the mice were sacrificed.

Gametocyte and ookinete production

Gametocyte production is defined as the percentage of ring forms developing into mature gametocytes during synchronized infections (Janse and Waters, 1995). Ookinete produc-

tion was determined in standard *in vitro* fertilization and ookinete maturation assays and is defined as the percentage of female gametes that develop into mature ookinetes under standardized *in vitro* culture conditions (van Dijk *et al*., 2001). Female gamete and mature ookinete numbers were determined in Giemsa-stained blood smears made 16–18 h post-activation.

Electron microscopy

Ookinetes were cultured *in vitro* as previously described (van Dijk *et al*., 2001); briefly, gametocytes for these assays were obtained from infected mice that had been pretreated with phenylhydrazine and treated with the antimalarial drug sulfadiazine (dissolved in the drinking water at a concentration of 30 mg l^{-1}) to obtain highly pure gametocyte populations (Beetsma *et al*., 1998). Ookinetes from these cultures were purified using a Nycodenz density gradient centrifugation. The purified ookinetes were diluted in RPMI medium (without serum) and fixed by resuspending them in an equal amount of 3% glutaraldehyde (Electron Microscopy Sciences, Hatfield, PA) in 0.2 M sodium cacodylate pH 7.4 (1 h at RT), washed twice with cacodylate buffer (spinning for 2 min at 425 *g*), post-fixed with 1% osmium tetroxide (Electron Microscopy Sciences, Hatfield, PA) in cacodylate buffer (1 h at RT), and washed again with cacodylate buffer. Subsequently, the samples were stained with an aqueous solution of 1% uranyl acetate for 40 min at RT, washed twice with demineralized water, resuspended in 3% agar (Difco Laboratories, Detroit, Michigan; in demineralized water at 60°C), centrifuged (for 2 min at 425 *g*) and stored at 4°C until the agar became solid. The samples were dehydrated in series of washes 70% (overnight), 80% (10 min), 90% (10 min) and 100% ethanol (1 h, refreshing two times), infiltrated with a 1:1 mixture of epon LX 112/propylene oxide (1 h) and pure epon (3 h), followed by embedding in epon and polymerization for 48 h at 60°C. The samples were cut using a Leica UC6 ultramicrotome at RT into 100nM sections with a Diatome ultra 45°diamond knife (Diatome, Switzerland) at a cutting speed of 1 mm s^{-1}. The sections were attached to slot copper grids (Stork Veco BV, Eerbeek, the Netherlands), covered with 1% formvar film and a 7 nm carbon layer; no post-staining was applied prior to data collection. Imaging was performed in a Tecnai 12 Twin transmission electron microscope (FEI Company). Transmission electron microscope was operated at an acceleration voltage of 80 kV, and binned images (2k × 2k) were acquired with a FEI Eagle CCD camera (FEI Company).

Oocyst and sporozoite production in Anopheles stephensi *mosquitoes*

For mosquito transmission experiments female *A. stephensi* mosquitoes were fed on mice infected with wild-type parasites or mutants. Oocyst development, oocyst production and sporozoite production was monitored in infected mosquitoes as described (Sinden, 1997). Oocyst and sporozoites numbers were counted in infected mosquitoes at 11–14 days and 19–22 days after infection respectively. Salivary gland sporozoites were isolated and counted as described (Annoura *et al*., 2012).

For Western blot analysis of CSP expression in oocysts or sporozoites, we isolated oocysts containing midguts from infected mosquitoes, or 100 000 midgut sporozoites, and proteins were separated on 8% polyacrylamide gels and transferred to nitrocellulose membranes by electroblotting. CSP expression was detected by incubation of membranes with monoclonal anti-CSP antibody (Potocnjak *et al*., 1980) followed by incubation with horseradish-peroxidase-conjugated anti-mouse antibody (Sigma). Immunostained protein complexes were visualized by enhanced chemiluminescence (Amersham). For the IFA, midguts of infected mosquitoes were isolated in RPMI-Medium and immobilized with 2% formaldehyde, 0.2% glutaraldehyde, 2 mM magnesium chloride, 0.02% Triton X-100 in phosphate-buffered saline (PBS). Subsequently midguts were permeabilized, using 2% Saponin in PBS and oocysts stained with monoclonal anti-CSP antibody and monoclonal Alexa-Fluor® 488 goat anti-mouse antibody. DNA was stained with Hoechst-33342.

Sporozoite infectivity and liver stage development

Sporozoites were collected at days 19–25 after infection by hand-dissection of the salivary glands as described (Annoura *et al*., 2012). Gliding motility of sporozoites was determined in assays that were performed on anti-P. *berghei* CSP antibody (3D11, monoclonal mouse antibody 25 μg ml^{-1}, 100 μl per well) pre-coated 10-well cell-line diagnostic microscope slides (7 mm, Thermo Scientific) to which 1×10^4 sporozoites were added (van Dijk *et al*., 2005). After 30 min of incubation at 37°C sporozoites were fixed with 4% paraformaldehyde and after washing with PBS, the sporozoites and the trails ('gliding circles') were stained with anti-CSP-antiserum (Yoshida *et al*., 1980) and anti-rabbit IgG-secondary antibody (Alexa Fluor® 488 Goat Anti-rabbit IgG; Molecular Probes®, Invitrogen). Slides were mounted with Vectorshield (Vector Laboratories) and 'gliding circles' were analysed using a Leica DMR fluorescence microscope at 1000× magnification.

Huh-7 cells, a human hepatoma cell line, were used in *in vitro* analysis of sporozoite infectivity. Huh-7 cells were cultured in 'complete' RPMI 1640 medium supplemented with 10% (vol/vol) fetal bovine serum (FBS), 1% (vol/vol) penicillin-streptomycin, 1% (vol/vol) GultaMAX (Invitrogen), and maintained at 37°C with 5% CO_2. Sporozoite hepatocyte traversal was determined in assays as described previously (Mota *et al*., 2001). Briefly, Huh-7 cells were suspended in 1 ml of 'complete' medium and were seeded in 24-well plates (10^5 cells ml^{-1}). After the Huh7 monolayers were > 80% confluent, 10^5 sporozoites were added with the addition of FITC- or Alexa-647-labelled dextran (Invitrogen, NL) for 2 h. No sporozoites were added to the negative control wells. *In vitro* invasion rates of mutants lacking expression of rhomboids and wild type parasites were determined by the ratio between the number of sporozoites inside the cells and the total number of sporozoites (both inside and outside of cells). Huh-7 cells (5×10^4 cells per well) were seeded into coverslips in 24-well plates and on the following day, cells were infected with 5×10^4 sporozoites. Three hours after infection, cells were fixed with 4% paraformaldehyde in PBS for 20 min. For the double staining, cells were incubated for 30 min in blocking buffer (10% FBS in PBS) followed by 1 h incubation with anti-CSP serum against *P. berghei* CSP protein (Yoshida

et al., 1980) diluted 1:500 in the same buffer. Cells were then washed with PBS and incubated for 45 min with a secondary antibody (anti-rabbit Alexa Fluor® 568) diluted 1:500 in blocking buffer. This procedure only stained the parasites outside the cells. After washing with PBS, cells were fixed with 4% paraformaldehyde in PBS for 30 min, then incubated in for 30 min in permeabilization buffer (1% Triton X-100 in PBS) followed by 1 h incubation with anti-CSP serum diluted 1:500 in the same buffer. Cells were then washed with PBS and incubated for 45 min with a secondary antibody (anti-rabbit Alexa Fluor® 488) diluted 1:500 in blocking buffer. This second staining allows visualization of all the parasites, whether inside or outside the cells. Nuclei were stained with Hoechst-33342. The parasites in both green and red channels were analysed using a DM-IRBE Flu Leica fluorescence microscope.

For analysis of *in vitro* EEF (exo-erythrocytic form) development, 5×10^4 sporozoites were added to a monolayer of Huh7 cells on coverslips in 24-well plates in 'complete' RPMI 1640 (see above). At different time points after infection, cells were fixed with 4% paraformaldehyde, permeabilized with 0.5% Triton X-100 in PBS, blocked with 10% FBS in PBS, and subsequently stained with primary and secondary antibodies for 2 h and 1 h respectively. Primary antibodies used were anti-PbEXP1 [raised in chicken (Sturm *et al*., 2006)] and anti-UIS4 [raised in rabbit (Mueller *et al*., 2005)], detecting the PVM-resident proteins; anti-PbHSP70 [raised in mouse (van Dijk *et al*., 2005)], detecting the cytoplasmic heat shock protein 70 (PBANKA_081890); and anti-MSP1 (mouse; MRA-78 from MR4; http://www.MR4.org) detecting MSP1 of *P. yoelii* and *P. berghei*. Anti-mouse, -chicken and -rabbit secondary antibodies, conjugated to Alexa Fluor® 488 and 594, were used for visualization (Invitrogen). Nuclei were stained with Hoechst-33342. Cells were mounted in Vectashield (Vector Laboratories) and examined using a DM-IRBE Flu Leica fluorescence microscope.

In addition, intracellular parasite development was determined by measuring the area of the EEFs inside fixed Huh-7 hepatoma cells. Huh-7 cells (5×10^4 cells per well) were seeded into coverslips in 24-well plates and, the following day, cells were infected with 4×10^4 sporozoites. Forty-eight hours after infection, cells were fixed with 4% paraformaldehyde in PBS for 20 min. Cells were stained by incubation for 30 min in blocking/permeabilization buffer (0.5% Triton X-100, 1% BSA in PBS) followed by 1 h incubation with monoclonal antibody 2E6 against *P. berghei* HSP70 diluted 1:500 in the same buffer. Cells were then washed with 0.5% Triton X-100 in PBS and incubated for 45 min with a secondary antibody (anti-mouse Alexa488) diluted 1:400 in blocking/permeabilization buffer. Nuclei were stained with DAPI. Images were acquired with a Zeiss Axiovert 200 M widefield fluorescence microscope and processed using ImageJ.

Hepatocyte infection was determined by measuring the luminescence intensity in Huh-7 cells infected with either the firefly luciferase-expressing Δ*rom9* and the corresponding control line PbGFP-Luc_{schz}. Huh-7 cells infection and culture conditions were as described above. At 57 h after infection, 50 µl of D-Luciferin (Firefly Luciferase Assay Kit, Biotium) were added to 30 µl of lysed samples in white 96-well plates. Luminescence intensity of the samples was measured using a microplate reader (Tecan Infinite M200). The viability of Huh-7 cells was assessed by the AlamarBlue assay (Invitrogen, UK) according to the manufacturer's protocol.

To determine parasite loads by qRT-PCR, sporozoites (5×10^4) were added to a monolayer of Huh7 cells (seeded the day before with 10^5 cells) in 24-well plates in 'complete' DMEM (Dulbecco's modified Eagle's medium) (see above). At different time-points after adding the sporozoites, culture medium was removed, cells washed once with PBS, and cells were resuspended in 200 µl of RLT buffer (Quiagen's MicroRNeasy kit). RNA from these samples was extracted following the manufacturer's instructions. The transcriptor first-strand cDNA synthesis kit (Roche) was used according to the manufacturer's recommendations to make single-stranded cDNA. Real time PCR analysis of *P. berghei* 18S rRNA and human β-actin was performed as described (Ploemen *et al*., 2009).

Flow cytometry analysis was used to determine the parasite load of Δ*rom9* in Huh-7 cell (57 h p.i) compared the wild type control (PbGFP-Luc_{schz}). The infection and culture condition was as described above. Fifty-seven hours after infection, samples for were washed with PBS, incubated with trypsin for 5 min at 37°C and collected in 400 µl of 10% v/v FBS in PBS. Cells were then centrifuged at 0.1 *g* for 5 min, resuspended in 300 µl of 2% v/v FBS in PBS. All samples were analysed on a LSR Fortessa cytometer with the appropriate settings for the fluorophores used. Data acquisition and analysis were carried out using the BD FACSDiva (BD Biosciences) and FlowJo (v6.4.7, FlowJo) software packages respectively.

To determine *in vivo* infectivity of sporozoites, Swiss OF1 mice were infected with 1×10^4 salivary gland sporozoites by intravenous injection, as previously described (Sinden, 1997). Blood stage infections were monitored by analysis of Giemsa-stained thin smears of tail blood collected on days 4–8 after inoculation of sporozoites. The prepatent period (measured in days post sporozoite infection) is defined as the day when a blood stage infection with a parasitemia of 0.5–2% is observed. In addition we determined parasite loads in livers of infected mice by *in vivo* imaging as described (Ploemen *et al*., 2009). In addition, a group of 10 male C57BL/6 mice were inoculated by i.v. injection of 1×10^4 freshly isolated sporozoites of Δ*rom9* or its wild type control PbGFP-Luc_{schz}. Luciferase activity in the livers of the animals was visualized 44 h after infection using an *in vivo* Imaging System (IVIS Lumina), following i.p injection of D-luciferin dissolved in PBS (100 mg kg^{-1}). Animals were kept under anesthesia during the measurements, which were performed within 3–5 min after the injection of D-luciferin. Bioluminescence imaging was acquired with a 10 cm field of view, medium binning factor and an exposure time of 180 s. Quantitative analysis of bioluminescence was performed by measuring the luminescence signal intensity using the ROI settings of the Living Image® 3.0 software. ROI measurements are expressed in total flux of photons. qRT-PCR is also used to determine the *in vivo* parasite load in liver. After measuring luminescence, livers from 5 mice were collected, homogenized in 4 ml denaturing solution (4 M guanidine thiocyanate; 25 mM sodium citrate pH 7, 0.5% sarcosyl and 0.7% β-Mercaptoethanol in DEPC-treated water) and total RNA was extracted using the RNeasy Mini kit (Qiagen). cDNA was obtained by reverse transcription (First-strand cDNA synthe-

sis kit, Roche) and qRT-PCR using the SybrGreen method (DyNAmoTM HS SYBR® Green qPCR Kit, Finnzymes) was performed with primers specific for *P. berghei* 18S rRNA for quantification of parasite load in the liver of each mouse. Relative amounts of *P. berghei* mRNA were calculated against the Hypoxanthine Guanine Phosphoribosyl Transferase (HPRT) housekeeping gene (Ploemen *et al.*, 2009).

Acknowledgements

We thank Inês S. Albuquerque and Hans Kroeze for technical assistance. Jing-wen Lin is supported by the China Scholarship Council-Leiden University Joint Program and Chris J. Janse, Andy Waters, Kai Matuschewski by a grant of the European Community's Seventh Framework Programme (FP7/2007–2013) under grant agreement no. 242095. Gunnar Mair is supported by FCT (PTDC/BIA-BCM/105610/2008, PTDC/SAU-GMG/104392/2008 and PTDC/SAU-MIC/122082/2010), Patrícia Meireles by FCT grant SFRH/BD/71098/2010 and Miguel Prudêncio by FCT project grant PTDC/SAUMIC/117060/2010.

References

Amani, V., Boubou, M.I., Pied, S., Marussig, M., Walliker, D., Mazier, D., and Renia, L. (1998) Cloned lines of *Plasmodium berghei* ANKA differ in their abilities to induce experimental cerebral malaria. *Infect Immun* **66:** 4093–4099.

Annoura, T., Ploemen, I.H., van Schaijk, B.C., Sajid, M., Vos, M.W., van Gemert, G.J., *et al.* (2012) Assessing the adequacy of attenuation of genetically modified malaria parasite vaccine candidates. *Vaccine* **30:** 2662–2670.

Baker, R.P., Wijetilaka, R., and Urban, S. (2006) Two *Plasmodium* rhomboid proteases preferentially cleave different adhesins implicated in all invasive stages of malaria. *PLoS Pathog* **2:** e113.

Beetsma, A.L., van de Wiel, T.J., Sauerwein, R.W., and Eling, W.M. (1998) *Plasmodium berghei* ANKA: purification of large numbers of infectious gametocytes. *Exp Parasitol* **88:** 69–72.

Ben-Shem, A., Fass, D., and Bibi, E. (2007) Structural basis for intramembrane proteolysis by rhomboid serine proteases. *Proc Natl Acad Sci USA* **104:** 462–466.

Brossier, F., Jewett, T.J., Sibley, L.D., and Urban, S. (2005) A spatially localized rhomboid protease cleaves cell surface adhesins essential for invasion by *Toxoplasma*. *Proc Natl Acad Sci USA* **102:** 4146–4151.

Brossier, F., Starnes, G.L., Beatty, W.L., and Sibley, L.D. (2008) Microneme rhomboid protease TgROM1 is required for efficient intracellular growth of *Toxoplasma gondii*. *Eukaryot Cell* **7:** 664–674.

Buguliskis, J.S., Brossier, F., Shuman, J., and Sibley, L.D. (2010) Rhomboid 4 (ROM4) affects the processing of surface adhesins and facilitates host cell invasion by *Toxoplasma gondii*. *PLoS Pathog* **6:** e1000858.

Charneau, S., Bastos, I.M., Mouray, E., Ribeiro, B.M., Santana, J.M., Grellier, P., and Florent, I. (2007) Characterization of PfDYN2, a dynamin-like protein of *Plasmodium falciparum* expressed in schizonts. *Microbes Infect* **9:** 797–805.

Cipolat, S., Rudka, T., Hartmann, D., Costa, V., Serneels, L., Craessaerts, K., *et al.* (2006) Mitochondrial rhomboid PARL regulates cytochrome *c* release during apoptosis via OPA1-dependent cristae remodeling. *Cell* **126:** 163–175.

van Dijk, M.R., Janse, C.J., Thompson, J., Waters, A.P., Braks, J.A., Dodemont, H.J., *et al.* (2001) A central role for P48/45 in malaria parasite male gamete fertility. *Cell* **104:** 153–164.

van Dijk, M.R., Douradinha, B., Franke-Fayard, B., Heussler, V., van Dooren, M.W., van Schaijk, B., *et al.* (2005) Genetically attenuated, P36p-deficient malarial sporozoites induce protective immunity and apoptosis of infected liver cells. *Proc Natl Acad Sci USA* **102:** 12194–12199.

Dowse, T.J., and Soldati, D. (2005) Rhomboid-like proteins in Apicomplexa: phylogeny and nomenclature. *Trends Parasitol* **21:** 254–258.

Ecker, A., Bushell, E.S., Tewari, R., and Sinden, R.E. (2008) Reverse genetics screen identifies six proteins important for malaria development in the mosquito. *Mol Microbiol* **70:** 209–220.

Ejigiri, I., Ragheb, D.R.T., Pino, P., Coppi, A., Bennett, B.L., Soldati-Favre, D., and Sinnis, P. (2012) Shedding of TRAP by a rhomboid protease from the malaria sporozoite surface is essential for gliding motility and sporozoite infectivity. *PLoS Pathog* **8:** e1002725.

Franke-Fayard, B., Djokovic, D., Dooren, M.W., Ramesar, J., Waters, A.P., Falade, M.O., *et al.* (2008) Simple and sensitive antimalarial drug screening in vitro and in vivo using transgenic luciferase expressing *Plasmodium berghei* parasites. *Int J Parasitol* **38:** 1651–1662.

Freeman, M. (2004) Proteolysis within the membrane: rhomboids revealed. *Nat Rev Mol Cell Biol* **5:** 188–197.

Freeman, M. (2009) Rhomboids: 7 years of a new protease family. *Semin Cell Dev Biol* **20:** 231–239.

Garnham, P.C., Bird, R.G., and Baker, J.R. (1962) Electron microscope studies of motile stages of malaria parasites. III. The ookinetes of *Haemamoeba* and *Plasmodium*. *Trans R Soc Trop Med Hyg* **56:** 116–120.

Garnham, P.C., Bird, R.G., Baker, J.R., Desser, S.S., and el-Nahal, H.M. (1969) Electron microscope studies on motile stages of malaria parasites. VI. The ookinete of *Plasmodium berghei yoelii* and its transformation into the early oocyst. *Trans R Soc Trop Med Hyg* **63:** 187–194.

Janse, C.J., and Waters, A.P. (1995) *Plasmodium berghei*: the application of cultivation and purification techniques to molecular studies of malaria parasites. *Parasitol Today* **11:** 138–143.

Janse, C.J., Boorsma, E.G., Ramesar, J., van Vianen, P., van der Meer, R., Zenobi, P., *et al.* (1989) *Plasmodium berghei*: gametocyte production, DNA content, and chromosome-size polymorphisms during asexual multiplication *in vivo*. *Exp Parasitol* **68:** 274–282.

Janse, C.J., Haghparast, A., Speranca, M.A., Ramesar, J., Kroeze, H., del Portillo, H.A., and Waters, A.P. (2003) Malaria parasites lacking *eef1a* have a normal S/M phase yet grow more slowly due to a longer G1 phase. *Mol Microbiol* **50:** 1539–1551.

Janse, C.J., Franke-Fayard, B., Mair, G.R., Ramesar, J., Thiel, C., Engelmann, S., *et al.* (2006a) High efficiency transfection of *Plasmodium berghei* facilitates novel selection procedures. *Mol Biochem Parasitol* **145:** 60–70.

Janse, C.J., Ramesar, J., and Waters, A.P. (2006b) High-

efficiency transfection and drug selection of genetically transformed blood stages of the rodent malaria parasite *Plasmodium berghei*. *Nat Protoc* **1:** 346–356.

Khan, S.M., Franke-Fayard, B., Mair, G.R., Lasonder, E., Janse, C.J., Mann, M., and Waters, A.P. (2005) Proteome analysis of separated male and female gametocytes reveals novel sex-specific *Plasmodium* biology. *Cell* **121:** 675–687.

Koonin, E.V., Makarova, K.S., Rogozin, I.B., Davidovic, L., Letellier, M.C., and Pellegrini, L. (2003) The rhomboids: a nearly ubiquitous family of intramembrane serine proteases that probably evolved by multiple ancient horizontal gene transfers. *Genome Biol* **4:** R19.

Lasonder, E., Janse, C.J., van Gemert, G.J., Mair, G.R., Vermunt, A.M., Douradinha, B.G., *et al*. (2008) Proteomic profiling of *Plasmodium* sporozoite maturation identifies new proteins essential for parasite development and infectivity. *PLoS Pathog* **4:** e1000195.

Lavazec, C., Moreira, C.K., Mair, G.R., Waters, A.P., Janse, C.J., and Templeton, T.J. (2009) Analysis of mutant *Plasmodium berghei* parasites lacking expression of multiple PbCCp genes. *Mol Biochem Parasitol* **163:** 1–7.

Lemberg, M.K., and Freeman, M. (2007) Functional and evolutionary implications of enhanced genomic analysis of rhomboid intramembrane proteases. *Genome Res* **17:** 1634–1646.

Levander, O.A., Fontela, R., Morris, V.C., and Ager, A.L., Jr (1995) Protection against murine cerebral malaria by dietary-induced oxidative stress. *J Parasitol* **81:** 99–103.

Lin, J.W., Annoura, T., Sajid, M., Chevalley-Maurel, S., Ramesar, J., Klop, O., *et al*. (2011) A novel 'Gene Insertion/Marker Out' (GIMO) method for transgene expression and gene complementation in rodent malaria parasites. *PLoS ONE* **6:** e29289.

Lin, J.W., Sajid, M., Ramesar, J., Khan, S.M., Janse, C.J., and Franke-Fayard, B. (2013) Screening inhibitors of *P. berghei* blood stages using bioluminescent reporter parasites. *Methods Mol Biol* **923:** 507–522.

McQuibban, G.A., Saurya, S., and Freeman, M. (2003) Mitochondrial membrane remodelling regulated by a conserved rhomboid protease. *Nature* **423:** 537–541.

Mair, G.R., Lasonder, E., Garver, L.S., Franke-Fayard, B.M., Carret, C.K., Wiegant, J.C., *et al*. (2010) Universal features of post-transcriptional gene regulation are critical for *Plasmodium* zygote development. *PLoS Pathog* **6:** e1000767.

Menard, R., Sultan, A.A., Cortes, C., Altszuler, R., van Dijk, M.R., Janse, C.J., *et al*. (1997) Circumsporozoite protein is required for development of malaria sporozoites in mosquitoes. *Nature* **385:** 336–340.

Mota, M.M., Pradel, G., Vanderberg, J.P., Hafalla, J.C.R., Frevert, U., Nussenzweig, R.S., *et al*. (2001) Migration of *Plasmodium* sporozoites through cells before infection. *Science* **291:** 141–144.

Mueller, A.K., Camargo, N., Kaiser, K., Andorfer, C., Frevert, U., Matuschewski, K., and Kappe, S.H. (2005) *Plasmodium* liver stage developmental arrest by depletion of a protein at the parasite-host interface. *Proc Natl Acad Sci USA* **102:** 3022–3027.

O'Donnell, R.A., Hackett, F., Howell, S.A., Treeck, M., Struck, N., Krnajski, Z., *et al*. (2006) Intramembrane proteolysis mediates shedding of a key adhesin during erythrocyte invasion by the malaria parasite. *J Cell Biol* **174:** 1023–1033.

Olivieri, A., Collins, C.R., Hackett, F., Withers-Martinez, C., Marshall, J., Flynn, H.R., *et al*. (2011) Juxtamembrane shedding of *Plasmodium falciparum* AMA1 is sequence independent and essential, and helps evade invasion-inhibitory antibodies. *PLoS Pathog* **7:** e1002448.

Otsuki, H., Kaneko, O., Thongkukiatkul, A., Tachibana, M., Iriko, H., Takeo, S., *et al*. (2009) Single amino acid substitution in *Plasmodium yoelii* erythrocyte ligand determines its localization and controls parasite virulence. *Proc Natl Acad Sci USA* **106:** 7167–7172.

Parussini, F., Tang, Q., Moin, S.M., Mital, J., Urban, S., and Ward, G.E. (2012) Intramembrane proteolysis of *Toxoplasma* apical membrane antigen 1 facilitates host-cell invasion but is dispensable for replication. *Proc Natl Acad Sci USA* **109:** 7463–7468.

Ploemen, I.H., Prudencio, M., Douradinha, B.G., Ramesar, J., Fonager, J., van Gemert, G.J., *et al*. (2009) Visualisation and quantitative analysis of the rodent malaria liver stage by real time imaging. *PLoS ONE* **4:** e7881.

Potocnjak, P., Yoshida, N., Nussenzweig, R.S., and Nussenzweig, V. (1980) Monovalent fragments (Fab) of monoclonal antibodies to a sporozoite surface antigen (Pb44) protect mice against malarial infection. *J Exp Med* **151:** 1504–1513.

Raine, J.D., Ecker, A., Mendoza, J., Tewari, R., Stanway, R.R., and Sinden, R.E. (2007) Female inheritance of malarial lap genes is essential for mosquito transmission. *PLoS Pathog* **3:** e30.

Saeed, S., Carter, V., Tremp, A.Z., and Dessens, J.T. (2010) *Plasmodium berghei* crystalloids contain multiple LCCL proteins. *Mol Biochem Parasitol* **170:** 49–53.

Santos, J.M., Ferguson, D.J., Blackman, M.J., and Soldati-Favre, D. (2011a) Intramembrane cleavage of AMA1 triggers *Toxoplasma* to switch from an invasive to a replicative mode. *Science* **331:** 473–477.

Santos, M., Graindorge, A., and Soldati-Favre, D. (2011b) New insights into parasite rhomboid proteases. *Mol Biochem Parasitol* **182:** 27–36.

Sinden, R.E. (1997) Infection of mosquitoes with rodent malaria. In *Molecular Biology of Insect Disease Vectors: A Method Manual*. Crampton, J.M., Beard, C.B., and Louis, C. (eds). London: Chapman and Hall, pp. 67–91.

Spaccapelo, R., Janse, C.J., Caterbi, S., Franke-Fayard, B., Bonilla, J.A., Syphard, L.M., *et al*. (2010) Plasmepsin 4-deficient *Plasmodium berghei* are virulence attenuated and induce protective immunity against experimental malaria. *Am J Pathol* **176:** 205–217.

van Spaendonk, R.M., Ramesar, J., van Wigcheren, A., Eling, W., Beetsma, A.L., van Gemert, G.J., *et al*. (2001) Functional equivalence of structurally distinct ribosomes in the malaria parasite, *Plasmodium berghei*. *J Biol Chem* **276:** 22638–22647.

Srinivasan, P., Coppens, I., and Jacobs-Lorena, M. (2009) Distinct roles of *Plasmodium* rhomboid 1 in parasite development and malaria pathogenesis. *PLoS Pathog* **5:** e1000262.

Stevenson, L.G., Strisovsky, K., Clemmer, K.M., Bhatt, S., Freeman, M., and Rather, P.N. (2007) Rhomboid protease AarA mediates quorum-sensing in *Providencia stuartii* by

activating TatA of the twin-arginine translocase. *Proc Natl Acad Sci USA* **104:** 1003–1008.
Sturm, A., Amino, R., van de Sand, C., Regen, T., Retzlaff, S., Rennenberg, A., *et al.* (2006) Manipulation of host hepatocytes by the malaria parasite for delivery into liver sinusoids. *Science* **313:** 1287–1290.
Sundaram, M.V. (2004) Vulval development: the battle between Ras and Notch. *Curr Biol* **14:** R311–R313.
Thathy, V., Fujioka, H., Gantt, S., Nussenzweig, R., Nussenzweig, V., and Menard, R. (2002) Levels of circumsporozoite protein in the *Plasmodium* oocyst determine sporozoite morphology. *EMBO J* **21:** 1586–1596.
Urban, S., Lee, J.R., and Freeman, M. (2001) Drosophila rhomboid-1 defines a family of putative intramembrane serine proteases. *Cell* **107:** 173–182.
Urban, S., Lee, J.R., and Freeman, M. (2002a) A family of Rhomboid intramembrane proteases activates all Drosophila membrane-tethered EGF ligands. *EMBO J* **21:** 4277–4286.
Urban, S., Schlieper, D., and Freeman, M. (2002b) Conservation of intramembrane proteolytic activity and substrate specificity in prokaryotic and eukaryotic rhomboids. *Curr Biol* **12:** 1507–1512.
Vera, I.M., Beatty, W.L., Sinnis, P., and Kim, K. (2011) *Plasmodium* protease ROM1 is important for proper formation of the parasitophorous vacuole. *PLoS Pathog* **7:** e1002197.
Verma, R., Varshney, G.C., and Raghava, G.P. (2010) Prediction of mitochondrial proteins of malaria parasite using split amino acid composition and PSSM profile. *Amino Acids* **39:** 101–110.
Wang, Y., Zhang, Y., and Ha, Y. (2006) Crystal structure of a rhomboid family intramembrane protease. *Nature* **444:** 179–180.
Wu, Z., Yan, N., Feng, L., Oberstein, A., Yan, H., Baker, R.P., *et al.* (2006) Structural analysis of a rhomboid family intramembrane protease reveals a gating mechanism for substrate entry. *Nat Struct Mol Biol* **13:** 1084–1091.
Yoshida, N., Nussenzweig, R.S., Potocnjak, P., Nussenzweig, V., and Aikawa, M. (1980) Hybridoma produces protective antibodies directed against the sporozoite stage of malaria parasite. *Science* **207:** 71–73.

Supporting information

Additional supporting information may be found in the online version of this article at the publisher's web-site.

Journal of Medicinal Chemistry

Article

pubs.acs.org/jmc

Tetraoxane–Pyrimidine Nitrile Hybrids as Dual Stage Antimalarials

Rudi Oliveira,[†] Rita C. Guedes,[†] Patrícia Meireles,[‡] Inês S. Albuquerque,[‡] Lídia M. Gonçalves,[†] Elisabete Pires,[§] Maria Rosário Bronze,[†,§] Jiri Gut,[∥] Philip J. Rosenthal,[∥] Miguel Prudêncio,[‡] Rui Moreira,*[,†] Paul M. O'Neill,*[,⊥] and Francisca Lopes[†]

[†]Instituto de Investigação do Medicamento (iMed.ULisboa), Faculdade de Farmácia, Universidade de Lisboa, Av. Prof. Gama Pinto, 1649-003 Lisboa, Portugal

[‡]Instituto de Medicina Molecular, Faculdade de Medicina da Universidade de Lisboa, Av. Prof. Egas Moniz, 1649-028 Lisboa, Portugal

[§]ITQB-UNL, Av. da República, Estação Agronómica Nacional, 2780-157 Oeiras, Portugal

[∥]Department of Medicine, San Francisco General Hospital, University of California, San Francisco, San Francisco, California 94143, United States

[⊥]Department of Chemistry, University of Liverpool, Liverpool, L69 3BX, U.K.

Supporting Information

ABSTRACT: The use of artemisinin or other endoperoxides in combination with other drugs is a strategy to prevent development of resistant strains of *Plasmodium* parasites. Our previous work demonstrated that hybrid compounds, comprising endoperoxides and vinyl sulfones, were capable of high activity profiles comparable to artemisinin and chloroquine while acting through two distinct mechanisms of action: oxidative stress and falcipain inhibition. In this study, we adapted this approach to a novel class of falcipain inhibitors: peptidomimetic pyrimidine nitriles. Pyrimidine tetraoxane hybrids displayed potent nanomolar activity against three strains of *Plasmodium falciparum* and falcipain-2, combined with low cytotoxicity. In vivo, a decrease in parasitemia and an increase in survival of mice infected with *Plasmodium berghei* was observed when compared to control. All tested compounds combined good blood stage activity with significant effects on liver stage parasitemia, a most welcome feature for any new class of antimalarial drug.

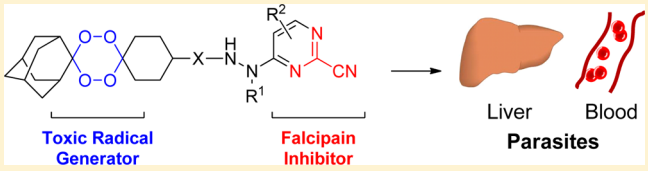

INTRODUCTION

Although the number of deaths caused by *Plasmodium falciparum* malaria has probably decreased in recent years, the disease remains a huge problem in much of the developing world.[1,2] Drug resistance is a major threat, and reports of resistance to artemisinins are alarming, as we are now highly dependent on the use of artemisinin-based combination therapies (ACTs) to treat *falciparum* malaria.[3−5] Semisynthetic artemisinin derivatives (Figure 1) were a major breakthrough in malaria chemotherapy because they produce a very rapid therapeutic response against malaria parasites. ACT, the current recommended treatment for uncomplicated *falciparum* malaria in most of the world, includes five standard regimens, each incorporating a rapid acting artemisinin derivative plus a slower acting drug to kill parasites that may escape the rapid action of the artemisinin and to limit selection of artemisinin-resistant parasites.[6] Artemisinins and other endoperoxides, such as tetraoxane **2** (Figure 1), are highly active against the asexual erythrocytic stage of infection. These compounds are reductively activated in the presence of high concentrations of iron(II) accumulated inside the parasite food vacuole after the digestion of large quantities of host hemoglobin. Although the mechanism of action of artemisinins is still a matter of debate,[7] it is generally accepted that the resulting radicals of this activation can alkylate several targets in the parasite, leading to its death.

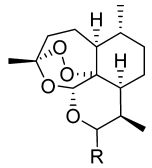

1, R = =O, ART
R = α-OH, DHA
R = β-OMe, AM
R = α-CO(CH$_2$)$_2$CO$_2$H, AS

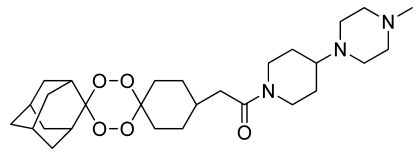

2

Figure 1. Structures of artemisinin, **1**, its derivatives dihydroartemisinin (DHA), artemether (AM), and artesunate (AS) and the tetraoxane RKA182, **2**.

A key feature of hybrid drugs is the presence of different mechanisms of action, against either a single target or different targets.[8] A recent publication associates artemisinin resistance

Received: March 22, 2014
Published: May 13, 2014

   dx.doi.org/10.1021/jm5004528 | J. Med. Chem. 2014, 57, 4916−4923

to a form of antioxidant defense system,[9] so it is particularly important that a distinct mechanisms of action is combined with endoperoxide drugs in the treatment of highly adaptable parasites.[10] We recently reported that tetraoxane−peptide vinyl sulfone hybrids, **3** (Figure 2), are rapidly activated by iron(II),

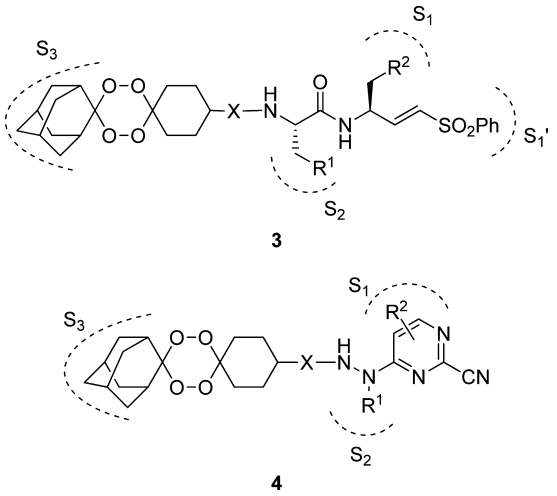

Figure 2. General structures: tetraoxane−vinyl sulfone hybrids **3**; tetraoxane−pyrimidine nitrile hybrids **4**.

releasing a potent irreversible inhibitor of falcipains inside the parasitedigestive vacuole.[11] Falcipain-2 and falcipain-3 are cysteine proteases from *P. falciparum* involved in the digestion of host hemoglobin in the digestive vacuole of the parasite, providing amino acids for its survival and development.[12] Although hybrid compounds **3** displayed weak to moderate falcipain inhibitory activity, they were able to inhibit hemoglobin digestion at low nanomolar concentrations, consistent with the release of the parent peptide vinyl sulfone triggered by iron(II).

To overcome selectivity issues often associated with irreversible inhibitors, it is desirable to develop nonpeptidic reversible inhibitors.[12,13] Nitriles inhibit cysteine proteases by forming a reversible thioimidate intermediate resulting from the nucleophilic attack of the catalytic cysteine residue.[14−18] Several heterocyclic and peptidomimetic compounds containing a nitrile warhead displayed excellent inhibitory activity against falcipain-2 and against cultured *P. falciparum*.[19] In particular, appropriately decorated pyrimidine and triazine scaffolds were shown to position vectors for the S_1, S_2, and S_3 binding pockets and to direct the thioimidate adduct toward the oxyanion hole of the enzyme.[18,19] An interesting feature of pyrimidine nitriles is the possibility to accommodate a wide variety of substituents at P_3, without significantly compromising enzyme inhibition.[19] This observation prompted us to hypothesize that tetraoxane−pyrimidine nitrile constructs with the general structure **4** (Figure 2), in which the peroxide moiety occupies the P_3 position, could be endowed with both falcipain and *P. falciparum* inhibitory activities, in contrast to their hybrid vinyl sulfone counterparts **3**.[11] This approach could provide a new class of hybrid compounds whose ability to inhibit falcipains would not be dependent on the rate of peroxide activation triggered by theiron(II) present in the digestive vacuole of the malaria parasite. We now report the synthesis of tetraoxane−pyrimidine nitrile hybrids **4**, and the evaluation of these compounds against the blood and liver stages of malaria infection, against falcipain-2, against mammalian cells, and in vivo using a murine model of malaria. The adamantane-based tetraoxane moiety was selected throughout this study, as it is known to provide adequate metabolic stability.

RESULTS AND DISCUSSION

Synthesis. Tetraoxane−pyrimidine nitrile hybrids were synthesized as depicted in Schemes 1 and 2. The tetraoxane

Scheme 1. Synthesis of Tetraoxanes 6 and 7[a]

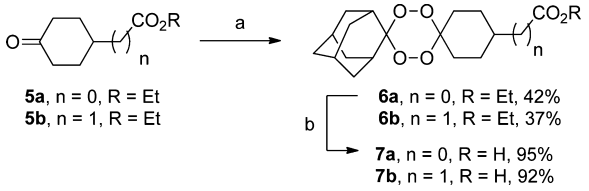

[a]Reagents and conditions: (a) (1) HCO_2H, H_2O_2 50%, ACN, rt, 45 min, (2) 2-adamantanone, Re_2O_7, DCM, rt, 3 h; (b) NaOH, MeOH/H_2O (2:1), 80 °C, 1 h 30 s.

moiety was prepared by reacting the appropriate ketone **5** with hydrogen peroxide 50% in acidic conditions to form a *gem*-dihydroperoxide intermediate, which was then reacted with 2-adamantanone in the presence of rhenium(VII) catalyst to give **6a−b** (Scheme 1).[20,21] The synthesis of the pyrimidine nitrile moiety followed the procedure reported by Coterón et al.[19] Reductive amination of *tert*-butyl carbazate, **8**, with the appropriate aldehyde or ketone and subsequent nucleophilic aromatic substitution reaction of the appropriate 2,4-dichloropyrimidine with hydrazines **9a−c** afforded the 5- and 6-substituted 2-chloropyrimidines **10a−f** (Scheme 2). Cyanation of **10a−f** using potassium cyanide gave the corresponding 2-cyanopyrimidines **11a−f**.[19] Boc removal with *p*-toluenesulfonic acid and subsequent coupling with the acid chloride derived from **7** yielded the final products **4** with poor to moderate yields (Scheme 2, method A). Alternatively, deprotection of the hydrazine **10a−f** followed by coupling with the acid chloride derived from **7** and cyanation of the 2-chloropyrimidine hybrid precursors **12** afforded the final products in moderate to good yields (Scheme 2, method B).

Iron(II) Activation. Compound **13**, lacking the tetraoxane core, was prepared from the reductive cleavage of tetraoxane **4a** using iron(II) bromide in dichloromethane (Scheme 3).[22] This reaction is intended to simulate the intraparasitic endoperoxide iron(II) mediated bioactivation process in the digestive vacuole of the parasite.[11,22] To confirm the proposed mechanism, an aqueous solution of **4a** was treated with high concentration of iron(II) sulfate, and the resulting mixture was analyzed by LC-MS.[22] Decomposition of **4a** into ketone **13** followed first-order decay kinetics, with a half-life of 5.1 h (Figure 3). This value is of the same order of magnitude as those observed with tetraoxanes and 1,2,4-trioxolane analogues with basic side chains, suggesting that the nature of the endoperoxide side chain does not significantly affect the rate of iron(II)-triggered activation.[22]

As depicted in Figure 3, ketone **13** accounts for 50% of the initial concentration of **4a**, indicating that another decomposition pathway is operating under the conditions used. Tetraoxane activation may involve coordination of iron(II) either with O2, leading to the formation of **13**, or with O1, which leads to 2-adamantanone (Supporting Information Scheme S1). Although we were not able to detect 2-

dx.doi.org/10.1021/jm5004528 | J. Med. Chem. 2014, 57, 4916−4923

Scheme 2. Synthesis of Tetraoxanes–Pyrimidine Nitrile Hybrids 4a–g[a]

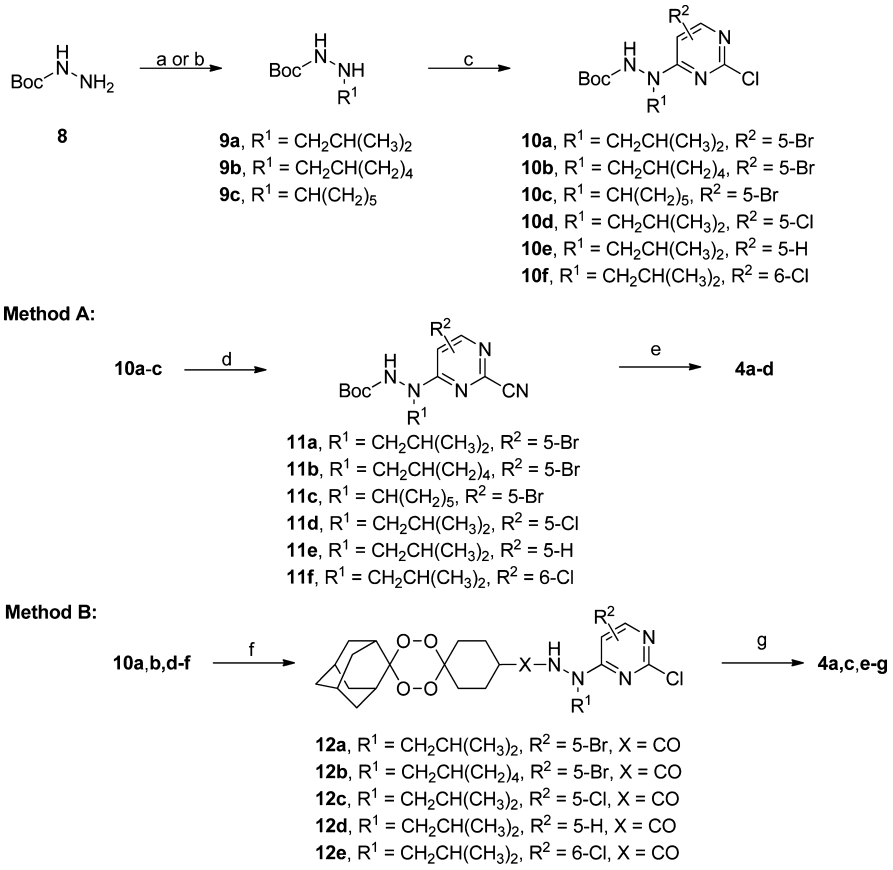

[a]Reagents and conditions: (a) (1) aldehyde, dry DCM, molecular sieves 3 Å (2) Et_3SiH, Pd/C, dry MeOH; (b) aldehyde or ketone, dry DCM, glacial AcOH, $NaBH(OAc)_3$, rt, ov; (c) 2,4-dichloropyrimidines, DIPEA, iPrOH, reflux, ov; (d) KCN, DABCO, DMSO/H_2O (9:1), rt, 3 h; (e) (1) pTsOH, ACN, rt, ov, (2) acid chloride of tetraoxane **7a–b**, DIPEA, dry THF, rt, ov; (f) (1) pTsOH, ACN, rt, ov, (2) acid chloride of tetraoxane **7a**, DIPEA, dry THF, rt, ov; (g) KCN, DABCO, DMSO/H_2O (9:1), rt, 3 h.

Scheme 3. Synthesis of Pyrimidine Nitrile 13[a]

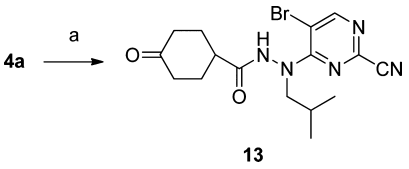

[a]Reagents and conditions: (a) $FeBr_2$, ACN/DCM (1:1), rt, 24 h.

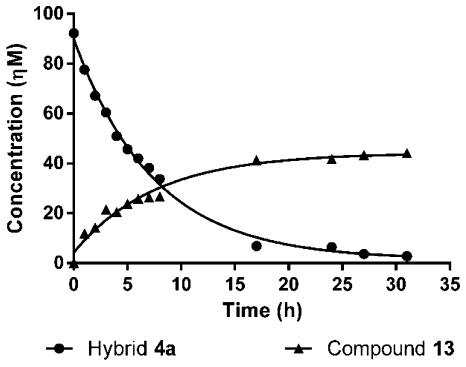

Figure 3. Time-dependence profile for the activation of hybrid **4a** by 18 equiv of $FeSO_4$ in aqueous acetonitrile.

adamantanone, these results are in agreement with similar assays, where radicals derived from both activation pathways were trapped with TEMPO and identified.[20,22]

Falcipain-2 Inhibition. Compounds **4** were screened against recombinant falcipain-2. They displayed a wide range of inhibitory activities, with IC_{50}s ranging from 978 nM for **4g** to 3.4 nM for **4e** (Table 1). These results suggest that pyrimidine nitriles, in contrast to their vinyl sulfone hybrid counterparts **3**,[11] can accommodate the bulky adamantane–tetraoxane moiety at P_3 without significantly affecting the enzyme inhibitory activity. Structure–activity data revealed that substituents at C-5 of the pyrimidine, which interact with the S_1 pocket, markedly affect the potency, with compounds bearing a chlorine and bromine 270 and 55 times more potent than their unsubstituted counterparts, respectively (**4a** and **4e** versus **4f**). In contrast, a chlorine atom at C-6 had a deleterious effect on the inhibitory capacity, compared to the unsubstituted compound (**4g** versus **4f**), suggesting that substituents at this position do not interact adequately with the S_1 binding site. Extending the linker between the two pharmacophoric moieties decreased the activity by 6-fold (**4a** versus **4b**). Finally, varying the P_2 moiety suggested that the isobutyl and cyclohexyl groups are well accommodated by the S_2 binding pocket, a result in line with that reported by Coterón et al.[19]

The predicted binding modes of hybrids **4** were further supported by covalent molecular docking calculations. The

dx.doi.org/10.1021/jm5004528 | J. Med. Chem. 2014, 57, 4916–4923

Table 1. Antiplasmodial Activity against Chloroquine-Sensitive (3D7), Chloroquine-Resistant (W2), and Atovaquone-Resistant (FCR3) Strains of *P. falciparum*, Falcipain-2 (FP-2) Inhibition, and Digestive Vacuole (DV) Swelling Induced by Hybrids 4a–g and Ketone 13

				IC_{50} (nM)				
compd	X	R^1	R^2	3D7	W2	FCR3	FP-2	DV swelling (123 nM)[a]
4a	CO	$-CH_2CH(CH_3)_2$	5-Br	58.1 ± 7.8	9.8 ± 1.5	ND[b]	16.4 ± 4.2	yes
4b	CH_2CO	$-CH_2CH(CH_3)_2$	5-Br	18.9 ± 4.2	22.8 ± 2.8	ND[b]	95.1 ± 0.4	yes
4c	CO	$-CH_2CH(CH_2)_4$	5-Br	70.7 ± 1.2	29.5 ± 11.7	ND[b]	112 ± 9	ND[b]
4d	CO	$-CH(CH_2)_5$	5-Br	78.5 ± 8.4	22.4 ± 12.3	81.2 ± 7.2	25.3 ± 7.1	yes
4e	CO	$-CH_2CH(CH_3)_2$	5-Cl	80.9 ± 17.2	33.8 ± 0	53.3 ± 7.6	3.4 ± 0.6	yes
4f	CO	$-CH_2CH(CH_3)_2$	5-H	13.1 ± 0.6	47.3 ± 1.7	30.3 ± 9.4	909 ± 93	no
4g	CO	$-CH_2CH(CH_3)_2$	6-Cl	28.4 ± 7.9	48.9 ± 2.5	37.7 ± 6.4	978 ± 205	no
13				48.2 ± 11.1	48.1 ± 3.2	ND[b]	58.4 ± 0.4	yes
ART				36.2 ± 4.7	14.1 ± 1.4	7.7 ± 8.7		
CQ				9.25 ± 3.5	64.7 ± 5.5	36.2 ± 0.4		

[a]Observation of DV swelling at 123 nM concentration. [b]ND: not determined.

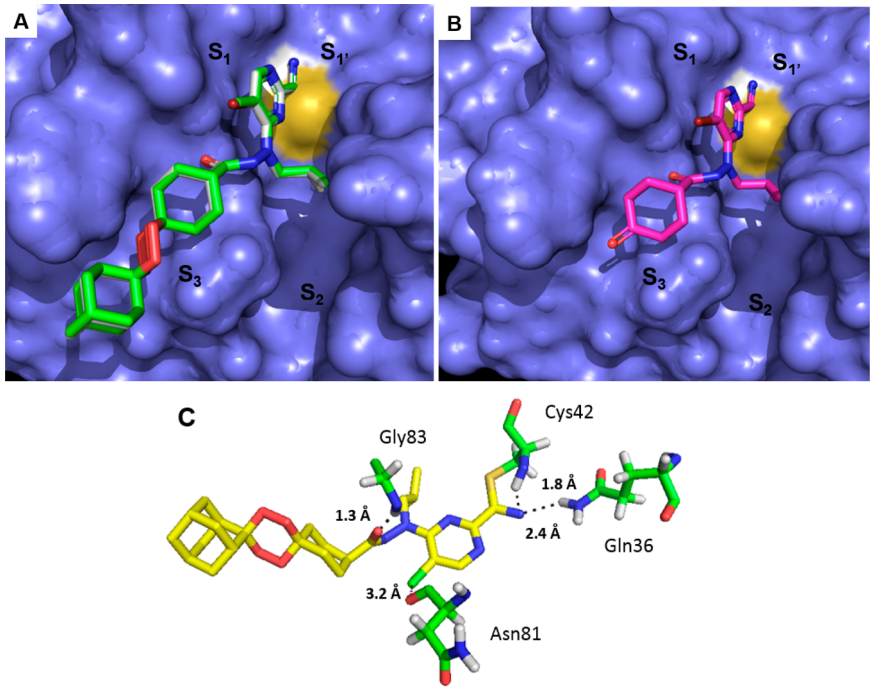

Figure 4. (A) Superimposition of docked conformations of hybrids **4a** (green) and **4e** (light-gray) inside FP-2 binding pocket. (B) Docked conformation of ketone **13** inside FP-2 binding pocket. (C) Closer view of the interactions between compound **4e** and residues present in the FP-2 binding pocket.

crystal structure of FP-2 complexed with the epoxysuccinate E64 at a resolution of 2.9 Å (PDB code: 3BPF) was employed in the docking calculations. Inspection of the top ranking solutions of **4a**, **4b**, **4e–g**, and **13** inside the falcipain-2 binding pocket (Figure 4A; see Supporting Information for a closer view), selected according to their goldscore fitness function, revealed that these compounds present the pyrimidine thioimidate adduct resulting from the nucleophilic attack of the active site cysteine sitting in the S_1 binding pocket, while the isobutyl group and tetraoxane moiety fit into the S_2 and S_3 binding sites, respectively. Remarkably, the parent ketone **13** adopts the same pose as **4a** and **4e** (Figure 4B), indicating that the adamantane group do not significantly disturb the positioning of the pyrimidine inside the active site. The best poses reveal that nitrogen atom of the thioimidate adduct is stabilized by hydrogen bonding with Gln36 (N···H ∼ 2.4 Å) and Cys42 (N···H ∼ 1.8 Å), while the carbonyl oxygen atom establishes a hydrogen bond with Gly83 (O···H ∼ 1.3 Å). But the most prominent feature observed for derivatives **4a**, **4b**, and **4e** is the strong halogen bond established between 5-Br/5-Cl and the Asn81 oxygen atom, ranging from 2.8 to 3.2 Å (Figure 4C). These values are lower than the sum of the van der Waals radii of 3.27 Å[23] and contrasts with the value of 3.54 Å observed for the less potent 6-Cl counterpart **4g**.

Target engagement in the parasites was confirmed by the observation that cultured parasites incubated with compounds **4** at 123 nM for 24 h beginning at the ring stage developed swollen digestive vacuoles with the staining characteristics of erythrocyte cytoplasm (Table 1). It has been previously shown that this specific abnormality is indicative of a block in hemoglobin hydrolysis caused by inhibition of falcipains.[24] Remarkably, compounds **4** with low nanomolar IC_{50} values against falcipain-2 were able to block hemoglobin degradation

dx.doi.org/10.1021/jm5004528 | J. Med. Chem. 2014, 57, 4916–4923

at 123 nM to the same extent as the parent pyrimidine nitrile **13**.

In Vitro Antimalarial Activity. Hybrid compounds **4** were screened against chloroquine-sensitive (3D7), chloroquine-resistant (W2), and atovaquone-resistant (FCR-3) *P. falciparum* strains to assess their potential as blood stage antimalarials (Table 2). Compounds **4a−g** inhibited the growth of the three

Table 2. In Vitro Cytotoxicity and Selectivity Index of Hybrids 4a−g and Ketone 13

	CC_{50} (μM)		selectivity index (SI)[a]	
compd	Hek293T	NIH3T	Hek293T	NIH3T
4a	>100	8.0 ± 0.7	>10000	816
4b	85.5 ± 6.7	2.3 ± 1.0	3750	101
4c	>100	5.5 ± 0.5	>3390	186
4d	>100	1.4 ± 0.1	>4464	63
4e	>100	4.5 ± 1.3	>2959	133
4f	>100	0.9 ± 0.1	>2114	19
4g	>100	1.7 ± 0.8	>2045	35
13	>100	>100	>2079	>2079

[a]SI was calculated as the ratio of IC_{50} for in vitro cytotoxicity on Hek293T and NIH3T to the IC_{50} of plasmodial inhibition against the strain W2.

P. falciparum strains with IC_{50} values ranging from 9.8 to 81.2 nM, while displaying negligible cytotoxicity, with EC_{50} values against HEK293T mammalian cells ranging from 85 to >100 μM.

Activity against liver-stage malaria parasites is highly desirable, in particular for radical cure of *Plasmodium vivax* and *Plasmodium ovale* infections and in drugs used for the prevention of malaria.[25,26] Thus, compounds **4** were also evaluated for their activity against liver stages of the rodent parasite *Plasmodium berghei* and for cytotoxicity to Huh-7 human hepatoma cells, employing previously reported methods.[27] Primaquine, the only approved drug to treat liver stage/relapsing malaria, and atovaquone were also included as positive controls for liver stage activity. Most hybrid compounds **4** significantly decreased the parasite load in Huh-7 cells when compared to untreated controls and were more active than primaquine at 10 μM (Figure 5) but less active than atovaquone at 2 μM (see Figure S3 in Supporting Information). A similar activity profile was observed for the parent compound **13**. The endoperoxide artemisinin was inactive at both dose levels. To our knowledge, this is the first report of endoperoxides and pyrimidine nitriles active against liver stage malaria. So far, only hybrid compounds based on known liver stage antimalarials[27−29] were noted to have both blood and liver stage activity.

In Vivo Efficacy. Hybrid **4e** was selected to evaluate the in vivo efficacy in a murine model of infection as it displayed excellent FP-2 inhibitory activity, high potency against all *P. falciparum* strains, low cytotoxicity, and very good activity in the liver stage assay. Hybrid **4e** was tested at 30 mg/kg/day, administered intraperitoneally for five consecutive days beginning when parasitemia reached 4% at day 4 postinfection. Infected mice receiving compound **4e** responded initially to the treatment, but parasitemia increased after day 8, to reach a mean valueof 51% at day 18 postinfection. However, all animals treated with compound **4e** survived to day 18 after initial inoculation with parasites (Figure 6).

CONCLUSIONS

In conclusion, we developed a series of tetraoxane−pyrimidine nitrile hybrids **4** endowed with two distinct mechanisms of action, a feature predicted to help prevent selection of drug resistance. Remarkably, appending a large adamantane-based tetraoxane moiety to the P_3 position of the pyrimidine scaffold did not affect inhibitory potency against falcipain-2 or general structure−activity relationship trends when compared to previously reported pyrimidine nitriles. Although this enzyme inhibitory profile translated into excellent in vitro potency against the erythrocytic stage malaria parasites, there was only moderate in vivo efficacy. Overall, this new class of hybrid antimalarial compounds displayed good activity against the blood and liver stages of malaria parasites and it is thus deserving of further exploration.[26]

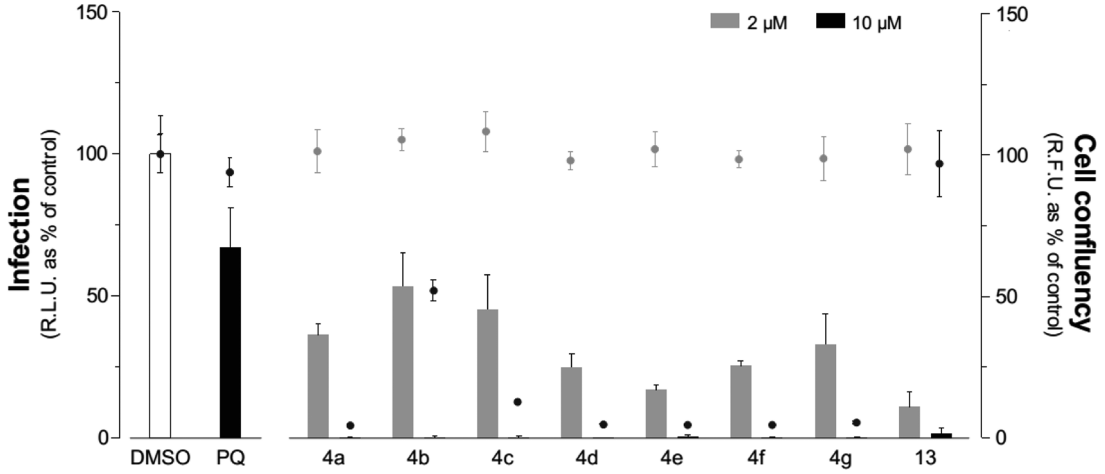

Figure 5. In vitro antimalarial activity against the liver stage of infection. In vitro inhibition of hepatic *P. berghei* infection by compounds **4a−g** and **13**. Compounds were added to Huh-7 hepatoma cells 1 h before infection with luciferase-expressing sporozoites. An amount of DMSO equivalent to that in the highest compound concentration tested was used as a control. Then 48 h after the addition of *P. berghei* sporozoites, cell confluence (dots on bar plots) was assessed by AlamarBlue fluorescence, and the infection rate (bars) was measured by quantifying the luciferase activity by luminescence. The effects of two concentrations (2 and 10 μM) of compounds **4a−g** and **13** are shown. Results are expressed as means ± standard deviations.

dx.doi.org/10.1021/jm5004528 | J. Med. Chem. 2014, 57, 4916−4923

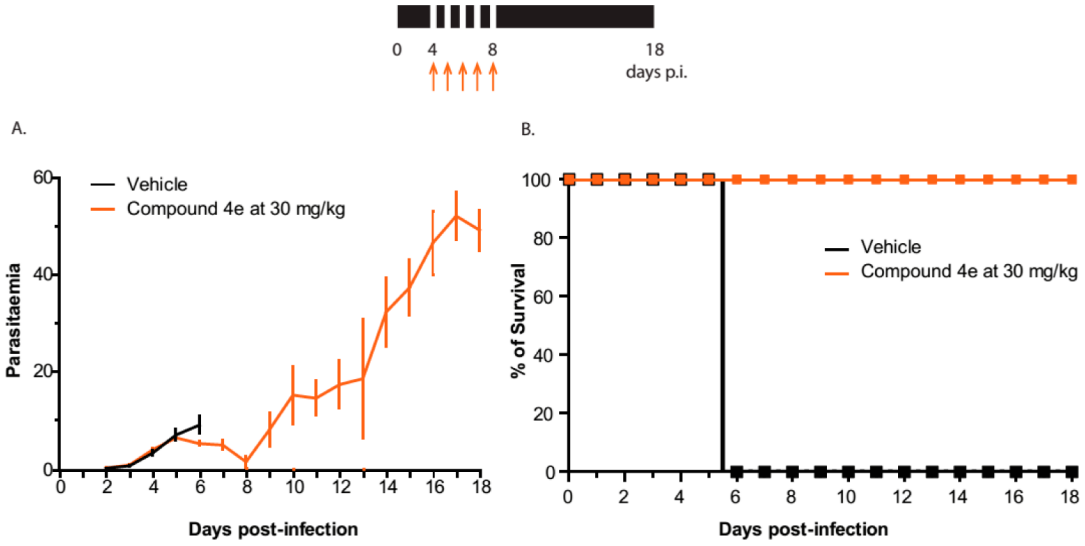

Figure 6. In vivo mouse efficacy studies for compound **4e** in the *P. berghei* mouse model. Mice were infected with parasites on day 0, and compound **4e** dosing began on day 4 and lasted for a total of 5 consecutive days (indicated by the arrows). Dosing was by ip administration at 30 mg/kg bw. (A) Parasitemia curve; (B) survival curve.

EXPERIMENTAL SECTION

Chemistry. All chemicals and solvents were of analytical reagent grade and were purchased from Alfa Aesar or Sigma-Aldrich. Tetrahydrofuran was dried before use. Thin layer chromatography was performed using Merck silica gel 60F254 aluminum plates and visualized by UV light, iodine, potassium permanganate dip, and/or *p*-anisaldehyde dip. Flash column chromatography was performed using Merck silica gel 60 (230−400 mesh ASTM) eluting with various solvent mixtures and using an air aquarium pump to apply pressure. NMR spectra were recorded on a Bruker 400 Ultra-Shield (400 MHz) in $CDCl_3$; chemical shifts, δ, are expressed in ppm, and coupling constants, J, are expressed in Hz. Mass analyses were determined using a Micromass Quattro Micro API spectrometer, equipped with a Waters 2695 HPLC module and Waters 2996 photodiode array detector. High resolution mass spectra were performed in Unidade de Espectrometria de Masas (HMRS-ESI-TOF), Santiago de Compostela, Spain. All compounds tested in the biological assays were determined to be >95% pure by elemental analysis (for C, H, and N). Melting points were determined using a Kofler Bock Monoscop M and are uncorrected.

Preparation of Compounds ***4*** *(Method A).* (1) To a solution of compound **11a−f** (0.2 mmol) in ACN (1.5 mL) was added *p*-toluenesulfonic acid (0.8 mmol). The mixture was stirred overnight at room temperature. Then the solvent was removed under reduced pressure and the crude taken up in EtOAc (30 mL) and washed with 1 M solution of Na_2CO_3 (30 mL). The aqueous phase was further extracted with EtOAc (2 × 20 mL). The combined organic phases were dried over Na_2SO_4, filtered, and concentrated to give the free amine. (2) A solution of tetraoxane **7a−b** (0.24 mmol) in thionyl chloride (2 mL) was refluxed for 2 h. The mixture was concentrated under reduced pressure, and then the acid chloride was taken up in dry THF (1 mL) in nitrogen atmosphere. A solution of the appropriate free amine (0.2 mmol) in dry THF (1 mL) was added to the acid chloride. After stirring for 30 min at room temperature under nitrogen, DIPEA (0.6 mmol) was added, followed by overnight stirring in the same conditions. The mixture was diluted with DCM (30 mL) and water (30 mL), and the phases were separated. The aqueous phase was further extracted with DCM (2 × 20 mL). The combined organic extracts were dried over Na_2SO_4, filtered, and concentrated. Purification by flash chromatography gave the pure compound.

Preparation of Compounds ***4*** *(Method B).* To a solution of compound **12a−e** (0.2 mmol) and DABCO (0.2 mmol) in DMSO/water (9:1, 2 mL) was added KCN (0.22 mmol). The solution was stirred for 5 h at room temperature. Then the mixture was poured into ice water (30 mL) and extracted with EtOAc (2 × 30 mL). The combined organic phases were washed with saturated solution of $NaHCO_3$ (30 mL), dried over Na_2SO_4, filtered, and concentrated. Purification by flash chromatography gave the pure compound.

Compound ***4a.*** White solid (method A: 38% yield/method B: 60% yield); mp 113−114 °C. ^{1}H NMR (400 MHz, $CDCl_3$) δ = 8.47 (s, 1H), 7.79 (s, 1H), 3.67 (bs, 2H), 2.38 (bs, 1H), 2.11−1.46 (m, 23H), 0.99 (d, J = 6.5 Hz, 6H) ppm. ^{13}C NMR (101 MHz, $CDCl_3$) δ = 171.9, 160.7, 160.7, 141.6, 115.4, 110.7, 106.7, 106.2, 59.0, 41.6, 36.9, 33.1, 27.0, 26.3, 20.2 ppm. HRMS-ESI: m/z $[M + Na]^+$ calcd for $C_{26}H_{34}BrN_5O_5$, 598.1641; found, 598.1618.

Compound ***4b.*** White solid (method A: 27% yield); mp 94−96 °C. ^{1}H NMR (400 MHz, $CDCl_3$) δ = 8.46 (s, 1H), 7.63 (s, 1H), 3.67 (bs, 2H), 2.19 (d, J = 6.7 Hz, 2H), 2.09−1.46 (m, 22H), 1.41−1.20 (m, 2H), 0.96 (d, J = 6.7 Hz, 6H) ppm. ^{13}C NMR (101 MHz, $CDCl_3$) δ = 169.6, 160.7, 160.6, 141.6, 115.4, 110.6, 107.5, 106.0, 59.1, 39.5, 36.9, 33.3, 33.1, 33.1, 27.0, 27.0, 26.3, 20.2 ppm. HRMS-ESI: m/z $[M + H]^+$ calcd for $C_{27}H_{37}BrN_5O_5$, 590.1978; found, 590.1961.

Compound ***4c.*** White solid (method A: 10% yield/method B: 66% yield); mp 190−191 °C. ^{1}H NMR (400 MHz, $CDCl_3$) δ = 8.44 (s, 1H), 7.69 (s, 1H), 3.75 (bs, 2H), 2.42−2.31 (m, 1H), 2.25−2.15 (m, 1H), 2.07−1.47 (m, 26H), 1.27 (m, 4H) ppm. ^{13}C NMR (101 MHz, $CDCl_3$) δ = 172.0, 160.7, 160.7, 141.8, 115.5, 110.9, 106.8, 106.2, 56.4, 41.7, 37.5, 37.0, 33.2, 30.7, 27.1, 27.1, 25.2 ppm. HRMS-ESI: m/z $[M + H]^+$ calcd for $C_{28}H_{37}BrN_5O_5$, 602.1978; found, 602.1962.

Compound ***4d.*** White solid (method A: 8% yield); mp 148−149 °C. ^{1}H NMR (400 MHz, $CDCl_3$) δ = 8.41 (s, 1H), 7.47 (s, 1H), 4.54 (bs, 1H), 2.42 (bs, 1H), 2.13−1.20 (m, 31H), 1.20−1.01 (m, 2H) ppm. ^{13}C NMR (101 MHz, $CDCl_3$) δ = 172.5, 160.4, 159.6, 141.7, 115.5, 110.7, 106.7, 106.3, 59.6, 36.9, 33.1, 27.0, 25.5 ppm. HRMS-ESI: m/z $[M + H]^+$ calcd for $C_{28}H_{37}BrN_5O_5$, 602.1978; found, 602.1971.

Compound ***4e.*** White solid (method B: 57% yield); mp 134−137 °C. ^{1}H NMR (400 MHz, $CDCl_3$) δ = 8.28 (s, 1H), 7.79 (s, 1H), 3.66 (bs, 2H), 2.40−2.27 (m, 1H), 2.08−1.46 (m, 23H), 0.97 (d, J = 6.7 Hz, 6H) ppm. ^{13}C NMR (101 MHz, $CDCl_3$) δ = 172.2, 159.8, 157.7, 141.1, 117.7, 115.3, 110.7, 106.7, 59.2, 41.6, 36.9, 33.1, 27.0, 27.0, 26.4, 20.2 ppm. HRMS-ESI: m/z $[M + H]^+$ calcd for $C_{26}H_{35}ClN_5O_5$, 532.2327; found, 532.2312.

Compound ***4f.*** White solid (method B: 43% yield); mp 196−197 °C. ^{1}H NMR (400 MHz, $CDCl_3$) δ = 8.22 (d, J = 6.0 Hz, 1H), 8.06 (bs, 1H), 6.61 (d, J = 6.0 Hz, 1H), 3.97−3.25 (m, 2H), 2.47−2.33 (m, 1H), 2.07−1.47 (m, 23H), 0.93 (d, J = 6.5 Hz, 6H) ppm. ^{13}C NMR (101 MHz, $CDCl_3$) δ = 158.5, 156.2, 144.1, 116.0, 110.7, 106.7, 105.6,

dx.doi.org/10.1021/jm5004528 | *J. Med. Chem.* 2014, 57, 4916−4923

41.8, 36.9, 33.1, 29.7, 27.0, 26.7, 20.1 ppm. HRMS-ESI: m/z [M − H]$^-$ calcd for $C_{26}H_{34}N_5O_5$, 496.2560; found, 496.2568.

Compound ***4g***. White solid (method **B**: 37% yield); mp 106−108 °C. ^{1}H NMR (400 MHz, $CDCl_3$) δ = 7.58 (s, 1H), 6.60 (s, 1H), 3.98−3.13 (m, 2H), 2.40 (bs, 1H), 2.14−1.46 (m, 23H), 0.95 (d, J = 6.4 Hz, 6H) ppm. ^{13}C NMR (101 MHz, $CDCl_3$) δ = 160.7, 143.5, 115.0, 110.8, 106.6, 104.6, 41.9, 36.9, 33.1, 27.0, 26.7, 20.1 ppm. HRMS-ESI: m/z [M − H]$^-$ calcd for $C_{26}H_{33}ClN_5O_5$, 530.2170; found, 530.2173.

In Vitro Activity Assay against Blood Stage of Infection. Synchronized ring-stage *P. falciparum* strain W2 parasites were cultured with multiple concentrations of test compounds (added from 1000× stocks in DMSO) in RPMI 1640 medium with 10% human serum. After 48 h of incubation, when control cultures contained new rings, parasites were fixed with 1% formaldehyde in phosphate-buffered saline (PBS), pH 7.4, for 48 h at room temperature; then they were labeled with YOYO-1 (1 nM; Molecular Probes) in 0.1% Triton X-100 in PBS. Parasitemia was determined from dot plots (forward scatter versus fluorescence) acquired on a FACSort flow cytometer using CellQuest software (Becton Dickinson). Fifty percent inhibitory concentrations (IC_{50} values) for growth inhibition were determined with GraphPad Prism software from plots of the percentage of parasitemia of the control relative to the inhibitor concentration. In each case, the goodness of the curve fit was documented by R^2 values of 0.95.

In Vitro Activity against Liver Stage of Infection. Inhibition of liver-stage infection by test compounds was determined by measuring the luminescence intensity in Huh-7 cells infected with a firefly luciferase expressing *P. berghei* line, PbGFP-Luc_{con}, as previously described.[30] Huh-7 cells, from a human hepatoma cell line, were cultured in 1640 rpmI medium supplemented with 10% v/v fetal calf serum, 1% v/v nonessential amino acids, 1% v/v penicillin/streptomycin, 1% v/v glutamine, and 10 mM 4-(2-hydroxyethyl)-1-piperazineethanesulfonic acid (HEPES), pH 7, and maintained at 37 °C with 5% CO_2. For infection assays, Huh-7 cells (1.2×10^4 per well) were seeded in 96-well plates the day before drug treatment and infection. The medium was replaced by medium containing the appropriate concentration of each compound approximately 1 h prior to infection with sporozoites freshly obtained through disruption of salivary glands of infected female *Anopheles stephensi* mosquitoes. Sporozoite addition was followed by centrifugation at 1700*g* for 5 min. Then 24 h after infection, the medium was replaced by fresh medium containing the appropriate concentration of each compound. Parasite infection load was measured 48 h after infection. The effect of the compounds on the viability of Huh-7 cells was assessed by the AlamarBlue assay (Invitrogen, U.K.) using the manufacturer's protocol.

Falcipain-2 Inhibition Assay. IC_{50}s against falcipain-2 were determined as described earlier.[24] Briefly, equal amounts (∼1 nM) of recombinant falcipain-2 were incubated with different concentrations of vinyl sulfones (added from 100× stocks in DMSO) in 100 mM sodium acetate (pH 5.5)−10 mM dithiothreitol for 30 min at room temperature before addition of the substrate benzoxycarbonyl-Leu-Arg-7-amino-4-methyl-coumarin (final concentration, 25 μM). Fluorescence was continuously monitored for 30 min at room temperature in a Labsystems Fluoroskan II spectrofluorometer. IC_{50}s were determined from plots of activity over enzyme concentration with GraphPad Prism software.

In Vivo Assay. C57Bl/6J mice were infected by intraperitoneal inoculations of 2×10^6 GFP-expressing *P. berghei* ANKA-infected erythrocytes. Parasitemias were monitored daily by microscopy and flow cytometry. Drug treatment was initiated when blood parasitemias were ca. 3.9%. At this point, 30 mg/kg bw of compound **4a** were administered once daily by intraperitoneal injection for 5 days. An equivalent amount of drug vehicle was injected in control mice. Parasitemias, disease symptoms, and survival were monitored daily from the onset of treatment until the end of the experiment. The experiment was terminated following 10 consecutive of growing blood parasitemia in treated mice. Parasitemias of control mice increased steadily until day 6 postinfection, when all mice died with symptoms of experimental cerebral malaria.

■ ASSOCIATED CONTENT

Ⓢ Supporting Information

Experimental details for the preparation of compounds **7a−b** and **11−13**, the description of iron(II) activation of hybrid **4a**, and computational methodology. This material is available free of charge via the Internet at http://pubs.acs.org.

■ AUTHOR INFORMATION

Corresponding Authors

*For P.M.O.: phone, 0151-794-3553; E-mail, p.m.oneill01@liverpool.ac.uk.

*For R.M.: fax, + 351 217946470; E-mail, rmoreira@ff.ul.pt.

Author Contributions

The manuscript was written through contributions of all authors. All authors have given approval to the final version of the manuscript.

Notes

The authors declare no competing financial interest.

■ ACKNOWLEDGMENTS

This work was supported by Fundação para a Ciência e Tecnologia, Portugal: grants PTDC/SAU-FAR/118459/2010, PEst-OE/SAU/UI4013/2014, REDE/1501/REM/2005, and PTDC/SAU-MIC/117060/2010; fellowship SFRH/BD/63200/2009 to R.O.), and FundaçãoLuso−Americana (award to R.M.).

■ ABBREVIATIONS USED

ACT, artemisinin-based combination therapy; ART, artemisinin; CQ, chloroquine; FP-2, falcipain-2

■ REFERENCES

(1) *World Malaria Report 2013*; World Health Organization: Geneva, 2013.

(2) White, N. J.; Pukrittayakamee, S.; Hien, T. T.; Faiz, M. A.; Mokuolu, O. A.; Dondorp, A. M. Malaria. *Lancet* **2014**, *383*, 723−735.

(3) White, N. J. Artemisinin Resistance—The Clock Is Ticking. *Lancet* **2010**, *376*, 2051−2052.

(4) Yeung, S.; Socheat, D.; Moorthy, V. S.; Mills, A. J. Artemisinin Resistance on the Thai−Cambodian Border. *Lancet* **2009**, *374*, 1418−1419.

(5) Dondorp, A. M.; Nosten, F.; Yi, P.; Das, D.; Phyo, A. P.; Tarning, J.; Lwin, K. M.; Ariey, F.; Hanpithakpong, W.; Lee, S. J.; Ringwald, P.; Silamut, K.; Imwong, M.; Chotivanich, K.; Lim, P.; Herdman, T.; An, S. S.; Yeung, S.; Singhasivanon, P.; Day, N. P. J.; Lindegardh, N.; Socheat, D.; White, N. J. Artemisinin Resistance in *Plasmodium falciparum* Malaria. *N. Engl. J. Med.* **2009**, *361*, 455−467.

(6) *Guidelines for the Treatment of Malaria*, 2nd ed.; World Health Organization: Geneva, 2010.

(7) O'Neill, P. M.; Barton, V. E.; Ward, S. A. The Molecular Mechanism of Action of Artemisinin—The Debate Continues. *Molecules* **2010**, *15*, 1705−1721.

(8) Meunier, B. Hybrid Molecules with a Dual Mode of Action: Dream or Reality? *Acc. Chem. Res.* **2008**, *41*, 69−77.

(9) Ariey, F.; Witkowski, B.; Amaratunga, C.; Beghain, J.; Langlois, A.-C.; Khim, N.; Kim, S.; Duru, V.; Bouchier, C.; Ma, L.; Lim, P.; Leang, R.; Duong, S.; Sreng, S.; Suon, S.; Chuor, C. M.; Bout, D. M.; Ménard, S.; Rogers, W. O.; Genton, B.; Fandeur, T.; Miotto, O.; Ringwald, P.; Le Bras, J.; Berry, A.; Barale, J.-C.; Fairhurst, R. M.; Benoit-Vical, F.; Mercereau-Puijalon, O.; Ménard, D. A Molecular Marker of Artemisinin-Resistant *Plasmodium falciparum* Malaria. *Nature* **2014**, *505*, 50−55.

(10) Martinelli, A.; Moreira, R.; Ravo, P. V. L Malaria Combination Therapies: Advantages and Shortcomings. *Mini-Rev. Med. Chem.* **2008**, *8*, 201−212.
(11) Oliveira, R.; Newton, A. S.; Guedes, R. C.; Miranda, D.; Amewu, R. K.; Srivastava, A.; Gut, J.; Rosenthal, P. J.; O'Neill, P. M.; Ward, S. A.; Lopes, F.; Moreira, R. An Endoperoxide-Based Hybrid Approach to Deliver Falcipain Inhibitors Inside Malaria Parasites. *ChemMedChem* **2013**, *8*, 1528−1536.
(12) Rosenthal, P. J.; Sijwali, P. S.; Singh, A.; Shenai, B. R. Cysteine Proteases of Malaria Parasites: Targets for Chemotherapy. *Curr. Pharm. Des.* **2002**, *8*, 1659−1672.
(13) Ettari, R.; Bova, F.; Zappala, M.; Grasso, S.; Micale, N. Falcipain-2 Inhibitors. *Med. Res. Rev.* **2010**, *30*, 136−167.
(14) Greenspan, P. D.; Clark, K. L.; Cowen, S. D.; McQuire, L. W.; Tommasi, R. A.; Farley, D. L.; Quadros, E.; Coppa, D. E.; Du, Z. M.; Fang, Z.; Zhou, H. H.; Doughty, J.; Toscano, K. T.; Wigg, A. M.; Zhou, S. Y. *N*-Arylaminonitriles as Bioavailable Peptidomimetic Inhibitors of Cathepsin B. *Bioorg. Med. Chem. Lett.* **2003**, *13*, 4121−4124.
(15) Altmann, E.; Cowan-Jacob, S. W.; Missbach, M. Novel Purine Nitrile Derived Inhibitors of the Cysteine Protease Cathepsin K. *J. Med. Chem.* **2004**, *47*, 5833−5836.
(16) Ehmke, V.; Heindl, C.; Rottmann, M.; Freymond, C.; Schweizer, W. B.; Brun, R.; Stich, A.; Schirmeister, T.; Diederich, F. Potent and Selective Inhibition of Cysteine Proteases from *Plasmodium falciparum* and *Trypanosoma brucei*. *ChemMedChem* **2011**, *6*, 273−278.
(17) Ehmke, V.; Kilchmann, F.; Heindl, C.; Cui, K.; Huang, J.; Schirmeister, T.; Diederich, F. Peptidomimetic Nitriles as Selective Inhibitors for the Malarial Cysteine Protease Falcipain-2. *MedChemComm* **2011**, *2*, 800−804.
(18) Ehmke, V.; Quinsaat, J. E. Q.; Rivera-Fuentes, P.; Heindl, C.; Freymond, C.; Rottmann, M.; Brun, R.; Schirmeister, T.; Diederich, F. Tuning and Predicting Biological Affinity: Aryl Nitriles as Cysteine Protease Inhibitors. *Org. Biomol. Chem.* **2012**, *10*, 5764−5768.
(19) Coterón, J. M.; Catterick, D.; Castro, J.; Chaparro, M. J.; Díaz, B.; Fernández, E.; Ferrer, S.; Gamo, F. J.; Gordo, M.; Gut, J.; de Las Heras, L.; Legac, J.; Marco, M.; Miguel, J.; Muñoz, V.; Porras, E.; de La Rosa, J. C.; Ruiz, J. R.; Sandoval, E.; Ventosa, P.; Rosenthal, P. J.; Fiandor, J. M. Falcipain Inhibitors: Optimization Studies of the 2-Pyrimidinecarbonitrile Lead Series. *J. Med. Chem.* **2010**, *53*, 6129−6152.
(20) O'Neill, P. M.; Amewu, R. K.; Nixon, G. L.; Bousejra-El Garah, F.; Mungthin, M.; Chadwick, J.; Shone, A. E.; Vivas, L.; Lander, H.; Barton, V.; Muangnoicharoen, S.; Bray, P. G.; Davies, J.; Park, B. K.; Wittlin, S.; Brun, R.; Preschel, M.; Zhang, K.; Ward, S. A. Identification of a 1,2,4,5-Tetraoxane Antimalarial Drug-Development Candidate (RKA 182) with Superior Properties to the Semisynthetic Artemisinins. *Angew. Chem., Int. Ed. Engl.* **2010**, *49*, 5693−5697.
(21) Ghorai, P.; Dussault, P. H. Broadly Applicable Synthesis of 1,2,4,5-Tetraoxanes. *Org. Lett.* **2009**, *11*, 213−216.
(22) Bousejra-El Garah, F.; Wong, M. H.-L.; Amewu, R. K.; Muangnoicharoen, S.; Maggs, J. L.; Stigliani, J.-L.; Park, B. K.; Chadwick, J.; Ward, S. A.; O'Neill, P. M. Comparison of the Reactivity of Antimalarial 1,2,4,5-Tetraoxanes with 1,2,4-Trioxolanes in the Presence of Ferrous Iron Salts, Heme, and Ferrous Iron Salts/phosphatidylcholine. *J. Med. Chem.* **2011**, *54*, 6443−6455.
(23) Sirimulla, S.; Bailey, J. B.; Vegesna, R.; Narayan, M. Halogen Interactions in Protein−Ligand Complexes: Implications of Halogen Bonding for Rational Drug Design. *J. Chem. Inf. Model.* **2013**, *53*, 2781−2791.
(24) Rosenthal, P. J.; Olson, J. E.; Lee, G. K.; Palmer, J. T.; Klaus, J. L.; Rasnick, D. Antimalarial Effects of Vinyl Sulfone Cysteine Proteinase Inhibitors. *Antimicrob. Agents Chemother.* **1996**, *40*, 1600−1603.
(25) Derbyshire, E. R.; Mota, M. M.; Clardy, J. The Next Opportunity in Anti-Malaria Drug Discovery: The Liver Stage. *PLoS Pathog.* **2011**, *7*, e1002178.
(26) malERA Consultative Group on Drugs. A Research Agenda for Malaria Eradication: Drugs. *PLoS Med.* **2011**, *8*, e1000402.
(27) Miranda, D.; Capela, R.; Albuquerque, I. S.; Meireles, P.; Paiva, I.; Nogueira, F.; Amewu, R.; Gut, J.; Rosenthal, P. J.; Oliveira, R.; Mota, M. M.; Moreira, R.; Marti, F.; Prudêncio, M.; O'Neill, P. M.; Lopes, F. Novel Endoperoxide-Based Transmission-Blocking Antimalarials with Liver- and Blood-Schizontocidal Activities. *ACS Med. Chem. Lett.* **2013**, *5*, 108−112.
(28) Capela, R.; Cabal, G. G.; Rosenthal, P. J.; Gut, J.; Mota, M. M.; Moreira, R.; Lopes, F.; Prudêncio, M. Design and Evaluation of Primaquine−Artemisinin Hybrids as a Multistage Antimalarial Strategy. *Antimicrob. Agents Chemother.* **2011**, *55*, 4698−4706.
(29) Lödige, M.; Lewis, M. D.; Paulsen, E. S.; Esch, H. L.; Pradel, G.; Lehmann, L.; Brun, R.; Bringmann, G.; Mueller, A.-K. A Primaquine−Chloroquine Hybrid with Dual Activity against *Plasmodium* Liver and Blood Stages. *Int. J. Med. Microbiol.* **2013**, *303*, 539−547.
(30) Ploemen, I. H. J.; Prudêncio, M.; Douradinha, B. G.; Ramesar, J.; Fonager, J.; van Gemert, G. J.; Luty, A. J. F.; Hermsen, C. C.; Sauerwein, R. W.; Baptista, F. G.; Mota, M. M.; Waters, A. P.; Que, I.; Lowik, C.; Khan, S. M.; Janse, C. J.; Franke-Fayard, B. M. D. Visualisation and Quantitative Analysis of the Rodent Malaria Liver Stage by Real Time Imaging. *PLoS One* **2009**, *4*, e7881.

ACS Medicinal Chemistry Letters

Letter

pubs.acs.org/acsmedchemlett

Novel Endoperoxide-Based Transmission-Blocking Antimalarials with Liver- and Blood-Schizontocidal Activities

Daniela Miranda,[†] Rita Capela,[†] Inês S. Albuquerque,[‡] Patrícia Meireles,[‡] Isa Paiva,[§] Fátima Nogueira,[§] Richard Amewu,[∥] Jiri Gut,[⊥] Philip J. Rosenthal,[⊥] Rudi Oliveira,[†] Maria M. Mota,[‡] Rui Moreira,[†] Francesc Marti,[∥] Miguel Prudêncio,[‡] Paul M. O'Neill,[∥] and Francisca Lopes*[,†]

[†]Research Institute for Medicines and Pharmaceutical Sciences (iMed.UL), Faculty of Pharmacy, University of Lisbon, Av. Prof. Gama Pinto, 1649-019 Lisbon, Portugal

[‡]Instituto de Medicina Molecular, Faculdade de Medicina da Universidade de Lisboa, Av. Prof. Egas Moniz, 1649-028 Lisboa, Portugal

[§]Centro de Malária e Outras Doenças Tropicais, IHMT, Universidade Nova de Lisboa, Rua da Junqueira No. 100, P-1349-008 Lisbon, Portugal

[∥]Department of Chemistry, University of Liverpool, Liverpool L69 7ZD, U.K.

[⊥]Department of Medicine, San Francisco General Hospital, University of California, San Francisco, San Francisco, California 94143, United States

Supporting Information

ABSTRACT: In a search for effective compounds against both the blood- and liver-stages of infection by malaria parasites with the ability to block the transmission of the disease to mosquito vectors, a series of hybrid compounds combining either a 1,2,4-trioxane or 1,2,4,5-tetraoxane and 8-aminoquinoline moieties were synthesized and screened for their antimalarial activity. These hybrid compounds showed high potency against both exoerythrocytic and erythrocytic forms of malaria parasites, comparable to representative trioxane-based counterparts. Furthermore, they efficiently blocked the development of the sporogonic cycle in the mosquito vector. The tetraoxane-based hybrid **5**, containing an amide linker between the two moieties, effectively cleared a patent blood-stage *P. berghei* infection in mice after i.p. administration. Overall, these results indicate that peroxide-8-aminoquinoline hybrids are excellent starting points to develop an agent that conveys all the desired antimalarial multistage activities in a single chemical entity and, as such, with the potential to be used in malaria elimination campaigns.

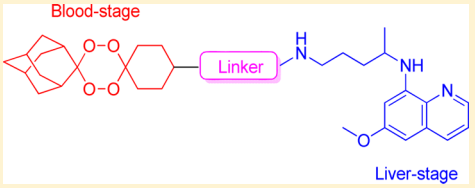

KEYWORDS: *Antimalarials, endoperoxide, sporogonic cycle, P. berghei*

Malaria is a potentially life-threatening disease caused by infection with parasites of the genus *Plasmodium* and transmitted to humans through the bite of infected female *Anopheles* mosquitoes.[1] Among the five *Plasmodium* species that commonly infect humans, *P. falciparum* is responsible for most of the mortality worldwide.[2] Parasite resistance to antimalarial drugs remains a real and ever-present danger. For this reason, the WHO recommends that *P. falciparum* malaria should be treated with artemisinin (ART, **1**)-based combination therapies (ACT), in which the ART-based component is combined with a second, longer-acting agent.[1,3] Artemisinin and its derivatives are potent blood schizontocides, acting rapidly against parasitic forms that invade erythrocytes and cause disease symptoms.[4]

The ultimate goal of eradicating malaria will benefit greatly from a drug that eliminates all life cycle stages of parasites.[5] Malaria parasites undergo an asymptomatic, obligatory developmental phase in the liver, which precedes the formation of red blood cell-infective forms.[6] Thus, the liver stage of infection offers important potential for disease prevention, as intervention at this stage acts before the onset of symptoms, providing a true causal prophylactic strategy.[7] In addition, *P. vivax*, the second most prevalent species causing human malaria, and *P. ovale* infections can generate cryptic parasite forms called hypnozoites that persist in the liver for long periods of time and that, upon reactivation, are responsible for relapses of malaria.[8] Thus, antiliver stage drugs would also be beneficial for a malaria eradication campaign through elimination of the long-lived hypnozoites of *P. vivax* and *P. ovale* in the liver.[8,9] Primaquine (**2**, PQ, Chart 1) is the only drug currently used for the radical cure of *P. vivax* and *P. ovale* malaria and is active against the transient liver forms of all *Plasmodium* species. Moreover, PQ is also used as a gametocytocidal, i.e., it is active against the blood-circulating sexual forms of the parasite that are transmitted to the mosquito upon a blood meal, and in this way, it is able to block the transmission of infection from the human host to mosquito vectors.[10,11] The liver and sporogonic stages of malaria parasites

Received: July 30, 2013
Accepted: December 20, 2013
Published: December 20, 2013

   dx.doi.org/10.1021/ml4002985 | *ACS Med. Chem. Lett.* 2014, 5, 108−112

Chart 1. Structures of Arteminisin, 1, Primaquine, 2, and an Artemisinin−Primaquine Hybrid, 3

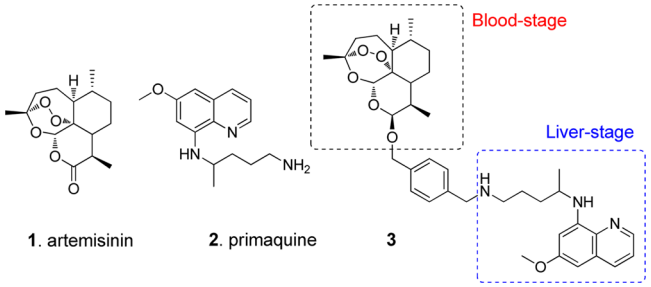

have remained largely underexploited as antimalarial targets due to the poorly understood biology of these life-cycle stages and the inherent technical difficulties in studying them.[7,11] Only recently have systematic efforts toward the identification of novel liver schizontocidal and transmission blocking scaffolds been reported.[4,12−14]

Endoperoxide-based hybrid compounds represent an attractive alternative to ACTs.[15−19] ART contains a 1,2,4-trioxane core that is reductively activated by iron(II) heme, a byproduct of host hemoglobin degradation, to form carbon-centered radicals capable of reacting with heme and proteins.[20] An alternative model for the antimalarial mechanism of endoperoxides has been put forward by Haynes and Monti whereby endoperoxides mediate their antimalarial activity through interaction with cofactors. The tetraoxanes reported here are also likely to be capable of oxidizing cofactors such as $FADH_2$ and differences in activity between trioxanes and tetraoxanes may reflect the different oxidizing capacities of the two heterocycles.[21,22]

We recently reported, for the first time, the ability of PQ-ART hybrid molecules, e.g., **3**, to impair the liver and erythrocyte stages of *Plasmodium*, a result that paves the way for the exploitation of this approach for malaria control and eradication.[23] We now extend this hybrid-based strategy to fully synthetic 1,2,4,5-tetraoxanes, a class of peroxides with potent blood schizontocidal activity.[24] The aims of this study were (i) to evaluate the efficacy of hybrid compounds **5**, **8**, **10**, and **12** (Scheme 1) against *Plasmodium* liver and erythrocyte stages and compare their activities to those of their 1,2,4-trioxane counterparts **16** and **18** (Schemes 2 and 3), and (ii) to determine their potential as transmission-blocking agents.

The preparation of hybrid compounds **5**, **8**, **10**, and **12** is outlined in Scheme 1. Compounds **5** and **10**, containing an amide linker between the two pharmacophoric moieties, were synthesized by reacting tetraoxanes **4** and **9** with PQ, using TBTU and methyl chloroformate as coupling agents, respectively. Tetraoxanes **4** and **9** as starting materials were prepared via a rapid three-step synthesis that was previously reported.[24−26]

The synthesis of hybrid **8**, the amine counterpart of **5**, started with the conversion of tetraoxane **4** to the Weinreb amide **6**, which was then reduced to the corresponding aldehyde **7** with $LiAlH_4$.[27−29] Reductive amination of **7** with PQ and $NaBH(AcO)_3$ gave compound **5** in moderate yield. Hybrid **12** was synthesized by reductive amination of tetraoxane **11** with PQ and $NaBH(AcO)_3$.[30] The 1,2,4-trioxane-based hybrid **16**, the amine counterpart of the previously reported amide **17**, was prepared as outlined in Scheme 2.[23] The synthetic pathway started with ART, which was converted to 10β-carboxymethyl-10-desoxy-dihydroartemisinin **13**.[31,32] Following the same procedure used for **6**, compound **13** was converted to the Weinreb amide **14** and then reduced to the corresponding aldehyde **15** with $LiAlH_4$. Reductive amination of **15** with PQ in acetic acid gave compound **16** in moderate yield. Finally, hybrid **18**, the amide counterpart of **3**, was prepared by reacting artelinic acid with PQ and TBTU.

Scheme 1. Synthesis of Tetraoxane-Primaquine Hybrids[a]

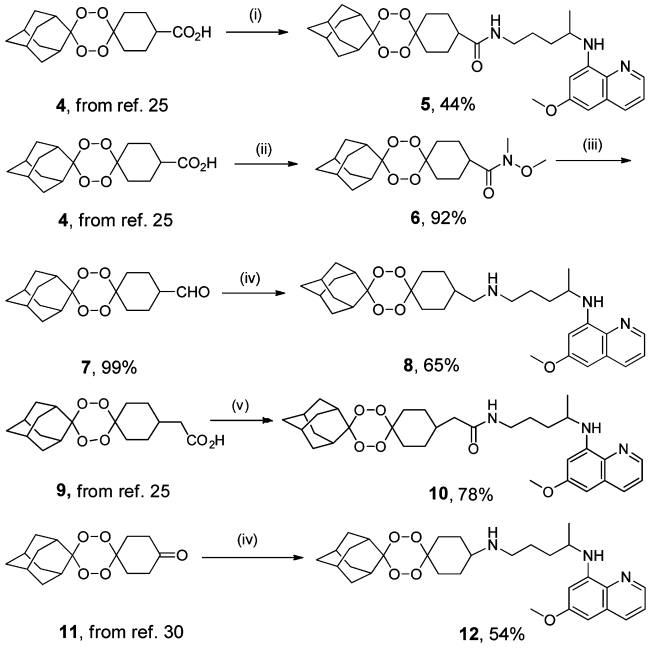

[a]Reagents and conditions: (i) *a*, TBTU, DCM, TEA, 0 °C, 1 h; *b*, PQ, DCM, TEA, rt. (ii) CH_3NHOMe, TBTU, DCM, TEA, rt, 7 h. (iii) $LiAlH_4$, THF, 0 °C, 1 h. (iv) *a*, PQ, DCM, rt, 30 min; *b*, $NaBH(AcO)_3$, AcOH, rt, 16 h. (v) *a*, CH_3OCOCl, TEA, DCM, 0 °C 1 h; *b* PQ, 0 °C 30 min, rt, 1.5 h.

Scheme 2. Synthesis of Trioxane−Primaquine Hybrid 16 and Structure of Hybrid 17[a]

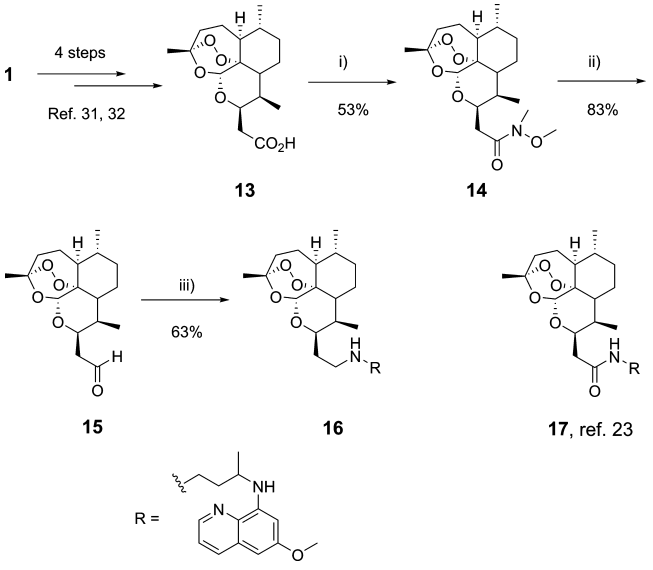

[a]Reagents and conditions: (i) CH_3NHOMe, TBTU, DCM, TEA, rt, 7 h. (ii) $LiAlH_4$, THF, 0 °C 2 h. (iii) *a*, PQ, DCM, rt, 30 min; *b*, $NaBH(AcO)_3$, AcOH, rt.

dx.doi.org/10.1021/ml4002985 | ACS Med. Chem. Lett. 2014, 5, 108−112

Scheme 3. Synthesis of Trioxane−Primaquine Hybrid 18[a]

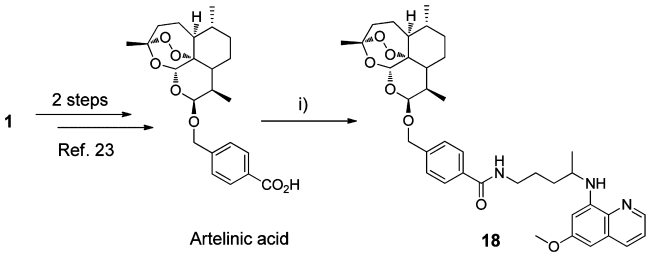

[a]Reagents and conditions: (i) *a*, TBTU, DCM, TEA, 0 °C, 1 h; *b*, PQ, DCM, TEA, rt.

Tetraoxanes **5**, **8**, **10**, and **12** and semisynthetic trioxanes **16** and **18** were first screened for activity against the erythrocyte-stage of chloroquine-resistant W2-strain *P. falciparum* (Table 1). Compounds **5**, **8**, **10**, and **12** inhibited the growth of parasites with IC_{50} values ranging from 21 to 45 nM, suggesting that the nature of the linker between the tetraoxane and PQ moieties does not significantly affect antiplasmodial activity. Trioxanes **16** and **18** were slightly more potent than tetraoxanes as antiplasmodial agents, with IC_{50} values of 9 and 5 nM, respectively (Table 1). These values are of the same order of magnitude as those reported for their counterparts **3**, **17**, and ART. As expected, PQ showed only modest activity in this assay.

Table 1. In Vitro Antimalarial Activity and Toxicity of Tetraoxanes 5, 8, 10, and 12 and Trioxanes 16−18

	in vitro activity (IC_{50}/nM)		cytotoxicity (IC_{50}/μM)
compd	blood-stage[a]	liver-stage[b]	Huh7
3	12.5[c]	155[c]	ND
5	21.1	538	>100
8	45.2	>1000	5.02
10	36.5	604	2.57
12	21.6	330	8.20
16	9.3	>1000	32.8
17	9.1[c]	523[c]	ND
18	5.1	67	73.0
4, ethyl ester	128.2	NA	ND
PQ	3300	7500	ND
ART	8.2	NA	ND
PQ + ART	ND	9714	ND

[a]Determined against the chloroquine-resistant *P. falciparum* W2 strain. [b]Determined against *P. berghei*; ND, not determined; NA, not active (>10 μM). [c]Ref 23.

To evaluate the abilities of hybrids **5**, **8**, **10**, **12**, **16**, and **18** to inhibit infection of liver cells by malaria parasites, the compounds were tested using an in vitro infection model that employs a human hepatoma cell line (Huh7) and the rodent malaria parasite *P. berghei*.[7] Parasite load was assessed by bioluminescence measurements following infection with luciferase-expressing parasites, as previously described.[33] The results were compared with those obtained for a tetraoxane lacking the 8-aminoquinoline moiety, the ethyl ester of **4** (Table 1). All hybrids showed high potency against the liver forms of the parasite, with most of the compounds displaying IC_{50} values in the low to mid nM range. In contrast, the parent tetraoxane showed to be inactive at 10 μM, suggesting that this scaffold is not intrinsically effective against the liver stages of the parasite. Furthermore, hybrids were significantly more potent than PQ and the 1:1 PQ−ART mixture. This is consistent with what has been previously reported for compounds **3** and **17**.[23] Additionally, none of the compounds significantly affected Huh7 cell proliferation, indicating that tetraoxane−PQ hybrids are selective and nontoxic antimalarial agents (Table 1).

Since PQ is known to undergo extensive oxidative deamination at the primary amine, the metabolic stability of tetraoxane-based hybrids **5** and **8** was evaluated in rat liver microsomes, at 37 °C. From the results presented in Table 2 it is possible to conclude that tetraoxane **5**, containing an amide linker between the two pharmacophoric moieties, displayed a high rate of metabolism in rat liver microsomes and predicted *in vivo* hepatic extraction ratio, E_H. In contrast, its amine counterpart **8** presented an intermediate E_H values, suggesting that metabolic susceptibility of tetraoxane hybrids are affected by the nature of the linker between the two moieties. Neither primaquine nor its oxidative deamination product, carboxyprimaquine,[10] were detected in the incubation mixtures, suggesting that other metabolic pathways might be operating for **5** and **8**. In addition, these hybrids did not degrade when incubated in 80% human plasma for 3 days.

Table 2. In Vitro Metabolism of Compounds 5 and 8 in Rat Liver Microsomes and Predicted in Vivo Metabolism Data

compd	$t_{1/2}$ (min)	$CL_{int,invitro}$ (μL/min/mg protein)	predicted E_H	putative metabolites[a]
5	10	132.8	0.81	Not detected
8	27	51.2	0.62	Not detected

[a]Primaquine and carboxyprimaquine.

Having determined the activity profile of tetraoxane-based hybrids against the blood- and liver-stage of infection, we then evaluated the in vivo antimalarial efficacy of compound **5** using GFP-expressing *P. berghei* ANKA-infected male C57Bl/6J mice. This compound was administered i.p. at 30 mg/kg dose once a day for 5 days. Parasitemias were monitored daily by microscopy and flow cytometry. Remarkably, compound **5** completely and irreversibly cleared the parasitemia by day 8 postinfection, and all treated animals survived until the end of the experiment, whereas all control mice succumbed with signs of experimental cerebral malaria at day 6 postinfection (Figure 1), clearly indicating that tetraoxane-based hybrids have curative value. Furthermore, no adverse reactions were observed following administration of **5** at the dosage regimen used in this study.

The potential of tetraoxane hybrids to inhibit the sporogonic cycle of the parasite within the mosquito was also evaluated using an established in vivo infection model consisting of BALB/c mice infected with *P. berghei* ANKA-GFP and *Anopheles gambiae* mosquitoes.[34,35] In this model, mice infected with parasitised erythrocytes were treated by a single i.p. injection of each compound at two dose levels (10 and 25 μmol·kg^{-1}). Two hours after administration, glucose-starved mosquitoes were allowed to feed on the anesthetized mice. The engorged mosquitoes were maintained at 19 ± 1 °C, for 10 days and then collected and dissected for microscopy detection of oocysts in midguts. The criteria used to assess the antimalarial activity of each compound were the percentage of mosquitoes with oocysts and the mean number of oocysts per infected mosquito, when compared to nontreated controls.

dx.doi.org/10.1021/ml4002985 | ACS Med. Chem. Lett. 2014, 5, 108−112

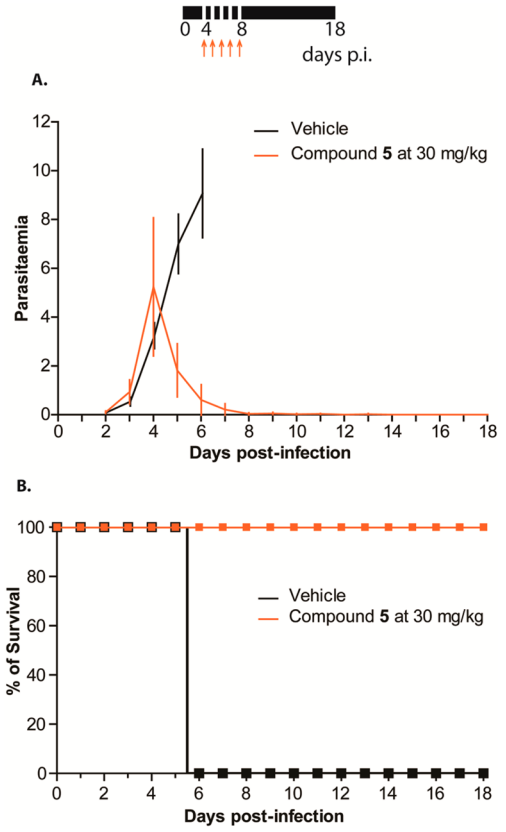

Figure 1. In vivo mouse efficacy studies for compound **5** in the *P. berghei* mouse model. Mice were infected with parasites on day 0, and compound **5** dosing began on day 4 and lasted for a total of 5 consecutive days (indicated by the arrows). Dosing was by i.p. administration at 30 mg/kg b.w. (A) Parasitemia curve; (B) survival curve.

Inspection of data presented in Table 3 shows that compounds **5**, **8**, **10**, and **12** affected the development of the sporogonic cycle of *P. berghei* in *A. gambiae* mosquitoes at the dose levels of 10 and 25 μmol·kg^{-1}. In particular, compound **5** was superior to PQ, and completely inhibited the appearance of oocysts in mosquito midguts when administered at 25 μmol·kg^{-1}. Compounds **8**, **10**, and **12** also markedly decreased the percentage of infected mosquitoes as well as the number of oocysts at the highest dose tested. Although it should be noted that this in vivo model cannot specifically ascribe the drug effect to either gametocytocidal or sporontocidal activity, the results clearly show that hybrids **5**, **8**, **10**, and **12** are effective at interrupting the transmission of malaria parasites to mosquitoes.

Table 3. Effect of Compounds 5, 8, 10, 12 and Primaquine on the Sporogonic Development of *Plasmodium berghei* ANKA in *Anopheles gambiae* Mosquitoes

	mean no. oocysts per mosquito ± SEM[a]		% infected mosquitoes	
compd	10 μmol·kg^{-1}	25 μmol·kg^{-1}	10 μmol·kg^{-1}	25 μmol·kg^{-1}
PQ	2.9 ± 1.1	1.0 ± 0.0	35.5	2.2
5	23.2 ± 5.1	0.0 ± 0.0	68.6	0.0
8	8.0 ± 3.6	1.0 ± 0.0	42.9	5.9
10	26.9 ± 6.1[b]	1.8 ± 0.8	66.7	11.4
12	19.3 ± 8.0[b]	1.0 ± 0.0	36.4	13.3
control	42.1 ± 4.4		83.6	

[a]Standard error of the mean. [b]Not significantly different from control ($P < 0.05$) using the Mann–Whitney test.

In conclusion, a new class of hybrid compounds combining endoperoxides and 8-aminoquinoline pharmacophores was developed to target both blood- and liver-stages of parasites and to block the transmission of infection to mosquito vectors. The in vitro antimalarial profile of these compounds reveals that they display potent inhibitory activity against the blood stage of infection, with IC_{50} values in the nanomolar range, a level of activity similar to that of artemisinin-based hybrid compounds. Screening against *P. berghei* liver stage of infection revealed that both the tetraoxane- and trioxane-based series are potent inhibitors of the exoerythrocytic forms of the parasite, with IC_{50} values in the submicromolar range, being superior to a 1:1 PQ–ART mixture.[23] In vivo studies revealed that compound **5** irreversibly cleared the parasitemia from infected mice, while screening of transmission-blocking activity showed that the tetraoxanes show potent activity in reducing the percentage of infected mosquitoes and the mean number of oocysts per mosquito. These results indicate that these hybrids are excellent starting points to develop agents with the potential to be used in malaria eradication campaigns since they display all the desired antimalarial multistage activities.

■ ASSOCIATED CONTENT

Supporting Information

General procedure and structural data for compounds **5**–**8**, **10**, **12**, **14**–**16**, and **18**; in vitro and in vivo assays. This material is available free of charge via the Internet at http://pubs.acs.org.

■ AUTHOR INFORMATION

Corresponding Author

*(F.L.) Phone: +351 217946476. Fax: +351 217946470. E-mail: fclopes@ff.ul.pt.

Author Contributions

The manuscript was written through contributions of all authors. All authors have given approval to the final version of the manuscript.

Funding

This work was supported by Fundação para a Ciência e Tecnologia, Portugal: grants PTDC/SAU-FAR/118459/2010, Pest-OE/SAU/UI4013/2011, PTDC/SAU-MIC/117060/2010 (to M.P.), SFRH/BD/63200/2009 (to R.O.). M.M.M. is a Howard Hughes Medical Institute International Scholar and P.J.R. is a Distinguished Clinical Scientist of the Doris Duke Charitable Foundation.

Notes

The authors declare no competing financial interest.

■ ACKNOWLEDGMENTS

We acknowledge Prof. Virgílio do Rosário for helpful discussions on the transmission-blocking assays.

■ REFERENCES

(1) WHO. *World Malaria Report 2011*; Geneva, Switzerland, 2011.
(2) Kantele, A.; Jokiranta, T. S. Review of cases with the emerging fifht human malaria parasite *Plasmodium knowlesi*. *Clin. Infect. Dis.* **2011**, *52*, 1356–1362.

(3) Martinelli, A.; Moreira, R.; Cravo, P. V. L Malaria combination therapies: Advantages and shortcomings. *Mini-Rev. Med. Chem.* **2008**, No. 8, 201−212.
(4) Delves, M.; Plouffe, D.; Scheurer, C.; Meister, S.; Wittlin, S.; Winzeler, E. A.; Sinden, R. E.; Leroy, D. The activities of current antimalarial drugs on the life cycle stages of plasmodium: A comparative study with human and rodent parasites. *PLoS Med.* **2012**, *9*, e1001169.
(5) The malERA Consultative Group on Drugs.. A research agenda for Malaria eradication: Drugs. *PloS Med.* **2011**, *8*, e1000402.
(6) Prudencio, M.; Rodriguez, A.; Mota, M. M. The silent path to thousands of merozoites: the Plasmodium liver stage. *Nat. Rev. Microbiol.* **2006**, *4*, 849−856.
(7) Prudencio, M.; Mota, M. M.; Mendes, A. M. A toolbox to study liver stage malaria. *Trends Parasitol.* **2011**, *27*, 565−74.
(8) Wells, T. N.; Burrows, J. N.; Baird, J. K. Targeting the hypnozoite reservoir of *Plasmodium vivax*: the hidden obstacle to malaria elimination. *Trends Parasitol.* **2010**, *26*, 145−51.
(9) Derbyshire, E. R.; Mota, M. M.; Clardy, J. The next opportunity in anti-malaria drug discovery: the liver stage. *PLoS Pathog.* **2011**, *7*, e1002178.
(10) Vale, N.; Moreira, R.; Gomes, P. Primaquine revisited six decades after its discovery. *Eur. J. Med. Chem.* **2009**, *44* (3), 937−953.
(11) Rodrigues, T.; Prudencio, M.; Moreira, R.; Mota, M. M.; Lopes, F. Targeting the liver stage of malaria parasites: A yet unmet goal. *J. Med. Chem.* **2012**, *55*, 995−1012.
(12) Meister, S.; Plouffe, D. M.; Kuhen, K. L.; Bonamy, G. M. C.; Wu, T.; Barnes, S. W.; Bopp, S. E.; Borboa, R.; Bright, A. T.; Che, J. W.; Cohen, S.; Dharia, N. V.; Gagaring, K.; Gettayacamin, M.; Gordon, P.; Groessl, T.; Kato, N.; Lee, M. C. S.; McNamara, C. W.; Fidock, D. A.; Nagle, A.; Nam, T. G.; Richmond, W.; Roland, J.; Rottmann, M.; Zhou, B.; Froissard, P.; Glynne, R. J.; Mazier, D.; Sattabongkot, J.; Schultz, P. G.; Tuntland, T.; Walker, J. R.; Zhou, Y. Y.; Chatterjee, A.; Diagana, T. T.; Winzeler, E. A. Imaging of Plasmodium liver stages to drive next-generation antimalarial drug discovery. *Science* **2011**, *334*, 1372−1377.
(13) Cruz, F. P.; Martin, C.; Buchholz, K.; Lafuente-Monasterio, M. J.; Rodrigues, T.; Sönnichsen, B.; Moreira, R.; Gamo, F.-J.; Marti, M.; Mota, M. M.; Hannus, M.; Prudêncio, M. Drug screen targeted at Plasmodium liver stages identifies a potent multistage antimalarial drug. *J. Infect. Dis.* **2012**, *205*, 1278−1286.
(14) Derbyshire, E. R.; Prudencio, M.; Mota, M. M.; Clardy, J. Liver-stage malaria parasites vulnerable to diverse chemical scaffolds. *Proc. Natl. Acad. Sci. U.S.A.* **2012**, *109*, 8511−8516.
(15) Walsh, J. J.; Bell, A. Hybrid drugs for Malaria. *Curr. Pharm. Des.* **2009**, *15*, 2970−2985.
(16) O'Neill, P. M.; Stocks, P. A.; Pugh, M. D.; Araujo, N. C.; Korshin, E. E.; Bickley, J. F.; Ward, S. A.; Bray, P. G.; Pasini, E.; Davies, J.; Verissimo, E.; Bachi, M. D. Design and synthesis of endoperoxide antimalarial prodrug models. *Angew. Chem., Int. Ed.* **2004**, *43*, 4193−4197.
(17) Benoit-Vical, F.; Lelievre, J.; Berry, A.; Deymier, C.; Dechy-Cabaret, O.; Cazelles, J.; Loup, C.; Robert, A.; Magnaval, J. F.; Meunier, B. Trioxaquines are new antimalarial agents active on all erythrocytic forms, including gametocytes. *Antimicrob. Agents Chemother.* **2007**, *51*, 1463−1472.
(18) Cosledan, F.; Fraisse, L.; Pellet, A.; Guillou, F.; Mordmuller, B.; Kremsner, P. G.; Moreno, A.; Mazier, D.; Maffrand, J. P.; Meunier, B. Selection of a trioxaquine as an antimalarial drug candidate. *Proc. Natl. Acad. Sci. U.S.A.* **2008**, *105*, 17579−17584.
(19) Araujo, N. C. P.; Barton, V.; Jones, M.; Stocks, P. A.; Ward, S. A.; Davies, J.; Bray, P. G.; Shone, A. E.; Cristiano, M. L. S.; O'Neill, P. M. Semi-synthetic and synthetic 1,2,4-trioxaquines and 1,2,4-trioxolaquines: synthesis, preliminary SAR and comparison with acridine endoperoxide conjugates. *Bioorg. Med. Chem. Lett.* **2009**, *19*, 2038−2043.
(20) O'Neill, P. M.; Posner, G. H. A medicinal chemistry perspective on artemisinin and related endoperoxides. *J. Med. Chem.* **2004**, *47*, 2945−2964.
(21) Haynes, R. K.; Chan, W. C.; Wong, H. N.; Li, K. Y.; Wu, W. K.; Fan, K. M.; Sung, H. H. Y.; Williams, I. D.; Prosperi, D.; Melato, S.; Coghi, P.; Monti, D. Facile oxidation of leucomethylene blue and dihydroflavins by artemisinins: Relationship with flavoenzyme function and antimalarial mechanism of action. *ChemMedChem* **2010**, *5*, 1282−1299.
(22) Haynes, R. K.; Cheu, K. W.; Tang, M. M. K.; Chen, M. J.; Guo, Z. F.; Guo, Z. H.; Coghi, P.; Monti, D. Reactions of antimalarial peroxides with each of leucomethylene blue and dihydroflavins: Flavin reductase and the cofactor model exemplified. *ChemMedChem* **2011**, *6*, 279−291.
(23) Capela, R.; Cabal, G. G.; Rosenthal, P. J.; Gut, J.; Mota, M. M.; Moreira, R.; Lopes, F.; Prudêncio, M. Design and evaluation of primaquine-artemisinin hybrids as a multistage antimalarial strategy. *Antimicrob. Agents Chemother.* **2011**, *55*, 4698−4706.
(24) O'Neill, P. M.; Amewu, R. K.; Nixon, G. L.; ElGarah, F. B.; Mungthin, M.; Chadwick, J.; Shone, A. E.; Vivas, L.; Lander, H.; Barton, V.; Muangnoicharoen, S.; Bray, P. G.; Davies, J.; Park, B. K.; Wittlin, S.; Brun, R.; Preschel, M.; Zhang, K. S.; Ward, S. A. Identification of a 1,2,4,5-tetraoxane antimalarial drug-development candidate (RKA 182) with superior properties to the semisynthetic artemisinins. *Angew. Chem., Int. Ed.* **2010**, *49*, 5693−5697.
(25) Wang, X. F.; Zhao, Q. J.; Vargas, M.; Dong, Y. X.; Sriraghavan, K.; Keiser, J.; Vennerstrom, J. L. The activity of dispiro peroxides against *Fasciola hepatica*. *Bioorg. Med. Chem. Lett.* **2011**, *21*, 5320−5323.
(26) Ghorai, P.; Dussault, P. H. Mild and efficient Re(VII)-catalyzed synthesis of 1,1-dihydroperoxides. *Org. Lett.* **2008**, *10*, 4577−4579.
(27) De Luca, L.; Giacomelli, G.; Taddei, M. An easy and convenient synthesis of Weinreb amides and hydroxamates. *J. Org. Chem.* **2001**, *66*, 2534−2537.
(28) Han, K. J.; Kim, M. Direct synthesis of Weinreb amides from carboxylic acids using triphosgene. *Lett. Org. Chem.* **2007**, *4*, 20−22.
(29) Liu, M.; Li, J.; Xiao, X.; Xie, Y.; Shi, Y. An efficient synthesis of optically active trifluoromethyl aldimines via asymmetric biomimetic transamination. *Chem. Commun.* **2013**, *49*, 1404−1406.
(30) Marti, F.; Chadwick, J.; Amewu, R. K.; Burrell-Saward, H.; Srivastava, A.; Ward, S. A.; Sharma, R.; Berry, N.; O'Neill, P. M. Second generation analogues of RKA182: synthetic tetraoxanes with outstanding in vitro and in vivo antimalarial activities. *MedChemComm* **2011**, *2*, 661−665.
(31) Stocks, P. A.; Bray, P. G.; Barton, V. E.; Al-Helal, M.; Jones, M.; Araujo, N. C.; Gibbons, P.; Ward, S. A.; Hughes, R. H.; Biagini, G. A.; Davies, J.; Amewu, R.; Mercer, A. E.; Ellis, G.; O'Neill, P. M. Evidence for a common non-heme chelatable-iron-dependent activation mechanism for semisynthetic and synthetic endoperoxide antimalarial drugs. *Angew. Chem., Int. Ed.* **2007**, *46*, 6278−6283.
(32) O'Neill, P. M.; Pugh, M.; Stachulski, A. V.; Ward, S. A.; Davies, J.; Park, B. K. Optimisation of the allylsilane approach to C-10 deoxo carba analogues of dihydroartemisinin: synthesis and in vitro antimalarial activity of new, metabolically stable C-10 analogues. *J. Chem. Soc., Perkin Trans. 1* **2001**, 2682−2689.
(33) Ploemen, I. H. J.; Prudencio, M.; Douradinha, B. G.; Ramesar, J.; Fonager, J.; van Gemert, G. J.; Luty, A. J. F.; Hermsen, C. C.; Sauerwein, R. W.; Baptista, F. G.; Mota, M. M.; Waters, A. P.; Que, I.; Lowik, C.; Khan, S. M.; Janse, C. J.; Franke-Fayard, B. M. D. Visualisation and quantitative analysis of the rodent malaria liver stage by real time imaging. *PLoS One* **2009**, *4*, e7881.
(34) Araujo, M. J.; Bom, J.; Capela, R.; Casimiro, C.; Chambel, P.; Gomes, P.; Iley, J.; Lopes, F.; Morais, J.; Moreira, R.; de Oliveira, E.; do Rosario, V.; Vale, N. Imidazolidin-4-one derivatives of primaquine as novel transmission-blocking antimalarials. *J. Med. Chem.* **2005**, *48*, 888−892.
(35) Vale, N.; Matos, J.; Gut, J.; Nogueira, F.; do Rosario, V.; Rosenthal, P. J.; Moreira, R.; Gomes, P. Imidazolidin-4-one peptidomimetic derivatives of primaquine: Synthesis and antimalarial activity. *Bioorg. Med. Chem. Lett.* **2008**, *18*, 4150−4153.